U.S. Department
of Transportation
**Federal Railroad
Administration**

Office of Research and
Development
Washington, D.C. 20590

Freight Car Dynamics

Field Test Results and Comparison with Theory

FRA/ORD-81/46
June 1981
Interim Report

N. K. Cooperrider
E. H. Law
R. H. Fries

Document is available to the U.S. public through the National Technical Information Service, Springfield, Virginia 22161

03 - Rail Vehicles &
Components

NOTICE

This document is disseminated under the sponsorship of the U.S. Department of Transportation in the interest of information exchange. The United States Government assumes no liability for the contents or use thereof.

NOTICE

The United States Government does not endorse products or manufacturers. Trade or manufacturer's names appear herein solely because they are considered essential to the object of this report.

Technical Report Documentation Page

1. Report No.	2. Government Accession No.	3. Recipient's Catalog No.
FRA/ORD-81/46		

4. Title and Subtitle	5. Report Date
FREIGHT CAR DYNAMICS: FIELD TEST RESULTS AND COMPARISON WITH THEORY	June, 1981
	6. Performing Organization Code
7. Author(s)	8. Performing Organization Report No.
N.K. Cooperrider, E.H. Law, R.H. Fries	

9. Performing Organization Name and Address		10. Work Unit No. (TRAIS)
Arizona State University Mechanical Engineering Dept. Tempe, AZ 85281	Clemson University Dept. of Mech. Engr. Clemson, SC 29631	11. Contract or Grant No. DOT-OS-40018
12. Sponsoring Agency Name and Address		13. Type of Report and Period Covered
U.S. Department of Transportation Federal Railroad Administration Washington, D.C. 20590		Interim
		14. Sponsoring Agency Code FRA/RRD-11

15. Supplementary Notes

Prepared in cooperation with Association of American Railroad Research Center Chicago, Illinois, and the Union Pacific Railroad

16. Abstract

Field tests of a conventional rail freight car were conducted to provide data for comparison with theoretical analyses of rail freight car dynamic behavior. These tests, carried out by the Association of American Railroads and the Union Pacific Railroad, were designed to provide experimental information concerning modal damping, modal frequencies, mode shapes, motion amplitudes, critical hunting speeds, wheel-rail forces, and creep coefficients for comparison with theoretical results.

Alternative techniques for theoretical freight car analysis, data processing, and comparison of theory and experiment are discussed. The 80-ton open-hopper test car parameters, the wheel-rail and roadbed geometry, the test conduct and the data analysis precedures are described. Field test results in the form of time series data, RMS values, modal frequency and damping characteristics, and spectral analysis results are presented and discussed. Comparisons of test results with theoretical results of linear eigenvalue analyses, quasi-linear random response analyses, and hybrid computer simulations are given.

17. Key Words	18. Distribution Statement
freight car dynamics, rail vehicle dynamics, field tests, validation freight car trucks	Document is available to the public through the National Technical Information Service, Springfield, Virginia 22161

19. Security Classif. (of this report)	20. Security Classif. (of this page)	21. No. of Pages	22. Price
UNCLASSIFIED	UNCLASSIFIED	143	

METRIC CONVERSION FACTORS

Approximate Conversions to Metric Measures

Symbol	When You Know	Multiply by	To Find	Symbol
		LENGTH		
in	inches	*2.5	centimeters	cm
ft	feet	30	centimeters	cm
yd	yards	0.9	meters	m
mi	miles	1.6	kilometers	km
		AREA		
in^2	square inches	6.5	square centimeters	cm^2
ft^2	square feet	0.09	square meters	m^2
yd^2	square yards	0.8	square meters	m^2
mi^2	square miles	2.6	square kilometers	km^2
	acres	0.4	hectares	ha
		MASS (weight)		
oz	ounces	28	grams	g
lb	pounds	0.45	kilograms	kg
	short tons (2000 lb)	0.9	tonnes	t
		VOLUME		
tsp	teaspoons	5	milliliters	ml
Tbsp	tablespoons	15	milliliters	ml
fl oz	fluid ounces	30	milliliters	ml
c	cups	0.24	liters	l
pt	pints	0.47	liters	l
qt	quarts	0.95	liters	l
gal	gallons	3.8	liters	l
ft^3	cubic feet	0.03	cubic meters	m^3
yd^3	cubic yards	0.76	cubic meters	m^3
		TEMPERATURE (exact)		
°F	Fahrenheit temperature	5/9 (after subtracting 32)	Celsius temperature	°C

*1 in. = 2.54 cm (exactly). For other exact conversions and more detail tables see NBS Misc. Publ. 286. Units of Weight and Measures. Price $2.25 SD Catalog No. C13 10 286.

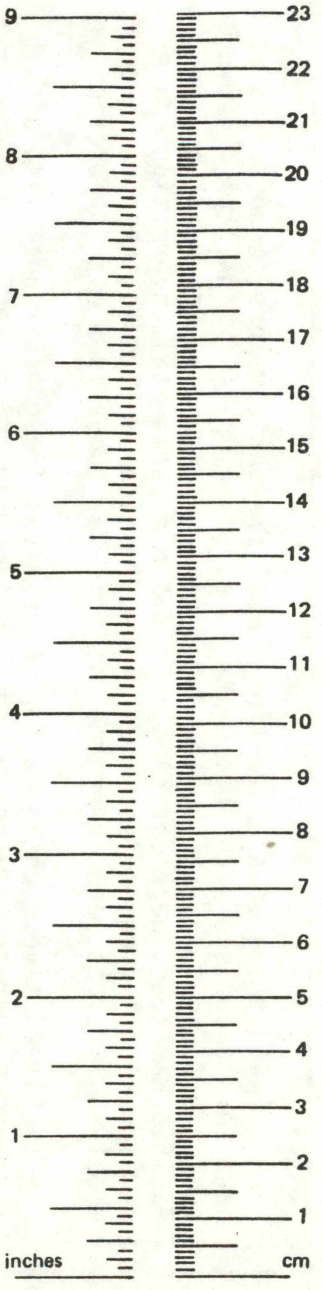

Approximate Conversions from Metric Measures

Symbol	When You Know	Multiply by	To Find	Symbol
		LENGTH		
mm	millimeters	0.04	inches	in
cm	centimeters	0.4	inches	in
m	meters	3.3	feet	ft
m	meters	1.1	yards	yd
km	kilometers	0.6	miles	mi
		AREA		
cm^2	square centimeters	0.16	square inches	in^2
m^2	square meters	1.2	square yards	yd^2
km^2	square kilometers	0.4	square miles	mi^2
ha	hectares (10,000 m^2)	2.5	acres	
		MASS (weight)		
g	grams	0.035	ounces	oz
kg	kilograms	2.2	pounds	lb
t	tonnes (1000 kg)	1.1	short tons	
		VOLUME		
ml	milliliters	0.03	fluid ounces	fl oz
l	liters	2.1	pints	pt
l	liters	1.06	quarts	qt
l	liters	0.26	gallons	gal
m^3	cubic meters	36	cubic feet	ft^3
m^3	cubic meters	1.3	cubic yards	yd^3
		TEMPERATURE (exact)		
°C	Celsius temperature	9/5 (then add 32)	Fahrenheit temperature	°F

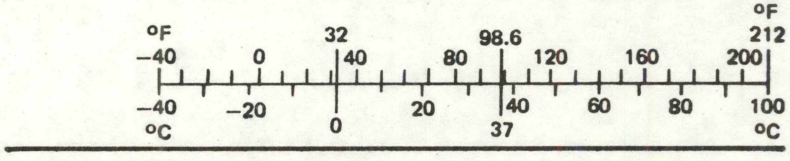

TABLE OF CONTENTS

TABLE OF CONTENTS

(Continued)

LIST OF FIGURES

LIST OF FIGURES

(Continued)

LIST OF FIGURES

(Continued)

LIST OF FIGURES

(Continued)

LIST OF FIGURES

(Continued)

LIST OF FIGURES

(Continued)

LIST OF TABLES

LIST OF TABLES

(Continued)

Chapter 1

INTRODUCTION

PROBLEM STATEMENT

An extensive effort to plan and conduct freight car dynamics tests and subsequently to analyze the test data and compare it with corresponding theoretical results was carried out by Clemson and Arizona State Universities in cooperation with the Association of American Railroads. This work, conducted over the period 1974-1978, constituted one aspect of the "Freight Car Dynamics" project carried out at Clemson and Arizona State under Federal Railroad Administration sponsorship. The field tests and efforts to compare the results with theory are described in this report.

The overall objective of this project was to develop tools and techniques for the analysis of railroad freight car dynamics. Both development and correlation of theoretical techniques for prediction of freight car dynamics were involved. The theoretical developments are described in other reports [1-1 through 1-8], while this report deals with the testing, data reduction, data analysis and theoretical comparison efforts.

PREVIOUS WORK

Very few efforts to compare theoretical and experimental rail vehicle dynamic results were conducted in the first century of railroading. Apparently experimentalists and theoreticians had very little interaction, working in different groups and organizations with very little contact or access to the others' tools and results. Only in the last two decades has there been significant advancement in this area.

Much of the experience with rail vehicle testing for validation has been surveyed by Cooperrider and Law [1-9]. Reasonably good agreement has been obtained between theory and experiment when the vehicle response does not involve the mechanics of the wheel-rail interaction. In particular, good agreement has been found for the response of vehicles to vertical roadbed irregularities [1-10, 1-11], and for the "rock and roll" response of freight cars to roadbed crosslevel irregularities [1-12, 1-13]. When the wheel-rail contact conditions are well controlled, as occurs on roller rig installations, good agreement for lateral stability has also been found [1-14, 1-15]. However, good agreement between theoretical and experimental vehicle lateral dynamics on actual roadbed has not been obtained, perhaps due in part to the complexities and uncertainties of the wheel-rail contact mechanics, and in part to incomplete knowledge of the roadbed characteristics.

In one approach to validating the lateral dynamics theory, experimental and theoretical values for the critical speed delineating the onset of vehicle hunting have been compared. However, this comparison involves only one value from theory and experiment, and is of relatively little use in assessing the fidelity of a theoretical model. This one value, the critical speed, is strongly dependent on system parameters that are often difficult to establish, such as the creep-force laws, the wheel-rail friction level, the suspension friction levels or the amplitudes of the vehicle component motions. A more comprehensive comparison is needed to establish the fidelity of the theory.

The most complete previous effort to compare theory and experimental results for rail vehicle lateral dynamic behavior was conducted by the British Rail Research Centre for the Office of Research and Experiments (ORE) of the International Union of Railways several years ago [1-9]. British Rail employed a two-axle experimental vehicle equipped with profiled wheels to obtain test data. Test data in the form of power spectra for vehicle accelerations was compared with theoretical power spectra obtained from linear theory. Laterally, the agreement between theory and experiment was rather poor. British Rail attributes this poor correlation to three factors:

1. The use of profiled wheels whose "effective conicity" depended on the amplitude of motion.

2. The unknown values of the actual creep coefficients.

3. The fact that the complete lateral roadbed input spectrum was not known because they did not measure the rolling line offset.

OBJECTIVES

The specific objective of this effort was to carry out a quantitative comparison of rail car lateral dynamic theory with experimental results in order to demonstrate the quantitative fidelity of the theory. Good agreement between experimental and theoretical motion amplitudes, motion frequencies, system damping, critical speeds, and mode shapes in a variety of vehicle configurations and operating situations was of particular interest.

Although the difficulties encountered by others in attempting such an effort in the past were known from the beginning, these difficulties were not fully appreciated initially. As explained in this report, the vehicle behavior was found to depend on a large number of environmental factors that, despite out best efforts, remained undetermined in our tests. In addition, due to the strongly nonlinear character of the test car suspension, the dynamic behavior depended on the amplitudes of the roadbed irregularities and other disturbances. Consequently, the effort reported here must be regarded as an early step in the long process of obtaining agreement between theory and experiment for lateral vehicle dynamics.

APPROACH

The total effort conducted in the "Freight Car Dynamics" project involved extensive develop-

ment of theoretical models and analysis as well as methods for planning, conducting and analyzing rail vehicle field tests. As mentioned earlier, the theoretical developments are reported elsewhere. This report deals with the field test plans, conduct, data analysis and reduction, and comparisons with theory.

In the following chapter, the methods that we considered for comparison of test data and theoretical results are discussed. This discussion includes a brief description of the theoretical models and available data-analysis methods.

The field test preparations and conduct are described in Chapter 3. The field tests were conducted by the Association of American Railroads (AAR) and the Union Pacific Railroad in accordance with our test conduct requests. The vehicle and roadbed characterization, instrumentation, data collection system and test conduct are discussed there.

The field test results are covered in Chapter 4. The test data is summarized, sample time series data cases presented and discussed, vehicle hunting characteristics described, the root mean square (RMS) response results given, frequency and damping characteristics surveyed and the spectral analysis results discussed.

The comparison of theory and experimental results is discussed in Chapter 5. Three models are compared with the experimental results: a linear eigenvalue-eigenvector analysis, a statistical linearization approach, and a hybrid computer analysis.

Our conclusions and suggestions for future work are presented in Chapter 6.

Chapter 2

EXPERIMENTAL AND THEORETICAL COMPARISON METHODS

BACKGROUND

In this exploratory study, our approach has been to develop and investigate a number of modeling, analysis and correlation techniques. For example, vehicle models with 5, 9, 17, 19 and 23 degrees of freedom have been developed. Solution techniques for the equations of vehicle motion ranging from linear eigenvalue techniques to hybrid computer integration have been utilized. Similarly, a variety of methods for processing the experimental data and comparing it with theoretical results have been pursued.

These theoretical models, analysis techniques, and comparison methods are outlined in this chapter. The suitability, efficiency and range of applicability of these various methods are discussed in Chapter 5.

THEORETICAL ANALYSES METHODS

A hierarchy of modeling and analysis techniques has been developed in this project. This approach is necessary due to the nonlinear nature of the freight car suspension and wheel-rail interaction, and due to varying requirements for dynamic behavior information. Conventional analysis methods for complex nonlinear systems (i.e., direct integration of the equations of motion using digital or analog/hybrid computers) are quite expensive, time consuming, and yield diffuse resuts in the form of time histories of the system variables. Our hierarchy of models, with varying degrees of detail and with solution techniques that include linear and quasilinear methods, permits less costly computation and yield more condensed results. The ultimate objective of this work is to establish the conditions and range of applicability of each model and analysis approach. This will allow a vehicle designer or analyst to select the most appropriate model and computer program for his purpose.

This hierarchical approach has been followed in each area of lateral freight car dynamics. For investigating hunting, we have developed six models (classified in terms of numbers of degrees of freedom) and four analytical techniques to solve the model equations of motion. For forced response to rail irregularities, two models and three analyses, and for curving behavior, two models and two analyses. These models and analyses are briefly described in the following sections, and are more fully discussed in other reports and papers [2-1, 2-2, 2-3].

Hunting Stability

The lateral stability of the freight vehicle can be found from analysis of the homogeneous equations of motion. The models developed for the lateral dynamics of a single railway vehicle are shown in Table 2-1 and are classified according to the number of degrees of freedom.

Eigenvalue/eigenvector stability analyses have been coded for linearized versions of each of these models. These analyses provide the frequency and damping of oscillatory modes, the time constants for overdamped modes, and the corresponding mode shapes. Critical hunting speeds and stability margins for the least-damped or hunting mode may be estimated with these analyses.

Selecting input data for use in these eigenvalue/eigenvector analyses is not a simple matter even when component test data are available. The lateral suspension characteristics of conventional North American freight trucks are dominated by dry friction and other nonlinearities. Thus, choosing equivalent linear characteristics for these input parameters requires considerable expertise and judgment as does interpretation of the results of the stability analyses.

Table 2-1. Vehicle Models

No. of DOF	Description of Degrees of Freedom
5*	Half car model; one roller bearing truck with warp, yaw, and lateral DOF; half car body with lateral and roll DOF.
9	Full car model; two roller-bearing trucks with warp, yaw, and lateral DOF; car body with lateral, yaw and roll DOF.
11	Half car model; one generalized truck with lateral, yaw, and torsional DOF of each of two wheelsets as well as lateral, warp, and yaw DOF of the truck frame; half car body with lateral and roll DOF.
19	Full car model; two generalized trucks with lateral and yaw DOF of each of two wheelsets as well as lateral, warp, and yaw DOF of the truck frame; car body with rigid body lateral, roll, and yaw DOF. The use of a two-mass approximation to the car body permits a first approximation to flexible car body torsion and lateral bending thus giving the car body a total of 5 DOF.
23	Full car model; this model is identical to the 19-DOF model discussed above with the addition of an axle torsional degree of freedom for each of the four axles. The effects of independently rotating wheels or axle torsional flexibility may be examined with this model.

*This model was developed in the early stages of the research when it was thought there was a possibility of performing tests with a similar physical configuration on the Japanese National Railways (JNR) roller rig.

These analyses have been used to examine the effects on stability of variations in design variables such as primary suspension and wheelset interconnection characteristics, truck-frame warping flexibility, and car-body flexibility [2-1, 2-2]. Questions dealing with maintenance and operational practice as well as those concerned with vehicle design have also been addressed with these tools. The primary advantages of these linearized models and analyses are that they are relatively economical with regard to computer costs and afford a means of obtaining a great deal of insight into rail vehicle stability.

North American freight car suspensions contain several nonlinear elements such as Coulomb friction, deadband, and hardening springs. Additionally, due to worn wheel profiles, the wheel/rail geometric constraints are often strongly nonlinear even for motions before flange contact occurs. Quasi-linear and direct integration analysis methods to solve the nonlinear equations of motion were employed in this effort.

Representative results obtained by a quasi-linear stability analysis of a 9-DOF freight car are shown in Figure 2-1 where amplitudes of stable and unstable limit cycles are shown plotted as functions of forward speed. Unstable limit cycles are stability boundaries while stable limit cycles represent possible hunting conditions. Other outputs that may be obtained are the wheel/rail forces, forces between suspension components, and acceleration levels in the vehicle during hunting. Quasi-linear analysis techniques applied to rail vehicle dynamics are discussed more completely in [2-4].

Due to machine capacity limitations of the Clemson University Engineering Computer Laboratory, we have focused our hybrid computation efforts on the 5-DOF half-car model described in Table 2-1. Nonlinearities considered are the wheel-rail geometric constraint characteristics and suspension friction. Random lateral rail alignment irregularities that conform to a specified spectrum have been input to the simulation. Typical results obtained from the hybrid simulation of the 5-DOF model are shown in Figure 2-2. The limit cycle amplitude characteristics are plotted versus forward speed for two vehicles in this figure. In one case, **equivalent** viscous damping is used for Coulomb friction in the suspension, while in the second the actual Coulomb friction characteristics are used. The predominant effect of the Coulomb friction in this case is to reduce the speed at which hunting may occur. These hybrid simulation efforts are discussed more completely in other reports [2-1, 2-5].

Forced Response

The forced response of the freight car to roadbed disturbances has been computed with several of the models. A computer program using frequency-domain techniques for the linearized 9-DOF model was developed [2-6]. This program determines both the model variable amplitudes and phase relationships in response to harmonic roadbed alignment or cross-level disturbances, and the model variable power spectral densities (PSDs) in response to random roadbed irregularities.

The nonlinear freight car response has been computed employing statistical linearization for the 9-DOF model. Although this approach is especially attractive as a cost-effective analysis tool, there are assumptions and approximations made that are not necessary when directly integrating the equations. These questions are considered more fully in [2-4].

The nonlinear vehicle response may also be computed by direct integration. Here too, our efforts have utilized a hybrid computer simulation of the 5-DOF model. The roadbed irregularities in this simulation may be of almost any form including dips, bumps, sinusoids, and random signals. Results of the analysis are time histories of the vehicle response variables. The resulting time histories may be processed using any of the data analysis techniques discussed in the next section.

Curving Behavior

We have used two models and two approaches to estimate the curving performance of freight cars. A 9-DOF model for a three-piece, roller bearing truck and a 17-DOF model that permits interconnected wheelsets and primary suspension elements have been used. The solution approaches were: 1) linearization and direct solution of the resulting linear algebraic equations, and 2) an iterative solution of the nonlinear equations that includes wheel-rail geometry and suspension nonlinearities.

Although curving tests were carried out in this project, the data obtained from them proved to be unusable for correlation purposes, as explained in Chapter 4. Consequently, results of these curving analyses have not yet been correlated with the actual curving behavior of rail freight cars. Such an effort should be addressed in the future.

EXPERIMENTAL DATA ANALYSIS TECHNIQUES

Field test data is gathered in the form of time-series data of displacement, velocity, acceleration and force measurements. This data may be utilized directly for comparison with theoretical data in time-series form, may be combined, or may be processed to reduce the time-series data to more manageable form. This data reduction can range from simple computation of a single value to transformation to frequency domain utilizing Fourier transform methods.

The data analysis method utilized depends on the nature of the tests. Two types of tests were conducted in this effort. In one type of test, a hydraulic truck forcer system applied a torque between the truck and the car body. This system caused an initial translation and angular displacement of the truck components. The objective

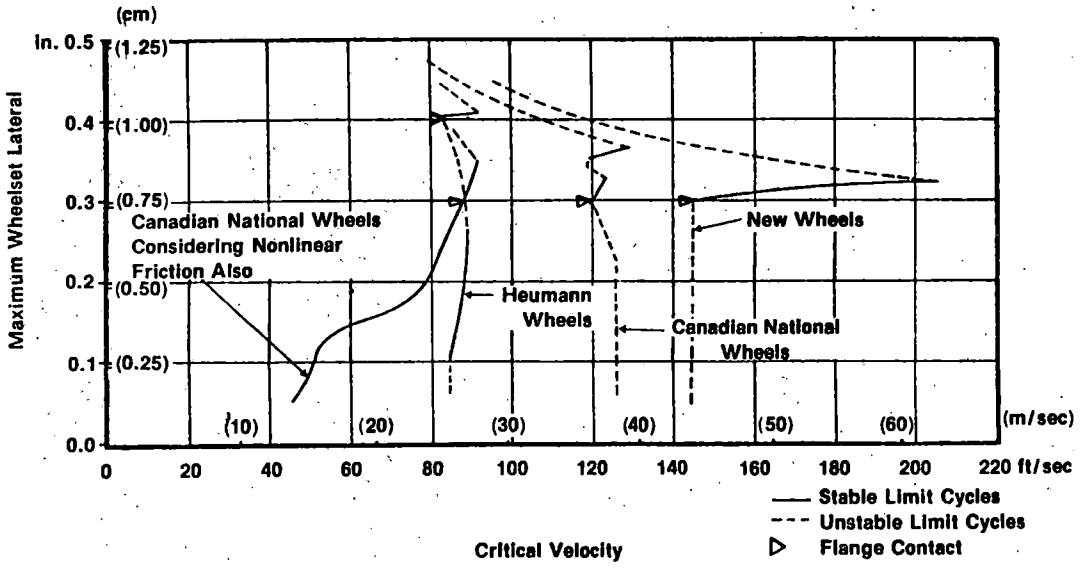

Figure 2-1. Limit Cycle Characteristics from Quasi-Linear Analysis

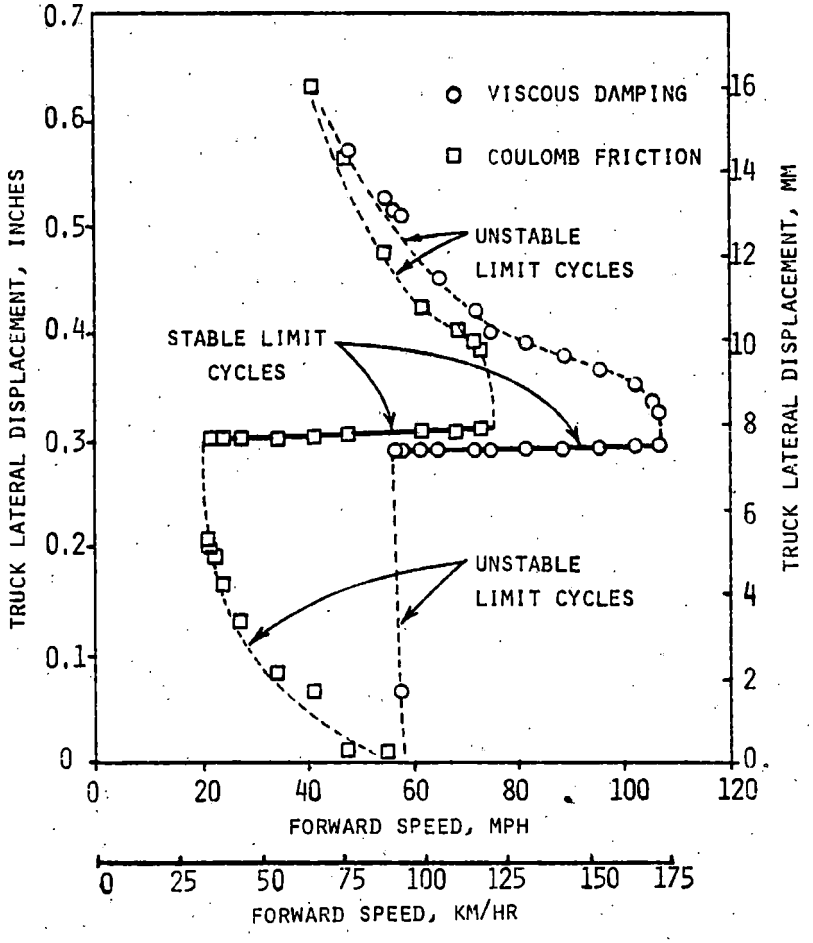

Figure 2-2. Limit Cycle Characteristics from Hybrid Simulation

in using the forcer was to obtain transient response data. Thus, analysis of this data provides estimates of natural frequencies and damping ratios.

The second type of test entailed merely recording the random response of the vehicle to roadbed irregularities. This time-series data can be analyzed in a variety of ways. In our study, histograms, mean values and standard deviations were computed to provide an overview of the test vehicle behavior. However, the comparison with theory utilized two other data reduction methods: spectral analysis and the Random-Decrement technique.

The Random-Decrement technique, originally developed for aircraft flutter test analysis, provides a transient "signature" [2-7]. Figure 2-3 illustrates a Random-Decrement signature obtained for the test vehicle at 15 mph. The damping ratio and frequency can be determined from such a signature.

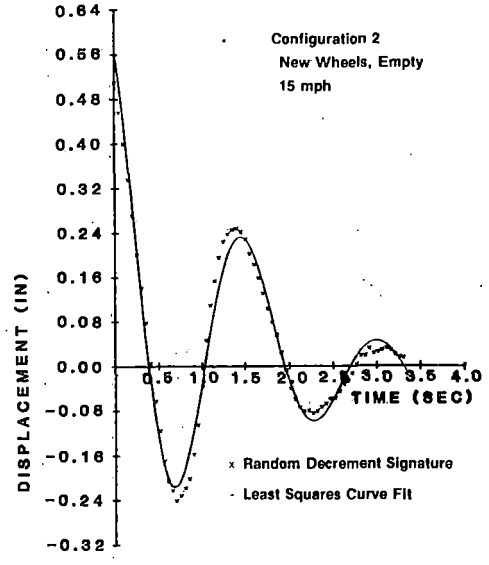

Figure 2-3. Random-Decrement Signature

Spectral-analysis techniques provide reduced data in several forms. The power spectral density (PSD) expresses the distribution of the random response over the frequency range. Cross-spectral densities yield the phase relationship between two signals and can be used together with the PSDs to compute transfer functions between variables.

The spectral analysis results, PSDs and transfer functions in particular, can be analyzed to infer damping, frequency and mode shapes of the system response.

COMPARISON METHODS

Validation or correlation of theoretical results with experimental data may be undertaken at many different levels. At the lowest level, a qualitative comparison is obtained between analytically predicted trends and experimentally observed behavior. For example, almost all linear stability analyses of rail car lateral dynamics predict that vehicles with wheelsets having high "effective" conicities will hunt at lower speeds than vehicles with wheelsets having a lower value of "effective" conicity. This trend agrees with observations of rail vehicle operation.

A great deal of qualitative validation has been done to strengthen confidence in the analytical tools. In stability analyses, the effects of primary yaw and warp stiffness on critical speeds have been qualitatively correlated. In curving analyses, the effects of yaw stiffness and wheelset conicity on L/V ratios have also been qualitatively correlated.

The value of qualitative validated analyses should not be underestimated. Models validated in this manner are invaluable in making design changes and in devising successful experiments because they provide information about the sensitivity of the vehicle behavior to parameter changes, and they also provide a framework for interpreting the test results.

A second level of validation entails correlation of a single, but usually critical, value from the analysis with experimental results. For example, the analytical predictions for the critical speed when hunting begins or the resonant speed for rock and roll behavior would be compared with experimental measurements or observations of the same variable. For example, the Japanese National Railroad (JNR) during development of the New Tokaido line equipment carried out a program of theoretical analysis, roller rig testing and subsequent field testing [2-8]. In the field tests, speeds to 256 km/hr were achieved. Vehicle hunting was experienced during some of these tests. The only quantitative correlation between theory and experiment in this program involved the critical speed of hunting. Theoretical predictions for critical speed did not agree well with experiment, although qualitative trends were reproduced.

It was apparent from the beginning of our project that an adequate validation procedure entails more than comparison of single theoretical and experimental values such as the critical speed for the onset of hunting. However, the best and most reliable approach was not clear initially. Consequently, several alternative approaches were planned to allow for possible shortcomings or failures with some of the methods.

Two methods for comparison of the tangent track theory with experimental results were pursued: 1) a comparison of theoretical and experimental PSDs, and 2) a comparison of theoretical and analytical modal frequency, modal damping and mode shape vs. speed characteristics. As explained below, both these approaches have drawbacks for nonlinear systems such as the freight car.

On curved track, comparison of theoretical and experimental values of wheelset lateral displacements, wheelsets yaw angles, and wheel/rail contact forces in curve entry and steady curving was planned. This curving validation could not be carried out due to difficulties with the instrumentation and test conduct. As a result of these difficulties the test data was not usable for curving theory validation.

Pre-test sensitivity studies indicated a strong influence of the creep coefficients on the vehicle behavior. In some cases, the critical speed of hunting predicted from a linear stability analysis would double when the creep coefficients were changed from 50% to 100% of the values predicted by Kalker's linear theory. For this reason, a third series of tests was planned and executed in an attempt to determine the creep coefficients more directly. These tests, run at slow speeds of approximately 10 mph, involved applying measurable torques between the truck and car body and recording the resulting displacements and angular positions of the wheelsets relative to the rails. The torques were applied with the hydraulic forcer system described earlier. The creep coefficients were to be determined by an identification procedure utilizing the equilibrium equations for the vehicle and the measured wheelset and car-component displacements. Unfortunately, the data from these creep tests also cannot be used because the initial conditions for the wheel-rail transducers were not recorded, and the tests were conducted on a poor quality passing track rather than the good quality track where the other tests were run. These two problems prevent extraction of the steady-state wheel-rail lateral and yaw displacements that are needed to determine the creep forces. Despite the failure of these creep tests, we believe that field testing to establish the creep force conditions should be a part of all future tests to validate rail vehicle lateral dynamics theory.

As a result of the problems mentioned above, the efforts completed in this project were limited to tangent track vehicle dynamics. Comparisons of theoretical results for both hunting stability and vehicle forced response to track irregularities were undertaken. These two methods allow us to look at the vehicle dynamics in different ways, and thus provide redundancy in the validation. The same theoretical model is used in obtaining stability and forced response results. Only the disturbances acting on the system differ between the two situations.

Stability Correlation

Sustained hunting oscillations are one of the most important problems associated with freight car dynamic behavior. A major objective of this project is the development of mathematical models that will predict the speed at which sustained hunting oscillations occur, the influence of design changes on this speed, and the stability margin available at lower speeds.

The rail freight car behavior at any speed can be loosely described as the sum of motions in several different modes. Each mode is characterized by a particular frequency, damping ratio and mode shape. The mode shape is a particular amplitude and phase relationship between the motions of the various system components often called the eigenvector. Terms such as upper center roll, lower center roll, nosing, and fish tailing are often used to describe such mode shapes.

The stability of the freight car dynamic response is determined by the mode that has the least amount of damping. For a linear system, the response of any variable is mathematically expressed as,

$$X_i(t) = \sum_{j=1}^{n} A_j e^{-\zeta_j \omega_{nj} t} \cos(\omega_j t + \phi_j)$$

where

- n - number of state variables
- ζ_j - damping ratio for mode j
- ω_j - frequency of mode j
- ω_{nj} - undamped natural frequency of mode j
- ϕ_j - phase angle for mode j

Thus, a stable system will have $\zeta_i > 0$ for all modes, and an unstable system will have at least one $\zeta_i < 0$. The pair, ζ_j and ω_j can be combined in a complex number called the eigenvalue for that mode. The transient response of a motion for several different damping ratios is depicted in Figure 2-4.

Results of a mathematical analysis can be compared with experimentally determined damping ratios, frequencies and mode shapes at several speeds. A linear analysis of freight car stability by the eigenvalue method produces damping ratios and frequencies for the least-damped mode that vary with speed in the manner shown in Figure 2-5. The intersection of the damping ratio curve with the horizontal axis occurs at the predicted speed of hunting. One of our correlation approaches was to compare theoretical and experimental results for damping ratio and frequency in the format shown above. However, obtaining information in this form posed difficulties both theoretically and experimentally.

Placing the data in the form shown in Figure 2-4 implies that the system behaves nearly linearly, and that only one mode has light damping. Additional lightly damped modes would require plotting other frequencies and damping ratios. The linearity implied by a response of the form shown in the preceding equation poses a more difficult problem. The vehicle behavior proved to be highly nonlinear, due to the high Coulomb friction levels at the centerplate, bolster/sideframe and sideframe/bearing adapter interfaces. Although the describing function technique was used to handle the amplitude dependence implied by this nonlinearity, difficulties in analyzing and interpreting the test data still occurred, as described later.

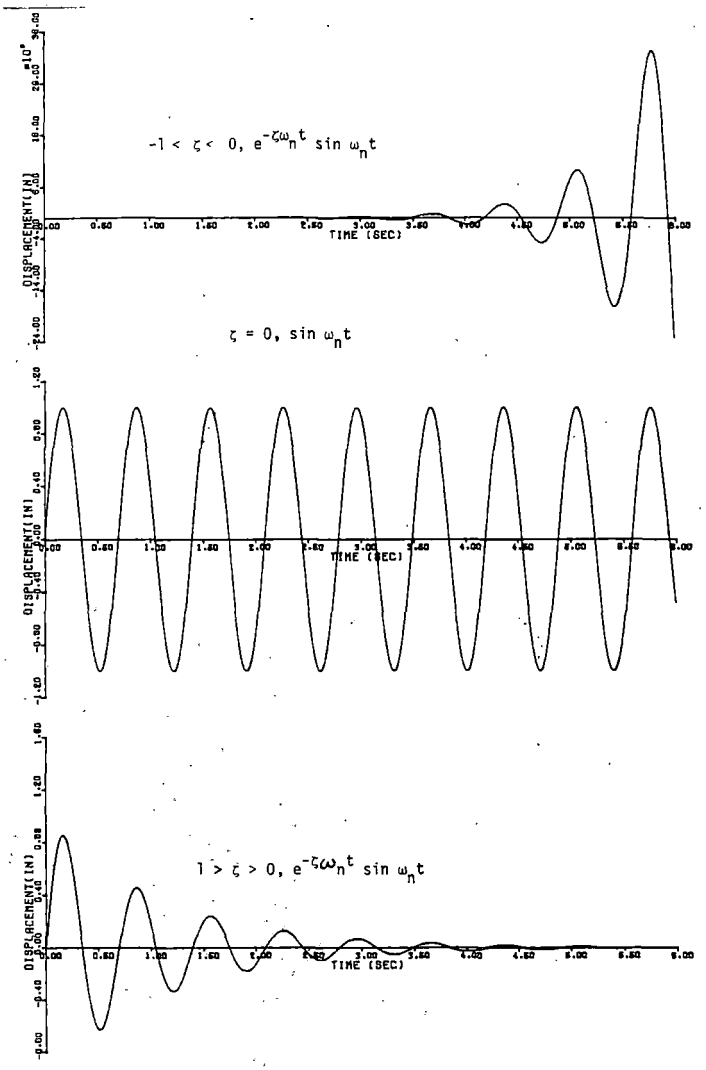

Figure 2-4. Typical System Dynamic Response

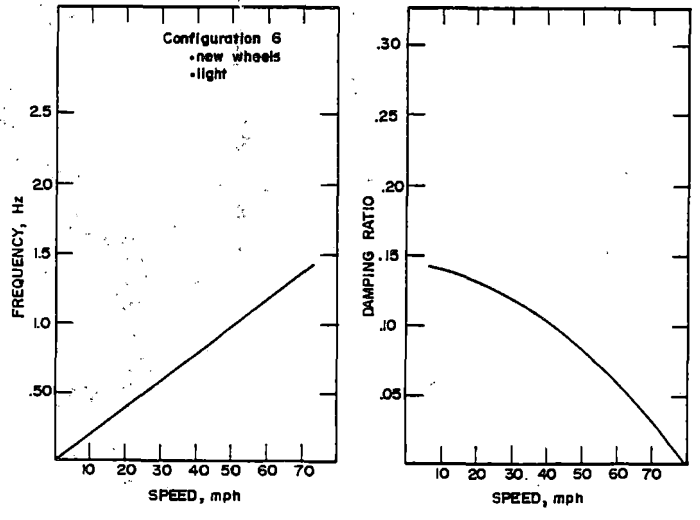

Figure 2-5. Eigenvalues for Least Damped Mode. Linear Freight Car Model.

The experimental system damping and frequency information needed for this comparison may be obtained from the forcer response time-series data or from the random response time series by utilizing the Random-Decrement or PSD methods. All three approaches were utilized in this study.

Forced Response

The process of comparing experimental and theoretical forced response is somewhat simpler. Previous studies have shown that the vehicle vertical and roll response to specific track irregularities, such as low joints [2-9], can be predicted fairly well by analytical means. For example, power spectral densities from experimental vertical acceleration measurement made in the TDOP tests [1-11] were compared with analytically computed PSDs. As seen in Figure 2-6, quite good agreement was obtained, despite the nonlinear friction present in the system.

Previous attempts to validate analyses for lateral response to random rail irregularities have not been very successful. As mentioned earlier these efforts revealed difficulties due to nonlinear wheel-rail geometry, unknown creep-force laws and the fact that the rolling line offset was not known. An attempt was made in this project to avoid these difficulties by testing with conical as well as profiled wheels, measuring rail head profiles to assess rolling line offset, and devising tests to determine the actual creep coefficients. Discussion of the power spectra computations and comparison with theoretical power spectra may be found in the following chapters.

One difficulty with correlation of forced response data is the necessity of knowing the track disturbances imposed on the vehicle. The unknown level of the rolling-line offset is one such problem; another is obtaining current track-geometry data. In the case of our tests, only limited track-geometry data is available due to two accidents involving track-geometry measurement equipment. In addition, we were able to measure rail head profiles at a limited number of stations and cannot construct a continuous estimate of rolling line offset.

The shape of the least-damped mode, and in some cases those of other modes, can also be obtained from the forced response data. Cross-spectral densities used in conjunction with PSDs provide transfer functions between the component motions. This provides additional information to strengthen confidence in the validity of the mathematical analysis.

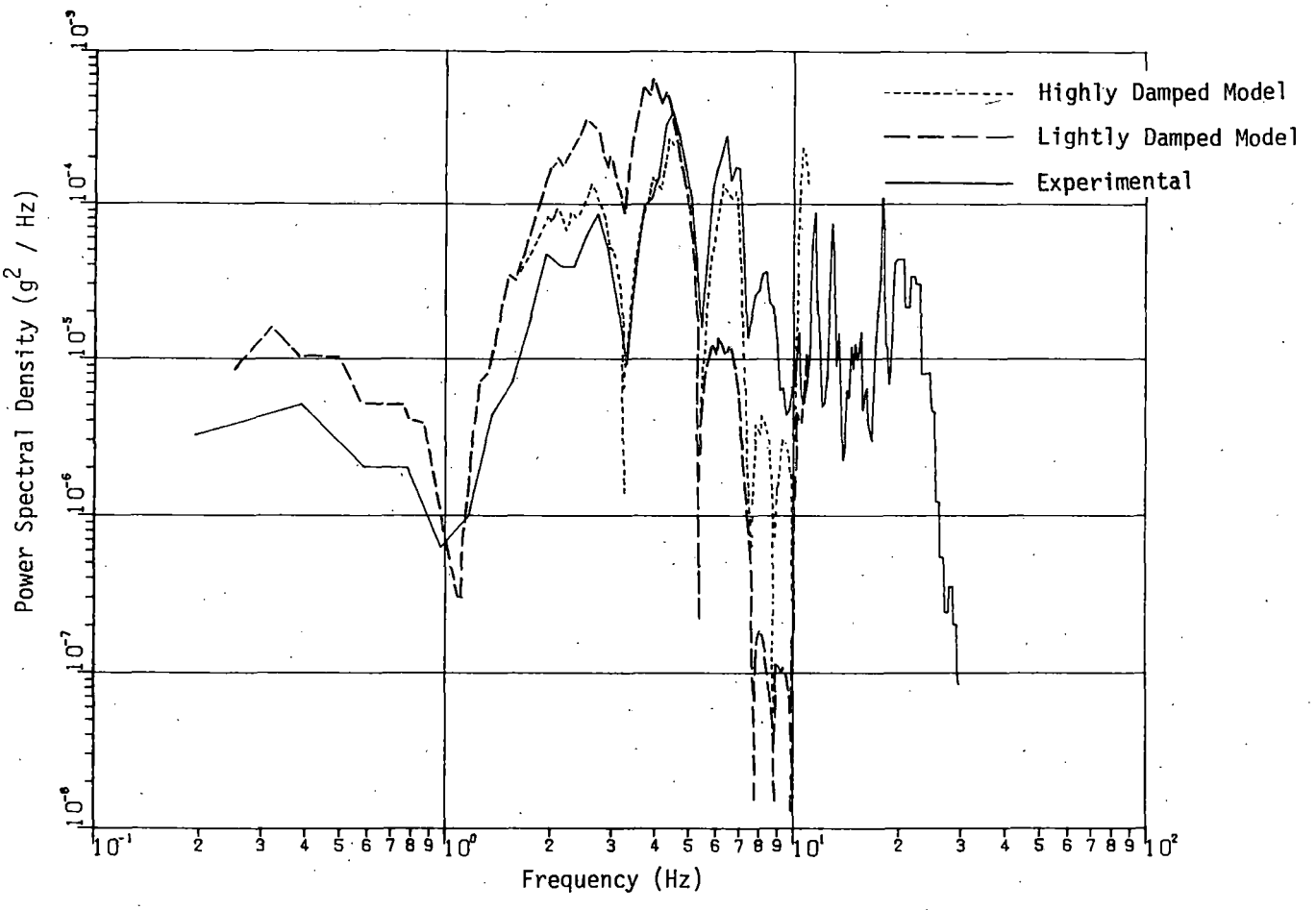

Figure 2-6. Theoretical and Experimental PSDs for Vertical Response of Refrigeration Car

SUMMARY

A battery of theoretical modeling and analysis techniques has been developed to study the freight car dynamic behavior. These approaches vary in the complexities of the modeling, in the method of handling nonlinear effects, in the roadbed configuration, and in the method of solution. Our objective in this effort has been to determine the limitations and appropriate application for each of these models and associated analysis techniques.

The original test objectives included tests to determine hunting stability, forced response on tangent track, curving behavior, and creep force relationships. An oversight in the test conduct procedures rendered the curving and creep force test data unusable. Consequently, only correlation of vehicle behavior on tangent track was carried out.

Several different approaches were taken to compare theoretical and experimental freight car dynamic behavior. Stability results obtained from random response and initial condition situations were compared. The experimental random response data was processed by the Random-Decrement technique and by spectral analysis methods to obtain frequency and system or modal damping versus vehicle speed characteristics. These frequency and damping characteristics were also obtained by analysis of the response to initial conditions imposed by a hydraulic force system. Correlation entailed comparison of the experimental frequency and damping characteristics obtained by eigenvalue and other analytical methods. The forced response data on tangent track was also used to compare with theoretical results in the form of power spectra.

The field tests to obtain the data needed to carry out these correlation approaches are described in the following chapters. The results of the comparison between experimental and theoretical results are presented in Chapter 5.

Chapter 3

FIELD TEST CONDUCT

INTRODUCTION

This field test program involved the cooperation of several organizations to characterize the test vehicle and roadbed, instrument the vehicle and conduct the test program. American Steel Foundries (ASF) and Martin Marietta Corporation carried out tests to characterize various elements of the vehicle trucks and car body. The Association of American Railroads instrumented the vehicle, managed the test program and collected the test data. The Union Pacific Railroad provided the manpower, motive power, and right-of-way for the conduct of the tests. Roadbed geometry data was provided by the Union Pacific Railroad and by ENSCO, Inc. Wheel and rail profile data was obtained using profilometers loaned by the Germany Federal Railways (DB). This data was partially processed at the U.S. DOT Transportation Test Center in Pueblo, Colorado. The reduction and analysis of the test data was carried out at Arizona State and Clemson Universities, who were also responsible for outlining the test requirements.

The conduct of this test program is discussed in this chapter. The discussion is divided into sections dealing with the vehicle and track characterization, the field tests themselves and a brief summary. The reduction of the field test data, a discussion of the test results, and the conclusions that we have drawn from the testing experience are covered in the following chapter.

VEHICLE AND ROADBED CHARACTERISTICS

A significant portion of this experimental program was devoted to obtaining data for characterization of the vehicle-roadbed system. This effort included laboratory testing of the test vehicle and its components; on-site measurements of vehicle, rail and roadbed characteristics; and extensive data analysis to derive the desired system parameter values. In addition, the vehicle was equipped with several devices and systems designed to provide variations in vehicle characteristics and to execute certain test maneuvers. In this section, the testing, data analysis and resulting parameter values are discussed. The test vehicle hardware is described, although description of the vehicle instrumentation is left to the following section.

Test Vehicle

The test vehicle, shown in Figure 3-1, was an 80-ton open hopper car on loan from the Louisville & Nashville (L & N) Railroad (LN 184701). The running gear consisted of a pair of ASF 70-ton A-3 Ride Control trucks. The fundamental component of this vehicle, like all rail vehicles, is the wheelset. The wheelset, consisting of two wheels rigidly fixed to the axle, provides a self-steering action through the wheel/rail contact forces. These forces arise from the tapered or profiled shape of the wheel treads.

The test vehicle truck consisted of two sideframes, a bolster, and two wheelsets. An illustration of such a truck, equipped with journal roller bearings is shown in Figure 3-2. The ends of the sideframe rest on the bearing adapters that rest in turn on the bearings of the wheelsets. A close-up view of the bolster-sideframe connection is given in Figure 3-3.

Data obtained from laboratory tests and corroborated by field test results indicate that the relative motion between the sideframes and wheelsets of the roller bearing truck is, for the most part, rotational. Relative translational motion at this interface is very small as long as the vehicle is not hunting. Consequently, it is reasonable to model this interface as the kinematic equivalent of a ball-joint. Such a model is not applicable to older freight trucks with plain bearings which have considerable lateral free-play between the wheelsets and sideframes.

In much of this investigation, the behavior of the test trucks was represented by three degrees of freedom (DOF): lateral motion (x_T), yaw of the centerline of the truck (θ_T), and parallelogramming or warping of the truck frames (θw) due to the relative rotational motion permitted by the sideframe-wheelset connection. Clearances in the actual truck are such that the maximum possible warp angle is about 2.5 degrees. A schematic of the truck with these degrees of freedom is shown in Figure 3-4.

Vehicle Geometry

The general layout of the test vehicle and details concerning its equipment are given in Figure 3-5. The brake rigging was removed from the trucks to allow for special instrumentation required for these tests. The geometric parameter values of importance in dynamic analysis are given with definitions in Table 3-1. The value for the height of the loaded carbody center of gravity is based on calculations for the car fully loaded with crushed rock [3-1].

Table 3-1. Test Vehicle Geometric Parameters

Sideframe semi-lateral spacing	3.25	ft
Truck Semi-wheelbase	2.83	ft
Carbody semi-truck center distance . .	16.85	ft
Wheel radius	1.375	ft
Truck sideframe c.g. height above rail	1.375	ft
Car body c.g. height above rail		
Light car	2.99	ft
Loaded car	4.62	ft

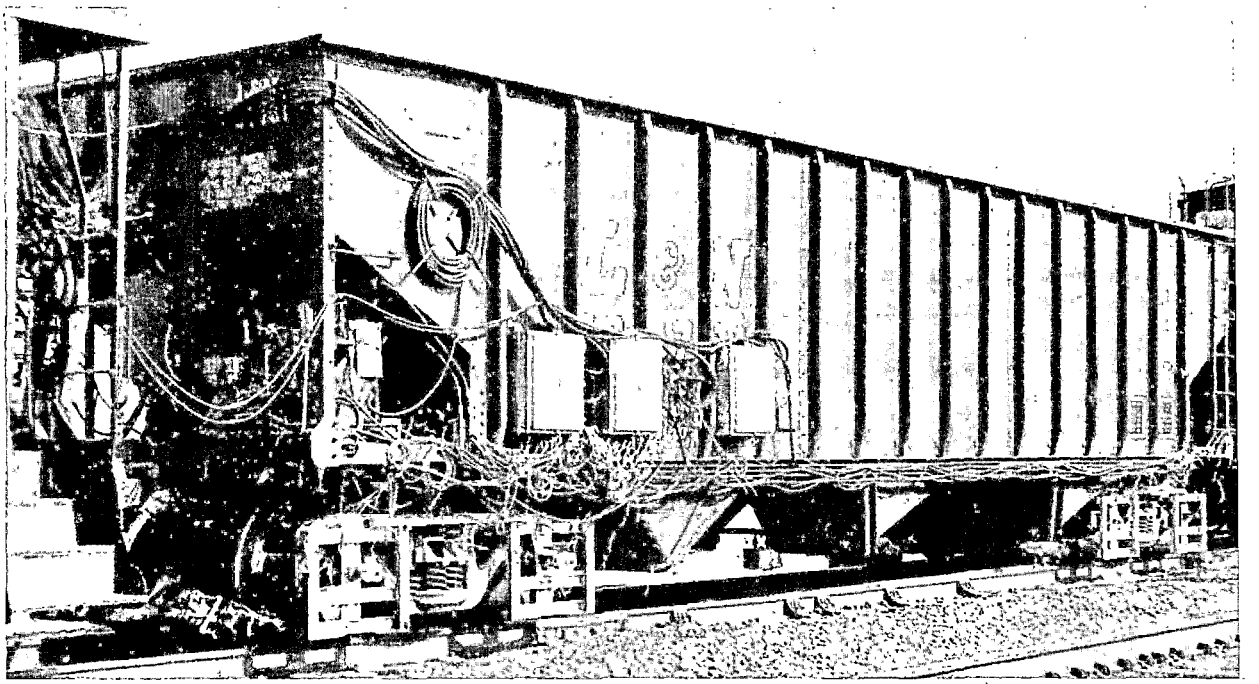

Figure 3-1. L & N Hopper Test Car

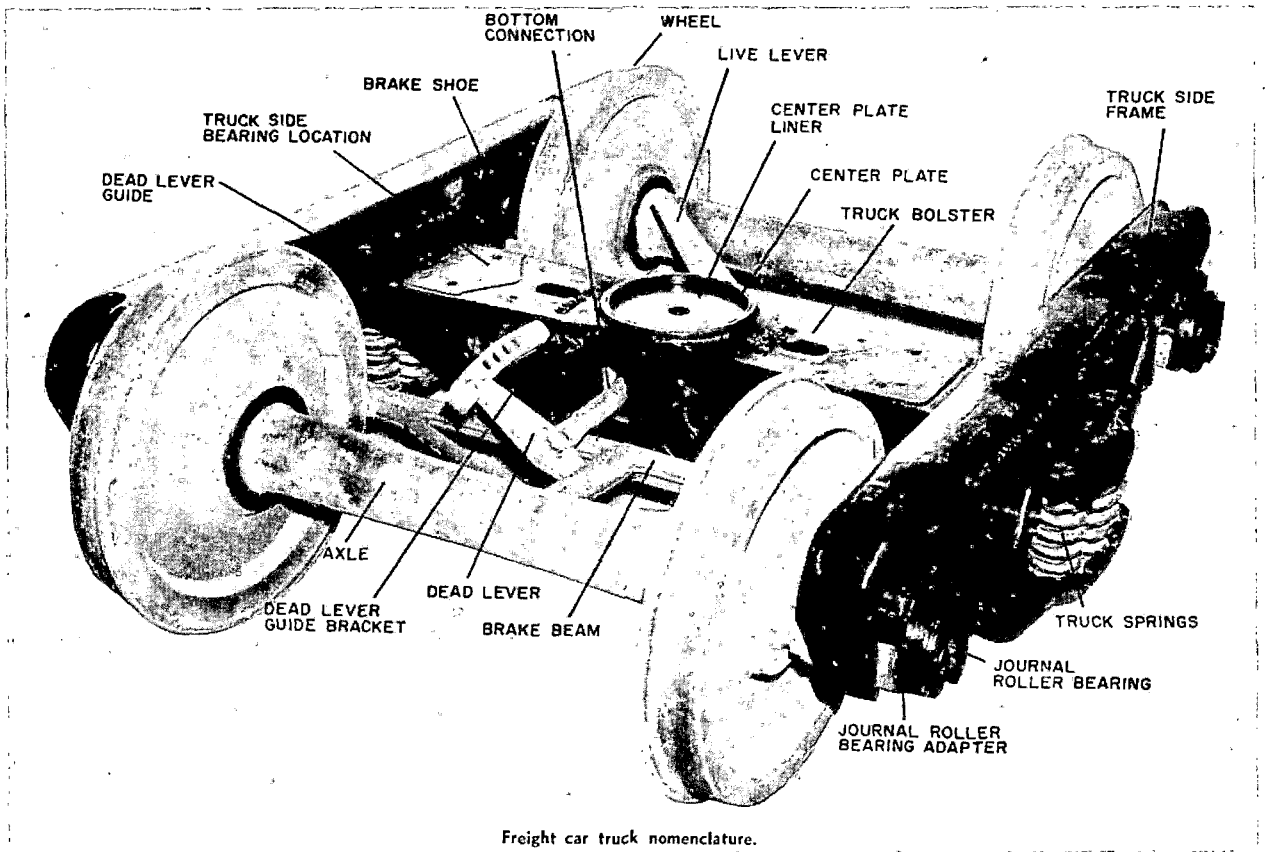

Figure 3-2. Conventional North American Freight Truck

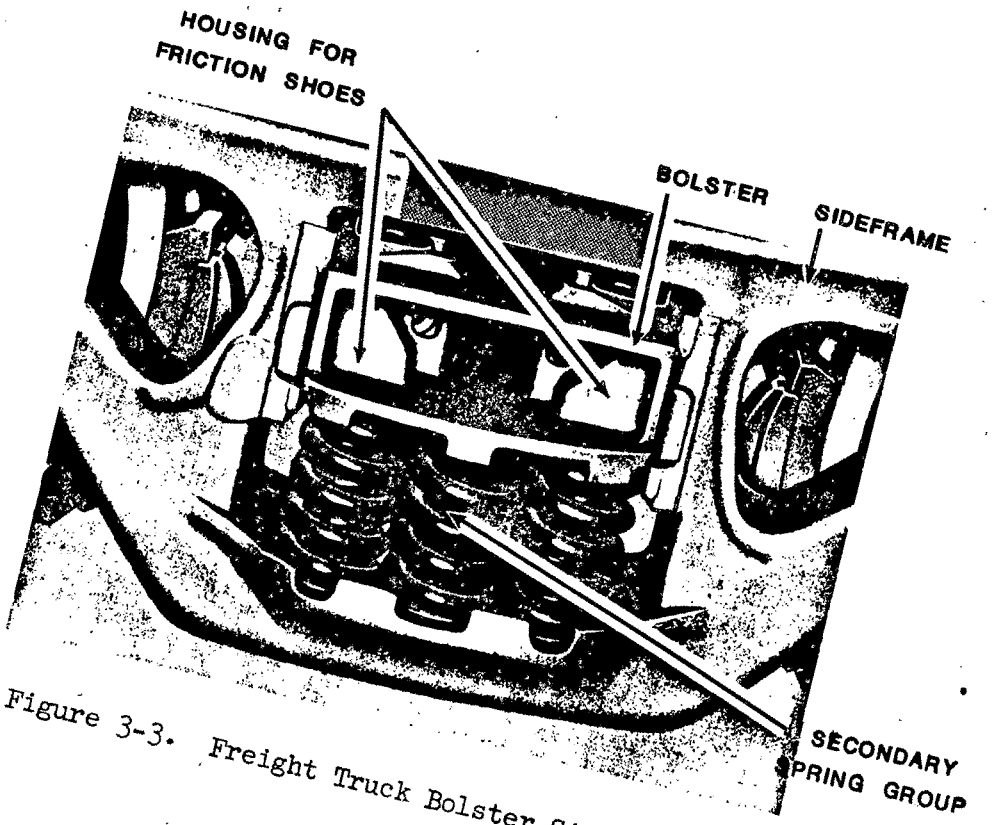

Figure 3-3. Freight Truck Bolster-Sideframe Connection

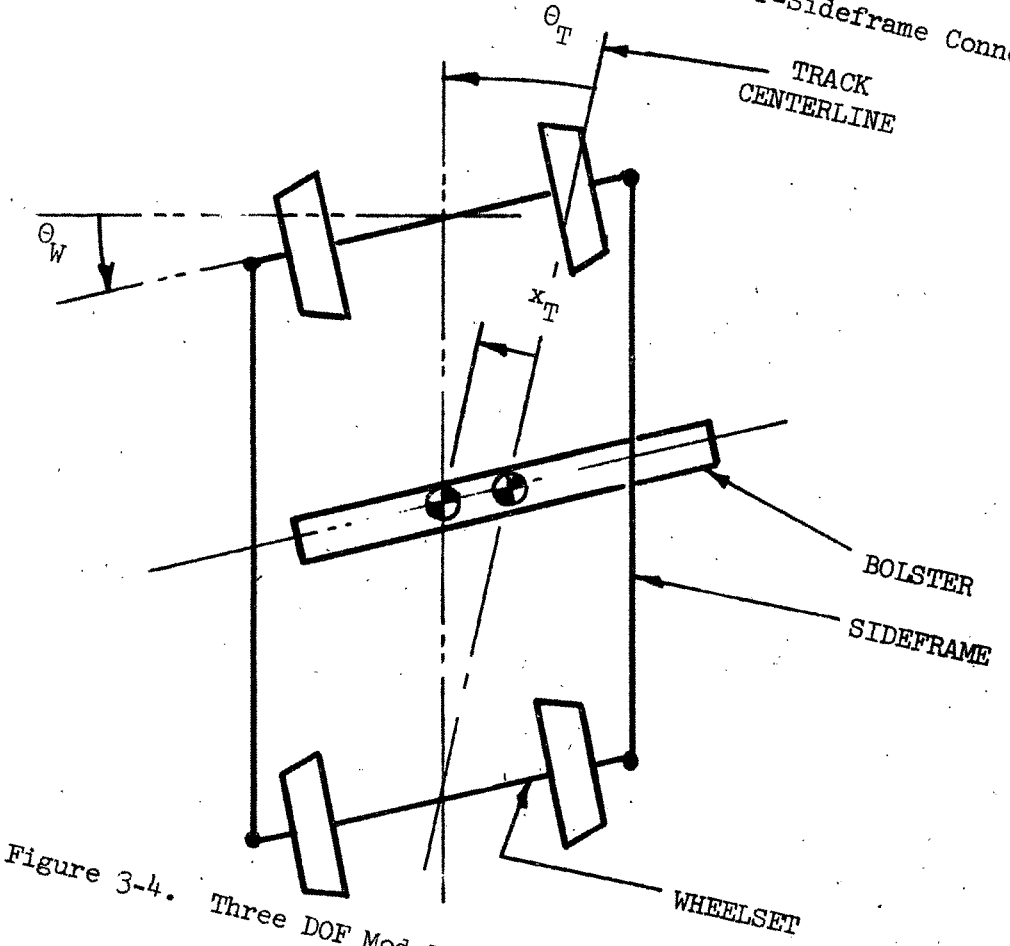

Figure 3-4. Three DOF Model for Freight Truck

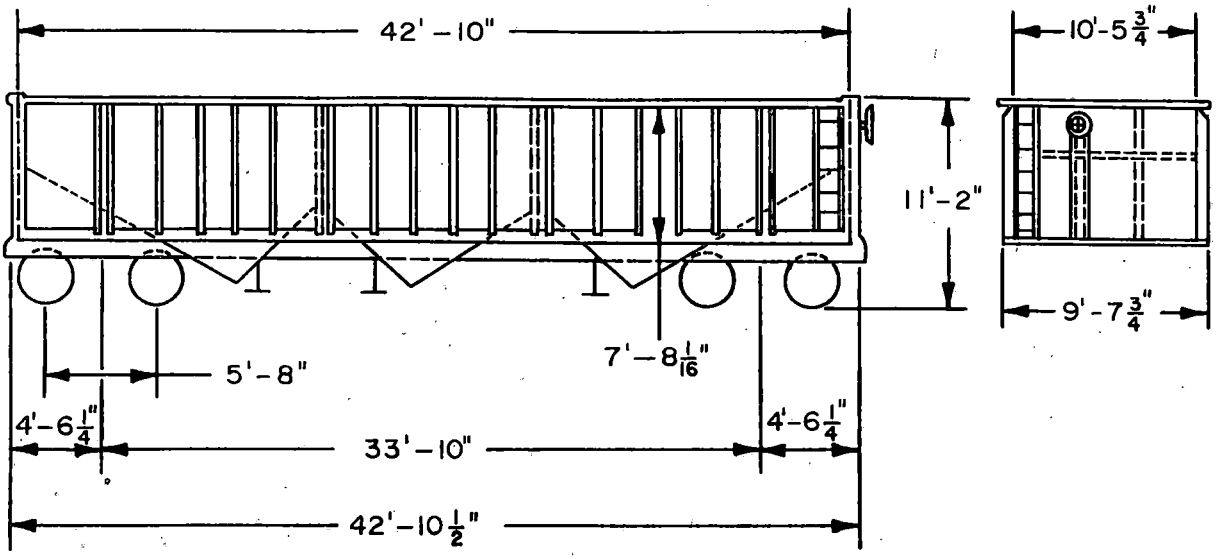

GENERAL CAR DATA

Built by P-S, Lot	9535
Built or Rebuilt	Oct, Nov, 1971
Average Light Weight, Lb.	53,200
Center of Gravity Height, Light, In.	46.8
Capacity, Cu. Ft.	2960

TRUCK DATA

No. 140 Type A-3, 70 Ton
Capacity, 6"x11", Weight, 8860 Lb, Bowl Dia., 14"
Side Frames: FS-4294
Bolster: FS-4416
Journals: Roller Bearings
Pedestal Adapter: FS-4282, E-21744
Axles: 6"x11"
Truck Springs, Per Truck:
Outer 14: D-5, Inner 12: D-5
Ride Control Springs Per Truck:
Outer 4: ASF DWG 54222

Figure 3-5. General Arrangement of Test Vehicle

Vehicle Inertia Properties

The vehicle component inertia properties were compiled from a variety of sources. The wheelset mass and inertia properties were determined by laboratory tests at the AAR Research Center [3-1]. The sideframe and bolster inertia properties were determined as part of the truck characterization tests conducted by American Steel Foundries [3-2]. The carbody inertia properties were calculated by the AAR Research Center [3-1]. These inertia properties are summarized in Table 3-2.

Vehicle Suspension Characteristics

The suspension characteristics of the test car were evaluated in tests conducted by the American Steel Foundries [3-2,3] and Martin Marietta [3-4]. The characteristics obtained for the four suspension elements of the truck, namely lateral, vertical, warp, and yaw, led Martin Marietta to propose a generic suspension element as shown in Figure 3-6. The characteristics of each of the four elements can then be interpreted in terms of the generic element.

The generic element is comprised of a parallel combination of the following sub-elements: (a) a linear spring (K_1); (b) a series combination of a linear spring (K_2) and a deadband or clearance (δ); and, (c) a series combination of a linear spring (K_F) and a Coulomb friction element (f). The characteristics of this element can represent the most general force-deflection test data.

The test data obtained by Martin Marietta together with the results obtained by ASF for the yaw breakout moment at the centerplate are presented in terms of the characteristics of the generic suspension element in Table 3-3. The tests were conducted for several values of preload on the centerplate corresponding to a range typical of light to loaded vehicles.

	Wheelset	Sideframe	Bolster	Carbody
Mass (slugs)	76.6	24.0	36.1	1102 (light) 6282 (loaded)
Principal centroidal moment of intertia about lateral axis (slug ft^2)	53.1	83.1	---	.227 x 10^6 (light) 1.050 x 10^6 (loaded)
Principal centroidal moment of inertia about vertical axis (slug ft^2)	448.5	77.6	178.6	.234 x 10^6 (light) 1.070 x 10^6 (loaded)
Principal centroidal moment of inertia about longitudinal axis (slug ft^2)	448.5	---	178.6	13,000 (light) 87,700 (loaded)

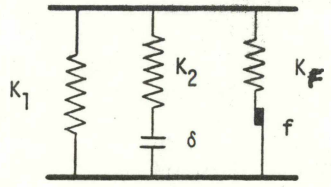

Figure 3-6. Generic Suspension Element

Table 3-3. Suspension Parameters

Linear Suspension	Preload on Centerplate, lb	K_1, LB/FT	K_2, LB/FT	K_F, LB/FT	f, LB	δ, RAD
VERTICAL (Two elements per truck)		2.5715 x 10^5		6 x 10^6	3500	
LATERAL (Two elements per truck)	*17742	6.1932 x 10^4		1.968 x 10^6	3669	
	20000	6.42 x 10^4		1.96 x 10^6	3650	
	50000	9.24 x 10^4		2.1 x 10^6	3400	
	100000	1.662 x 10^5		2.52 x 10^6	3000	
	**101140	1.6784 x 10^5		2.6 x 10^4	2960	
ROTATIONAL Suspension	Preload on Centerplate, lb	K_1, FT-LB/RAD	K_2, FT-LB/RAD	K_F, FT-LB/RAD	f,FT-LB	δ, RAD
WARP (One element per truck)	*17742	3.729 x 10^6	4.238 x 10^6	2.509 x 10^7	4687	2.18 x 10^{-3}
	20000	3.691 x 10^6	4.291 x 10^6	2.5 x 10^7	5000	
	50000	3.191 x 10^6	5.0 x 10^6	2.375 x 10^7	9166	
	100000	2.858 x 10^6	5.833 x 10^6	2.141 x 10^7	11666	
	**101140	2.48 x 10^6	5.84 x 10^6	2.10 x 10^7	11650	
YAW (One element per truck)	*17742				606	
	**101140				3450	

*unloaded vehicle
**loaded vehicle

The parameters of the generic element vary with centerplate preload for the lateral, yaw, and warp suspensions while those of the vertical element are unaffected by centerplate preload. The values for the nominally loaded and unloaded (or light) configurations are indicated in Table 3-3.

It should be emphasized that this data is our best estimate of these characteristics, but may not be accurate. Only one of the two trucks was tested at Martin Marietta. The other truck may have had very different characteristics. The centerplate friction data was taken from the ASF tests of an entirely different bolster. Friction levels are also liable to change with environmental conditions and wear. Methods to make vehicle component characterization tests during the course of a validation test should be developed to eliminate these uncertainties in furture efforts of this sort.

Truck Stiffener

In order to evaluate the effect of warp stiffness, the resistance of the frame formed by the sideframes and wheelsets to "parallelogramming" motion, a truck stiffening device was employed in one test series. This device consisted of structural steel members bolted transversely between ends of the side frames, as shown in Figure 3-7. Brackets welded to the side frames provided the attachment means for the cross members. The effect of the truck stiffener was to transform the truck to a very rigid box frame configuration.

The dimensions of the truck stiffener are given in Figure 3-8. A warp-stiffness value for the truck with the stiffner in place was not computed.

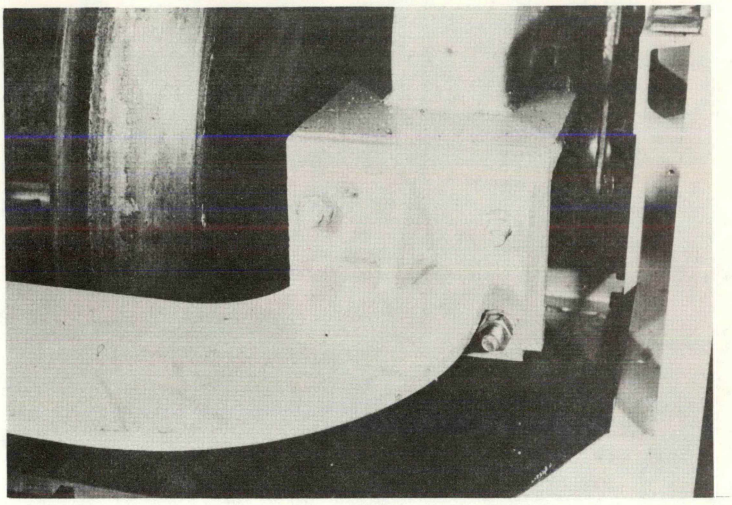

Figure 3-7. Truck Stiffener Device

Air Bag Side Bearings

The influence of variations in rotational resistance in yaw between the truck and car body bolsters was investigated by replacing the conventional side bearings with air bag units. These side bearings, pictured in Figure 3-9, allow adjustment of the bearing contact load.

The friction characteristics of the side bearing devices were determined through tests conducted by the AAR [3-5]. Friction coefficients in the range of 0.33 to 0.42 were found for the side bearing surfaces under cnditions approximating those in service. It appears that a value of friction coefficient equal to 0.40 would be reasonable.

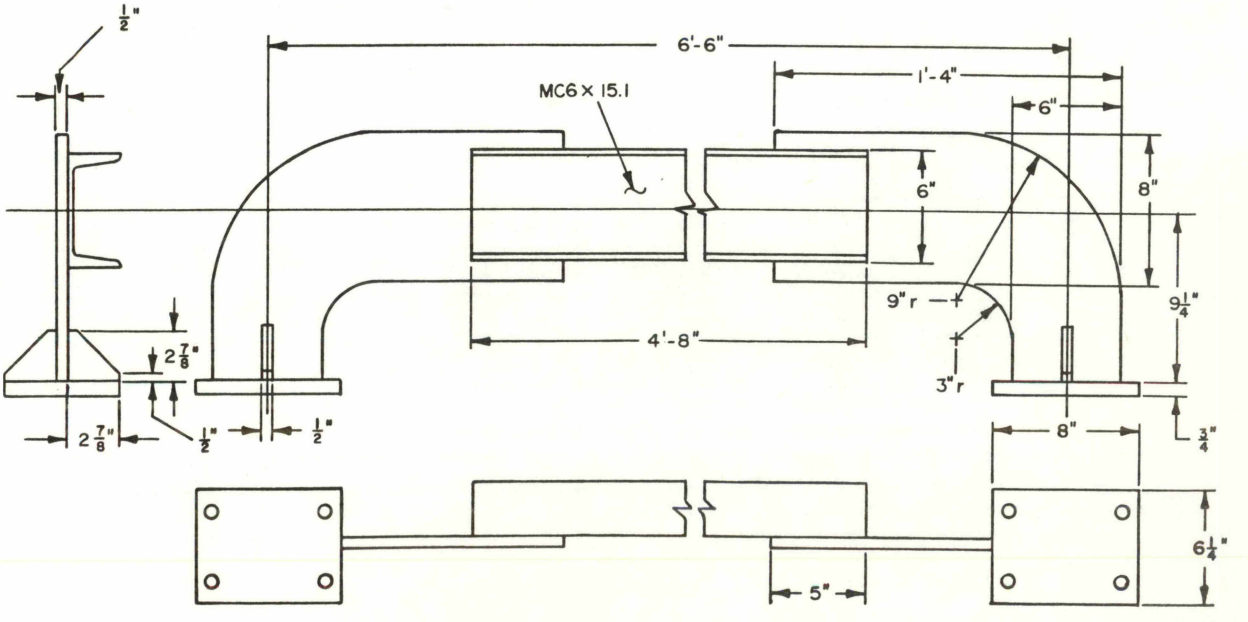

Figure 3-8. Truck Stiffener Schematic.

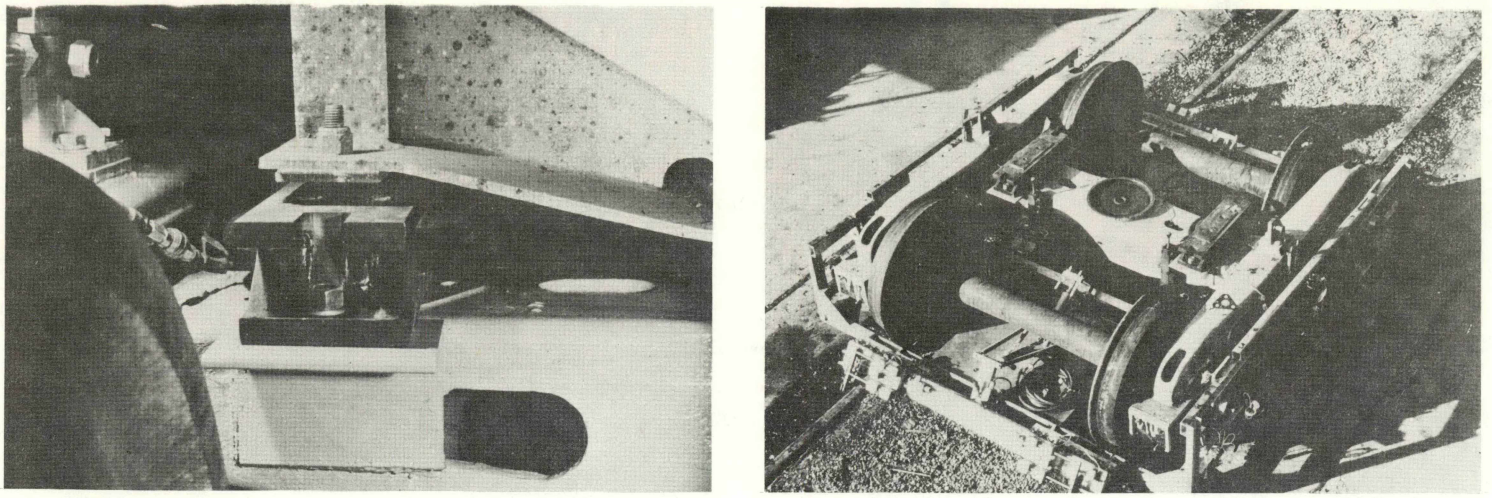

Figure 3-9. Air Bag Side Bearings

Three side bearing conditions were tested with the side bearing loads at 0, 2000 and 6000 pounds per bag. Because the air bags will unload the centerplate, the total frictional yaw resistance must account for the reduced centerplate frictional torque. The resulting torque for the three test conditions is given in Table 3-4 for the unloaded car.

Table 3-4. Truck Yaw Torques with Side Bearings

Side Bearing Force (LB)	Bolster-Car Yaw Friction Torque (FT-LB)
0	606
2000	3800
6000	10,200

Wheel Profiles

Two wheel profile conditions were chosen for the test vehicle. One of these, the AAR Standard 1/20 tapered wheel profile was selected to provide wheel-rail characteristics that should be well defined and insensitive to rail head characteristics. This profile is defined as shown in Figure 3-10. The actual wheel profiles on the 8 wheels of the test vehicle were also directly measured and compared. This wheel profile data after digitization and data smoothing is shown in Figure 3-11. Note that the wheel profiles appear nearly identical in the tread region but appear to have different flange slopes as well as different gauge clearances. These differences may be due to the fact that one set of wheels had previously seen about 5000 miles of service during "L/V" tests at the U.S. Dept. of Transportation Test Center. This set was placed under the truck tested at Martin Marietta. The other wheels came directly from the manufacturer with slightly rough as cast surfaces. This difference in wheel surface condition probably contributed to observed differences in behavior of the two trucks during the tests, as discussed later.

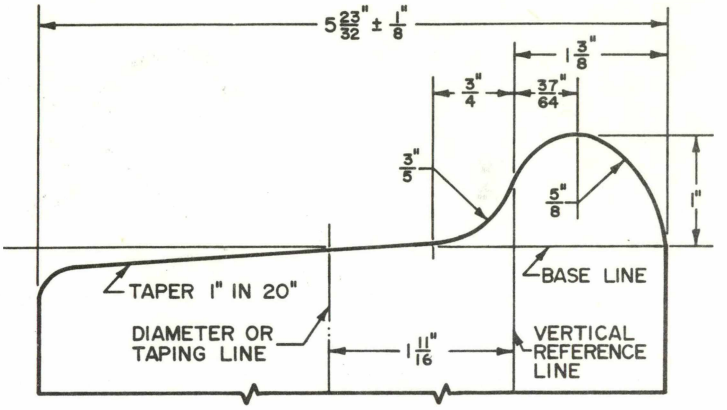

Figure 3-10. AAR Standard Tread and Flange Contour-Wide Flange Wheel.

The second wheel profile was developed by the Canadian National Railroad to approximate the worn wheel profiles found on that railroad. This profile, named the "Profile A", is defined as shown in Figure 3-12. The actual wheel profiles as measured are shown in Figure 3-13.

Wheel-Rail Geometry Characteristics

The wheel-rail geometric constraint functions such as effective conicity and gravitational stiffness strongly affect the lateral dynamic response of rail vehicles. The shapes of the wheel and rail head profiles determine these functions [1-2]. When small contact angles are assumed to prevail between the axle centerline and the wheel-rail contact plane, the geometric constraint functions that appear explicitly in the equations of motion are $(r_L - r_R)/2a$, $(\delta_L - \delta_R)/2$, and ϕ. These are, respectively, the normalized difference in rolling radii between left and right wheels, half the difference in contact angles at the left and

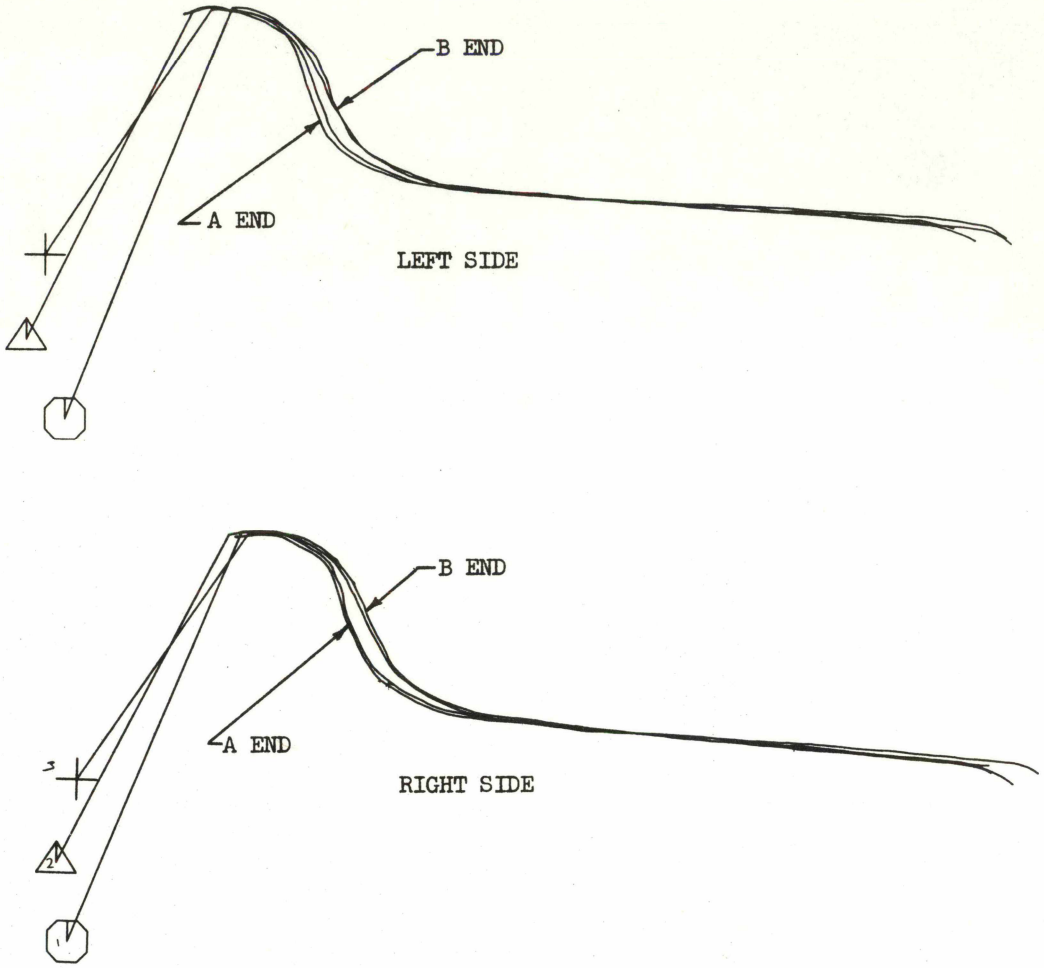

Figure 3-11. Test Vehicle Wheel Profiles, AAR Standard Profile

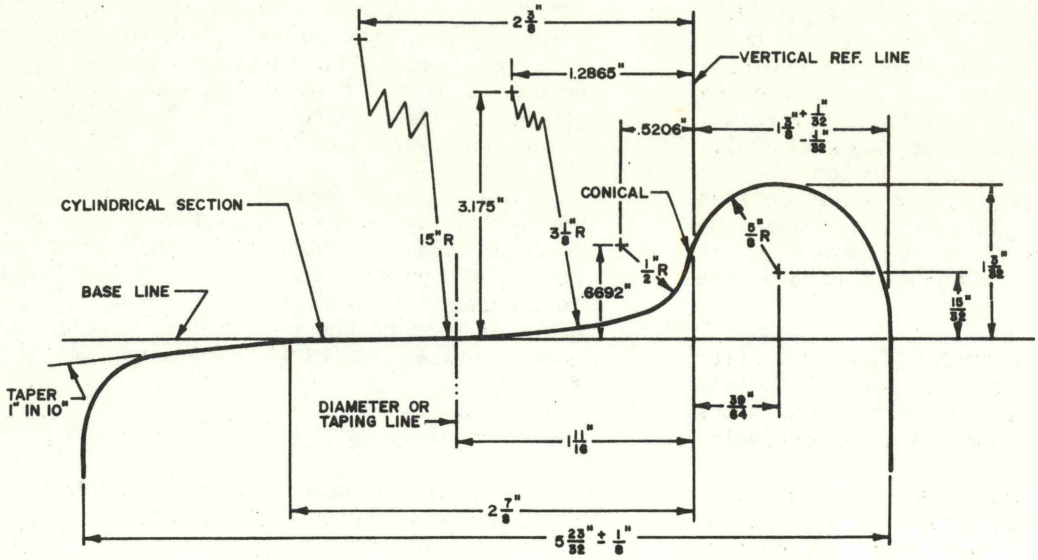

Figure 3-12. CN Profile A Wheel Contour

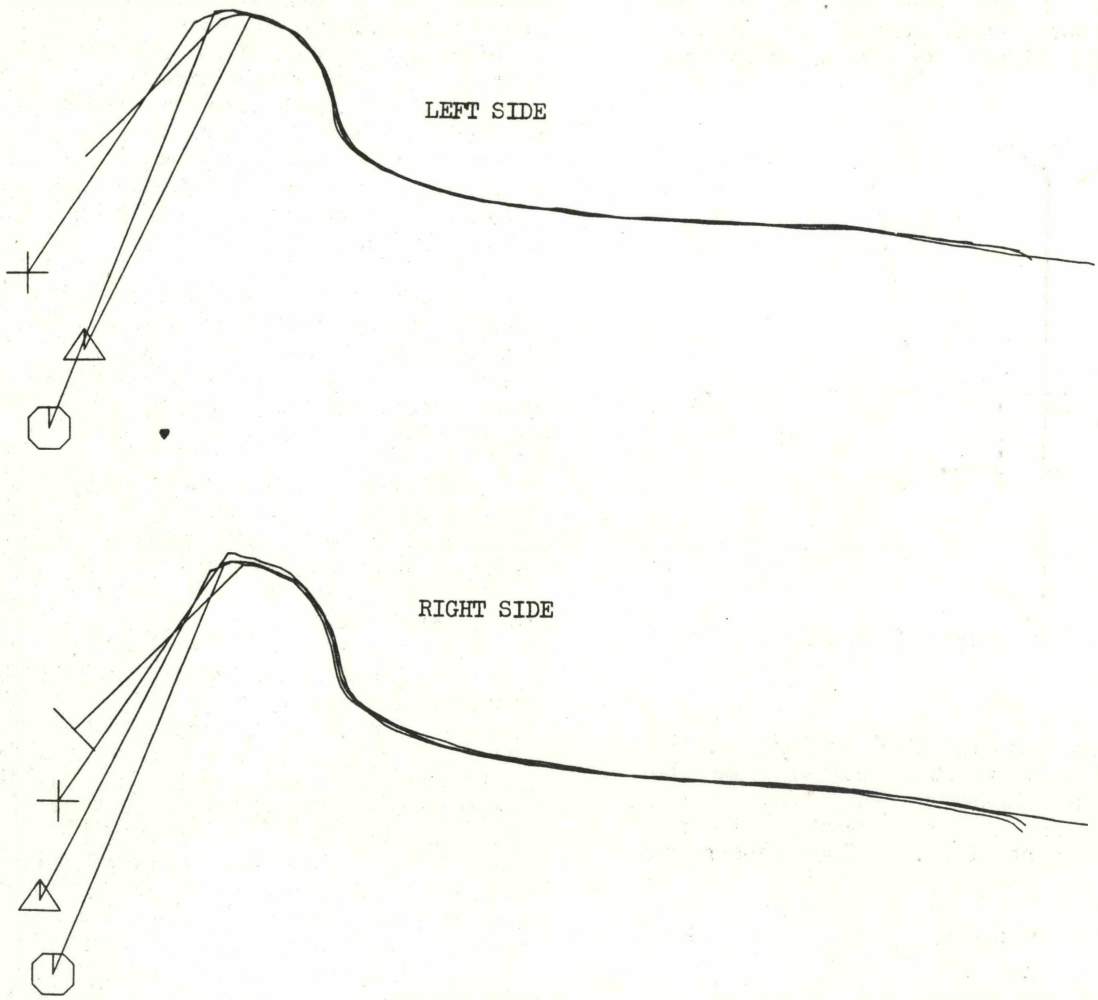

Figure 3-13. Test Vehicle Wheel Profiles, CN A

right wheels, and the wheelset roll angle with respect to the rail plane. The first of these may be linearized to yield the effective conicity while the sum of the latter two (multiplied by the axle load) gives the gravitational stiffness. If the contact angles cannot be assumed small, the rolling radii and contact angles do not appear in this form. Rather, sines and cosines of the contact angles appear in both the expressions for the lateral creep forces and in the lateral resultant of the normal forces of the rails on the wheels.

Examples of the constraint functions (for small contact angles) for the new AAR 1/20 wheels and the CNA wheels at a station on the test track are given in Figures 3-14 and 3-15, respectively.

Rail vehicle forcing due to the track results from: (1) irregularities in the lateral and vertical alignment of each rail; (2) changes in the rail head profiles and rail cant angles along the track; and, (3) differences in rail head profile and cant angle between left and right rails. Combinations of these latter two effects lead to changes in the functional form of the constraint functions and also to variations along the track of the zero offsets in the constraint functions. An example of this latter is the rolling line offset, x_{R_o}, shown in Figure 3-16.

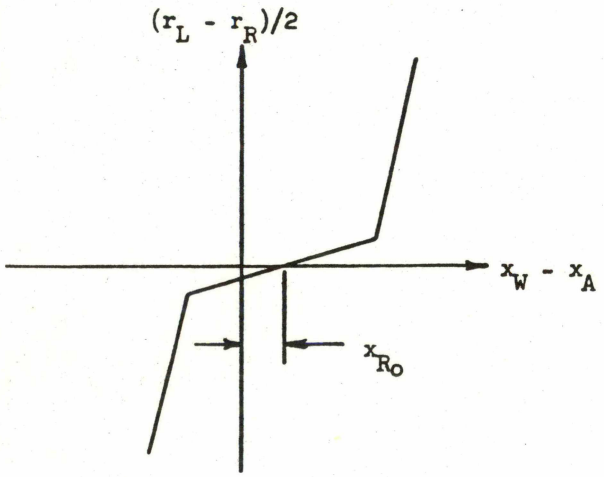

Figure 3-16. Rolling Line Offset Illustration

For irregular track, this rolling radius difference constraint function actually may be expressed as a function of $x_w - x_A$, the displacement of the wheelset relative to the disturbed track centerline. The centerline alignment is x_A.

$$(r_L - r_R)/2 = f(x_w - x_A) \qquad (3\text{-}1)$$

If the function is linearized,

$$(r_L - r_R)/2 = \lambda[(x_w - x_A) - x_{R_o}] \qquad (3\text{-}2)$$

where λ is the effective conicity. In the formulation of the equations of motion, the term $\lambda(x_A - x_{R_o})$ appears on the right hand side of the equations as a forcing term. Similar terms also appear in the equations due to offsets in the other constraint functions.

Due to the predominant influence of the wheel-rail geometry characteristics upon the lateral dynamic response through parameters in the equations as well as forcing terms, it was considered essential to measure both the wheel profiles used on the test car as well as the rail head profiles at various stations in the test sections.

Measurement of Rail Head and Wheel Profiles

The device used to measure the rail head profiles was borrowed from the German Federal Railways (DB) for this purpose. This is shown in Figure 3-17 and is similar to the device (also borrowed from the DB) that was used to measure the wheel profiles, as shown in Figure 3-18. Profiles for both left and right rails are measured and reproduced on microdot encapsulated paper by a stylus attached by a mechanical linkage to a sharp-edged follower that was traversed manually over the rail head. Immediately after set-up of the device at a station, it is "locked down" and vertical and horizontal reference lines scribed on paper newly mounted at each station. The location and orientation of these reference lines for left and right rails are known and constant and do not depend on the orientation of the pieces of paper on the device.

Checks for repeatability were made by mounting the profilometer at a station, recording the profiles, disengaging the device from the rails and then repeating the process. No discrepancies could be detected in the two sets of profiles.

Rail head profiles were also measured at a station as close as possible to one of the axles of a loaded 80-ton hopper car. No differences could be detected between these profiles and the profiles obtained at the same station when the rails were unloaded.

Rail head profiles were recorded at 159 stations in the various test zones. These included two sites on the tangent test section (MP 208.5 west for 320 feet - 65 stations; MP 206.5 east for 320 feet - 25 stations), two curves (the 6 and 1 degree curves - about 800 feet along each - 23 and 15 stations respectively), and the passing track (about 450 feet - 31 stations). As will be discussed later, deficiencies in the test conduct procedure rendered useless the dynamic response data taken during curve negotiation and traversal of the passing track. Consequently, summary data for the wheel-rail geometry characteristics in the curves and on the passing track are included in Appendix A but not discussed here.

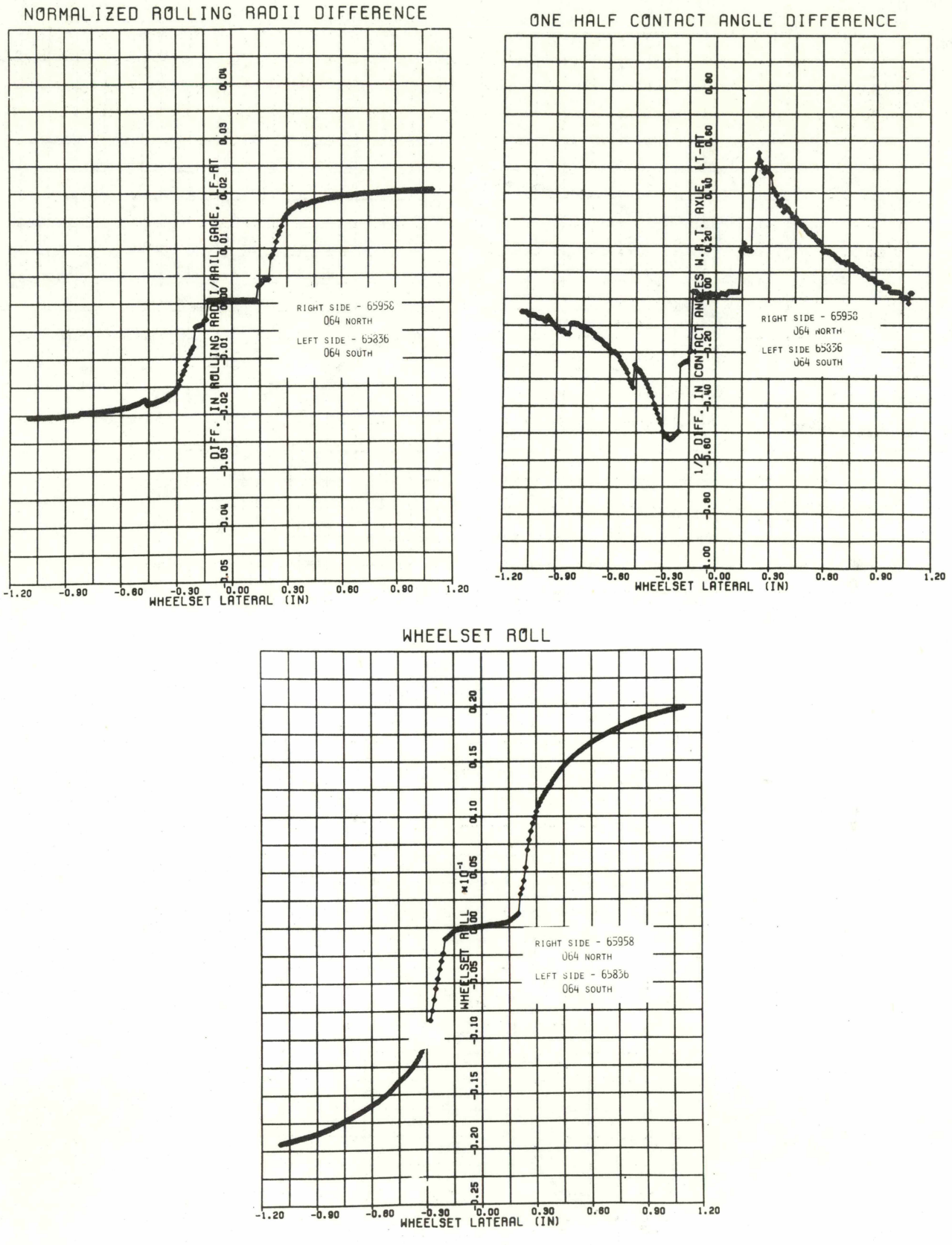

Figure 3-14. Constraint Functions for AAR Wheels

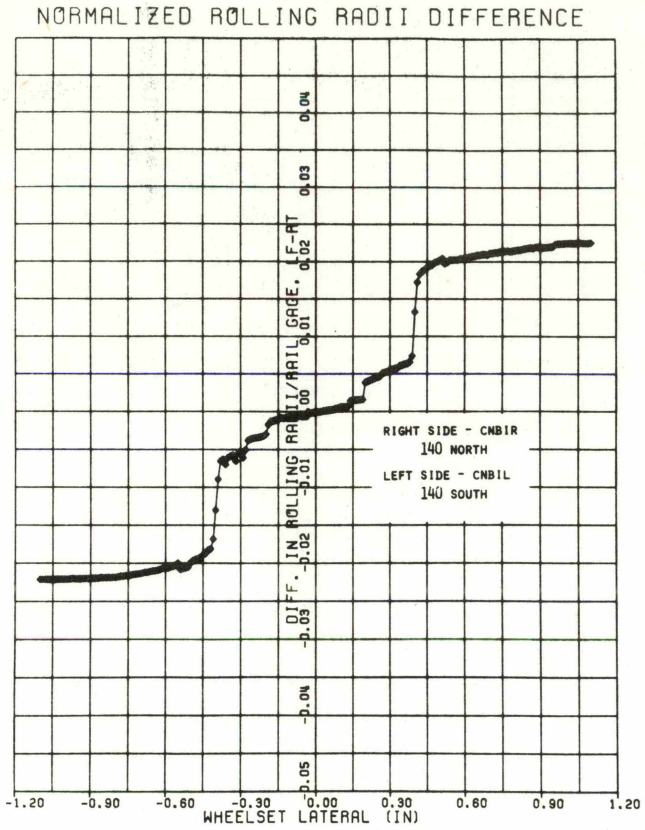

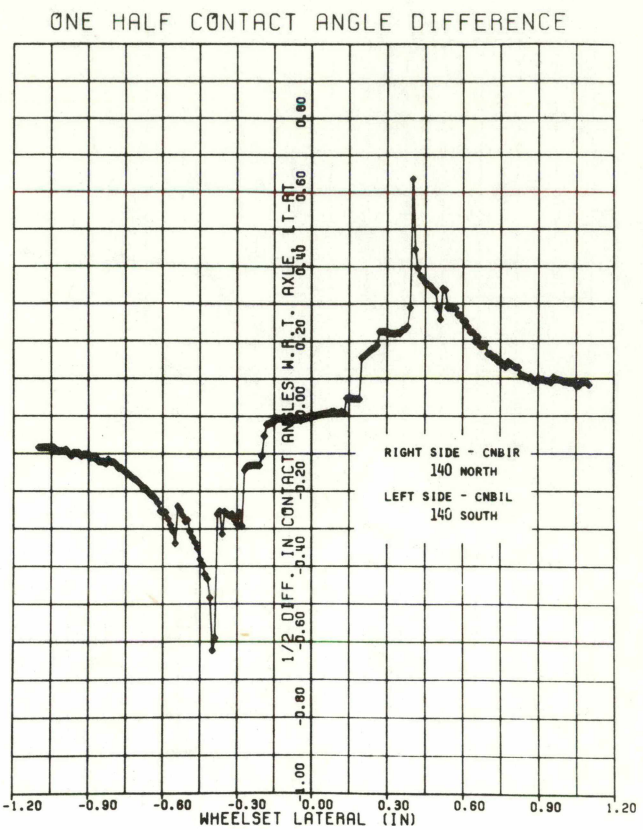

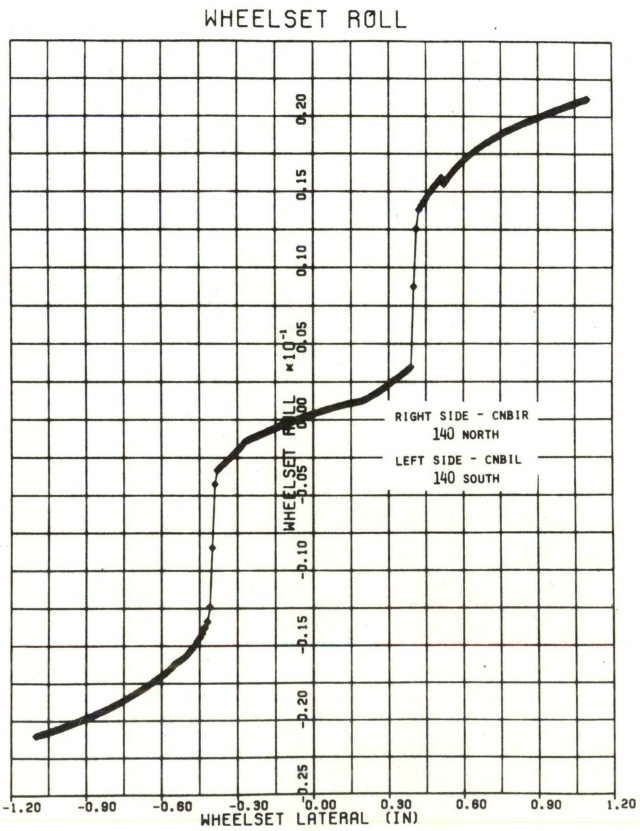

Figure 3-15. Constraint Functions for CN A Wheels

a. Rail Profilometer on Track

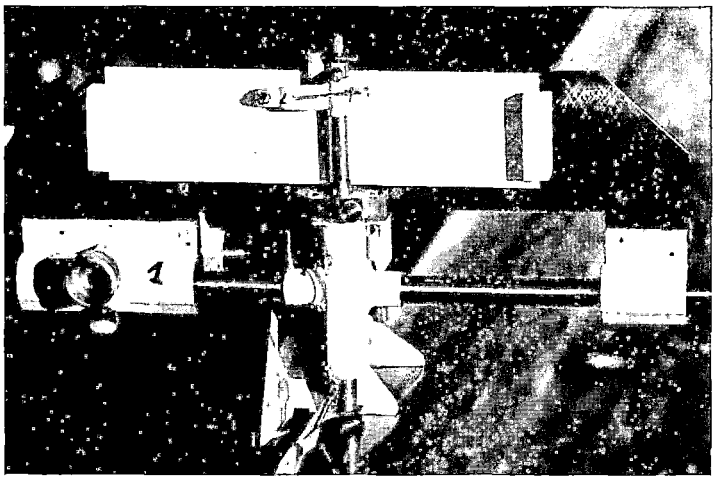

b. Close-up View

Figure 3-17. DB Rail Profile Measuring Device

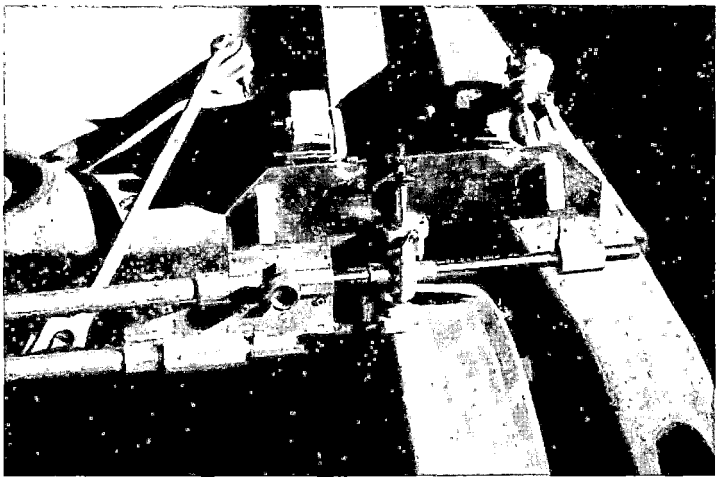

a. Wheel Profilometer on Wheelset

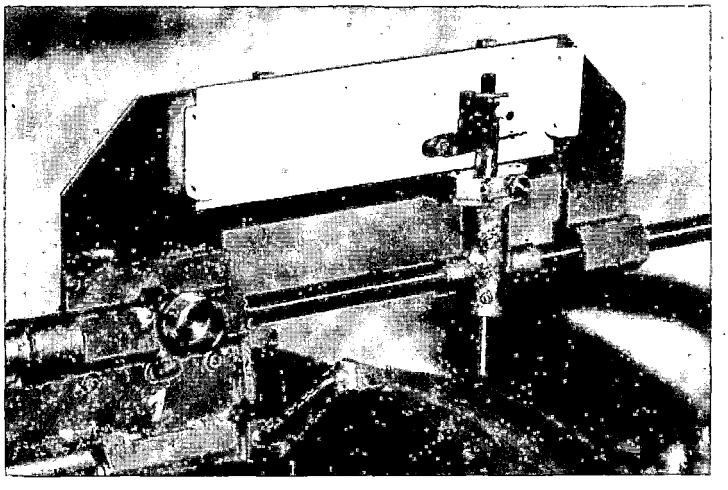

b. Close-up View

Figure 3-18. DB Wheel Profile Measuring Device

As discussed previously, the wheel profiles were measured for all axles of the test car with AAR 1/20 wheels and with the CNA wheels. This was done using the device (shown in Figure 3-18) borrowed from the DB. The operation of this device and the subsequent processing of the profile data obtained were essentially identical to the techniques used in measuring and processing the rail head profile data.

Processing and Analysis of Wheel-Rail Geometry

The rail profile data required extensive processing before it could be used in the wheel-rail geometry analysis. The individual profile tracings were photographically enlarged; the enlargements were digitized at the U.S. DOT Transportation Test Center; the digitized data was recorded on magnetic tape; the profile data was resorted, labeled, and edited; and finally the data was again recorded on tape. Details of this process are given in Appendix A.

The data from the above process was used as input to the wheel-rail geometry computer program [1-3]. The output of this program, in the form of numerical geometric constraint functions for both the AAR 1/20 wheels and CNA wheels at each rail station was then stored for subsequent analysis.

Data analysis of these results was carried out to compute the offsets and slopes of the constraint functions for the various track sections. Details of this analysis, and summary tables of the results are given in Appendix A.

A summary of these results for one tangent track site is shown in Table 3-5. For the AAR 1/20 wheels, the values given represent the entire region of flange contact, but values over relative wheelset-rail motion of ± 0.15 inch and ± 0.25 inch are given for the CNA wheels. These tables describe the parameters λ, x_{R_o}, Δ, x_{δ_o}, Γ and x_{ϕ_o} in the following equations:

Table 3-5. Linear Estimates of Wheel-Rail Geometric Constraint Functions

(a) SECTION 0: Tangent Track; MP 208.5 West for 320 ft.		WHEEL PROFILE		
		AAR 1/20	CNA (±0.15 in)	CNA (±0.25 in)
GAUGE	MEAN (IN)	56.464	56.462	56.462
	STD. DEV. (IN)	0.050 (64:64)	0.052 (64:64)	0.052 (64:64)
	90% CONF. LIM.	(56.453, 56.474)	(56.451, 56.473)	(56.451, 56.473)
EFFECTIVE CONICITY, λ	MEAN	0.0291	0.3463	0.4154
	STD. DEV.	0.0314 (61:64)	0.1006 (64:64)	0.0586 (64:64)
	90% CONF. LIM.	(0.0224, 0.0358)	(0.3253, 0.3673)	(0.4032, 0.4276)
ROLLING LINE OFFSET, x_{R_o}	MEAN (IN)	-0.2723	-0.0376	-0.0348
	STD. DEV. (IN)	1.4630 (60:64)	0.0281 (63:64)	0.0215 (64:64)
	90% CONF. LIM.	(-0.5877, 0.0431)	(-0.0435, -0.0317)	(-0.0393, -0.0303)
CONTACT ANGLE DIFFERENCE, Δ	MEAN	-0.8811	9.3899	13.5453
	STD. DEV.	3.3621	4.1979 (64:64)	2.7055 (64:64)
	90% CONF. LIM.	(-1.5829, -0.1793)	(8.5136, 10.2662)	(12.9805, 14.1101)
CONTACT ANGLE OFFSET, x_{δ_o}	MEAN (IN)	-0.0071	-0.0060	-0.0196
	STD. DEV. (IN)	0.2688 (60:64)	0.0327 (63:64)	0.0189 (64:64)
	90% CONF. LIM.	(-0.0651, +0.0509)	(-0.0129, 0.0009)	(-0.0235, -0.0157)
ROLL ANGLE, Γ	MEAN	0.0623	0.1552	0.1619
	STD. DEV.	0.0119 (64:64)	0.0104 (63:64)	0.0123 (63:64)
	90% CONF. LIM.	(0.0598, 0.0648)	(0.1530, 0.1574)	(0.1593, 0.1645)
ROLL ANGLE OFFSET, x_{ϕ_o}	MEAN	-0.0848	-0.0644	-0.0535
	STD. DEV. (IN)	0.0666 (64:64)	0.0390 (64:64)	0.0339 (64:64)
	90% CONF. LIM.	(-0.0987, -0.0709)	(-0.0725, -0.0563)	(-0.0606, -0.0464)
AVERAGE CONTACT ANGLE, δ_o	MEAN (RAD)	0.0647	0.1371	0.1519
	STD. DEV. (RAD)	0.0101 (64:64)	0.0125 (64:64)	0.0132 (64:64)
	90% CONF. LIM.	(0.0626, 0.0668)	(0.1345, 0.1397)	(0.1491, 0.1547)

$$(r_L - r_R)/2 = \lambda(x_w - x_{R_o}) - \lambda x_A \qquad (3\text{-}3)$$

$$(\delta_L - \delta_R)/2 = \Delta(x_w - x_{\delta_o})/a - \Delta x_A/a \qquad (3\text{-}4)$$

$$\phi_w = \Gamma(x_w - x_{\phi_o})/a - \Gamma x_A/a \qquad (3\text{-}5)$$

$$(\delta_L + \delta_R)/2 = \delta_o \qquad (3\text{-}6)$$

The table entries are explained more fully in the Appendix A.

Ideally, one would like to construct power spectra for the offset terms so that they, together with the spectrum of the track lateral alignment, could be used to calculate spectra of the various vehicle response variables. However, rail head profiles would have to be measured at many more stations (and subsequently processed and analysed) to have sufficient data to construct these spectra. To the authors' knowledge, only one attempt to construct spectra for offsets has been made [3-6].

In analyzing the data from this process, the first thing to be noted is that the system parameters λ, Δ, and Γ vary appreciably along the track. This tendency is most pronounced for the AAR 1/20 profile. This fact is surprising since we expected from previous experience that the characteristics of the constant taper 1/20 profile would be insensitive to variations in the rail head profiles from station to station. In particular, we expected that the mean values of λ, Γ and Δ would be very close to 0.05, 0.05, and 0, respectively, and that the limits on the 90% confidence interval would be very tight. We examined plots of the constraint functions at several stations on the track for the 1/20 wheels and found that the functions $(r_L - r_R)/2a$ and $(\delta_L - \delta_R)/2$ were very irregular in the tread contact region. This was contrary to previous experience [1-3]. Upon further investigation, we found that the digitized wheel and rail profiles were very irregular or "bumpy" whereas the original traces of the profiles obtained directly from the DB profile machines were extremely smooth. The "bumpiness" introduced in the digitization process caused the calculated contact points to jump around somewhat erratically over the wheel and rail profiles, thus leading to "bumpy" functions for $(r_L - r_R)/2a$ and $(\delta_L - \delta_R)/2$. Only the ϕ_w function was relatively insensitive to this induced error. In

addition to broadening the confidence intervals for λ, Δ, and Γ, this digitization error caused poor estimates for the offset terms, particularly x_{R_o}. This is unfortunate as x_{R_o} together with x_A is probably the most important input into the system.

For the curved CNA profiles, there was also a considerable amount of "bumpiness" introduced during the profile digitization process. However, the curved CNA profile is not nearly as sensitive to this type of error as is the constant taper 1/20 profile. This relative insensitivity may be seen by comparing the tighter 90% confidence intervals of the CNA profile to those of the 1/20 profile for both the system parameters λ, Δ, and Γ and the offsets x_{R_o}, x_{δ_o}, and x_{ϕ_o}.

Due to the errors introduced in the profile digitization process, the results presented in Appendix A for the AAR 1/20 profile are probably unreliable. However, it is felt that the data presented for the CNA profile is reliable due to the relative insensitivity of the CNA profile to this source of error.

As expected, the values for λ, Δ, and Γ are larger for the CNA profile with the straight line fit over $\pm$ 0.25 in. as compared with $\pm$ 0.15 in. This is because for the CNA profile the corresponding constraint function values increase rapidly as flange contact is approached. The somewhat wider gauge of track Section A as compared with 0 also gives lower values for λ, Δ, and Γ on Section A. This is due to the fact that for wide gauge the constraint function values are lower than for a narrower gauge at a given value of x_w.

The 90% confidence intervals for the offset terms of the CNA profile are about the same for either $\pm$ 0.15 in. or $\pm$ 0.25 in. straight line fits. They are also all rather tight and close to zero as expected. However, with the sole exception of x_{δ_o} for the $\pm$ 0.15 in. straight line fit on Section 0, none of the confidence intervals include zero. This might indicate the presence of a constant bias due to slightly unequal wheel radii or some other cause.

It should be noted that in using the DB wheel profiler, a line connecting the top of the wheel flanges (the "horizontal" reference line) is assumed to be parallel to the axle centerline. This is the only apparent drawback of this profiler. Ideally, the "horizontal" reference of the profiler should be exactly parallel to the axle centerline. As it is now configured, any wheel mismatch due to different radii to the tops of the flanges would not be detected by the profiler. For the wheel profiles measured in this project, the radii were measured by other means and found to be nominally identical for each wheelset.

It is interesting to note that the values of the standard deviations for x_{R_o}, x_{δ_o}, and x_{ϕ_o} for the CNA profile on Sections A and 0 are small, on the order of 0.02 to 0.04 inches. Our best estimate of the standard deviation of the centerline alignment for the entire length of the tangent test section that includes Sections A and 0 (MP 206.8 to MP 208.5 on the UP main line east of Barstow, CA) is 0.095 inches for the spatial frequency range, $f > 0.002$ cyc/ft. Previous work by Gilchrist [3-7] for the RD6 wheel gave values for rolling line offset and conicity at three test sites. Excerpts of Gilchrist's results are given in Tables 3-6 and 3-7. Note that the standard deviation of the rolling line offset is the same order as the rms centerline alignment. Gilchrist's values (Table 3-7) for the standard deviation of the rolling line offset are somewhat larger than ours for the CNA profile. However, they are of the same order as ours and should be expected to be different because of the strong dependence on the particular wheel profile. It would be expected from Gilchrist's results, and to a somewhat lesser extent from ours, that rolling line offset would act as a strong input together with centerline alignment to the lateral dynamic response.

Gilchrist's results (Table 3-7) for conicity are rather interesting as at two sites (Etwall A and Widmerpool B) the ratio of the standard deviation to the mean value is about the same as we obtained (Table 3-8) for the CNA profile with a $\pm$ 0.25 inch straight line fit. At site Etwall B the ratio was about the same as we obtained for a $\pm$ 0.15 inch straight line fit.

One of the major impressions to be gained from these results for conicity (as well as from the results for Δ and Γ) is that conicity can be a function of amplitude of wheelset motion (a nonlinear effect) and also change as the wheelset travels along the track (a phenomenon leading to parametric excitation). These results also indicate that to estimate the system parameters λ, Δ and Γ for a wheel profile, it is necessary to evaluate them at several stations along the track and then calculate the sample averages and standard deviations. In this way, confidence intervals for the true mean values of the parameters may be established.

Roadbed Characteristics

Since the roadbed is the primary source of disturbances to a vehicle traveling over it, it is important to know its characteristics. This section of the report describes efforts to characterize the roadbed used for the field tests.

Tangent-track test runs were conducted on a section of the Union Pacific mainline between Las Vegas, Nevada and Los Angeles, California. The actual test section was between mileposts 206.8 and 208.5 near Barstow, California. Continuous welded rail is in place in the test zone.

The roadbed characteristics were first measured in August, 1975 using the Union Pacific's Plasser-American Corp model EM-80 track evaluation car. Track measurements were recorded on magnetic tape in FM analog format. The signals were later digitized and provided to ASU by the AAR.

Table 3-6. Summary of Rolling Line Offset Results With RD6 Wheel (from [3-7]).

Site	No. of Stations	Rolling Line Offset, in		RMS Centerline Alignment, in	
		Mean	Std. Deviation	f>0.01 cyc/ft	f>0.02 cyc/ft
Etwall A	92	+ 0.033	0.086	0.064	0.038
Widmerpool A	23	- 0.034	0.095	0.051	0.033
Widmerpool B	44	- 0.015	0.040	0.058	0.034

Table 3-7. Summary of Conicity Results with RD6 Wheel (from [3-7]).

Site	No. of Stations	Mean Value	Std. Deviation	% Std. Deviation/Mean
Etwall A	92	0.145	0.018	13%
Widmerpool A	23	0.127	0.042	33%
Widmerpool B	44	0.169	0.026	16%

Table 3-8. Summary of Conicity Results with CNA Wheel Profile

Section	No. of Stations	Mean Value		Standard Deviation		% Std. Deviation/Mean	
		± 0.15 in	± 0.25 in	± 0.15 in	± 0.25 in	± 0.15 in	± 0.25 in
0	64	+ 0.3463	+ 0.4154	+ 0.1006	+ 0.0586	29%	14%
A	24	+ 0.3116	+ 0.3012	+ 0.0959	+ 0.0403	31%	13%

Two attempts to measure the roadbed characteristics during the field tests in late 1976 and early 1977 were unsuccessful because the measurement cars were damaged in accidents.

In November of 1977 a final track geometry evaluation was made by ENSCO, Inc., using the FRA T-3 track geometry car. ENSCO evaluated results of the measurements and reported results in reference [3-8]. A digital magnetic tape of the ENSCO data was furnished to ASU for analysis. With some slight differences due probably to different analysis techniques, our analysis results and ENSCO's were essentially the same. These results are contained in reference [3-8] and will therefore not be included here. This data is incomplete for our purposes, however, since we need alignment data, which is not measured by the T-3 car.

We analyzed the data from the UP EM-80 car to obtain the results shown in Figures 3-19 and 3-20. These figures show the shapes of the PSD and probability density functions of the track superelevation and alignment. The alignment PSD shown is adjusted to compensate for errors believed to exist in the original recorded data. The standard deviation of the raw alignment data was 0.0129 inch, a value we think is too low for several reasons. We expect the alignment standard deviation to be about the same value as the gauge and surface profile standard deviations, which were 0.092 and 0.112 inches. In addition we believe it is unreasonable to expect alignment as good as the above would indicate even on the best of track. In an attempt to resolve this problem, the AAR redigitized the original data and furnished it to ASU for analysis. We analyzed the data again in early 1978 and repeated the results found earlier.

We attempted three methods to correct this discrepancy. In the first we plotted the track parameters as functions of time. One such plot, of the left alignment measurement, is shown in Figure 3-21. The steady state offset in left alignment in the 6-degree curve was found to be 0.88 inch using the calibration values furnished with the digital tape recording. We then calculated the midspan deviation for a 62-foot chord on a 6-degree curve and found the result to be 6.04 inch. The UP's track geometry car had used a 62-foot chordal measurement, so we discovered a gain difference of 6.04/0.88 or 6.86. We then adjusted the standard-deviation values by this factor of 6.86 so that the centerline alignment became 0.088 inch. The 0.088-inch value is an uncompensated value meaning that no

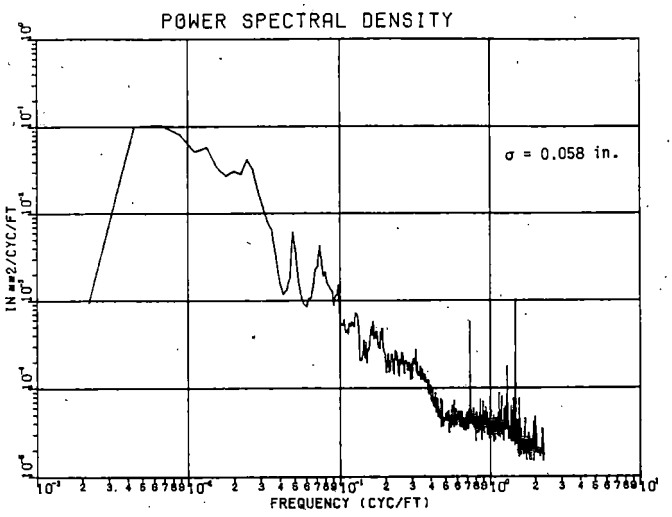

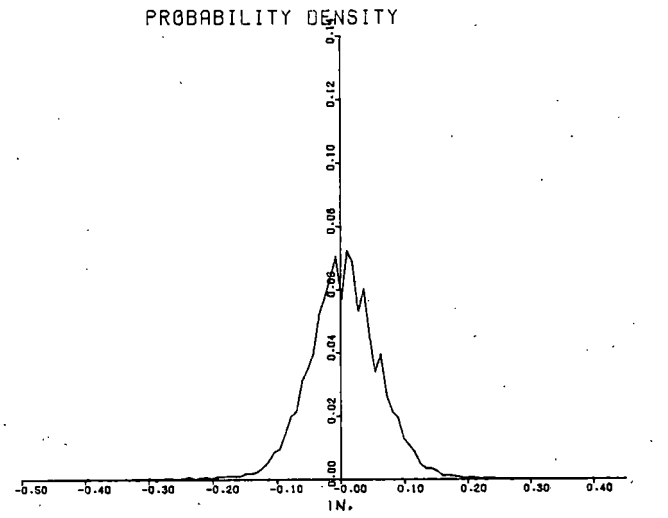

Figure 3-19. Superelevation PSD and Probability Density

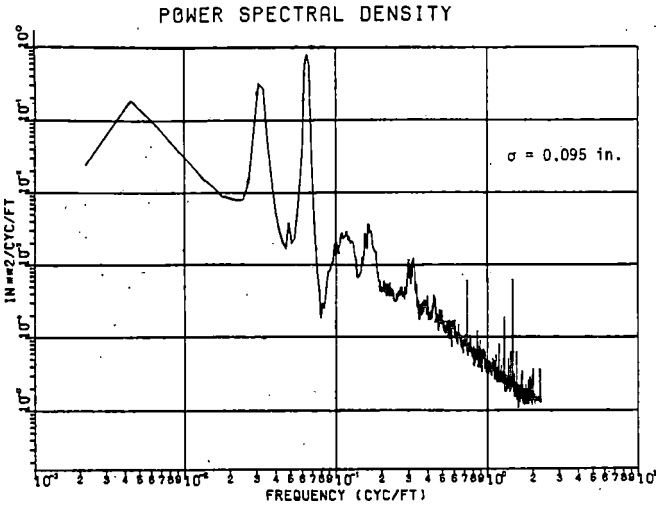

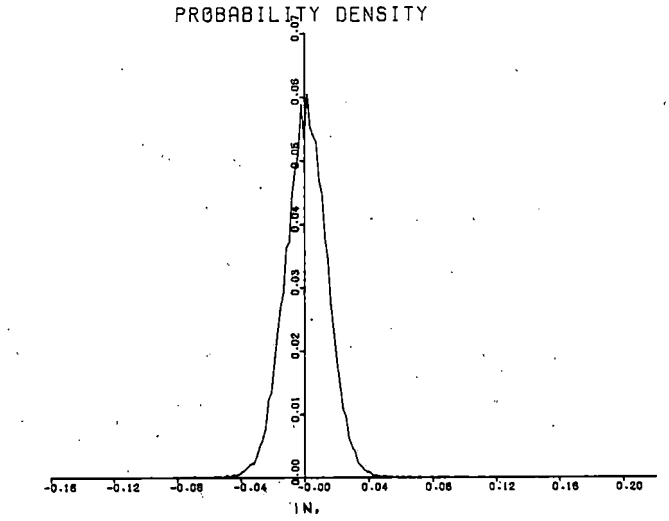

Figure 3-20. Alignment PSD and Probability Density

correction has been applied to account for errors caused by the chordal offset measuring technique. By compensating for this measuring technique [1-11], we have found that the standard deviation increases by about 1.8 times, so that the compensated value corresponding to 0.088 inch would be 0.158 inch.

In another attempt to find the alignment value, we computed a variable representing track gauge by taking the difference between left and right alignment data from the EM-80 tests. We found the standard deviation of our computed gauge data to be 0.023, just one-fourth of the 0.092 value we obtained from the measured data. We then compensated for the chordal offset measurement and multiplied by 4 to obtain the PSD shown in Figure 3-20. We then integrated the PSD omitting values associated with the peaks near 3.5 and 7.0 Hz to obtain a standard deviation of 0.095. The 3.5 and 7.0 Hz peaks were not included because they are introduced as a result of the compensation process, and they do not therefore represent actual track data.

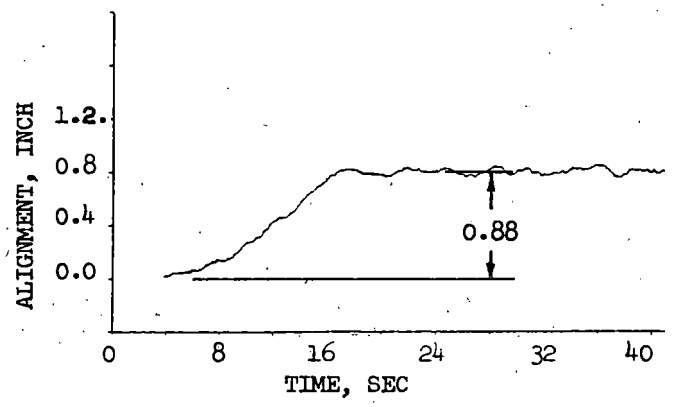

Figure 3-21. Alignment in 6-Degree Curve

We attempted another method to obtain the centerline alignment standard deviation, this time using ENSCO's data. It can be shown mathematically that curvature is very nearly equal to the second derivative of alignment when the curvature is small. So we twice integrated

the curvature data we obtained from the ENSCO tape and obtained a centerline alignment standard deviation estimate. Using this method we obtained a value of standard deviation that was significantly lower than the estimate discussed above. This analysis showed the dependency of alignment signal on spatial frequency to be -60 dB/decade instead of the -40 dB/decade shown in the PSD's from the UP data. So while this method of analysis appears to be valid theoretically, there are obviously some practical problems that need to be investigated further.

We should summarize this effort by observing that we don't really know what the track alignment was at the time of the tests. Figure 3-20 with a standard deviation of 0.095 inch is our best estimate, and we believe the order of magnitude is correct.

Three parameters provide the primary lateral disturbing forces to a rail vehicle. These are alignment, crosslevel, and rolling-line offset. Rolling-line offset is more a wheel-rail geometry property than a roadbed property and is not discussed here. The remaining two, alignment and crosslevel, are used as the forcing functions in the theoretical analysis discussed later in this report. For analysis purposes it is convenient, although not necessary, to assume that alignment and crosslevel are statistically independent, that is, not related to each other. To test the validity of making this assumption we performed a cross-spectral-density analysis of the two parameters. The coherence function between alignment and crosslevel is shown in Figure 3-22.

Coherence is a frequency-dependent function that varies from zero to one in value. A value of one indicates that the two variables being analyzed are statistically dependent; a value of zero indicates they are statistically independent. In this case the value of the coherence function is sufficiently low, with an average value near 0.05, to warrant the assumption of statistical independence between alignment and crosslevel.

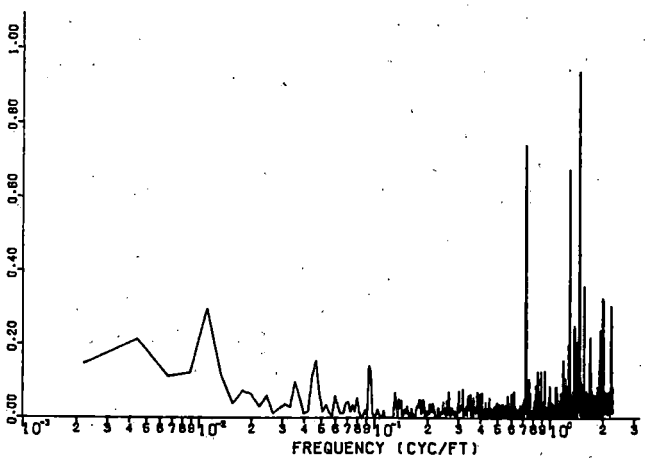

Figure 3-22. Coherence Between Alignment and Crosslevel

TEST CONDUCT

Most of the important aspects of the actual test conduct are covered in an AAR report [3-9]. The following is intended to provide enough background information on the tests to permit interpretation of the test results and comparisons discussed later. Therefore, most of the details of the test conduct are omitted.

Test-Vehicle and Consist

The test-vehicle consist is shown in Figure 3-23. It comprised two locomotives, the AAR-100 Research Car, a buffer car, the L&N 80-Ton Open-Hopper Car, and a caboose.

The hopper car was tested in eight different configurations to provide a variety of test conditions. The different configurations were achieved by the use of different wheelsets, the truck stiffener, the constant-contact sidebearings, the unlubricated or lubricated centerplate, and the presence of a load in the vehicle. Table 3-9 summarizes the eight configurations.

Table 3-9. Test Configurations

Configuration	Wheels	Load	Side-Bearings	Truck Stiffener	Centerplate
1	CN Profile A	0	0	None	Dry
2	CN Profile A	0	0	None	Lubricated
3	CN Profile A	0	2000 LB	None	Lubricated
4	CN Profile A	0	6000 LB	None	Lubricated
5	CN Profile A	0	0	ON	Lubricated
6	New	0	0	None	Lubricated
7	New	83.4 T	0	None	Lubricated
8	CN Profile A	83.4 T	0	None	Lubricated

Test-Vehicle Instrumentation and Equipment

The test vehicle was equipped by the AAR to measure 22 accelerations, 49 displacements, 8 wheel forces, and train speed. The instrumentation included 6 (sometimes 8) transducers to measure lateral and angular displacements of wheels and axles relative to the rails.

A system of nomenclature was devised in which the name of the measured variable indicates the location of the transducer used to measure it. Table 3-10 lists the measured variables and gives their channel assignments, transducer types, and ranges. Slight variations in the channel arrangements were occasionally made during the tests to accomodate failures. Wheel forces were available only with the AAR 1/20 wheels since the CN wheels were not strain gauged.

Each truck of the test vehicle was equipped with a hydraulic system capable of exerting a torque between the truck and the carbody. This system was used to provide an initial condition to the vehicle consisting of lateral and angular

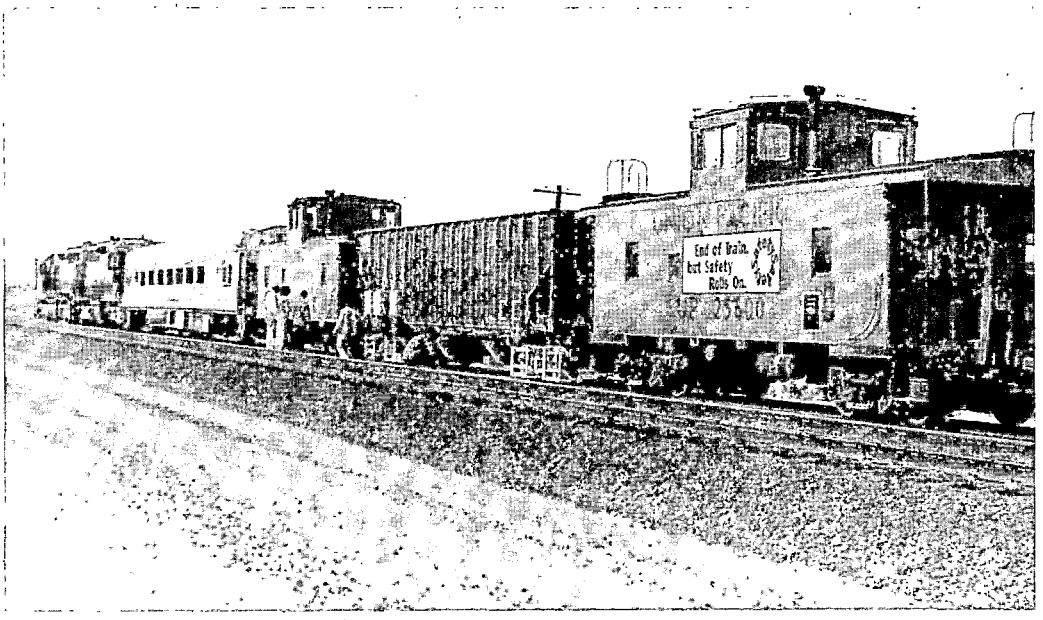

Figure 3-23. Test Consist

displacements of the trucks away from their equilibrium positions on the track. Hydraulic cylinders provided the actual forces. Pressures in one of the hydraulic cylinders were measured and recorded.

Data Acquisition System

All data was recorded on board the AAR-100 Research Car. The data was sampled at 100 samples per second and recorded digitally on magnetic tape. In addition, selected channels were recorded on strip charts so they could be observed during or shortly after a particular test.

The computer operator and the test director maintained logs to document test conduct and significant events. The computer operator also wrote real-time messages onto the data tape as significant events occurred.

Test Sequence

Four different types of tests were made with each of the eight configurations. Table 3-11 summarizes the sequence of the testing and lists the nominal speeds for each test type. The four test types are described below:

1) Curves: 6-degree and 1-degree curves were traversed at 3 speeds. The speeds were intended to be below, near, and above balance speeds for both curves.

2) Unforced: The unforced tests were conducted at several speeds on tangent mainline track. No activation from the on-board hydraulic forcing system was used. Therefore, the primary forces acting on the test vehicle were those from the track irregularities.

3) Forced: The forced tests were also conducted on tangent mainline, but for this series the on-board hydraulic forcer system was used to provide initial angular and lateral displacements of the test vehicle away from the equilibrium position. Upon rapid release of the imposed forces, the vehicle's response to the initial condition and also the track irregularities was recorded.

4) Creep: The creep tests were conducted on tangent passing track at a speed sufficiently slow so that the dynamic forces in the test vehicle were negligible. The hydraulic forcing system was used to apply a known moment between the trucks and the body of the test vehicle. The purpose of the creep tests was to permit estimation of the wheel-rail creep forces.

DATA ANALYSIS PROCESS

The primary purpose of conducting the field tests was to provide real vehicle response data for comparison with predicted or calculated response data from several freight car mathematical models. Consequently, the first step in the data analysis process was to combine the signals recorded from individual transducers in a manner that constructs the variables of a 19-degree-of-freedom model of the test vehicle [1-1]. For example, the Truck A lateral displacement variable was constructed by summing 16 individual signals with appropriate weights.

Time histories of all the signals to be analyzed were plotted and studied. Portions of test data from each configuration and speed of interest were selected for analysis. For most of the analysis, truck lateral displacements proved to be the most useful signals, although other variables were used as well.

Table 3-10. Instrumentation List and Channel Assignments

Channel	Name	End of Car	Side of Car	Wheel	Side of Part	Transducer Type	Range
1	BUF - 1					ACC	±10G
2	CVRT - A L					ACC	± 2G
3	CVRT - A R					ACC	± 2G
4	BOLAT - A					ACC	±25G
5	SFLAT - A R 3					ACC	±25G
6	SFLAT - A R 4					ACC	±25G
7	SFLAT - A L 3					ACC	±25G
8	SFLAT - A L 4					ACC	±25G
9	SFLNG - A L					ACC	±25G
10	SFLNG - A R					ACC	±25G
11	CRBOV - A R					SP	3.5 IN
12	SFLOD - A R					SP	15 IN
13	SFLOD - A L					SP	15 IN
14	SPTR - A R					SP	10 IN
15	SPTR - A L					SP	10 IN
16	AXDSP - A R 4					SP	1 IN
17	AXDSP - A L 4					SP	1 IN
18	WRLD - A R 4 a					SP	3.5 IN
19	WRLD - A R 4 b					SP	3.5 IN
20	WRLD - A L 3 a					SP	3.5 IN
21	WRLD - A L 3 b					SP	3.5 IN
22	WRLD - A L 4 a					SP	3.5 IN
23	WRLD - A L 4 b					SP	3.5 IN
24	WRLD - A R 3 a					SP	3.5 IN
25	WRLD - A R 3 b					SP	3.5 IN
26	WRVD - A R 4 a					SP	1 IN
27	WRVD - A R 4 b					SP	1 IN
28	WRVD - A L 3 a					SP	1 IN
29	WRVD - A L 3 b					SP	1 IN
30	WRVD - A L 4 a					SP	1 IN
31	WRVD - A L 4 b					SP	1 IN
32	ASLAT - A R 3up					SP	3.5 IN
33	ASLAT - A R 3dn					SP	3.5 IN
34	ASLAT - A R 4up					SP	3.5 IN
35	ASLAT - A R 4dn					SP	3.5 IN
36	ASLAT - A L 3up					SP	3.5 IN
37	ASLAT - A L 3dn					SP	3.5 IN
38	ASLAT - A L 4up					SP	3.5 IN
39	ASLAT - A L 4dn					SP	3.5 IN
40	BOSF - A R					SP	3.5 IN
41	BOSF - A L					SP	3.5 IN
42	SFAX - A R 4					SP	3.5 IN
43	SFAX - A L 4					SP	3.5 IN
44	LATFO - A R 3					SG	30 KIPS
45	LATFO - A R 4					SG	30 KIPS
46	LATFO - A L 3					SG	30 KIPS
47	LATFO - A L 4					SG	30 KIPS
48	VRTFO - A R 3					SG	40 KIPS
49	VRTFO - A R 4					SG	40 KIPS
50	VRTFO - A L 3					SG	40 KIPS
51	VRTFO - A L 4					SG	40 KIPS
52	CYPSH - A L (BR)					SG	
53	CYPUL - A L (BR)					SG	
54							
55							
56	Not Used						
57							
58							
59							
60							
61							
62	CVRT - B R					ACC	± 2G
63	CVRT - B L					ACC	± 2G
64	BOLAT - B					ACC	±25G
65	SFLAT - B R 1					ACC	±25G
66	SFLAT - B R 2					ACC	±25G
67	SFLAT - B L 1					ACC	±25G
68	SFLAT - B L 2					ACC	±25G
69	SFLNG - B R					ACC	±25G
70	SFLNG - B L					ACC	±25G
71	CRBOV - B R					SP	3.5 IN
72	SFLOD - B L					SP	15 IN
73	SFLOD - B R					SP	15 IN
74	SPTR - B R					SP	10 IN
75	SPTR - B L					SP	10 IN
76	AXDSP - B R 2					SP	1 IN
77	AXDSP - B L 2					SP	1 IN
78	WRLD - B R 1 a					SP	3.5 IN
79	WRLD - B R 1 b					SP	3.5 IN
80	WRLD - B L 1 a					SP	3.5 IN
81	WRLD - B L 1 b					SP	3.5 IN
82	WRLD - B L 2 a					SP	3.5 IN
83	WRLD - B L 2 b					SP	3.5 IN
84	BOSF - B R					SP	3.5 IN
85	BOSF - B L					SP	3.5 IN
86	SFAX - B R 1					SP	3.5 IN
87	SFAX - B L 1					SP	3.5 IN
88							
89	TSPD						
90	TLOC						

NOTES: ACC - Accelerometer
SP - String Potentiometer
SG - Strain Gauge

Table 3-11. Test Sequence Summary

AAR Tape ID	Tape File	Config-uration	Test Type	Test Date	Nominal Speeds (MPH)
THMV1	1	1	Curves	11-8-76	6-Deg: 20, 30, 35
		1	Curves	11-8-76	1-Deg: 10, 30, 35
	2	1	Unforced	11-11-76	15, 25, 30, 35, 40
THMV2	1	1	Creep	11-12-76	5
	2	1	Forced	11-12-76	15, 25, 30, 35, 40
THMV3	1	2	Unforced	11-13-76	15, 25, 35, 40
		3	Unforced	11-13-76	25, 35, 45, 50
		4	Unforced	11-13-76	40, 50
THMV4	1	4	Unforced	11-13-76	60, 65
	2	4	Unforced	11-15-76	70, 75
	3	4	Forced	11-15-76	50, 60, 65, 70
		3	Creep	11-15-76	5
THMV5	1	2	Creep	11-16-76	5
		4	Forced	11-16-76	65
		3	Forced	11-16-76	20, 30, 35, 40
		2	Forced	11-16-76	20, 30, 35, 40
THMV6	1	5	Unforced	11-16-76	50
	2	5	Unforced	11-16-76	35, 45, 55
		5	Forced	11=16-76	35, 40, 45, 50
		5	Creep	11-16-76	5
THMV7	1	5	Curves	11-29-76	6-Deg: 250, 30, 40
		5	Curves	11-29-76	1-Deg: 10, 30, 40
	2	2	Curves	11-29-76	6-Deg: 20, 30, 40
		2	Curves	11-29-76	1-Deg: 10, 30, 40
		4	Curves	11-29-76	6-Deg: 20, 30, 40
		4	Curves	11-29-76	1-Deg: 10, 30, 40
		3	Curves	11-29-76	6-Deg: 20, 30, 40
		3	Curves	11-29-76	1-Deg: 10, 30, 40
THMV8	1	6	Creep	12-3-76	5
	2	6	Forced	12-3-76	25, 35, 45, 55
			Unforced	12-3-76	25, 35, 45, 55
THMV9	1	6	Curves	12-6-76	6-Deg: 20, 30, 40
		6	Curves	12-6-76	1-Deg: 20, 30, 40
	2	7	Creep	12-8-76	5
	3	7	Unforced	12-8-76	40, 50, 80
		7	Forced	12-8-76	40, 70, 80
THMV10	1	7	Unforced	12-9-76	60, 70
		7	Forced	12-9-76	50, 60
	2	7	Curves	12-10-76	6-Deg: 20, 30, 40
		7	Curves	12-10-76	1-Deg: 10, 30, 40
THMV11	1	8	Unforced	1-12-77	20, 30, 40, 50
		8	Forced	1-12-77	50
	2	8	Curves	1-14-77	6-Deg: 20, 30, 40
	2	8	Curves	1-14-77	1-Deg: 10, 30, 40

The frequency and damping characteristics reported here for the unforced runs were obtained using the Random-Decrement technique [2-7]. This process yields estimates of the natural frequency and damping ratio of the least-damped mode of the system. See Figure 2-3 for a typical Random Decrement signature. It should be noted that each Random Decrement signature represents the average of approximately 100 time records.

Random-Decrement is a time-domain analysis procedure. For comparison purposes damping ratios were also computed using a frequency-domain method based on determining the bandwidth of the resonant peak on a PSD plot. Similar results were obtained using both methods.

The final step in the damping ratio estimation process refines the initial damping ratio estimates. The least-damped mode for the hopper car is usually the kinematic mode. This mode has the characteristic that the natural frequency is very nearly proportional to vehicle speed. Thus when the speed varies over the duration of a data run, the dynamics of the process also vary. This variation results in a smearing of the data in the frequency domain, and a broadening of the resonant peak associated with the least-damped mode. The broadening of the resonant peak represents an apparent increase in the damping ratio of the process. The net result is that damping ratio estimates are too high.

A computer program has been developed that refines the damping ratio estimates by accounting for the vehicle speed variations during a particular test run. The train-speed channel is used in this program to determine the actual damping ratio that would have resulted in the observed damping ratio, given the known train speed variations. The assumptions are made that the vehicle dynamics are second order and lightly damped, and that natural frequency is proportional to train speed. This adjustment is negligible for large damping ratios but can be substantial for damping ratios of the order of 0.1 and smaller.

Test vehicle response following application of the truck forcers was studied using the logarithmic decrement technique. The truck forcers apply a moment between the car body and the truck bolster, forcing the truck away from its equilibrium position near the center of the track. The vehicle dynamic behavior can be studied from the initial condition response that ensues when the forcers are released. Figure 3-24 shows a typical time history of the Truck A lateral displacement during a forced run. Damping ratio information is contained in the shape of the decay envelope, which is defined by the peaks in the response curve. Both positive and negative pairs of successive peaks were used to compute a large number of damping ratios for each speed. The damping ratios were then averaged to obtain a single damping ratio for each speed.

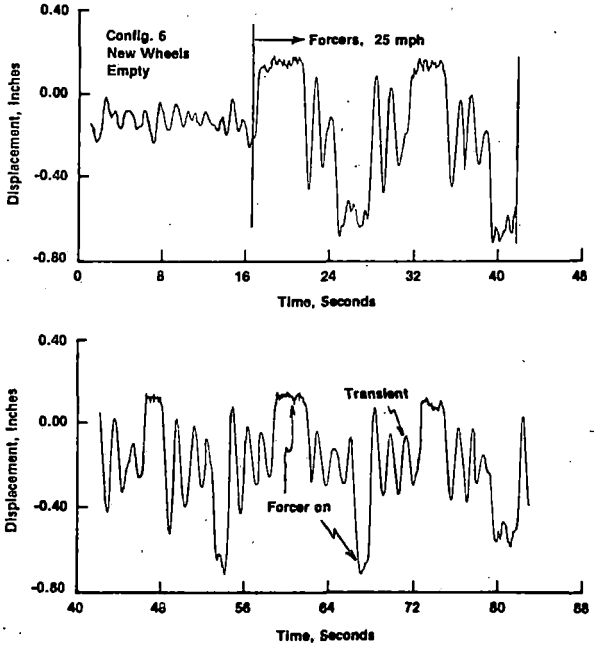

Figure 3-24. Truck Lateral Displacement Using Hydraulic Forcers

Random response of the test vehicle was also analyzed using a spectral analysis computer program developed specifically for this test program [1-11]. Histograms, autocorrelation functions, PSDs and RMS values were computed for many variables.

OBSERVATIONS AND CONCLUSIONS

We have accumulated several observations and conclusions concerning the test planning and conduct that we believe may be useful to others involved in similar tests. Concerning the vehicle, a very thorough effort was made to characterize the test vehicle. However, only one truck was characterized, and that effort was carried out in Denver many months prior to the test. Consequently, differences in suspension stiffness and friction between the two trucks, and the variations in suspension friction with environmental conditions remain undetermined. It would be desirable to identify these characteristics at the test site.

The wheel tread profile data obtained from the German Federal Railroad (DB) measurement machine was quite suitable for computing the wheel-rail geometric constraint functions. However, we believe that the wheel surface condition may strongly influence the creep force laws that govern the wheel-rail forces. It would be useful, in future tests, to determine these creep force laws at the test site using a procedure similar to that attempted, unsuccessfully, in this test series.

One of the shortcomings of our tests was the roadbed geometry characterization. As explained earlier, alignment, profile and gauge data was only gathered one year before and after the tests. The actual roadbed condition during the tests was not known, nor were we able to synchronize the vehicle test data with roadbed measurements. This proved to be particularly unfortunate, because we found that nonlinear friction in the vehicle suspension causes the vehicle behavior to depend strongly on the roadbed disturbances.

The DB rail profilometer proved as easy as its companion, the wheel profilometer, to use. However, conversion of the graphical output to digital data was time consuming. Direct electrical readout of the data would be extremely helpful. This improvement will prove particularly useful if more rail head profiles are measured, as we recommend. The data gathered in these tests indicated that the wheel-rail geometric constraint functions very significantly along the track, but did not provide enough information to characterize this variation.

The vehicle instrumentation and data recording system used in these tests were well thought out and performed well during the tests. The wheel-rail displacement probes, in particular, provided reliable and useful data. The greatest shortcoming of the tests, however, was the failure to obtain initial conditions for these devices. A simple procedure to zero these probes is needed.

The instrumented wheel data were not used at all. The fundamental problem with this data was the lack of a reference calibration. It appears that considerable care and effort must be taken to obtain reliable wheel/rail force data. Future test planners should be aware of the magnitude of care and effort needed.

Several small matters should be remedied in future testing. Close attention should be paid to the A/D converter discretization level. If this level is too high, the wheel-rail angle of attack measurements may not be reliable. Changing data channels during the test also poses problems. The data processing comptuer programs may not be flexible enough to accomodate such variations in location of the test data.

During the tests, several problems occured that can be traced to a lack of understanding of the test objectives on the part of the test personnel. We believe that such misunderstandings can only be minimized when someone familiar with the theory of rail vehicle dynamics, preferably a user of the test data, is on the test site for the duration of the tests.

We would have preferred, given the limitations of testing resources, to have more test data for fewer vehicle configurations. Longer runs at the same speed, and runs at more speeds would have given enough data to analyze the anomolous behavior that often occured. More constant speed during the test runs also would have made the data more useful.

The data collection system performed superbly. We had very few problems in reading the data tapes and processing the test data.

In summary, we regard these tests as one of a series of tests to obtain data for comparison with theoretical vehicle dynamic analyses. We believe that a great deal of useful information was obtained in this project, and that better information will be obtained in future tests by avoiding the problems mentioned above.

Chapter 4

FIELD TEST RESULTS

DATA ANALYSIS SUMMARY

This chapter contains the results of the field-test data analysis. Results from the analysis methods described in Chapter 3 are discussed in a separate section of this chapter. A summary of the various types of analyses performed on the test data is shown in Table 4-1. For reference purposes, this table also contains the data identifiers used by the AAR and ASU for the magnetic tapes containing raw and processed test data. More detailed information concerning the portions of data used in each analysis is contained in subsequent sections.

TIME SERIES DATA

Data from all of the tangent track test runs was processed to form variables corresponding to the 19-DOF model variables described earlier. Plots of this data show several types of vehicle behavior such as sustained hunting, intermittent hunting, and stable random response. Examples of these behavior types are presented below.

Sustained Hunting with Flange Contact

Figure 4-1 shows a typical test run during which sustained hunting occurred. In Figure 4-1 and subsequent figures, time starts at zero at the beginning of each magnetic tape file identified in Table 4-1. The variable plotted in the figure is truck lateral displacement, which is a combination of twelve recorded signals. The hunting oscillation has a peak-to-peak amplitude of about 0.80 inch indicating frequent flange contact. With this wheelset and rail combination, flange contact occurs with peak-to-peak amplitudes greater than 0.65 inch. In general, hunting in these tests exhibited this high-amplitude, high-frequency, uniform-magnitude behavior.

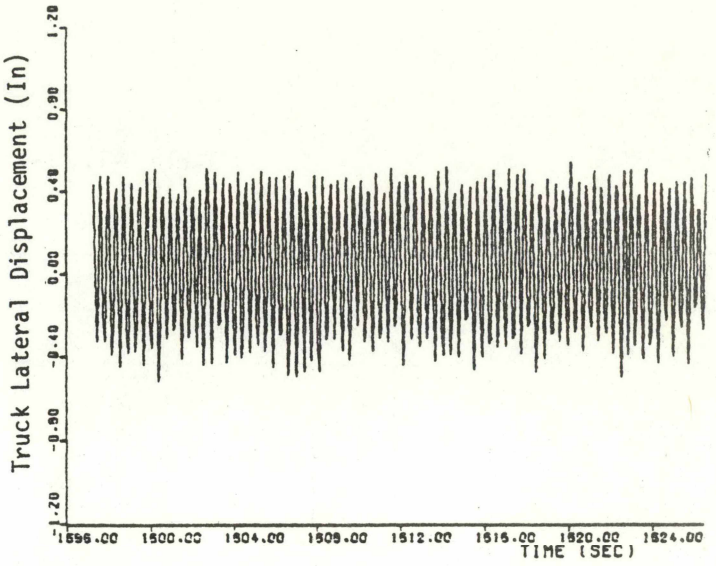

Figure 4-1. Typical Sustained Hunting Response

Typical Stable Response

Most of the recorded test data represented the stable response of the test vehicle to the random track irregularities. Figure 4-2 shows a portion of a test run that is typical of this behavior. Some low-amplitude oscillations can be observed at the natural frequency of the least-damped mode of the vehicle. Some high-frequency and lower-frequency oscillations can also be seen in the figure.

In non-hunting situations the time response of Truck A and Truck B were essentially of the same shape, but with slightly different amplitude, and with a transport delay in the response of the trailing truck. To illustrate this we have removed the transport lag and plotted the lateral displacements of Trucks A and B on the same axes in Figure 4-3.

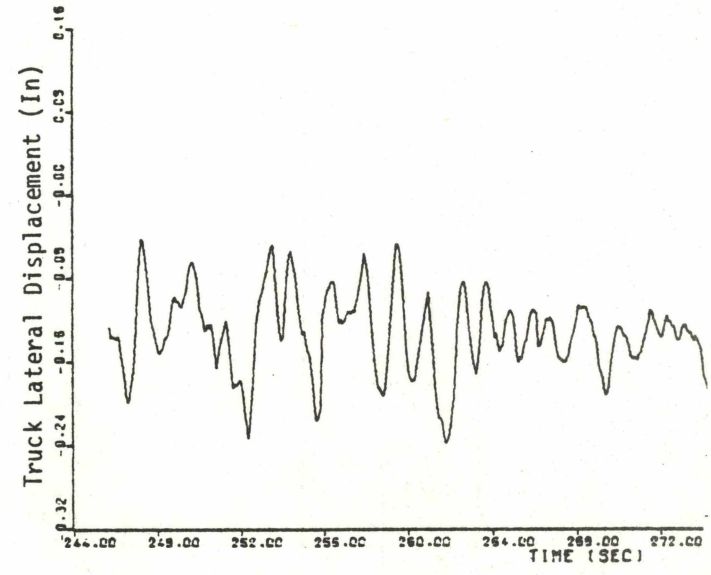

Figure 4-2. Stable Response to Track Forcing

Intermittent Hunting

We observed two somewhat different types of intermittent hunting in the test data distinguished by the amplitude of the limit-cycle motion. Both types occurred a number of times. Figure 4-4 shows a typical truck lateral response in which a relatively short (about 12 seconds) burst of hunting occurred with an amplitude limited by flange contact between wheels and rail. This is essentially a short period of the type of hunting shown in Figure 4-1 with an abrupt beginning and ending. Train speed was nearly constant during the time period shown.

Table 4-1. Data Analysis Summary

AAR Tape ID	Tape File	Config.	Data Type	Raw Data on ASU Tape	Reduced Data on ASU Tape	Types of Data Analysis Performed
THMV1	1 2	1 1	Curves Unforced	U0866	U0512 U0944	MV, P MV, P, PSD, R
THMV2	1 2	1 1	Creep Forced			
THMV3	1	2, 3, 4	Unforced	U0524	U0512	MV, P, PSD, R, JD
THMV4	1 2 3	4 4 3 4	Unforced Unforced Creep Forced	U0803	U0694 U0512	MV, P, PSD, R MV, P, PSD, R
THMV5	1	2, 3, 4	Forced	U0268		
THMV6	1 2	5 5	Unforced Unforced/ Forced	U0940	U0962 U0944	MV, P, PSD MV, P, PSD
THMV7	1 2	5 2, 3, 4	Curves Curves			
THMV8	1 2	6 6	Creep Forced/ Unforced	U0732	U0694	MV, P, PSD, R, XPSD, L, JD
THMV9	1 2	6 7	Curves Creep	U0592	U0694	MV, P
THMV9	3	7	Forced/ Unforced	U0649	U0512	MV, P, PSD
THMV10	1 2	7 7	Forced/ Unforced Curves	U0801	U0694	MV, P, PSD
THMV11	1 2	8 8	Forced/ Unforced Curves	U0838	U0694	MV, P, PSD

MV = Obtain Model Variables, Speed Channel, and other Selected Variables
P = Plot Speed Channel, Truck Lateral Displacements and Other Selected Variables
PSD = Obtain Power Spectral Density of Truck Lateral Displacements and Other Selected Variables
R = Perform Random Decrement Analysis on Truck Lateral Displacements
XPSD = Perform Cross Spectral Analysis
L = Conduct Logarithmic Decrement Analysis of Forced Response
JD = Obtain Displacements Across Nonlinear Elements of Test Vehicle

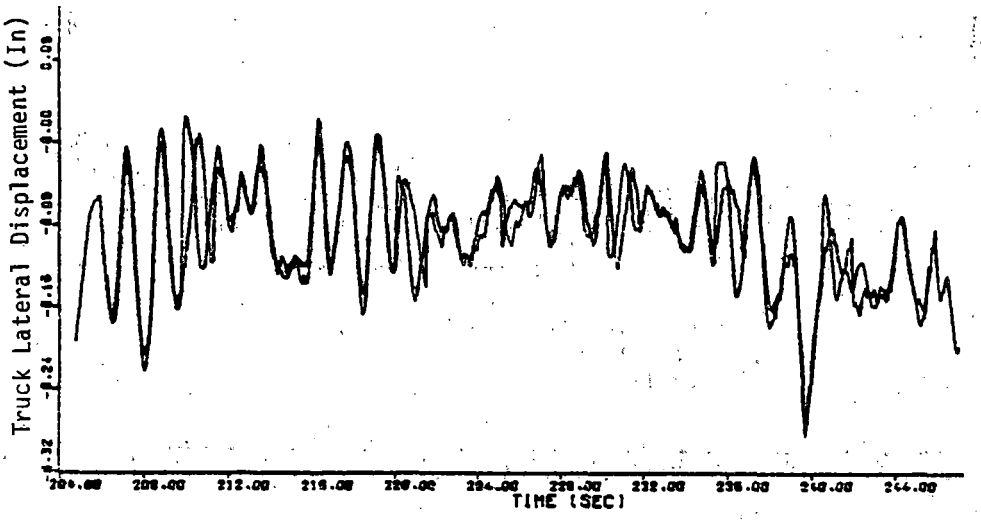

Figure 4-3. Stable Response of Trucks A and B Plotted on Same Axes

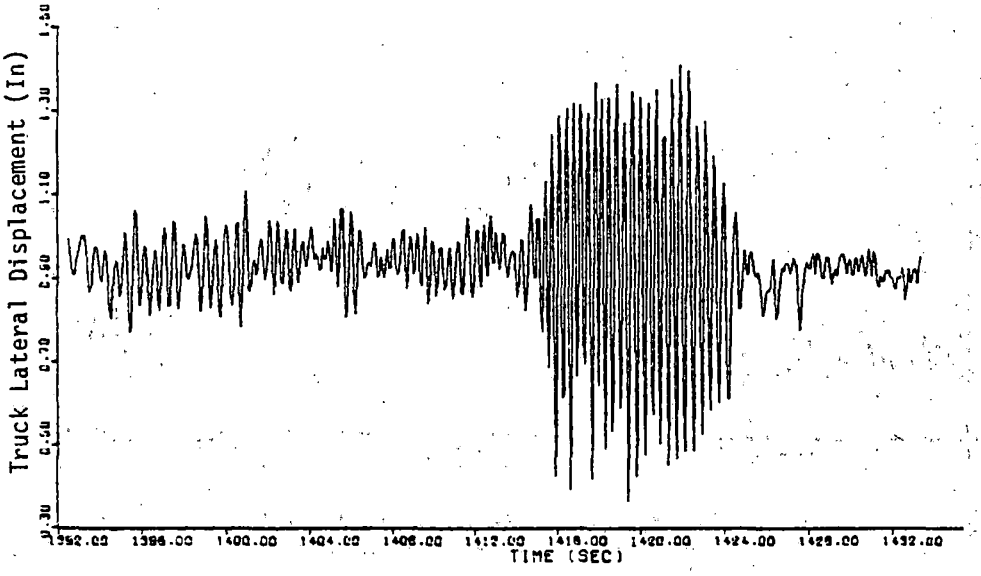

Figure 4-4. High Amplitude Intermittent Hunting

The other type of intermittent hunting also occurred during short time periods, but in contrast to the first type, it had an amplitude well below the flange-contact amplitude. This type of response is shown in Figure 4-5. Beginning at about 1492 seconds into this test period, three short bursts of low-amplitude hunting occurred. The frequency of these short bursts of hunting is about 30% higher than the non-hunting response exhibited in the 1474-to 1492-second time period. Once started, this type of hunting either died out or grew in amplitude to sustained high-amplitude hunting. The latter case occurred in the hunting burst starting at about 1510 seconds in Figure 4-5.

Curving Response

Figure 4-6 shows a typical lateral-displacement response, WRLD-AR3B, to a 6-degree curve. The lateral displacement increases during curve entry, indicating movement of the wheel away form the rail. An equilibrium condition reflected in a non-zero mean displacement is reached during the curve negotiation, and the lateral displacement returns to its zero mean value upon curve exit.

A typical plot for the 1-degree curve appears identical to the stable response shown in Figure 4-2 for tangent track. It is difficult or impossible to detect the 1-degree curve by observing the plots because the steady-state average lateral displacement changed so little.

In one situation the initiation of hunting was observed at the exit from the curve. This response, although not typical during these tests, is shown in Figure 4-7. The small-amplitude hunting oscillations shown began as the configuration 1 test vehicle exited the 6-degree curve at 40 mph. The beginning of this run was truncated, so it is not known if the vehicle was hunting upon curve entry. Both trucks began hunting upon curve exit.

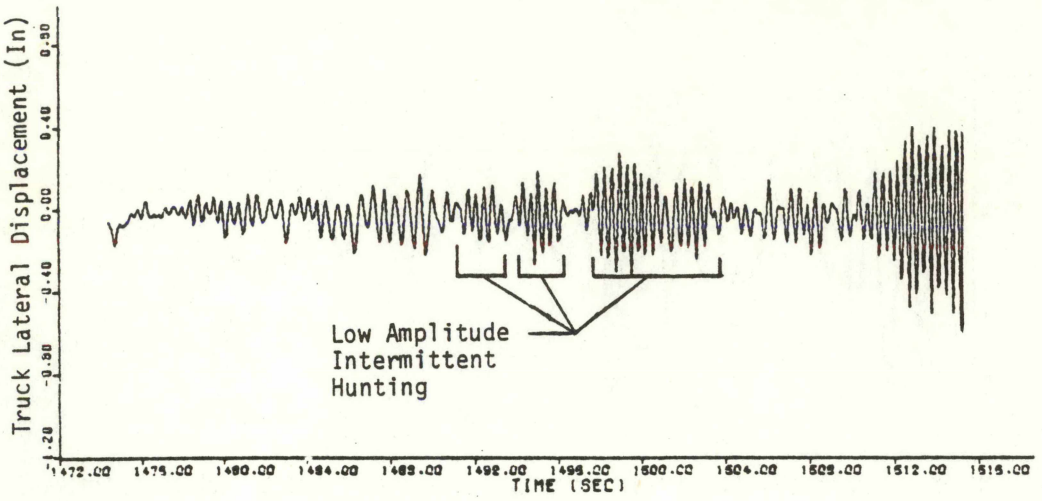

Figure 4-5. Low Amplitude Intermittent Hunting

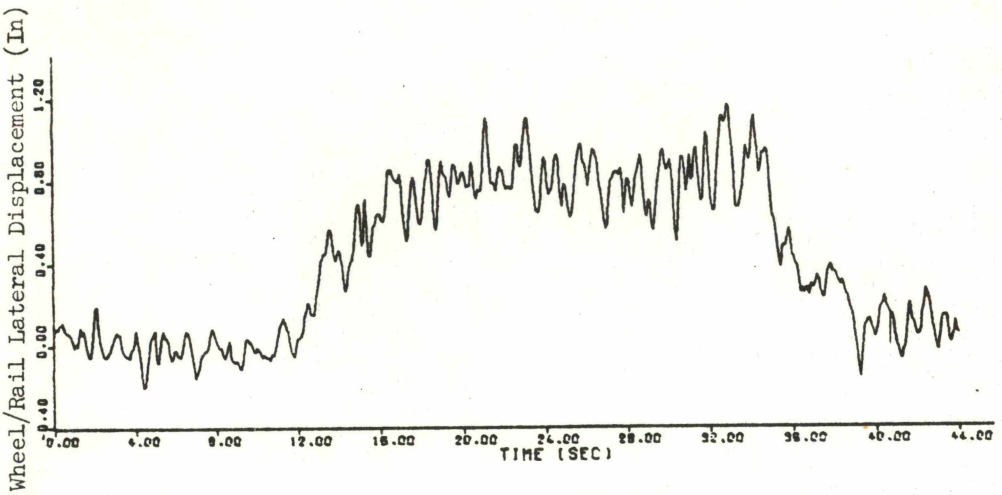

Figure 4-6. Typical Lateral Response During 6-Degree Curve Negotiation

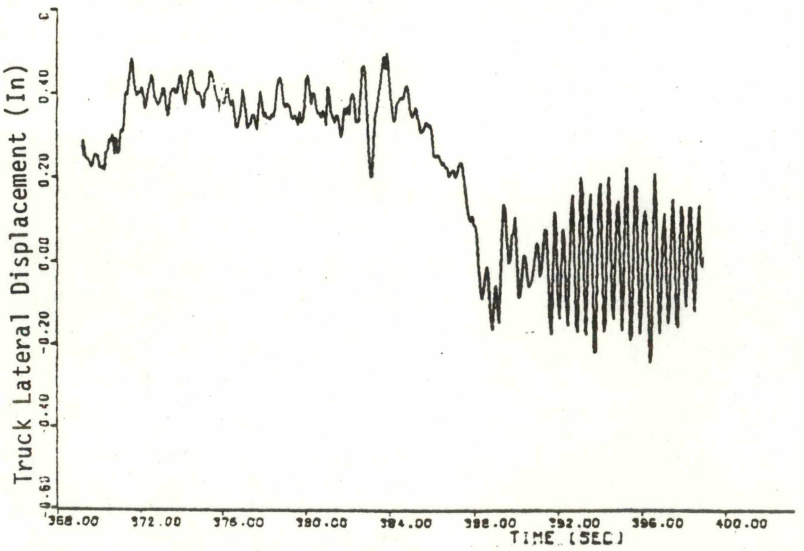

Figure 4-7. Hunting Initiated upon Exit from 6-Degree Curve at 40 MPH

VEHICLE HUNTING CHARACTERISTICS

An interesting and important result of the field tests is a characterization of the hunting performance of the test vehicle in its eight configurations. Discussions of hunting behavior are often conducted in terms of "the hunting speed" of a vehicle as though hunting speed were a unique property of a vehicle. One of the points that we wish to emphasize in this report is that, in reality, hunting speed can not be characterized by a single number with the dimension of speed. There is actually a transition speed range in which intermittent hunting occurs. Below this range hunting never occurs, and above it sustained hunting always occurs.

Three effects seen in our analysis of the test data illustrate the impossibility of associating a unique hunting speed with a given vehicle configuration.

1) At speeds in the transition range between no hunting and sustained hunting, hunting behavior is intermittent. For example, Figure 4-4 shows that a period of intermittent hunting occurs between two periods of stable behavior during a constant 48-mph test run of Configuration 2.
2) The behavior of a freight vehicle depends upon a number of characteristics that are not constant in time. During the field tests the hunting behavior of the test vehicle was observed to differ from one day to the next. It is not surprising that this should occur since, as noted above, the behavior was not always constant during a test run.
3) Different types of hunting occurred during the field tests. The obvious type is exemplified in Figure 4-1, which shows hunting during which flange contact occurred regularly. Another type is shown in Figure 4-5, where hunting occurred in short bursts at an amplitude well below flange contact. For analysis purposes we called both of these behaviors hunting in determining the percentage of time during a test run that hunting occurred.

Figure 4-8 summarizes the hunting characteristics of the eight configurations. The data points used in constructing the graphs are shown. The ordinate on these bar-type charts is percent of time the vehicle was hunting at a given speed. In every case a point is shown for zero-percent hunting. This point represents the speed at and below which no hunting was observed to occur. A point is also shown, when available, for 100-percent hunting, which is the speed at and above which sustained hunting was always observed to occur.

In most cases the points represent tape-recorded data. In some cases, however, points come from written observations of the test crew. This is the case with the 100-percent hunting points for C3 Truck B, C5 Truck B and both trucks of C8. The 50-percent hunting on C6 Truck B at 82 mph is also from test crew observations, and was called "moderate hunting" and "marginal hunting" in the test log. It was

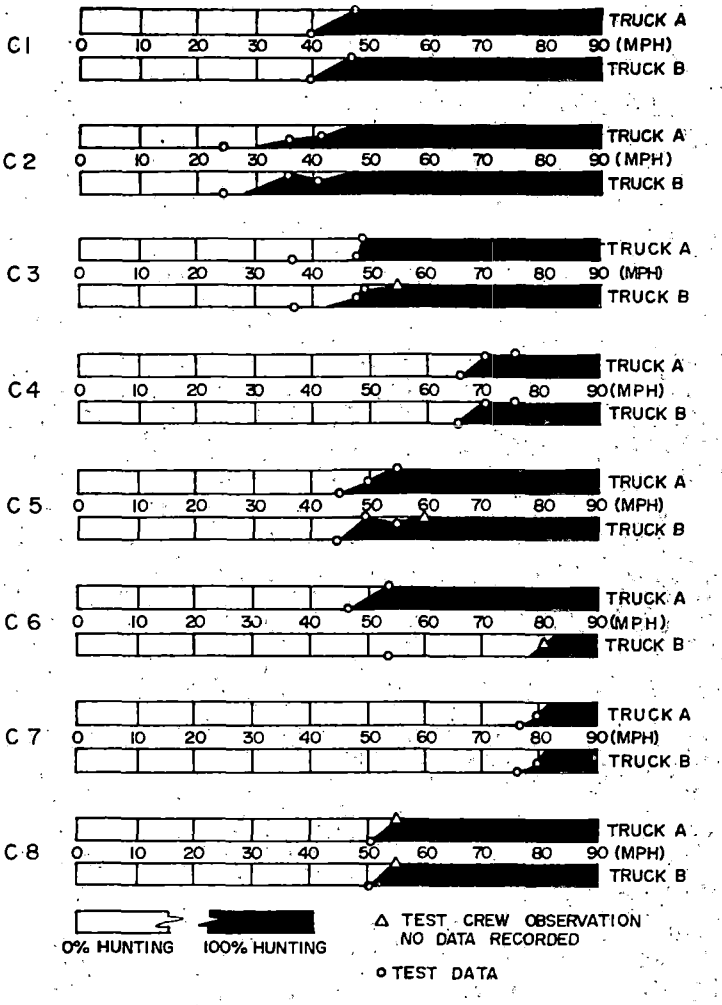

Figure 4-8. Test Vehicle Hunting Characteristics

somewhat arbitrarily set at 50 percent hunting.

The lines connecting the data points represent an estimate of the behavior at speeds between and beyond the test speeds. Since we have no real information at intermediate speeds, the actual behavior may differ in these regions.

Some observations on each of the configurations are given below:

C1. No intermittent hunting was recorded for C1, the empty vehicle with CN wheels and unlubricated centerplates. The slope of the transition between no hunting and sustained hunting could be considerably greater.

C2. The C2 vehicle was the C1 vehicle with centerplates lubricated. The obvious effects were to lower the speed for hunting initiation and also to spread out the transition-speed range. The effect on the speed at which sustained hunting always occurred is not known, because no test runs were made for C2 at speeds exhibiting sustained hunting. C2 Truck B data shows an unusual trend in which hunting occurred a lower percentage of time at 41.5 mph than it did at 35.7 mph. This also occurred on C5 Truck B test data.

C3. Addition of the constant-pressure sidebearing device to the C2 vehicle made the C3 vehicle. C3 exhibited an upward shift in the hunting-speed transition range.

C4. With a higher pressure in the side-bearing device in C4, the hunting speed transition range became even higher.

C5. The C5 vehicle was the C2 vehicle with addition of a warp stiffener. The hunting speed transition region was narrower and occurred at a higher speed than that of C2.

C6. The C6 vehicle was the basic empty hopper car with lubricated centerplates and AAR straight-taper wheels. The Truck B wheels were quite new, with much of the wheel tread in a rough as-manufactured condition. Truck-A wheels had accumulated considerably more miles, and the treads were fairly well polished. It should be noted that the zero-percent hunting speed is shown as 46 mph for Truck-A since no hunting occurred during the 46-mph unforced test run. However, on the 45-mph test run using truck forcers, sustained hunting occurred between application of truck forcers, and it ceased when the forcers were applied. To our knowledge the wheel surface conditions were the only significant differences between Trucks A and B that could account for the vastly different hunting characteristics. An attempt was made to correlate hunting speed differences to direction of travel of the test vehicle, but no significant correlation was found.

C7. The loaded C6 vehicle became C7. Hunting characteristics for both trucks were about the same, the highest found during the test series.

C8. The C8 vehicle was the loaded hopper car with the CN wheels. Because no intermittent hunting was recorded, the nature of the transition is not known. The C8 vehicle had higher hunting speeds than the C2 vehicle, which was the empty C8 vehicle.

RMS RESPONSE CHARACTERISTICS

The root mean square (RMS) value of any variable gives a good overall measure of the amplitude of motion occurring during a particular test run. We computed RMS values for certain of the model variables and for several variables which represent displacements across the nonlinear elements in the test vehicle.

Model Variables

Figure 4-9 shows the RMS values of the model variables as a function of speed for each of the configurations. For Configuration 6, we computed RMS values of all the model variables except MV5, carbody lateral bending, which was not available. In addition we computed the RMS values of two

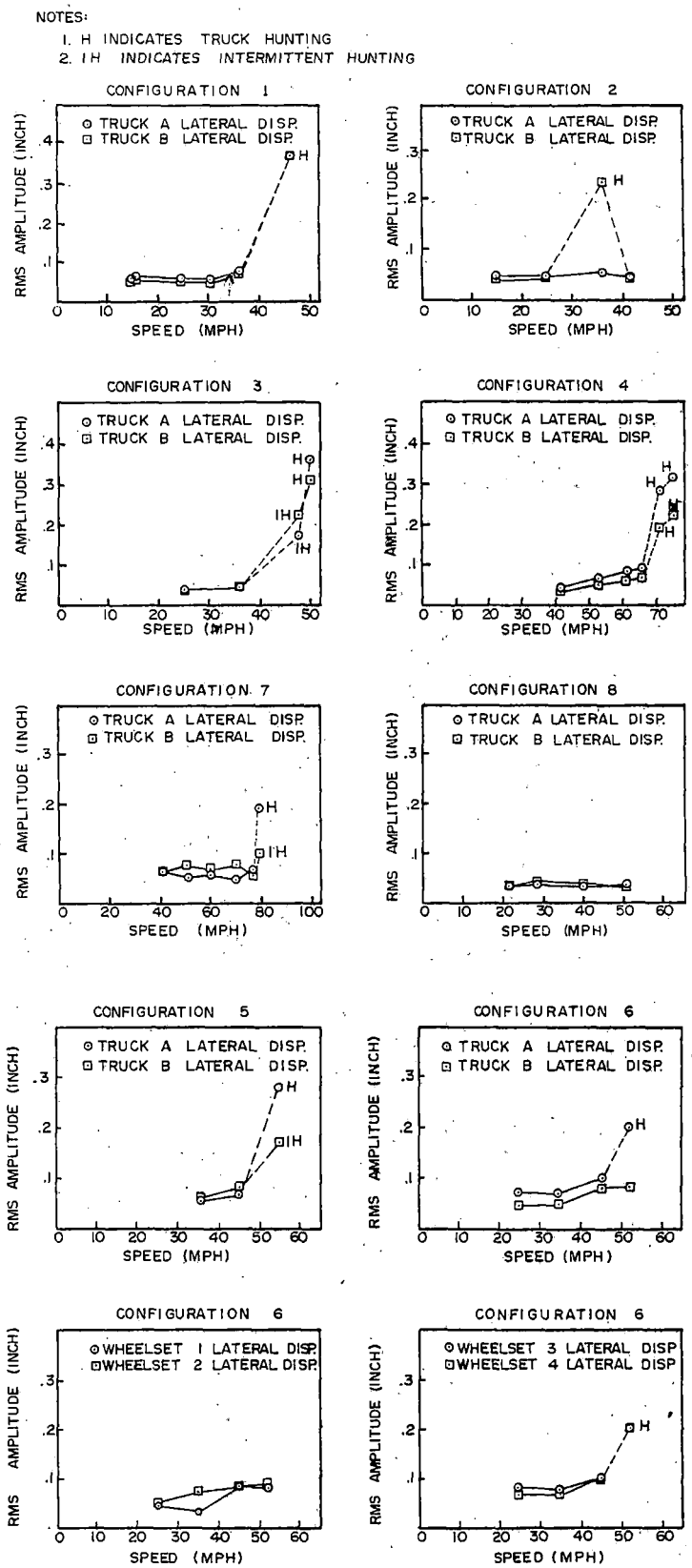

Figure 4-9. RMS Values of Model Variables

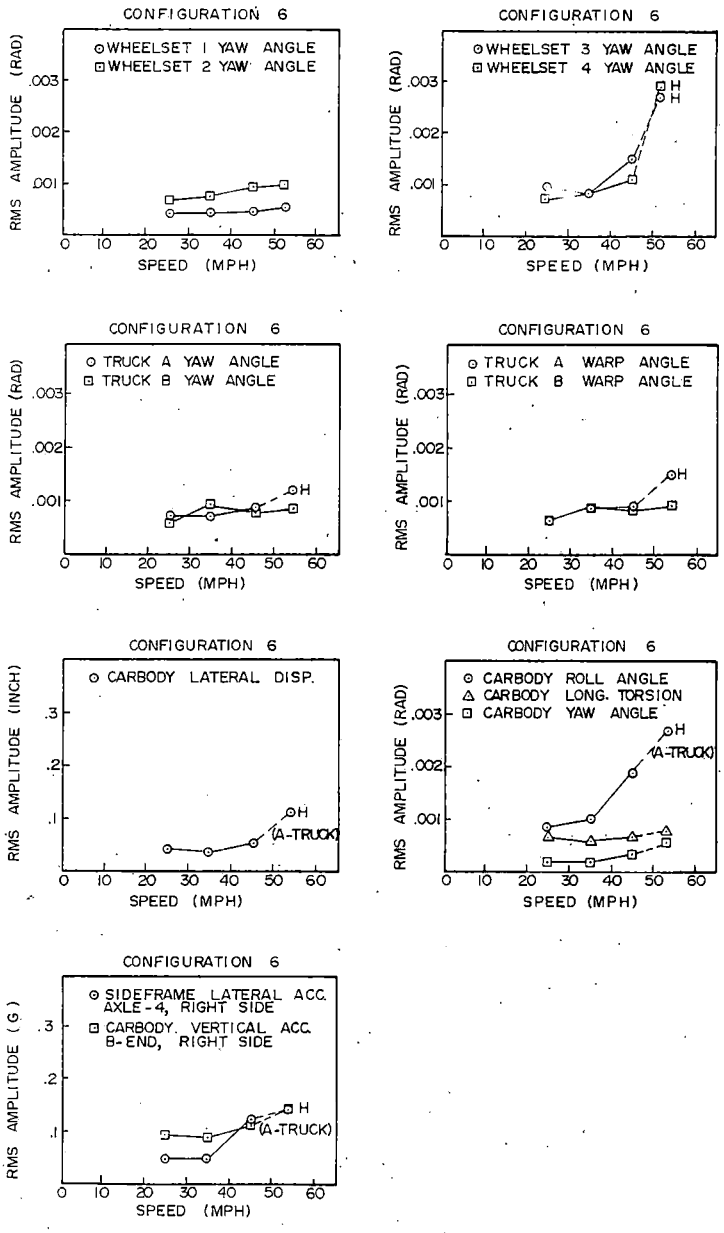

Figure 4-9. (cont) RMS Values of Model Variables

accelerations. For the other seven configurations we computed RMS values of the truck lateral displacements only.

Truck lateral displacement is an excellent indicator of hunting. In every case analyzed, when the RMS value of truck lateral displacement exceeded 0.1 inch, either sustained or intermittent hunting occurred. Likewise, when the RMS value of truck lateral displacement was less than 0.1 inch, no hunting occurred. A good hunting sensor for this field test series would have been a detector of truck lateral displacements exceeding 0.1 inch RMS.

The highest RMS value computed for truck lateral, 0.37 inch, occurred on the Configuration 1 test at 36.7 mph for both Truck A and Truck B. Assuming a sinusoidal response, this value corresponds to a peak-to-peak amplitude of about one inch, indicating continual flange contact. The actual response contains higher harmonics.

Table 4-2 contains the RMS values plotted in Figure 4-9. These are provided in the event they are required in some further analysis with an accuracy greater than can be obtained by taking values from the graphs in Figure 4-9. The table also shows the sections of the test runs used in the analysis. Time begins at zero at the beginning of each magnetic tape file shown in Table 4-1. Truck hunting status is also shown in Table 4-2. Table 4-3 defines the variables shown in Table 4-2.

Joint Displacements

In order to linearize the equations of motion of the test vehicle, estimates of the amplitudes of motions across the nonlinear elements in the vehicle model are needed. For this purpose, we computed a number of these displacements. The method used to compute these variables is given in Appendix C. The amplitudes, in the form of standard deviations, were computed from the test data for selected test runs. The results of these computations appear in Table 4-4. Spaces in the table indicate that the data for a particular variable was not directly usable due to noise contamination from a malfunctioning transducer, or from gross slips across the joints. Plots of the joint-displacement variables showed either excessively high levels or large discontinuities in the data in these cases.

In Table 4-4 CPROTA and CPROTB represent rotations of the Truck A and B centerplates relative to the carbody. BOSF-A and BOSF-B are bolster-to-sideframe lateral displacements for Truck A and B. SFVERT is the average of the four sideframe displacements for Truck A and B. SFVERT is the average of the four sideframe vertical displacements.

FREQUENCY AND DAMPING CHARACTERISTICS

We used three different methods on two different types of data to estimate the natural frequency and damping ratio of the least-damped mode of the test vehicle. Results of frequency and damping-ratio estimates made by the Random-Decrement and PSD methods on the unforced, tangent-track test runs are in substantial agreement with each other. Natural frequency estimates made from the forced runs are slightly higher than those made from the unforced runs, and damping ratios estimated using logarithmic decrement methods on the forced runs are substantially lower than those from the unforced runs.

Random-Decrement and PSD Results

Figures 4-10 through 4-13 show the estimates of natural frequency and damping ratio for Configurations 1, 2, 4, and 6. These estimates come from the Random-Decrement analysis of unforced tangent-track test runs. The data for these figures is given in Table 4-5. The table indicates the nominal test speed, actual test speed, data segment analyzed, natural frequency, raw and adjusted damping ratios, and the goodness of fit measure from the Random-Decrement analysis. See Chapter 3 for details of the analysis.

Table 4-2. RMS Values for Selected Variables from AAR Field Test Data

Config.	Nominal Speed (MPH) and Direction	Start Time (Sec)	Stop Time (Sec)	Actual Speed (MPH)	Variable Name	Hunting Status	RMS Value
1	15E	0	143	14.8	MV6		5.6×10^{-2}
	15E	149	292	15.7			6.5×10^{-2}
	25W	481	625	24.9			6.2×10^{-2}
	30E	783	927	30.5			6.3×10^{-2}
	35W	1029	1173	36.1			7.5×10^{-2}
	40E	1244	1388	46.7		H	3.7×10^{-1}
	15E	0	143	14.8	MV9		5.1×10^{-2}
	15E	149	292	15.7			5.9×10^{-2}
	25W	481	625	24.9			5.2×10^{-2}
	30E	783	927	30.5			5.7×10^{-2}
	35W	1029	1173	36.1			6.5×10^{-2}
	40E	1244	1388	46.7		H	3.7×10^{-1}
2	15E	0	143	15.0	MV6		4.6×10^{-2}
	25W	476	620	25.0			5.0×10^{-2}
	35E	809	952	35.7			5.8×10^{-2}
	40W	1009	1091	41.5			4.7×10^{-2}
	15E	0	143	15.0	MV9		4.2×10^{-2}
	25W	476	620	25.0			4.8×10^{-1}
	35E	809	952	35.7		H	2.4×10^{-2}
	40W	1009	1091	41.5			4.5×10^{-2}
3	25E	1157	1270	25.1	MV6		3.9×10^{-2}
	35E	1311	1382	36.2			4.7×10^{-1}
	45W	1398	1541	47.9		IH	1.7×10^{-1}
	50E	1567	1710	49.2		H	3.6×10^{-2}
	25E	1157	1270	25.1	MV9		3.7×10^{-2}
	35E	1311	1382	36.2			4.6×10^{-2}
	45W	1398	1541	47.9		IH	2.2×10^{-1}
	50E	1567	1710	49.2		H	3.1×10^{-2}
4	40E	1720	1864	41.5	MV6		4.1×10^{-2}
	50W	1900	2022	52.8			6.5×10^{-2}
	60W	56	179	61.0			8.0×10^{-2}
	65W	189	292	65.3			9.0×10^{-2}
	70W	108	210	70.5		H	2.8×10^{-1}
	75W	0	102	75.1		H	3.1×10^{-2}
	40E	1720	1864	41.5	MV9		3.2×10^{-2}
	50W	1900	2022	52.8			5.0×10^{-2}
	60W	56	179	61.0			5.7×10^{-2}
	65W	189	292	65.3			6.6×10^{-2}
	70W	108	210	70.5		H	1.9×10^{-1}
	75W	0	102	75.1		H	2.2×10^{-1}
5	35E	15	169	36.5	MV6		5.6×10^{-2}
	45E	358	512	45.5			6.7×10^{-2}
	50E	164	215	*			*
	50E	220	261	*		H	*
	55W	215	348	55.0		H	2.8×10^{-1}
	35E	15	169	36.5	MV9		6.0×10^{-2}
	45E	358	512	45.5			8.0×10^{-2}
	50E	169	215	*		H	*
	50E	220	261	*		H	*
	55W	215	348	55.0		IH	1.7×10^{-1}
6	25E	609	742	24.9	MVI		4.1×10^{-2}
	35W	896	988	34.3			3.5×10^{-2}
	45E	0	143	46.0			5.4×10^{-1}
	55E	307	430	53.8		H**	1.1×10^{-4}
	25E	609	742	24.9	MV2		8.4×10^{-4}
	35W	896	988	34.3			9.9×10^{-3}
	45E	0	143	46.0			1.9×10^{-3}
	55E	307	430	53.8		H**	2.7×10^{-4}
	25E	609	742	24.9	MV3		2.0×10^{-4}
	35W	896	988	34.3			2.1×10^{-4}
	45E	0	143	46.0			3.6×10^{-4}
	55E	307	430	53.8		H**	5.6×10^{-4}
	25E	609	742	24.9	MV4		6.9×10^{-4}
	35W	896	988	34.3			6.0×10^{-4}
	45E	0	143	46.0			6.7×10^{-4}
	55E	307	430	538		H**	7.9×10^{-2}
	25E	609	742	24.9	MV6		7.1×10^{-2}
	35W	896	988	34.3			6.9×15^{-1}
	45E	0	143	46.0			1.0×10^{-1}
	55E	307	430	53.8		H**	2.0×10^{-4}
	25E	609	742	24.9	MV7		7.2×10^{-4}
	35W	896	988	34.3			7.0×10^{-4}
	45E	0	143	46.0			8.8×10^{-4}
	55E	307	430	53.8		H**	1.2×10^{-4}
	25E	609	742	24.9	MV8		6.7×10^{-4}
	35W	896	988	34.3			8.8×10^{-4}
	45E	0	143	46.0			8.9×10^{-4}
	55E	307	430	53.8		H**	1.5×10^{-3}
6	25E	609	742	24.9	MV9		4.5×10^{-2}
	35E	896	988	34.3			4.9×10^{-2}
	45W	0	143	46.0			8.0×10^{-2}
	55E	307	430	53.8			8.2×10^{-4}
	25E	609	742	24.9	MV10		6.0×10^{-4}
	35E	896	988	34.3			9.1×10^{-4}
	45W	0	143	46.0			8.0×10^{-4}
	55E	307	430	53.8			8.5×10^{-4}
	25E	609	742	24.9	MV11		6.3×10^{-4}
	35E	896	988	34.3			9.0×10^{-4}
	45W	0	143	46.0			8.2×10^{-4}
	55E	307	430	53.8			8.9×10^{-2}
	25E	609	742	24.9	MV12		4.4×10^{-2}
	35E	896	988	34.3			3.4×10^{-2}
	45W	0	143	46.0			8.7×10^{-2}
	55E	307	430	53.8			8.3×10^{-4}
	25E	609	742	24.9	MV13		4.1×10^{-4}
	35E	896	988	34.3			4.2×10^{-4}
	45W	0	143	46.0			4.9×10^{-4}
	55E	307	430	53.8			5.2×10^{-2}
	25E	609	742	24.9	MV14		5.1×10^{-2}
	35E	896	988	34.3			7.7×10^{-2}
	45W	0	143	46.0			8.6×10^{-2}
	55E	307	430	53.8			9.0×10^{-2}
	25E	609	742	24.9	MV15		6.8×10^{-4}
	35E	896	988	34.3			7.3×10^{-4}
	45W	0	143	46.0			9.6×10^{-4}
	55E	307	430	53.8			9.8×10^{-4}
	25E	609	742	24.9	MV16		8.1×10^{-2}
	35E	896	988	34.3			7.3×10^{-1}
	45W	0	143	46.0			1.1×10^{-1}
	55E	307	430	53.8		H**	2.0×10^{-1}
	25E	609	742	24.9	MV17		9.7×10^{-4}
	35E	896	988	34.3			8.3×10^{-4}
	45W	0	143	46.0			1.5×10^{-3}
	55E	307	430	53.8		H**	2.7×10^{-2}
	25E	609	742	24.9	MV18		6.8×10^{-2}
	35E	896	988	34.3			6.7×10^{-2}
	45W	0	143	46.0			9.8×10^{-2}
	55E	307	430	53.8		H**	2.0×10^{-2}
	25E	609	742	24.9	MV19		7.0×10^{-4}
	35W	896	988	34.3			8.2×10^{-4}
	45E	0	143	46.0			1.1×10^{-3}
	55E	307	430	53.8		H**	2.4×10^{-3}
	25E	609	742	24.9	CH6		5.7×10^{-2}
	35W	896	988	343			4.9×10^{-2}
	45E	0	143	46.0			1.2×10^{-1}
	55E	307	430	53.8		H**	1.4×10^{-2}
7	40E	0	164	40.0	MV6		6.4×10^{-2}
	50E	604	748	50.1			5.0×10^{-2}
	60E	266	389	***			5.7×10^{-2}
	70E	0	102	***			4.9×10^{-2}
	80W	189	220	79.4		IH	1.9×10^{-1}
	80W	225	277	76.2			6.9×10^{-2}
	40E	0	164	40.0	MV9		6.4×10^{-2}
	50E	604	798	50.1			7.6×10^{-2}
	60E	266	389	***			6.9×10^{-2}
	70E	0	102	***			7.6×10^{-2}
	80W	189	220	79.4		IH	1.0×10^{-1}
	80W	225	277	76.2			5.5×10^{-2}
8	20W	0	154	21.2	MV6		3.6×10^{-2}
	30W	189	292	28.8			3.8×10^{-2}
	40E	297	471	39.9			3.2×10^{-2}
	50W	476	579	503			3.7×10^{-2}
	20W	0	154	21.2	MV9		3.7×10^{-2}
	30W	189	292	28.8			4.7×10^{-2}
	40E	297	471	39.9			3.8×10^{-2}
	50W	476	579	50.3			3.5×10^{-2}

* Calibration Error. Actual Values Not Known.
** Speed Channel Inoperative This Run.
*** Speed Channel Inoperative This Run

Table 4-3. Model Variable and Channel List

Model Variable or Channel (CH)	Unit	Name
MV1	in	Carbody lateral displacement
MV2	rad	Carbody roll angle
MV3	rad	Carbody yaw angle
MV4	rad	Carbody longitudinal torsion
MV6	in	Truck A lateral displacement
MV7	rad	Truck A yaw angle
MV8	rad	Truck A warp angle
MV9	in	Truck B lateral displacement
MV10	rad	Truck B yaw angle
MV11	rad	Truck B warp angle
MV12	in	Wheelset 1 lateral displacement
MV13	rad	Wheelset 1 yaw angle
MV14	in	Wheelset 2 lateral displacement
MV15	rad	Wheelset 2 yaw angle
MV16	in	Wheelset 3 lateral displacement
MV17	rad	Wheelset 3 yaw angle
MV18	in	Wheelset 4 lateral displacement
MV19	rad	Wheelset 4 yaw angle
CH6	g	Sideframe lateral acceleration Axle-4 right side
CH62	g	Carbody vertical acceleration B-end right side

Table 4-4. Joint Displacement Summary

SPEED (MPH)	START TIME (SEC)	STOP TIME (SEC)	CONFIG-URATION	TAPE (ASU NO.)	DIR.	STANDARD DEVIATIONS SPEED (MPH)	MV8(TRUCK A WARP) (RAD)	MV11(TRUCK B WARP) (RAD)	CPROT-A (RAD)	CPROT-B (RAD)	BOSF-A (IN)	BOSF-B (IN)	SFVERT (IN)	HUNTING STATUS
15.0	0	143	C2		EB	0.324	0.775×10^{-3}	0.814×10^{-3}	0.524×10^{-3}	0.506×10^{-3}	0.506×10^{-2}	0.518×10^{-2}	0.142×10^{-1}	
25.0	476	620		U0524	WB	0.423	0.103×10^{-2}	0.942×10^{-3}	0.847×10^{-3}	0.570×10^{-3}	0.356×10^{-2}	0.567×10^{-2}	0.262×10^{-1}	
35.7	809	952		File 1	EB	1.100	0.113×10^{-2}	0.431×10^{-2}	0.941×10^{-3}	0.476×10^{-2}	0.901×10^{-2}	0.242×10^{-1}	0.989×10^{-1}	(1)
41.5	1009	1091			WB	0.647	0.125×10^{-2}	0.942×10^{-3}	0.869×10^{-3}	0.107×10^{-2}	0.801×10^{-2}	0.670×10^{-2}	0.101	
25.1	1152	1265	C3	U0524	EB	2.115	0.173×10^{-2}	0.137×10^{-3}	0.104×10^{-2}	0.129×10^{-2}	0.129×10^{-1}	0.270×10^{-1}	0.325×10^{-1}	
36.2	1311	1382		File 1	EB	0.800	0.877×10^{-3}	0.972×10^{-3}	0.592×10^{-3}	0.516×10^{-3}	0.451×10^{-2}	0.405×10^{-2}	0.387×10^{-1}	
47.9	1398	1541			WB	1.315	0.245×10^{-2}		0.358×10^{-2}		0.530×10^{-1}	0.618×10^{-1}	0.882×10^{-1}	(2)
41.5	1720	1864	C4	U0524	EB	1.548	0.912×10^{-3}		0.462×10^{-3}		0.642×10^{-2}	0.496×10^{-2}	0.540×10^{-1}	
52.8	1900	2022		File 1	WB	0.934	0.907×10^{-3}		0.800×10^{-3}		0.647×10^{-2}	0.854×10^{-2}	0.486×10^{-1}	
61.0	56	179		U0803	WB	1.883	0.100×10^{-2}		0.106×10^{-2}		0.882×10^{-2}	0.869×10^{-2}	0.485×10^{-1}	
65.3	189	292		File 1	WB	1.732	0.103×10^{-2}		0.123×10^{-2}		0.973×10^{-2}	0.135×10^{-1}	0.518×10^{-1}	
70.5	108	210		U0803	WB	1.668	0.204×10^{-2}	0.186×10^{-2}	0.365×10^{-2}	0.178×10^{-2}	0.566×10^{-1}	0.438×10^{-1}	0.107	(3)
75.1	0	102		File 2	WB	2.016	0.256×10^{-2}	0.223×10^{-2}	0.423×10^{-2}	0.232×10^{-2}	0.851×10^{-1}	0.616×10^{-1}	0.121	(3)
24.9	609	742	C6		EB	0.403	0.802×10^{-3}					0.187×10^{-2}	0.313×10^{-1}	
34.3	896	988		U0732	WB	0.301	0.108×10^{-2}					0.530×10^{-2}	0.433×10^{-1}	
46.0	0	143		File 2	EB	0.657	0.946×10^{-3}					0.690×10^{-2}	0.808×10^{-1}	
53.8	307	430			EB	1.398	0.149×10^{-2}					0.853×10^{-2}	0.103	(4)

NOTES: (1) B-Truck Hunting
(2) Intermittent Hunting, Both Trucks
(3) Both Trucks Hunting
(4) Truck A Hunting

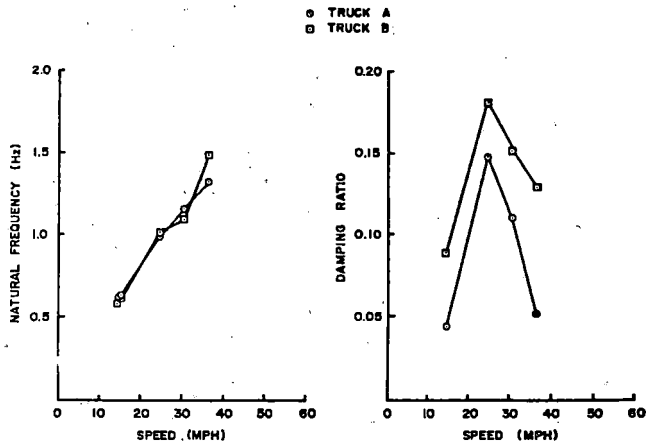

Figure 4-10. Configuration 1 Frequency and Damping Characteristics

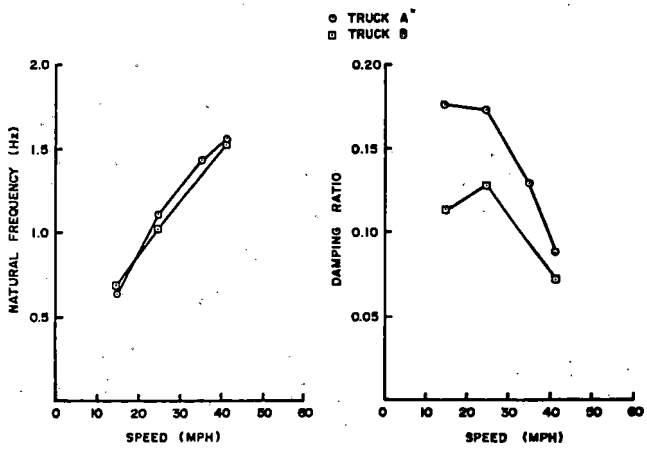

Figure 4-11. Configuration 2 Frequency and Damping Characteristics

In Figure 4-10 the Configuration 1 damping-ratio plot shows a very uncharacteristic shape in that is has low damping ratios at the slowest speeds. A second estimate of the lowest speed (15 mph) damping ratios for both Trucks A and B from a different time segment yielded adjusted values of zero damping indicating unstable or nearly unstable behavior. These latter data points are not shown in the figure. Two separate portions of the 15-mph Configuration 1 test run were chosen for analysis because the time responses appeared somewhat different in nature between the two. The portions yielding the zero damping-ratio estimates actually contained portions of oscillatory behavior somewhat like the low-amplitude intermittent hunting discussed earlier in this chapter. Observations of track data plots revealed no differences in track between the two test sections, so the reasons for the different behavior are not known.

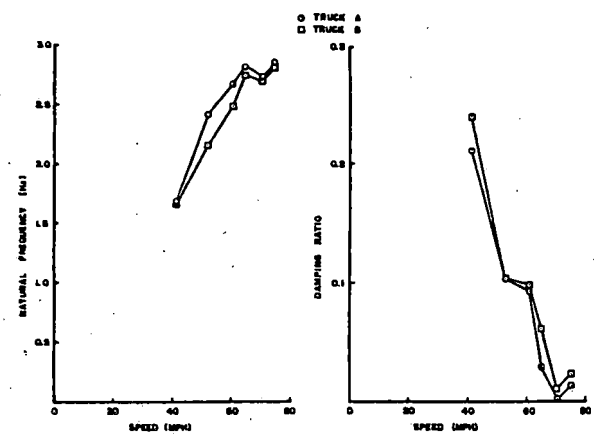

Figure 4-12. Configuration 4 Frequency and Damping Characteristics

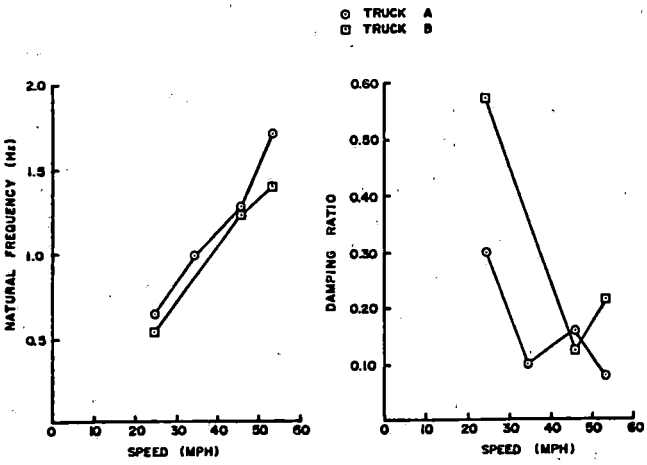

Figure 4-13. Configuration 6 Frequency and Damping Characteristics

In Figure 4-11 the Configuration 2 damping-ratio estimates are plotted without the 35-mph Truck B data point because Truck B was hunting during this test run. As shown in Table 4-5 the frequency is higher, and the damping ratio lower for this speed on Truck B. The high frequency, low damping behavior is characteristic of most of the hunting conditions we analyzed from the field tests.

The Configuration 3 data from Table 4-5 is not plotted because only two speeds below hunting were recorded. Typically, the 45-mph data for this configuration shows the high-frequency, low-damping behavior characteristic of hunting. We should also point out that the goodness-of-fit measure from our Random-Decrement analysis was generally lower (indicating a better fit) for hunting test runs than for others. This means that the Random-Decrement signature was closer in shape to the assumed exponentially decaying sine wave curve for these runs than it was for others.

Table 4-5. Random Decrement Analysis Results

CONFIG-URATION	NOMINAL SPEED (MPH) AND DIRECTION	TRUCK A RESULTS							TRUCK B RESULTS							HUNTING STATUS
		START TIME (SEC)	STOP TIME (SEC)	ACTUAL SPEED (MPH)	NATURAL FREQUENCY (Hz)	DAMPING RATIO	FIT	ADJUSTED DAMPING RATIO	START TIME (SEC)	STOP TIME (SEC)	ACTUAL SPEED (MPH)	NATURAL FREQUENCY (Hz)	DAMPING RATIO	FIT	ADJUSTED DAMPING RATIO	
1	15E	0	148	14.8	0.63	0.096	24%	0.044	0	148	14.8	0.58	0.127	17%	0.089	
	15E	148	297	15.7	0.62	0.073	14%	(1)	148	297	15.7	0.64	0.080	9%	(1)	
	25W	481	630	24.9	0.98	0.173	26%	0.147	481	630	24.9	1.01	0.201	29%	0.181	
	30E	783	932	30.5	1.15	0.131	34%	0.110	783	932	30.5	1.09	0.167	28%	0.151	
	35W	1029	1178	36.1	1.31	0.086	25%	0.051	1029	1178	36.1	1.49	0.159	17%	0.129	
2	15E	0	148	15.0	0.64	0.180	20%	0.176	0	148	15.0	0.69	0.117	7%	0.112	
	25W	476	625	25.0	1.11	0.173	12%	0.173	476	625	25.0	1.03	0.131	17%	0.128	
	35E	870	968	35.7	1.44	0.137	20%	0.128	809	957	35.7	2.46	0.076	24%	0.058	
	45W	1009	1157	41.5	1.56	0.091	30%	0.088	1009	1091	41.5	1.53	0.078	36%	0.073	
3	25E	1152	1265	25.2	1.15	0.203	15%	0.197	1152	1265	25.2	1.06	0.208	15%	0.202	
	35E	1311	1388	36.2	1.56	0.116	17%	0.110	1311	1388	36.2	1.49	0.247	43%	0.247	
	45W	1398	1546	47.9	2.76	0.021	5%	(1)	(2)							
4	40E	1720	1869	41.5	1.69	0.220	13%	0.212	1720	1869	41.5	1.66	0.248	22%	0.240	
	50W	1900	2022	52.8	2.43	0.108	22%	0.103	1900	2022	52.8	2.16	0.103	17%	0.103	
	60W	56	184	61.0	2.68	0.106	33%	0.093	56	184	61.0	2.49	0.111	28%	0.098	
	65W	189	297	65.3	2.84	0.051	27%	0.027	189	297	65.3	2.75	0.075	18%	0.061	
	70W	108	210	70.5	2.74	0.026	7%	(1)	108	210	70.5	2.70	0.035	9%	0.010	(4)
	75W	0	102	75.1	2.86	0.034	12%	0.013	0	102	75.1	2.83	0.045	16%	0.023	(4)
6	25E	609	748	24.9	0.64	0.301	14%	0.301	609	748	24.9	0.53	0.570	8%	0.570	
	35W	896	993	34.3	0.99	0.101	16%	0.101	(3)							
	45E	0	148	46.0	1.29	0.161	16%	0.161	0	148	46.0	1.24	0.125	28%	0.125	
	55E	297	430	53.8	1.71	0.092	16%	0.077	307	430	53.8	1.40	0.218	32%	0.214	(5)

NOTES:
(1) *No solution obtained from damping ratio adjustment program.*
(2) Not enough stable data to analyse.
(3) Noisy data--not able to analyse.
(4) Both trucks hunting.
(5) Truck A hunting.

The Configuration 4 data shown in Figure 4-12 shows unusual behavior at both the 70- and 75-mph speeds. Two observations need be made about these test speeds. First, because hunting occurred at both of these speeds, it is not unexpected that discontinuities would occur in the frequency and damping-ratio curves. However, on other configurations hunting was accompanied by increases in natural frequency above expected values, not decreases, as shown here. The second observation is that the 70- and 75-mph runs were made on a different day than the lower speed runs introducing the possibility that conditions may have changed over time. One possibility is that the pressure in the air bags may have changed due to temperature changes, leakage or some other cause. The friction characteristics of the truck may also have changed. The actual reasons for the anomolous behavior at these two speeds are not known, however.

Figure 4-13 shows the Configuration 6 frequency and damping-ratio estimates. Most notable here are the very high damping ratios of Truck B. This is consistent with observations that Truck B hunting began at about 80 mph, substantially above the speed shown here. The 35-mph data point is not plotted for Truck B because a very poor Random-Decrement signature was obtained for this speed. The time history of Truck B Lateral Displacement at this speed showed the presence of fairly high amplitude, short-duration (about one cycle) transients. These transients are believed to be spurious. They interfered with the Random-Decrement signature formation process sufficiently to render the frequency and damping-ratio estimates suspect for the 35-mph test run.

We also attempted analysis of the damping ratio and natural frequency for one of the loaded vehicle (Configuration 8) tests, but we had little success in obtaining a good random decrement signature for these cases. This difficulty probably indicates the presence of two or more closely spaced dynamic modes in the test vehicle. The lack of a single well-defined peak on the PSD plots can be observed on the plots of Appendix B for these test runs.

In addition to the Random-Decrement analysis, we obtained damping ratios from the PSDs using the method described in Chapter 3. A comparison of estimates made by the two methods on the same data is shown in Table 4-6. Both methods yielded what is for practical purposes the same estimates. Because the PSD estimates are unadjusted, they are compared to the unadjusted values of from the Random-Decrement analysis in this table.

Table 4-6. Comparison of Damping Ratios Estimated from PSD and Random Decrement Methods

Config-uration	Speed (MPH)	Damping Ratio	
		PSD	Random Decrement
2	15	0.19	0.18
	25	0.17	0.17
	35	0.080	0.14
	45	0.072	0.091
3	25	0.27	0.20
	35	0.12	0.17
	45	0.068	0.021
6	25	0.27	0.30
	35	0.11	0.10
	45	0.13	0.16
	55	0.072	0.092

Hydraulic Forcer Results

The hydraulic forcer system described in Chapter 3 provided a set of initial displacement and rotation conditions for the test vehicle. Upon release of the pressure in the hydraulic forcers, the test vehicle responded to the imposed initial conditions. The Configuration 6 Truck A forcer response was analyzed using the logarithmic decrement technique, as described in Chapter 3.

Figure 4-14 shows a typical response of the Truck A Lateral Displacement during a forced test run at 25 mph. Both positive and negative pairs of successive peaks were used to compute a large number of damping ratios for each test speed. Damping ratios were averaged to give the results shown in Figure 4-15. The bands shown in the figure delineate the plus and minus one standard deviation levels. Figure 4-15 also shows the natural frequencies found during the forcer runs.

The damping ratios shown in Figure 4-15 are about an order or magnitude less than those found for Configuration 6 during the unforced runs. Two reasons may account for this discrepancy.

First, the logarithmic-decrement technique is derived assuming there are no forces on the system after release from the initial conditions. In our application the forces due to random rail irregularities are always present. The section of track on which these tests were run was selected because it was relatively good track. Nonetheless, the forcer-response data is contaminated by the random track forcing. It can be observed in Figure 4-14 that there are several occasions when the displacement increased between successive peaks. These increases in peak value result from the rail forcing.

The forced response for the loaded test car suffered even greater contamination from the rail irregularities. During these runs, it is impossible to determine when the forcers were applied by observing time responses. The forcers provided a relatively small portion of the input for these cases, and the resulting motion was almost entirely due to rail forcing.

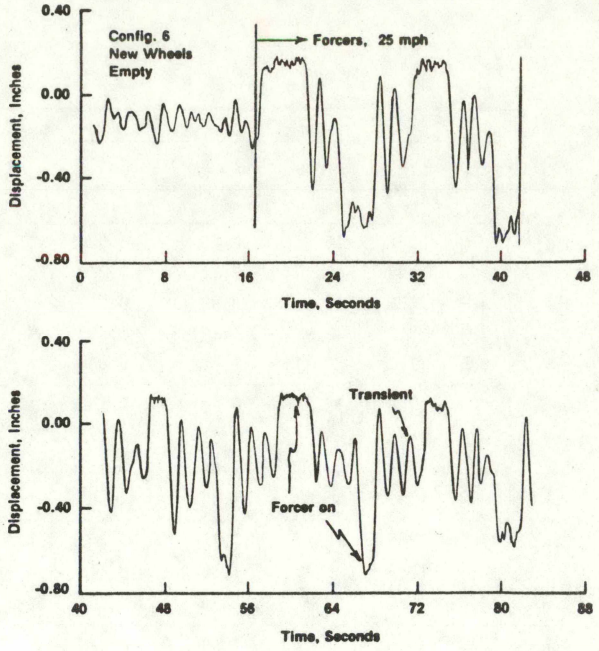

Figure 4-14. Truck Lateral Displacement Using Hydraulic Forcers

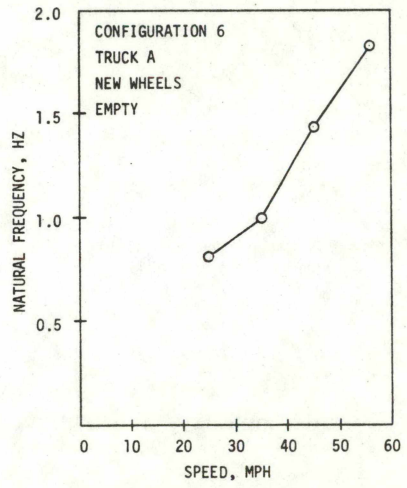

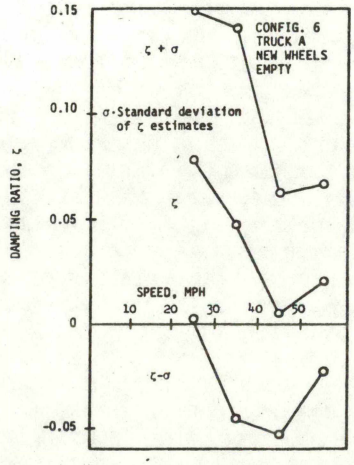

Figure 4-15. Natural Frequency and Damping Ratio Estimates from Forcer Tests

Nonlinearities in the test vehicle also account for some of the differences between the damping-ratio estimates from the forced and unforced tests. For a nonlinear system such as the test vehicle the effective damping decreases with increased amplitudes of motion. Because the forced runs began with the flanges hard against the rails during the unloaded vehicle runs, the amplitudes were near maximum values. In contrast during unforced runs the amplitudes were smaller. As a result, smaller estimates of damping ratio would be expected for the forcer test runs.

The particularly low value of damping ratio found for the 45-mph run can be explained by viewing a portion of time response from the run. See Figure 4-16. This figure shows that the truck is actually hunting between forcer applications. Hunting subsides as the forcers cause flange contact to occur. This behavior is in contrast to the stable 45-mph behavior observed during the unforced runs and is believed to be due in part to the large-amplitude initial displacement caused by the forcers. This does not, however, explain the essentially stable behavior at 55 mph during the forced runs, when Truck A hunted continuously during the 54 mph unforced run.

The natural frequency estimates shown in Figure 4-15 are in every case somewhat higher than those from the unforced runs. This is probably due to the high amplitudes of motion occurring in the forced runs. The test results in general show a fairly consistent trend in which higher amplitudes of motion are associated with higher frequencies.

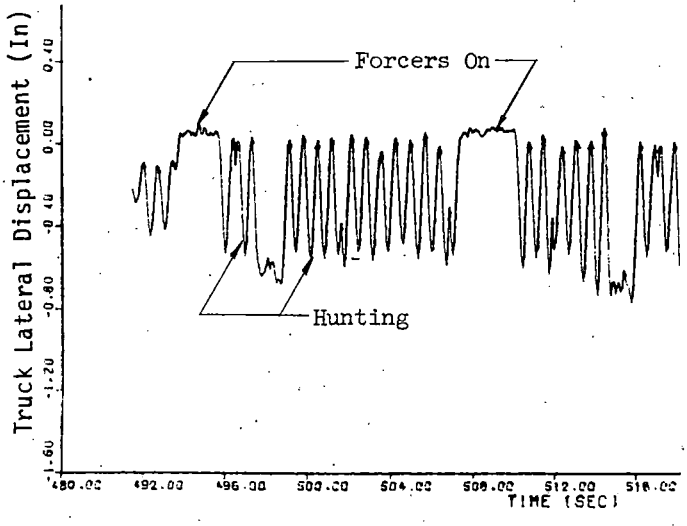

Figure 4-16. Hunting between Forcer Applications on the 45-MPH Test Run for Configuration 6

RANDOM-RESPONSE ANALYSIS

The random-response analysis described in this section utilized the random-data-analysis computer program discussed in Chapter 3. This type of analysis has proven to be useful in studying the dynamic behavior of the test vehicle. In particular, the PSD results can be compared directly to predictions of power spectra from analysis, and they can be analyzed directly to obtain information about the test vehicle behavior. We discuss below typical results from the various types of random response analysis performed.

Power Spectral Densities

Power spectral densities were computed for both Truck A and B Lateral Displacements for all configurations on tangent track at all test speeds. In addition, for the Configuration 6 runs PSDs were computed for all available 19-DOF model variables. Plots of these results, consisting of 150 different data sets, are contained in Appendix B. These PSDs correspond to the test runs described in Table 4-2 where the standard deviations for each of the test runs analyzed are tabulated.

When viewing or using the results of our PSDs it should be remembered that we plot only the positive half of a two-sided PSD spectrum. Our plotted values are therefore just one half the value of those corresponding to a single-sided spectrum.

Figure 4-17 shows a typical set of PSD plots taken from the set included in Appendix B. Of primary importance are the dominant peaks on these plots, which range in frequency from about 0.6 Hz for the 14.8-mph run to about 2.5 Hz for the 46.7-mph run. Each peak represents the energy associated with the least-damped system mode, which for this vehicle was the kinematic mode. The center frequencies of these peaks are the damped natural frequencies of the corresponding least-damped modes. These are essentially the frequencies plotted in Figures 4-10 through 4-13.

As we indicated earlier, the shape of the predominant peak contains information about the damping ratio of the associated dynamic mode. The low-amplitude, wide peak shown on the Truck B Lateral Displacement plot for 14.8 mph in Figure 4-17 represents fairly high damping, while the high-amplitude, narrow peak of the Truck A Lateral Displacement plot at 46.7 mph represents low damping. Truck A was actually hunting during the 46.7-mph test run. As discussed earlier, the PSDs were used to estimate damping ratios.

The minor peak at about 8Hz in the Truck A Lateral Displacement plot for 46.7 mph is associated with the wheel rotation rate. This peak is observable on many of the PSD plots.

The noise spikes at 20 and 40 Hz have been associated with the motor-generator set on the AAR-100 Research Car. This noise in no way interfered with the analysis of the data since the frequency range was above the range in which we are interested.

Autocorrelation Functions

Autocorrelation functions were computed for many of the test runs. Figures 4-18 and 4-19 show autocorrelation functions for stable and hunting runs respectively. On a stable test run, where the dominant peak on the PSD plot is small, oscillations of the autocorrelation function will

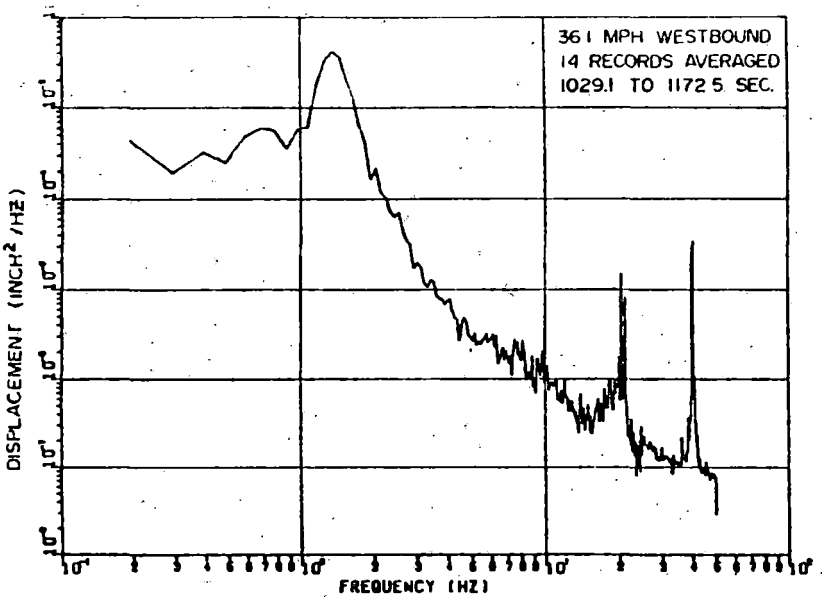

a. TRUCK-A LATERAL DISPLACEMENT

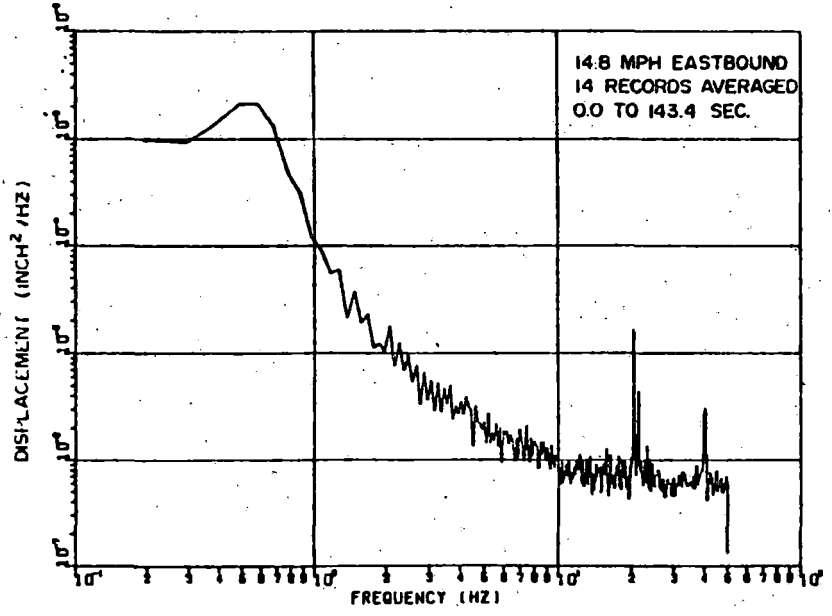

c. TRUCK-B LATERAL DISPLACEMENT

Figure 4-17. Selected Configuration

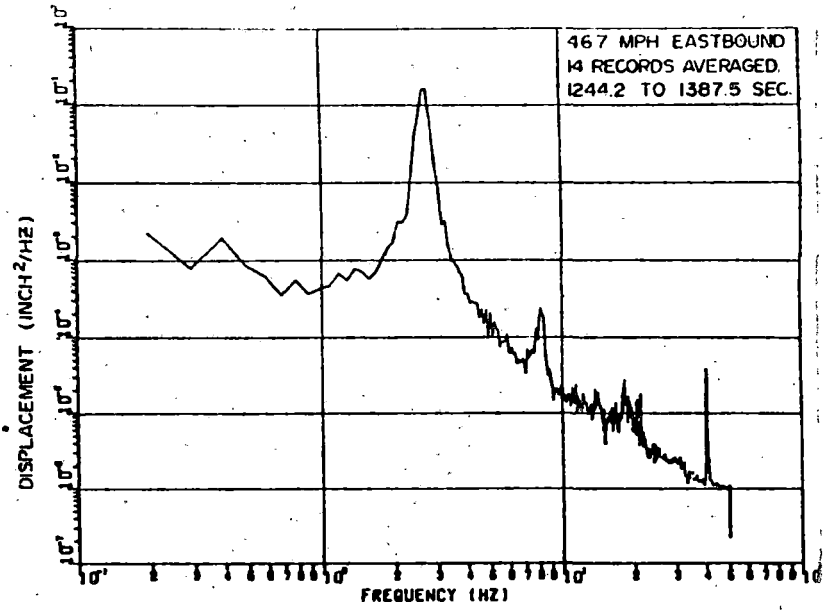

b. TRUCK-A LATERAL DISPLACEMENT

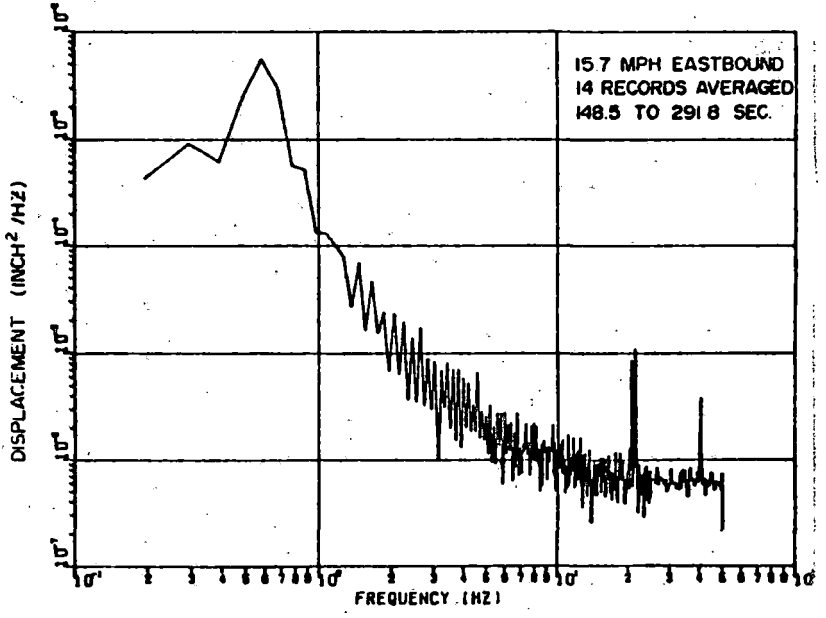

d. TRUCK-B LATERAL DISPLACEMENT

1 Power Spectral Densities

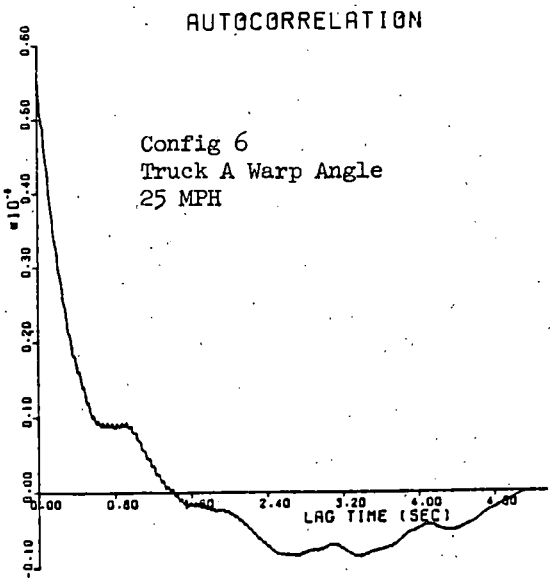

Figure 4-18. Typical Autocorrelation Function for Stable Behavior

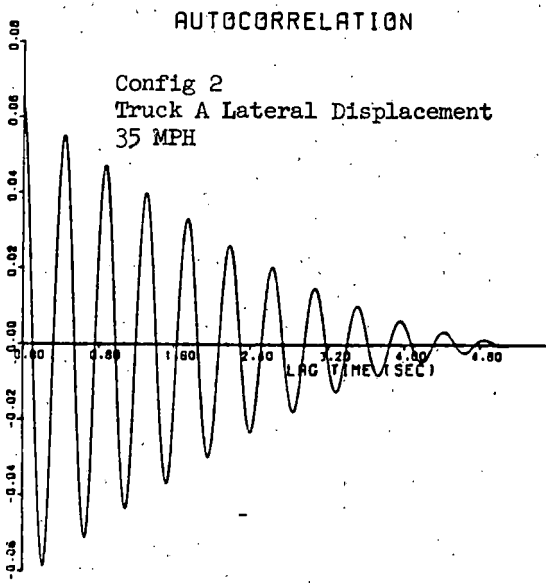

Figure 4-19. Typical Autocorrelation Function for Hunting Behavior

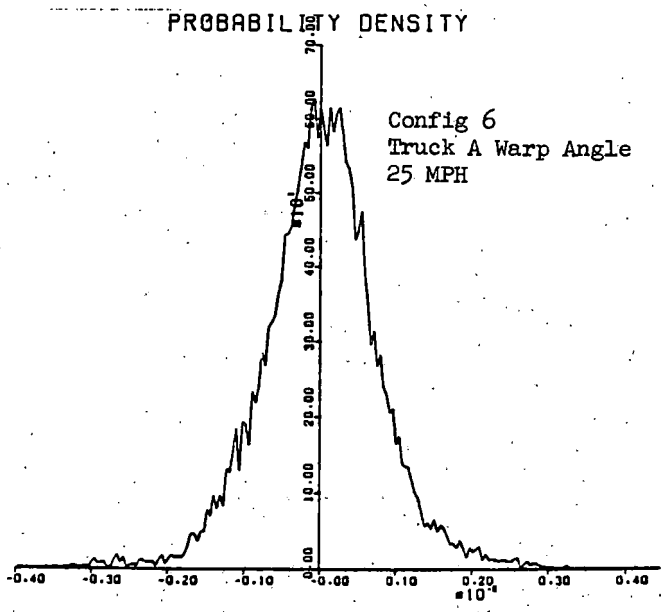

Figure 4-20. Typical Probability Density Function for Stable Behavior

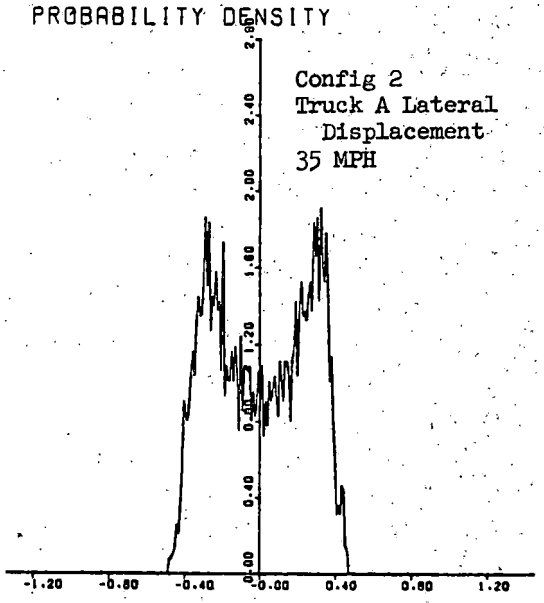

Figure 4-21. Typical Probability Density Function for Hunting Behavior

be small, as seen on Figure 4-18. In contrast when the behavior of the test vehicle is highly oscillatory, as it is in hunting situations, the PSD plot will have a narrow peak and the autocorrelation function will be highly oscillatory as seen in Figure 4-19. In this case the frequency of the oscillation on the autocorrelation function corresponds to the damped natural frequency of the least-damped mode, and damping information is contained in the shape of the envelope of the signal although it cannot be readily obtained by log decrement methods. The frequency shown on Figure 4-19 is about 2.3 Hz and corresponds to the hunting frequency of Configuration 2 Truck A at 35 mph.

Probability Density Functions

In conducting theoretical analysis of randomly forced dynamic systems in general, and of rail vehicles in particular, it is important to know the shape of the probability density functions of the random signals. We computed a sufficient number of probability density functions to conclude that for stable conditions, most of the variables had Gaussian-like density functions. Figure 4-20 shows an example of this form the Configuration 6 25-mph test run.

In contrast, for a hunting vehicle the probability density function exhibits a shape that is characteristic of the density function for a sine wave plus random noise. This may be seen in the Configuration 2 density function of Figure 4-21.

We should note that our probability density functions are actually histograms that show the relative number of data points falling into uniformly spaced regions of the test variable. Therefore they do not integrate to a value of one as a true probability density function does. If they are normalized to an integral value of one then they actually become probability density functions.

Transfer Function Analysis

We conducted a limited analysis of the field test data using the transfer function capability of the random-data-analysis computer program. This analysis was confined to Configuration 6 at 25 and 55 mph.

The three functions of primary interest to us in this analysis are the transfer function magnitude, transfer function phase, and the coherence function. The transfer function magnitude and phase give information on the mode shapes, and the coherence function provides a measure of the confidence one can place in the analysis. These three functions are shown in Figures 4-22 through 4-24 for the Configuraton 6 55-mph test run. The transfer function plotted in Figure 4-22 is the ratio of Truck B Lateral Displacement to Truck A Later Displacement. The corresponding phase angle is plotted in Figure 4-23. At low frequencies it can be observed that the magnitude is about one and the phase angle is about -180°.

At the system eigenvalues or natural frequencies the transfer function can be related to the system eigenvectors or amplitude and phase relationships. For example, a large negative spike occurs in the transfer function at about 1.9 Hz in Figure 4-22. The phase angle here is 180°. This is believed to be associated with Truck A hunting behavior during the 55-mph run. The amplitude of Truck A lateral displacement was high since it was hunting, so the transfer function ratio is low.

The highest positive peak, at about 1.7 Hz, is believed to be associated with the Truck B least-damped mode. The magnitude is larger than one indicating a larger amplitude for Truck B lateral displacement. Here the phase angle is -180°.

It is tempting to compare these mode shapes with those predicted analytically, but we should first look at the coherence function of Figure 4-24. The coherence function can be viewed as a measure of confidence in the results of the transfer function analysis.

A little background information on coherence function will be useful for this discussion. For a linear system in which both variables of the transfer function are caused by the same inputs, and the variables are measured without noise, the coherence function has a value of one at all frequencies. In the field test results, the same inputs operate on both variables, in this case track irregularities forcing both trucks. The measurements also have good signal-to-noise

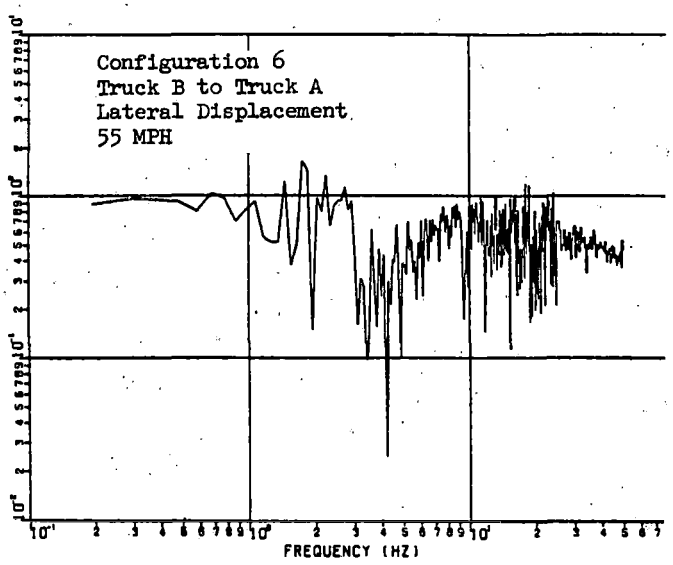

Figure 4-22. Transfer Function Magnitude

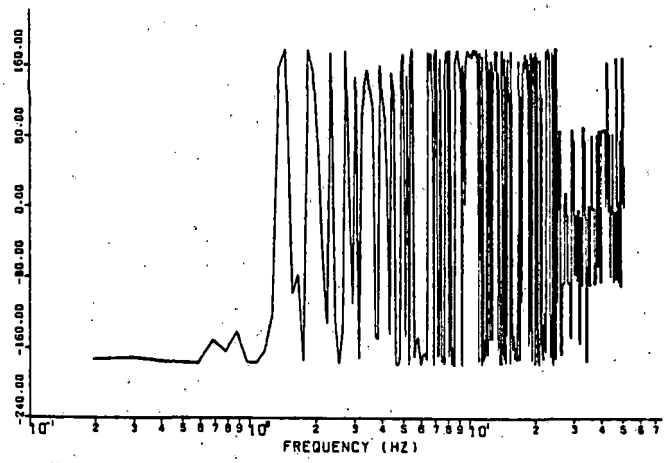

Figure 4-23. Transfer Function Phase

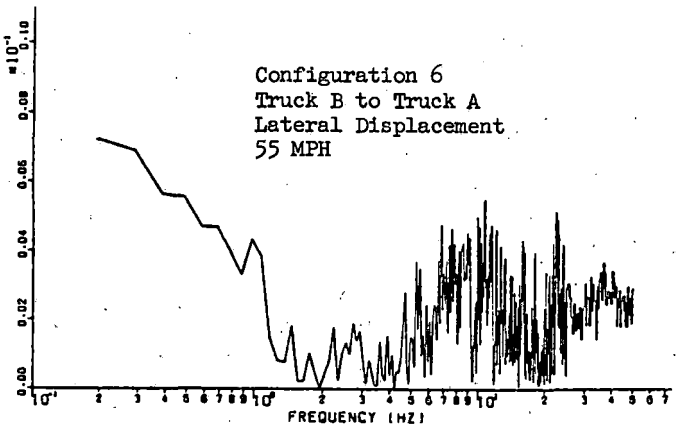

Figure 4-24. Coherence Function

ratios. Thus, if the system were linear, then a high value of coherence function, near unity, would be expected. In this case, the coherence is between two and three orders of magnitude below unity. We have concluded this low value of coherence results from the nonlinearities in the test vehicle.

In view of the low value of coherence we are reluctant to put a large amount of confidence in the results of the transfer function analysis. More investigation is required before these results can be interpreted with confidence.

OBSERVATIONS AND CONCLUSIONS

A number of useful observations and conclusions can be drawn from analysis of the test results presented in this chapter. Since the test vehicle is in many ways typical of freight vehicles in use in North America, many of the trends observed in these tests would also be found in vehicles in revenue service.

Observations

1. No such thing as a unique hunting speed exists for a given vehicle configuration. Instead, a hunting speed range exists. In the slower portion of this speed range, hunting may be intermittent. Above some speed in this range sustained hunting always occurs.
2. Two types of intermittent hunting have been identified. We have called these low-level and high-level intermittent hunting, as distinguished by their magnitude. All sustained hunting we observed was of high amplitude. All three types of hunting can occur on a test vehicle in a given configuration.
3. The hunting speed ranges for the eight configurations are shown in Figure 4-8. C2, the unloaded car with lubricated centerplates and CN wheels, had the lowest hunting speed range. C1, the same vehicle with dry centerplates, had a slightly higher hunting speed range. C3 and C5 followed C1 in order of increasing speed range. C3 was the C2 vehicle with the addition of a lightly loaded constant-pressure side-bearing device, and C5 was the C2 vehicle with a yaw stiffener. C8, the loaded C2 vehicle, came next. C6, the unloaded vehicle with lubricated centerplates and AAR wheels, showed vastly different hunting characteristics between its two trucks. The average hunting speed range of the two C6 trucks was about the same as that of C4; C4 was the C2 vehicle with a heavily loaded constant-pressure sidebearing device. The highest hunting speed range belonged to C7, the loaded C6 vehicle.
4. All of the vehicle stabilizaton devices tested increased the hunting speed range of the vehicle. This can be seen by observing that C3, C4, and C5 all had higher hunting speed ranges than C2.
5. In general the test vehicle's least-damped natural frequency increased nearly linearly with speed, and the associated damping ratio decreased with speed.
6. Trucks A and B of C6 showed substantially different hunting and damping characteristics. Trucks A and B of all other configurations showed nearly the same characteristics. The same trucks were used in all test configurations; only the wheelsets were changed. C6 and C7 shared the AAR wheelsets, and the other configurations shared the CN wheelsets. Truck B of C6 had a much higher hunting speed than Truck A, and it had higher damping than Truck A at speeds below hunting. The Truck B wheelsets were quite new, while the Truck A wheelsets had accumulated more miles. The Truck B wheelsets had a very narrow wear band outside of which the wheels were in the as-cast condition. The Truck A wheelsets had a much wider polished area on the tread surface.
7. Damping ratios estimated from the forced runs were substantially lower than those estimated from the unforced runs. During the forced runs, the wheels were forced into flange contact then released resulting in substantially larger wheelset excursions on the forced runs than on the unforced runs.
8. Power spectral densities showed large power levels to be associated with the test vehicle's least-damped mode. The PSDs for the unloaded configurations generally showed no other dominant peaks.
9. Very low coherence was found to exist between the lateral motions of Trucks A and B. In contrast, when time histories of these lateral motions were superimposed, the responses were found to be strikingly similar.
10. Vehicle motions became more nearly sinusoidal at and near hunting speeds, and more nearly Gaussian at speeds well below hunting.

Conclusions

1. The test vehicle contained significant nonlinearities. These nonlinearities strongly influence the behavior of the vehicle in all configurations. The hunting characteristics give a clear indication of nonlinear behavior. If the test vehicle had been linear, a single critical speed could have been identified above which hunting always occured and below which it never occured. If the test vehicle had been linear, the same damping ratios would have been estimated from both forced and unforced tests. If the vehicle had been linear, a high value of coherence would have been found between lateral displacements of Trucks A and B. Clearly the hopper car was nonlinear.
2. The kinematic mode of the test vehicle dominated the response of the vehicle. It is fairly well recognized by now that the

kinematic mode of a rail vehicle exhibits a frequency that is nearly directly proportional to speed. This was found to be the case in our tests. The PSD analysis clearly shows the majority of energy to be associated with the kinematic mode. This mode is so strong that it can be observed directly in the time response of the vehicle.

3. Surface conditions at the interface between the wheel and rail significantly affect the vehicle's behavior. The only identifiable difference between Trucks A and B in the C6 tests was the wheel condition. Yet these Trucks responded quite differently during the tests, with the truck having the newer wheelsets possessing more stability than the other truck.
4. The stability of the vehicle on tangent track is increased by adding rotational stiffness to the truck. This can be observed directly by noting that C5, which used truck stiffeners, had greater stability than C2 which was identical except for the stiffeners.
5. The stability of the vehicle on tangent track is increased by adding rotational friction to the trucks. This can be observed by noting that C1, the vehicle with dry centerplates, had greater stability than C2. In addition C3 and C4, with the constant-contact sidebearing devices, showed greater stability than C2. The increased rotational friction of C1, C3, and C4 over that of C2 was achieved by means of increased Coulomb or sliding friction. It is important to recognize that when these friction elements are not sliding, that is, they are locked, the net effect is to add rotational stiffness. Consider that a truck with locked centerplate is very stiff. So the increased rotational friction has the effect of increasing rotational stiffness during times when the friction surfaces do not slide.

CHAPTER 5
EXPERIMENTAL AND THEORETICAL COMPARISONS

INTRODUCTION

The results of our efforts to compare and obtain agreement between experimental and theoretical, results for the dynamic behavior of a rail freight car are discussed in this chapter. These results must be regarded as a first step, as our effort in this aspect of the project was limited by several factors. The lack of zero calibration values for the wheel-rail transducer data precluded determination of the absolute wheel-rail displacements needed for comparison of behavior in curving and creep situations. Thus, the scope was limited to tangent track dynamics. Furthermore, our efforts in the comparison of behavior on tangent track were also limited by the time and manpower available to the project. Numerous ideas that might lead to better correlation between theory and experiment could not be pursued within the time and effort constraints of the project.

A nine degree of freedom freight car model and sub-sets of this model were used throughout this effort. The model and associated analysis techniques are described in [5-1, 5-2]. Experimental data was compared with results from the following three analysis methods: linear eigenvalue-eignevector analysis, quasi-linear statistical linearization analysis, and direct analog integration employing a hybrid computer. The discussion that follows is organized around these three analysis approaches.

LINEAR STABILITY ANALYSIS

The first step in this effort involved comparing the damping ratio and frequency versus speed characteristics obtained via random decrement and spectral analysis of the experimental data with corresponding characteristics obtained by a linear eigenvalue analysis. The nine degree of freedom model described in [5-1], was chosen here for two reasons. First, a theoretical comparison of the 9 and 17 DOF linear analyses indicated that the two results approached the same result when the sideframe to axle connections were relatively rigid in translation [5-1]. In the case of the 3 piece freight truck, these conditions are met as long as there is no sliding at the bearing adapter. Secondly, the measurements of axle-sideframe motion demonstrated that virtually no relative translational motion occurs here unless the vehicle is hunting. Thus, for speeds below hunting, the 9 DOF model should be adequate.

Model Description

The nine degree of freedom model accounts for the lateral, yaw and warp motions of each truck, as depicted in Figure 3-4. The remaining 3 degrees of freedom describe the lateral, yaw and roll behavior of the car body.

The linear analysis approach requires estimates of linear equivalent values for the nonlinear suspension elements and wheel-rail geometric functions. Sinusoidal input describing functions were used to obtain these values. In the case of the wheel-rail geometry, the describing function values are nearly constant for both the AAR Standard and CN Profile A wheels if the wheel-rail relative motion does not reach flange contact. These values, corresponding to small wheelset motions, were used. Equivalent linear values and corresponding creep coefficients obtained by Kalker's linear theory [5-3] for the CN Profile A (Configurations 1-5, 8) and AAR Standard profile (Configurations 6, 7) wheels are given in Table 5-1. Keep in mind that the actual creep values depend on wheel and rail surface conditions, and may be as low as 10% of the values computed here.

Table 5-1. Wheel-Rail Geometry and Creep Coefficients

	AAR 1/20 STD	CN PROFILE A
Conicity,	0.050	0.1550
Contact Angle Coef.,	0.0	6.159
Wheelset Roll Coef.,	0.050	0.0516
Lateral Creep Coef.*	1.150×10^6 lb	1.362×10^6 lb
Longitudinal Creep Coef.*	1.262×10^6 lb	1.451×10^6 lb
Lateral/Spin Creep Coef.*	6750 lb-ft	8851 lb-ft

*Values are from Kalker's theory [5-3] for the light car.

The suspension nonlinearities posed a more difficult problem. In the first step, "nominal" amplitudes and frequencies were chosen to calculate the sinusoidal input describing functions. Statistics for the actual motions across the nonlinear suspension elements were not initially available. Consequently, "nominal" amplitudes were chosen after a brief survey of the raw test data. These nominal values and corresponding sinusoidal input values for the freight truck suspension elements are given in Table 5-2.

Table 5-2. Nominal Sinusoidal Input Describing Function Values

COMPONENT	DISPLACEMENT	STIFFNESS	DAMPING*
VERTICAL BOLSTER/SIDEFRAME	± 0.10 inch	443,000 lb/ft	39,580 $\frac{lb}{(ft/sec)}$
LATERAL BOLSTER/SIDEFRAME	± 0.10 inch	390,700 lb/ft	34,630 $\frac{lb}{(ft/sec)}$
WARP	± 0.005 radian	5.99×10^6 $\frac{ft\text{-}lb}{rad}$	91,420 $\frac{ft\text{-}lb}{(rad/sec)}$
YAW CENTERPLATE	± 0.005 radian	0	72,000 $\frac{ft\text{-}lb}{(rad/sec)}$

*Damping values computed for f = 2.0 Hz

Comparison of Theoretical and Experimental Results

Configuration 6, the light car with AAR Standard wheel profiles, was chosen for the initial comparisons in an attempt to eliminate the effects of nonlinear wheel-rail geometry and rail head profile variations. The low conicity, straight taper wheel profile leads to very linear geometric constraint functions (until flange contact is reached) that are insensitive to the rail head profile.

The equations of motion and eigenvalue solution method for the 9 degree of freedom freight car model used in this study are described in another report [5-2]. Frequency and damping ratios found for the least damped mode (a "kinematic" mode) for Configuration 6 are plotted as a function of vehicle speed in Figure 5-1, along with the experimental data for this configuration. The percentage of the theoretical creep coefficients computed by Kalker's theory [5-3] is a parameter in this figure. Note the strong dependence of the damping ratio and critical speed on the creep coefficients. A change in these coefficients from 25% to 100%

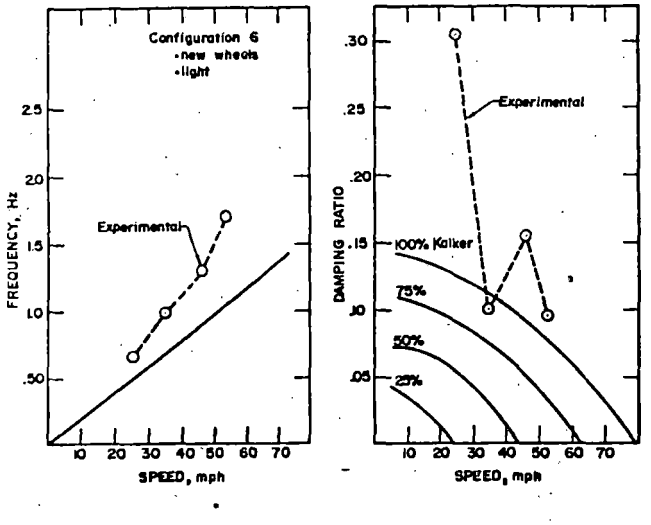

Figure 5-1. Damping Ratio and Frequency for Nominal Describing Function Values

of the theoretical values increases the critical speed from 24 mph to 78 mph. This trend runs counter to our expectation that the vehicle is increasingly stable as the creep coefficients decrease. Quite obviously, neither the frequencies nor the damping ratios of the experimental points are close to the theoretical values shown in this figure.

A closer look at the amplitudes of the motion across the nonlinear elements indicated that in many cases, particularly at lower speeds, these relative motions were smaller than those given in Table 5-2. A new set of relative displacement estimates, all smaller than those previously used, was assembled. This new set of displacements, and the corresponding sinusoidal input describing function values are given in Table 5-3.

Table 5-3. Small Amplitude Sinusoidal Input Describing Function Values

COMPONENT	DISPLACEMENT	STIFFNESS	DAMPING*
VERTICAL BOLSTER/SIDEFRAME	± 0.02 inches	2.129×10^6 lb/ft	3.688×10^5 ft-lb/rad/sec
LATERAL BOLSTER/SIDEFRAME	± 0.02 inches	2.030×10^6 lb/ft	0
WARP	± 0.0005 rad.	1.228×10^7 ft-lb/rad	1.586×10^6 lb/ft/sec
CENTERPLATE YAW	± 0.0005rad.	2.485×10^6 ft-lb/rad	1.538×10^6 ft-lb/rad/sec

*Damping values are computed for f = 0.75 Hz.

Frequency and damping ratios of the least damped mode as a function of vehicle speed for Configuration 6 with the suspension parameters of Table 5-3 are shown in Figure 5-2. The experimental data for this configuration is also shown in this figure. Note that the damping ratio still demonstrates a strong dependence on the creep coefficients, but that here increasing creep coefficients causes a decrease in stability, in line with our expectations. In this figure, the experimental damping ratio data falls within the range of uncertainty in the creep coefficients. However, the effect of the smaller amplitudes has been to stiffen the truck, particularly in yaw and warp motions, and cause a decrease in the frequency of motion at any speed. As a result the frequency agreement is even poorer.

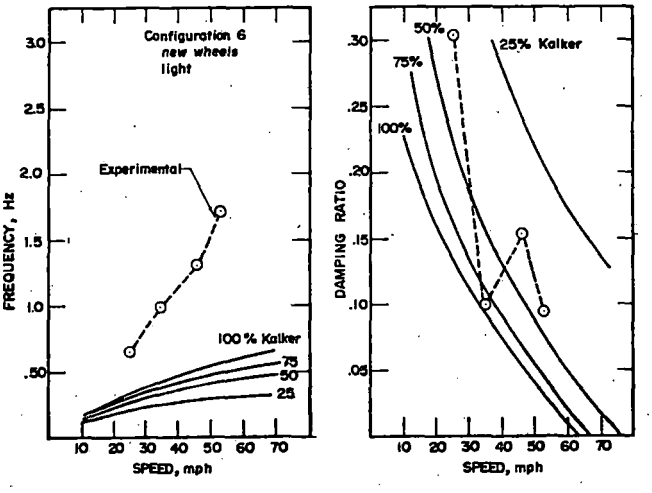

Figure 5-2. Damping Ratio and Frequency for Small Amplitude Describing Function Values

The frequency-speed relationship for the least damped mode at sub-critical speed is known to depend on the wheel conicity and the suspension characteristics. For a free wheelset,

$$f = \frac{V}{2\pi}\sqrt{\frac{\lambda}{r_o\, a}} \qquad (5\text{-}1)$$

and for a rigid truck without a primary suspension,

$$f = \frac{V}{2\pi}\sqrt{\frac{\lambda}{r_o a(1+h^2)}} \qquad (5\text{-}2)$$

where: λ = wheelset conicity

r_o = wheel radius

a = semi-rail gauge

h = ratio of wheelbase to gauge

f = frequency, Hz

V = speed

One expects that the actual kinematic frequency for a flexible truck will lie between these extremes. However, the experimental data for Configuration 6 lies on the free wheelset boundary at speeds below 45 mph, and is above this value at higher speeds. This suggests that the actual suspension characteristics are somewhat softer than those used in the analysis and/or the effective conicity experienced in actual running, particularly at higher speeds, was larger than the 0.05 value used in the results presented in Figures 5-1 and 5-2. For example, if the wheel tread conicity and corresponding values for the wheelset roll and contact angle difference terms are raised to 0.075 while the small amplitude parameters of Table 5-3 are used the results shown in Figure 5-3 are obtained. The effects of this change in wheel characteristics are to increase the frequencies while shifting the damping ratio curves to the left, a decrease in stability.

The higher effective conicity indicated by these results may be due to differences in the rail head profile along the track as well as occasional large wheelset excursions that cause flange contact. The rail head profile measurement and data reduction process described earlier indicates that the average conicity for the AAR Standard wheels on the tangent test track may be as large as 0.06. The standard deviation of the "effective" conicity for new wheels was about 0.03. Thus, large "effective" conicities are possible. Frequent flange contact would also cause larger "effective" conicities.

On the basis of the data presented thus far, the agreement between theory and experiment does not appear good. This apparent poor agreement may be due to one or more of the following reasons:

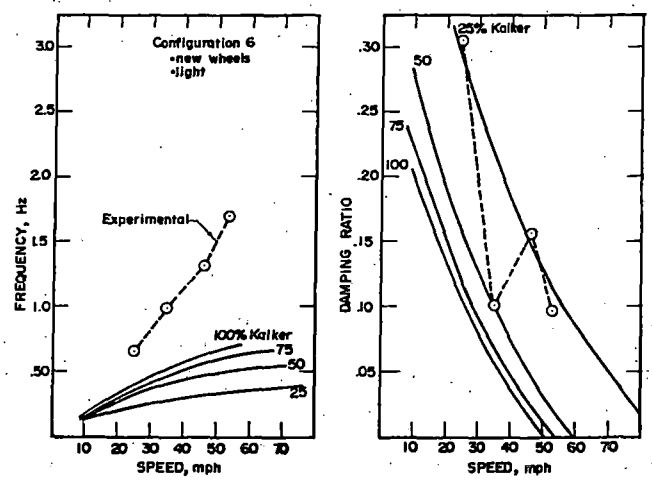

Figure 5-3. Damping Ratio and Frequency for Small Amplitude Describing Functions and Wheel Conicity of 0.075

1. Experimental data analysis inaccurate or incorrect.
2. Quasi-linearization of the nonlinear elements is incorrect or not applicable.
3. The theoretical model is incomplete or incorrect.

Ideally, one would like to compare theory and experimental data for other configurations before analyzing these three possibilities. However, the time and effort limitations placed on this research project preclude further investigation at this time. Consequently, each of the possible causes for the discrepancies between theory and experiment were considered briefly using the information available to us at this stage in the comparison process.

Data Analysis Shortcomings

Consider first the potential errors or inaccuracies in the experimental data. The freight car eigenvalue study conducted in connection with this effort revealed a possible explanation for the wide discrepancies between experimental and theoretical values. In the analysis of the empty car condition (Configurations 1-6), we usually find two modes with the following complex eigenvalue pairs:

$$\lambda_{1,2} = -\alpha_1 \pm j\omega', \quad \lambda_{3,4} = -\alpha_2 \pm j\omega'$$

where: $j = \sqrt{-1}$

α_1, α_2 = real values representing modal damping

ω' = real value representing modal frequency

i.e. two modes at virtually the same frequency. When the suspension stiffnesses are relatively soft, as occurs with the "nominal" amplitude case given in Figure 5-1, the damping ratios are also nearly identical in these two modes. However, when the stiffnesses are larger, as occurs with

the "small" amplitude parameters, then the damping values α_1 and α_2, differ considerably.

The eigenvectors associated with these two eigenvalues have the two truck lateral displacements and the car body lateral motion moving in phase but at different amplitudes. As a result, the two modes appear to be a "nosing" and a "fishtailing" motion as depicted in Figure 5-4.

These results, if valid for the freight car, have strong implications as far as the random decrement analysis is concerned. The system response to a step input under these conditions should include a term of the form

$$x(t) = (A_1 e^{-\alpha_1 t} + A_2 e^{-\alpha_2 t}) \cos \omega' t$$

where A_1 and A_2 are real numbers that depend on the initial condition amplitude and the mode shapes. This term represents the portion of the system response that would be detected by the random decrement analysis. Such a combination of modal responses may appear similar to a single, exponentially damped, sinusoidal response mode, but at a damping value different from α_1 or α_2.

It is quite likely that the random decrement results reported earlier may actually represent this two mode response. In such a case, one would like to know the relationship between the actual damping values α_1 and α_2 and the damping value detected by the random decrement process. We have not been able to prove that the damping ratio value computed from the random decrement signature must lie between α_1 and α_2, because the damping perceived by the random decrement analysis process will depend on the trigger level and the system response mode shapes. However, this has been true in the few cases that we have studied.

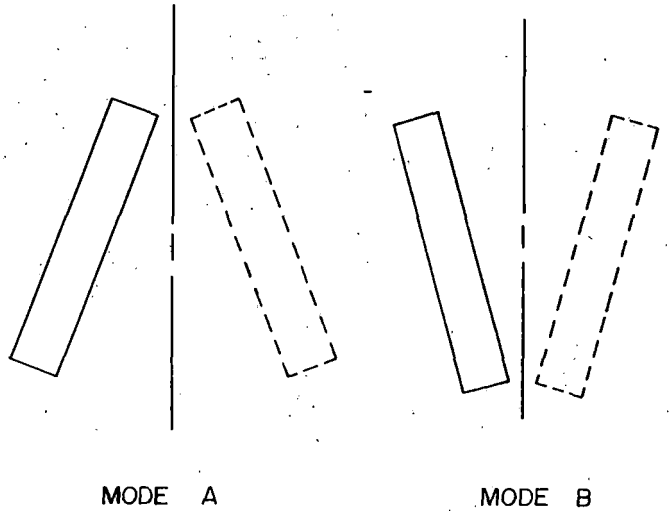

Figure 5-4. Typical Kinematic Mode Shapes

The procedure used to determine modal damping values from PSDs will also yield erroneous values when two modes with the same frequency exist. This procedure is based on the assumption that a single mode exits at the frequency of interest, and interprets the spectrum as representing a second order system in the vicinity of the modal frequency. It is not clear whether this analysis process would yield the same value as that found via the random decrement signature in the case where two modes occur very near the same frequency. These questions should be addressed in future studies.

In light of this new interpretation of the experimental modal damping data, we should re-examine the comparisons presented earlier. The two least damped "kinematic" modes found with the "nominal" amplitude data are nearly identical in damping as well as frequency. Thus the results shown in Figure 5-1 can not be reinterpreted in a more favorable light. However, the eigenvalue analysis for the "small" amplitude case produced significantly different damping values for the two "kinematic" modes. In this case, the experimental values lie between the two modes at all speeds, although the frequency agreement problem remains. Nevertheless, these results suggest that the presence of two modes in the experimental data may be one cause of the relatively poor agreement found between theory and experiment.

Nonlinearities

A second cause of the differences between theory and experiment may be due to the nonlinear nature of the vehicle system, and the associated difficulties in analyzing such system behavior with linear models. As discussed earlier, a linear analysis of this nonlinear vehicle system utilizes equivalent linearization techniques such as the describing function method. This method requires assumptions about the nature of the inputs to the nonlinear elements. The results presented earlier assumed that the wheel-rail geometric constraint functions were linear over the range of interest, essentially an assumption that flange contact did not occur. As mentioned earlier, the possibility that flange contact occured is indicated by the experimental results. An improved linear estimate should account for this possibility.

Two different sets of assumptions, "nominal" and "small" amplitude motions were made concerning the inputs to the suspension system nonlinearities. In each case, the same assumptions were used to calculate the response at all speeds. These assumptions have several shortcomings that may also help explain the differences between theoretical and experimental results. First, the inputs to the different nonlinearities are not the same at all speeds, but rather vary with speed. Thus a different set of inputs is appropriate for 15 mph than for 45 mph. Additionally, the strong dependence of the vehicle behavior on the amplitude of the truck warp and centerplate rotations in our theoretical studies [5-1], indicates that more accurate values for these motions are particularly important.

The difficulty in finding appropriate equivalent linear values can be attributed, in

general, to the sensitivity of the nonlinear freight car response to the disturbance inputs. This sensitivity, found in our accompanying theoretical work [5-1] makes interpretation of the behavior in linear terms difficult. The PSD and random decrement processes are applied to the response of a system whose behavior may vary considerably over the period of observation. Thus, in the deterministic sense, there may not be appropriate input amplitudes and frequencies to use in the sinusoidal input describing functions. This difficulty can be overcome with the statistical linearization approach discussed later in this chapter.

An attempt to obtain better statistics concerning the actual relative displacements across the suspension elements during the Configuration 6 tests was made. We intended to use this data to improve our estimates for the equivalent linear values of the suspension damping and stiffnesses. However, examination of this data revealed that certain transducers were operating improperly during this test series, possibly due to loose mounts. Consequently, reliable data for an entire run could not be obtained, although an attempt was made to "eyeball" maximum values for each value. These values were used to compute sinusoidal input describing function values and those values were used in an eigenvalue analysis at the corresponding speed. We do not place much credence in the results due to uncertainties in the data, although there was a slight improvement in agreement with the experimental damping values. The frequency agreement remained unsatisfactory.

The importance of the input amplitudes, is also illustrated by the forcer response data. As discussed in the previous chapter, one of the most likely reasons for the wide discrepancy between the forcer response data and the random decrement and PSD data is the nonlinear nature of the system. In the forcer tests, the truck wheelsets were forced into flange contact causing perceptible warp and centerplate displacements. Thus the relative wheel-rail, centerplate rotation and warp motion amplitudes were greater during these tests than during the random response tests. As a result, we would expect to find better agreement between the forcer test results and the "nominal" amplitude theoretical results. Figure 5-5 illustrates that this is indeed true. One should note, however, that the differences between forcer and random response data may be due to other factors as well, as previously discussed.

Linear Model Validity

These difficulties in studying nonlinear system response with a linear model bring into question the validity of the model itself. Our tentative conclusion, based on the brief study reported above, is that it is nearly impossible to accurately represent the actual freight car behavior in a given situation with a purely linear model, due to the strong nonlinearities such as Coulomb friction present in this vehicle. The detailed information concerning inputs to the nonlinearities that are needed for such a linear analysis is extremely difficult to obtain. That is not to say that the linear model has no validity or utility. The linear model, with

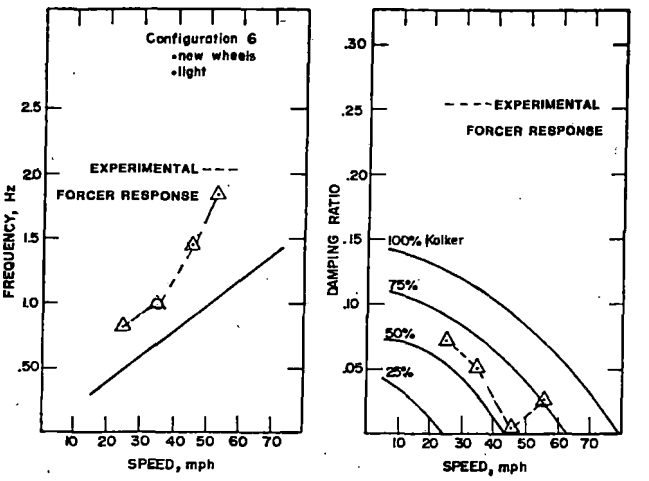

Figure 5-5. Comparison of Theoretical Results and "Forcer" Experimental Data

appropriate equivalent linear values, can reasonably represent the nonlinear system response. However, a difficulty lies in finding those appropriate linear values. The linear model is a useful tool to explore the sensitivity of the vehicle design to parameter changes. In such a study, however, one must recognize the wide variation in model variables likely in actual operation. More realistic results can only be obtained with quasi-linear or nonlinear analysis.

STATISTICAL LINEARIZATION ANALYSIS

Introduction

As discussed in the preceding section, choosing equivalent linear values for nonlinear elements is not straightforward. Different choices of values, all within a reasonable range, can give very different results for vehicle dynamic response. One method for calculating the response of a nonlinear vehicle to random roadbed inputs is the method of statistical linearization [5-4]. This method uses statistical describing functions (also known as random input describing functions) to represent the input-output characteristics of the nonlinear elements. The values of these describing functions depend on the root mean square (rms) value of the input signal to the nonlinearities. For a given power spectrum of the random forcing function (e.g., rail alignment irregularities), the power spectra of the response variables may be calculated and then integrated and combined to calculate new estimates for the rms values of the input signals to the nonlinear elements. An iteration scheme must be used to determine new estimates for the rms input values and re-calculate the response spectra. The iteration is continued until prescribed convergence criteria are met.

The statistical linearization procedure is potentially a very powerful tool for analyzing the forced response of rail vehicles. However, computer implementation of the technique is not without problems. Essentially, the analysis reduces to the solution of nonlinear simultaneous algebraic equations. Convergence of the iterative solution procedure is not always obtained.

We were able to find solutions for models representing configurations 1, 6, and 8 under certain conditions.

Rail and Track Irregularity Models

The computer program that implements the iterative algorithm for the method of statistical linearization provides only for forcing due to centerline lateral alignment, x_A. However, as discussed previously, preliminary estimates of the size of the rolling line offset contribution to the forcing are that it can be of the same order as the alignment. Obviously, if both centerline and offset estimates can be obtained and combined spectrum of $x_A + x_{R_o}$ formulated, this spectrum can be used as an input in the computer program. The spectrum of centerline lateral alignment used as input to the nonlinear vehicle analysis is shown in Figure 5-6. This has a general form that is similar to those measured for actual track. The value of the spectrum is constant at low frequency (or long wavelengths) out to a value of about 9.5 x 10^{-3} cycle/ft (105 ft/cycle) where it then decreases with frequency raised to the second power. In most of the studies used in this work, the root mean square of the rail lateral alignment was 0.08 inches. As mentioned previously, attempts were made to measure the lateral alignment of each of the test sections. These attempts were unsuccessful. However, as previously discussed, it is felt that an rms level of about 0.1 inch is realistic for good mainline track.

Vehicle Model

In [5-4], the vehicle model used to illustrate the technique of statistical linearization is that of a 9 degree-of-freedom model of a North American freight car with roller bearing trucks. The nonlinear elements considered were the wheel-rail geometric constraint functions [5-5] and the suspension elements. The nonlinear constraint functions for each wheelset are (1) the difference in left and right rolling radii; (2) the difference in left and right contact angles; and (3) the roll angle. The nonlinear suspension elements are as follows: (1) lateral motion between truck and car body (linear spring in parallel with dry friction); (2) roll motion between truck and car body (linear spring in parallel with dry friction); (3) yaw rotation of the truck bolster relative to the car body (dry friction); and, (4) warping motion of the truck frame (linear spring in parallel with dry friction). This model is discussed more completely in [5-4]. It should be noted that the form of the nonlinear suspension element implemented in this model is simpler than the general element model suggested by the Martin-Denver tests [3-4], Figure 3-6. The characteristics of the general element model were described in Table 3-3. The simplified model neglects the clearance, δ, and its series spring, k_2, as well as the spring in series with the friction, k_F. The form of the simplified suspension element model used in the present studies is shown in Figure 5-7.

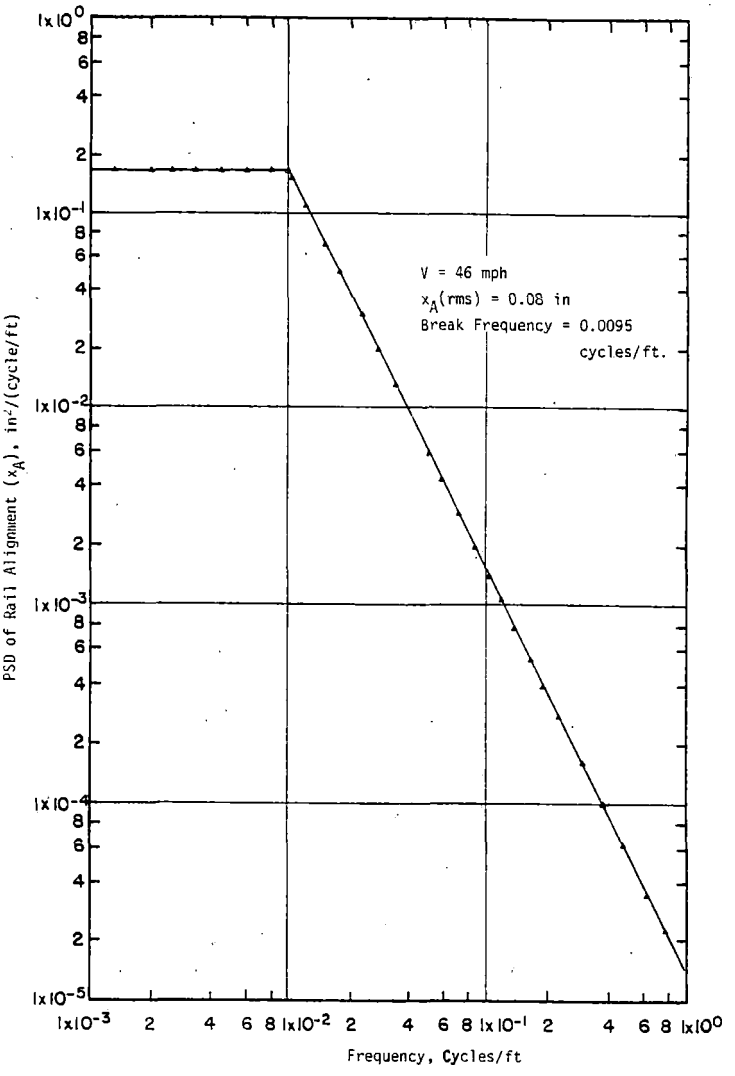

Figure 5-6. PSD of Centerline Lateral Alignment

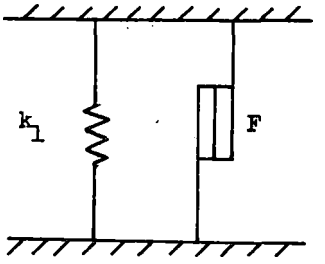

Figure 5-7. Simplified Form of Suspension Element for Nonlinear Model

Actually, two versions of the vehicle model were used in these studies. The first is the 9 degree-of-freedom model as noted. The second is an 11 degree-of-freedom model where each of the additional two degrees of freedom defines the lateral displacement of the end of a lateral spring in series with dry friction. This suspension element is a modified version of the element used to represent the lateral force/deflection characteristics of each of the trucks relative to the car body. It has the advantage of being more representative of the test data [3-4] and the added advantage of improving the convergence properties of the iterative solution algorithm.

We used both the 9 and the 11 degree-of-freedom models described above and a computer program implementing the forced response algorithm of [5-4] to calculate the forced response characteristics of the L&N test vehicle. The results of these calculations are presented in the following sections.

Measured vs. Absolute Truck Lateral Displacement

Signals from the wheel-rail displacement transducers were combined to yield truck lateral displacement. However, this combined signal is not the absolute lateral displacement of the truck, x_T, but the lateral displacement relative to the track centerline, x_{TFT}.

As shown in Figure 5-8, the gauge at any point on the track is given by 2ζ where ζ can vary along the track. The left and right wheel-rail transducers measure (to within a constant) Δ_L and Δ_R where for small wheelset yaw angles,

$$\Delta_L = \zeta - (x_w - x_A) \tag{5-3}$$

$$\Delta_R = \zeta + (x_w - x_A) \tag{5-4}$$

Now, the wheelset displacement relative to the disturbed track centerline is $x_w - x_A$ which may be obtained by subtracting Δ_L from Δ_R and averaging, or

$$(\Delta_R - \Delta_L)/2 = \{\zeta + (x_w - x_A) - [\zeta - (x_w - x_A)]\}/2 = x_w - x_A \tag{5-5}$$

For the complete truck, these differences were averaged for the front and rear wheelsets to produce a truck lateral displacement relative to the average of the front and rear track alignments. Using subscripts 1 and 2 to denote the front and rear wheelsets,

$$[(\Delta_{R1} - \Delta_{L1}) + (\Delta_{R2} - \Delta_{L2})]/2 = (x_{w_1} - x_{A_1} + x_{w_2} - x_{A_2})/2$$

$$= (x_{w_1} + x_{w_2})/2 - (x_{A_1} + x_{A_2})/2$$

$$= x_T - (x_{A_1} + x_{A_2})/2$$

$$\triangleq x_{T_{FT}} \tag{5-6}$$

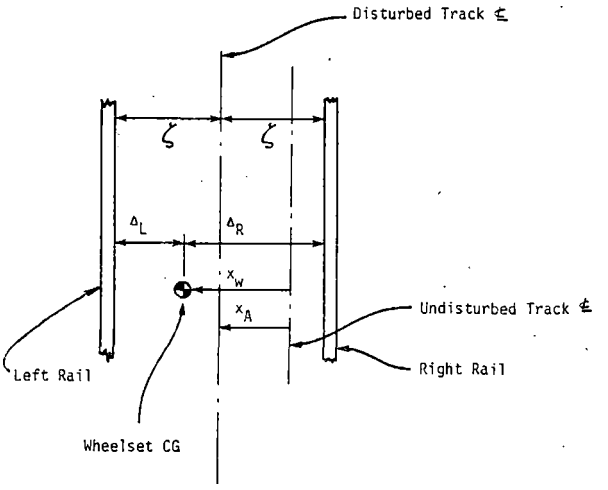

Figure 5-8. Definition of Quantities Measured by Wheel-Rail Displacement Transducers

This combined signal, x_{TFT}, is the "truck lateral displacement" that was measured during the field tests. In the analytical estimates of the power spectrum for truck lateral displacement, both x_T and x_{TFT} were calculated. An example of this is shown in Figure 5-9 where the spectra for both x_T and x_{TFT} for the front truck of Configuration 6 at 35 mph are presented. Note that the x_{TFT} signal is significantly different from the x_T signal at both low and high frequencies. As might be expected from comparison with results obtained for a single wheelset, the PSD for x_T should be about the same as that for the rail alignment for frequencies below that of the hunting mode and then fall off rapidly with frequency above the hunting frequency. Conversely, the PSD for x_{TFT} should be very small at low frequencies and approach the PSD of the alignment at high frequencies. This is essentially the case in Figure 5-9 with the addition of drop-outs in the x_{TFT} spectrum at high frequency.

Linear and Nonlinear Forced Response

Response spectra calculated for a nonlinear vehicle using the statistical linearization approach are quite different from those calculated for a linearized model of the same vehicle. This may be seen from results shown in Figures 5-10 and 5-11. For the linearized model, equivalent linear viscous damping values were calculated for the Coulomb friction portion of the suspension element of Figure 5-7. Constant values were also chosen for the wheel-rail geometry characteristics. The values of the equivalent linear suspension elements are given in Table 5-4 based on assumptions as noted for the relative displacements at a frequency of 2.0 Hz. The stiffness values are those of k_1 in the simple model of Figure 5-7 as obtained from [3-4] and the damping values as obtained from the expression

$$D_{eq} = 4F/\pi A\omega \tag{5-7}$$

Table 5-4. Equivalent Linear Suspension Characteristics (Configuration 6)

Suspension Element	Assumed Relative Displacement Across Suspension Element	Stiffness, k_l	Damping, D_{eq}*
Vertical Bolster/Sideframe	± 0.10 in	0.25715 x 10^6 lb/ft	0.40803 x 10^5 lb/(ft/sec)
Lateral Bolster/Sideframe	± 0.10 in	0.61930 x 10^5 lb/ft	0.43248 x 10^5 lb/(ft/sec)
Warp	± 0.005 rad	0.37290 x 10^7 ft lb/rad	0.80854 x 10^5 ft lb/(rad/sec)
Yaw Centerplate	± 0.005 rad	0	0.12280 x 10^5 ft lb/(rad/sec)

* Damping values computed for f = 2 Hz

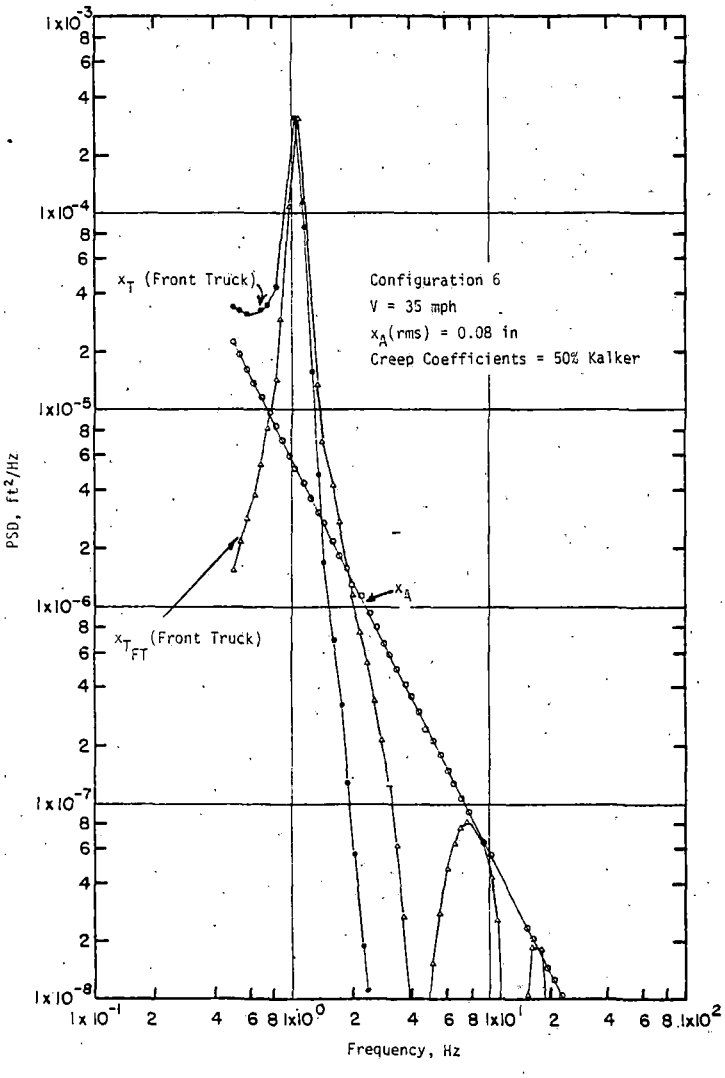

Figure 5-9. PSDs for Absolute and Relative Truck Lateral Displacement (x_T and x_{TFT}, respectively)

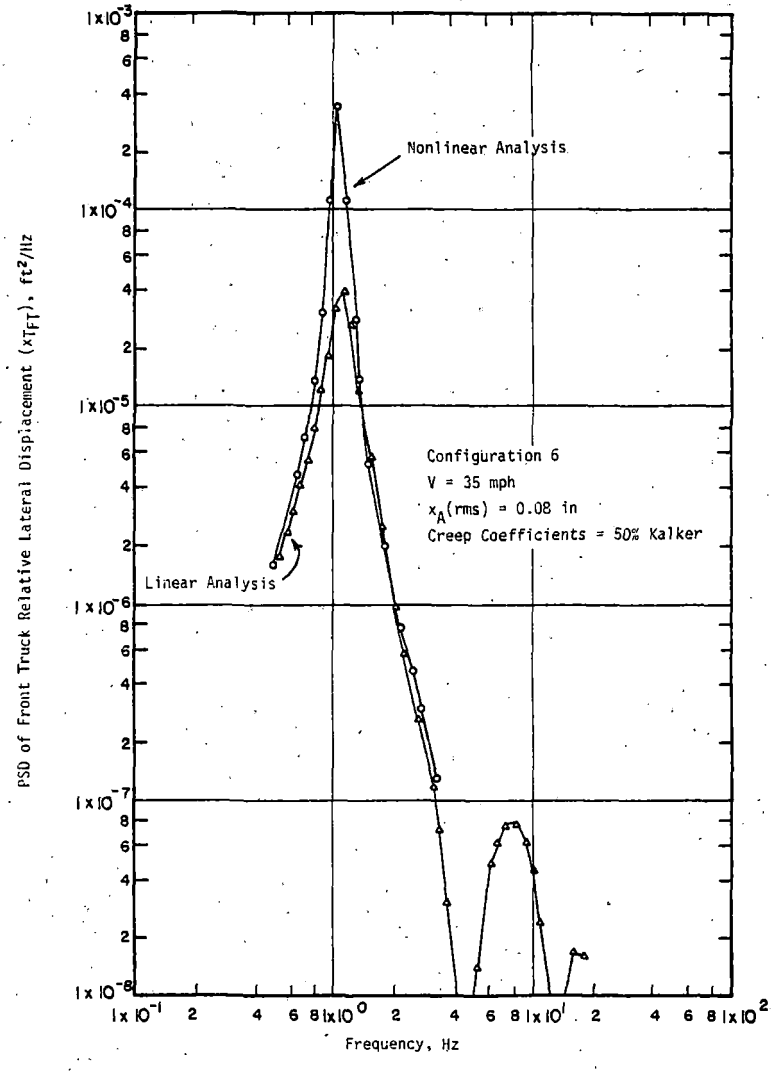

Figure 5-10. PSDs for x_{TFT} using Linear and Statistical Linearization (Nonlinear) Analyses

where F is the breakout force (or moment) and A is the linear (or angular) displacement across the element.

In Figure 5-10 we see that the response x_{TFT} to centerline lateral alignment has much lighter damping when the nonlinear as opposed to the linear analysis is used. Above and below the frequency for peak response (1 Hz), the spectra are fairly close.

Another manifestation of nonlinear behavior is shown in Figure 5-11. Power spectra for the relative lateral displacement of the front truck are shown for two levels of rail alignment input for Configuration 6 at 35 mph. For a linear vehicle the response to the 0.2 inch rms level should be merely scaled up from that for the 0.08 inch level (as shown in Figure 5-12). Clearly, this is not the case here. The effect of increasing the rms lateral alignment from 0.08 to 0.2 inches is to shift the peak response of the vehicle in the hunting mode from about 1.0 Hz to about 1.4 Hz. There is no increase in the level of the PSD at the hunting frequency.

One might expect that, in a simple sense, the higher level of forcing due to the rougher track would lead to larger responses of the wheelset lateral displacements. At 0.08 inches rms track lateral alignment, the front and rear trucks have rms displacements of 0.101 and 0.010 inches respectively. At 0.2 inches rms track lateral alignment, the front and rear trucks have about 0.168 and 0.154 inches rms displacement. Correspondingly, the rms response levels for the other variables are smaller with the 0.08 in rms alignment as compared with those for 0.2 inches.

This large increase in the lateral response of the rear truck at 0.2 in. rms track lateral alignment is shown in Figure 5-13. Note that no hunting mode peak is apparent at the 0.08 in. rms forcing while at 0.2 in. rms, there is a very large hunting mode peak at about 1.4 Hz. This is also a manifestation of nonlinear behavior.

As the truck lateral responses are larger for the rougher track, one might then postulate that, on the average, higher levels of effective conicity would prevail due to the more frequent

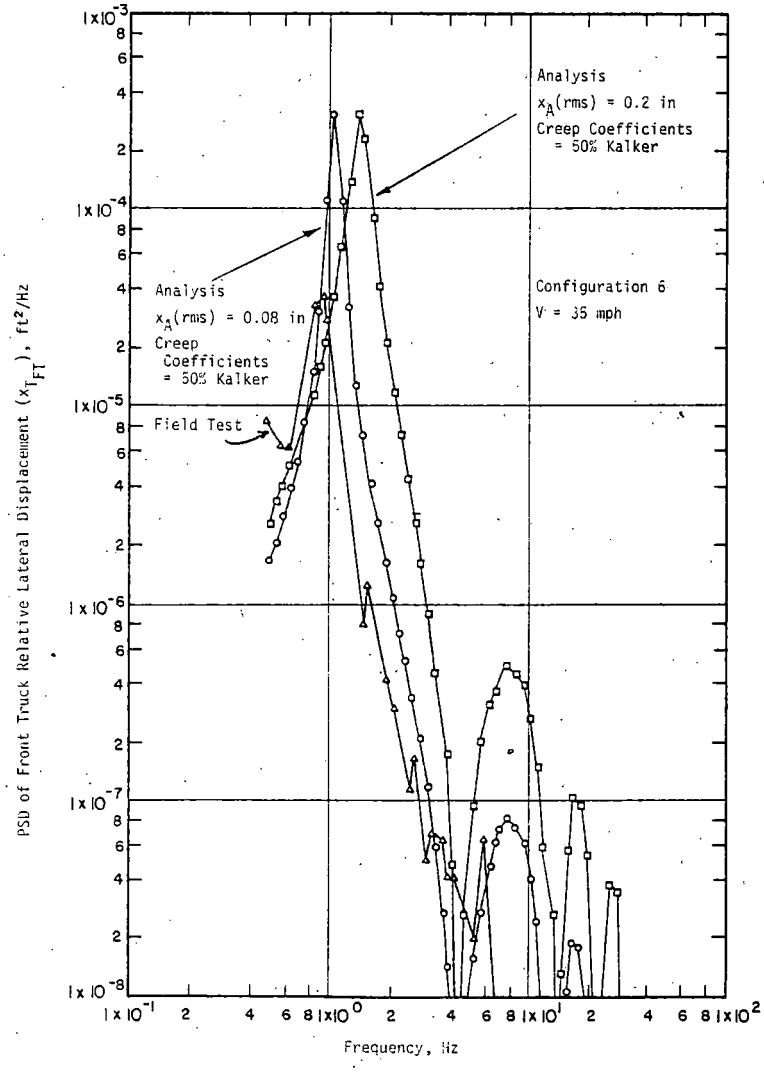

Figure 5-11. PSDs for x_{TFT} of the Front Truck at Two Levels of Alignment Input (Nonlinear Analysis)

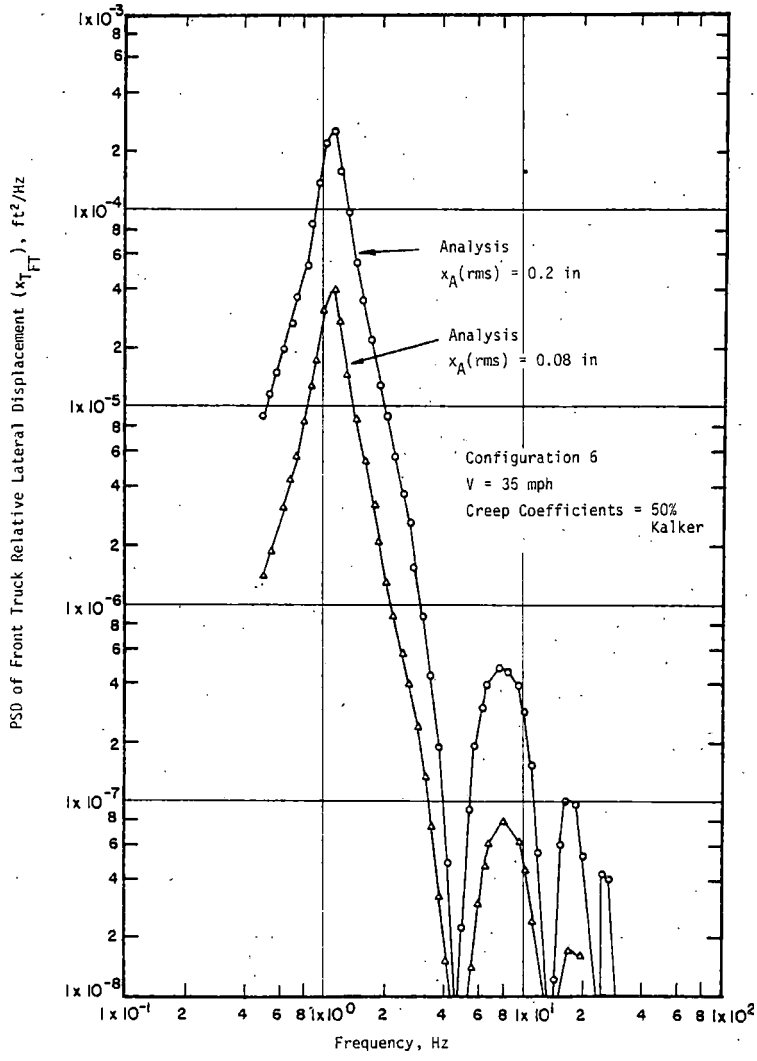

Figure 5-12. PSDs for x_{TFT} at Two Levels of Alignment Input (Linear Analysis)

flange contact on rougher track. This, if true, should lead to two effects: (a) a reduction in damping in the least damped or kinematic mode, and (b) an increase in the frequency of the least damped mode. An increase in frequency was observed, but it is difficult to assess how the damping changed.

In addition to higher levels of effective conicity acting to increase the frequency of the hunting or kinematic mode, one might also expect that with the larger levels of response on rougher track, the effective suspension damping would be lower. This should tend to "loosen up" the trucks and increase the frequency of motion at any speed. (This behavior trend was explained earlier in this chapter in connection with a linear stability analyses). This expected behavior is observed for the present case.

Effects of Creep Coefficient

As discussed previously, the values of creep coefficients that actually existed for the test vehicle were not known. Tests were conducted in an attempt to determine these values, but errors in the test conduct precluded the use of the data obtained for this purpose.

Initial results obtained with the statistical linearization analysis for Configuration 6 at 35 mph are shown in Figures 5-14 and 5-15. Both figures show the PSDs obtained for the front truck relative displacement (x_{TFT}) at x_A = 0.08 in. rms. In Figure 5-14, results for creep coefficients equal to 50 and 75% of the nominal Kalker values are shown, while results are shown in Figure 5-15 for the 50 and 100% levels. The results for 75% and 100% of the Kalker values are quite close and seem to indicate that the hunting mode occurs at a lower frequency than 0.5 Hz. At 50% of the Kalker nominal values, there is a pronounced peak in the response that indicates the probable presence of the hunting mode at about 1 Hz. Recall that test results for Configuration 6 (Figure 4-13) indicated the frequency of the hunting mode was on the order of 0.8 to 1.0 Hz at 35 mph. Above the hunting mode frequency (starting at 2 to 3 Hz), the responses are quite similar regardless of the creep values used. It appears that creep coefficient levels (below 75%) have a very strong influence on the vehicle response, even stronger than might be expected on the basis of a linear analysis.

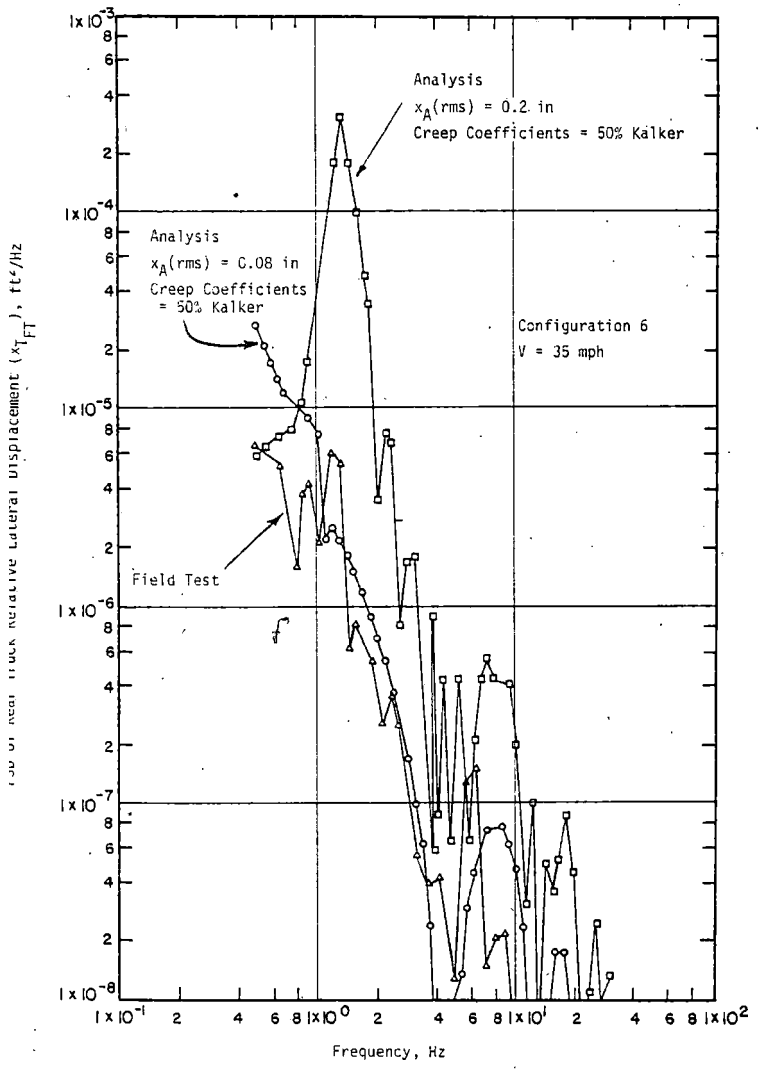

Figure 5-13. PSDs for x_{TFT} of the Rear Truck at Two Levels of Alignment Input (Nonlinear Analysis)

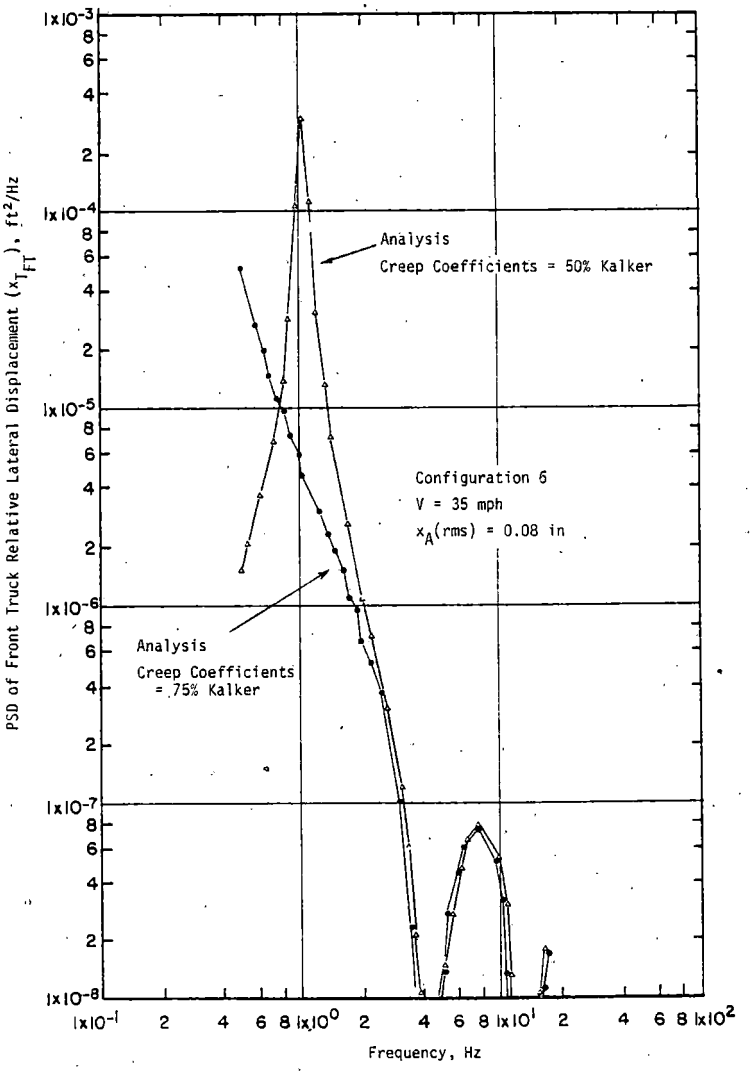

Figure 5-14. PSDs for x_{TFT} at 50 and 75% of the Nominal Kalker Creep Coefficients

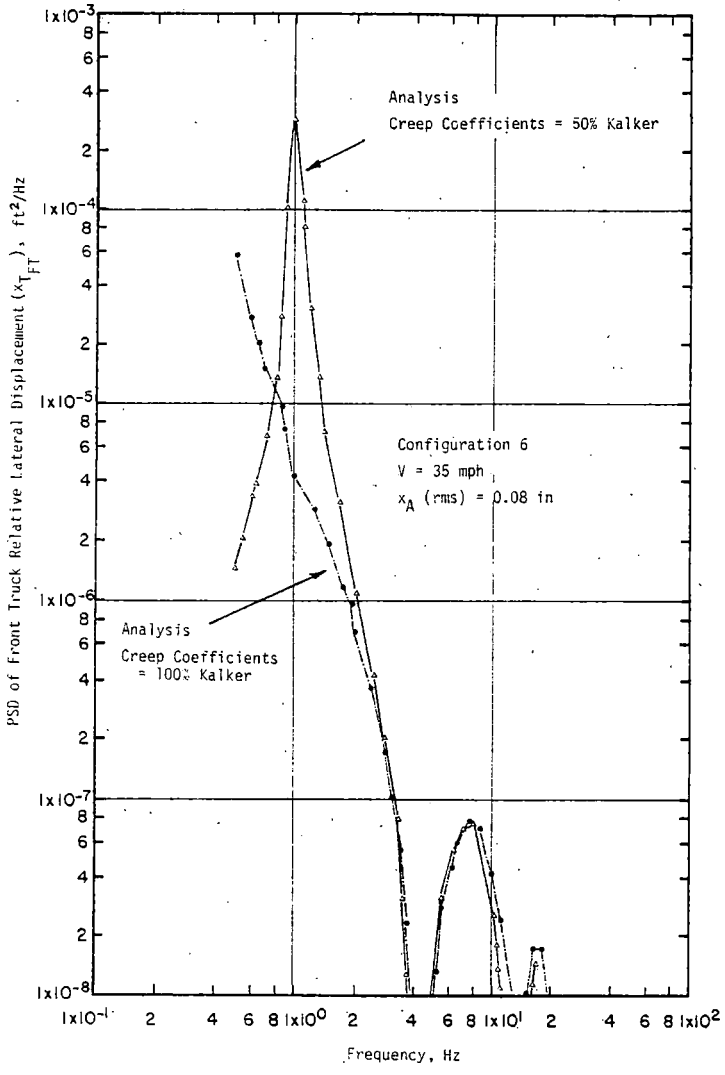

Figure 5-15. PSDs for x_{TFT} at 50 and 100% of the Nominal Kalker Creep Coefficients

However, on the basis of the frequency obtained for the least damped mode, it would appear that the 75 and 100% Kalker results are not as realistic as those for the 50% level.

Comparison of Theory and Field Test

There were a number of unknown parameters that very probably had a significant effect on the dynamic response of the test vehicle. Two of these are the actual creep force characteristics (the creep coefficients for a linear creep law) and the inputs due to wheel-rail geometry offsets (rolling line offset, etc.). In addition, for Configuration 6, the 1/20 wheels on one truck still had the mill scale present on the treads while those for the other truck had been polished through use. In all likelihood, the creep force characteristics were different for the two trucks. As described earlier, response characteristics for Configuration 6 seemed quite sensitive to this discrepancy.

To use either the 9 or 11 DOF model described earlier required choosing creep coefficients that would be the same for all eight wheels. In addition, although the nonlinear suspension elements were modeled, they were simpler models than the actual characteristics determined from tests. Crosslevel inputs were not provided for. The spectrum input for centerline alignment was chosen to approximate our "best guess" for the actual spectrum but was probably not completely accurate. Rolling line and other offsets were not used as inputs to the analysis.

In sum, the models used in this statistical linearization analysis were somewhat simplified and not all the parameters and inputs necessary to calculate the response were known. Because of these unknowns and deficiencies, the comparisons below should be considered as representative of a first step in a model validation process.

Results were shown previously for the relative truck lateral displacement for Configuration 6 at 35 mph (Figure 5-11 and 5-13). These plots showed the calculated response at two levels of rms track alignment, 0.08 and 0.20 in. At an rms alignment input of 0.08 in, the calculated frequency of the peak in the PSD characterizing the least damped or hunting mode was fairly close to that obtained during tests for the front truck (Figure 5-11). Also the rate of fall-off of the calculated and test PSDs were about the same. However, it is difficult to justify the level of response obtained via analysis. This is especially difficult since additional inputs due to the wheel-rail geometry offsets and crosslevel were present in the tests that were not included in the analysis.

Interestingly, the analytical PSD obtained for the rear truck relative lateral displacement for x_A(rms) = 0.08 in.(Figure 5-13) is reasonably close to that obtained during field tests. Even the first drop-outs compare well.

When 75% of the nominal values for the Kalker creep coefficients are used, the agreement between calculation and test for x_{TFT} of the front truck for Configuration 6 at 35 mph is generally good (Figure 5-16). However, test results show a well-defined peak due to a lightly damped hunting mode whereas no peak is present in the calculated results.

At 25 mph, (and 50% Kalker creep coefficients) the calculated PSD of x_{TFT} for the front truck (Configuration 6) shows good comparison with test at frequencies above about 1 Hz (Figure 5-17) but very poor comparison below 1 Hz for 50% Kalker creep coefficients. When the creep coefficient level is increased to 75% of the nominal Kalker values for this same configuration and speed, the comparison between test and calculation is good for the PSDs of x_{TFT} for both front and rear trucks (Figures 5-18 and 5-19).

Time and resources available did not permit more extensive analysis of Configuration 6. Two other Configurations, 1 and 8, were briefly examined. Results are shown in Figures 5-20 and 5-21 respectively. Configuration 1 was the empty vehicle with CNA wheels and dry or unlubricated centerplate. Configuration 8 was the loaded vehicle with CNA wheels and lubricated centerplate.

The calculated PSD for x_{TFT} of the front truck at 30 mph for Configuration 1 shows a much larger response in the hunting mode than does the field test PSD. In addition the calculated frequency of the hunting mode is about 1.6 Hz

whereas the hunting mode peak of the field test PSD is at about 1.2 Hz. The rates of fall-off for frequencies above the hunting frequency do compare reasonably well, however. When the vehicle was loaded and the centerplate lubricated to change Configuration 1 to 8, the comparison for the PSDs of the front truck x_{TFT} was even worse. At low frequencies the calculated PSD was significantly less than the field test. The hunting mode frequency determined from the field test PSD was slightly greater than 1 Hz while the calculated value was about 2 Hz. In addition, the calculated response at the hunting frequency was much higher than that obtained during field tests.

Summary

Although this application of statistical linearization was limited by time and resources, the following conclusions can be drawn from the results obtained by comparison of theory and experiment for Configuration 6:

(1) The best agreement of the PSD for the front truck, x_{TFT} at 35 mph was obtained with x_A (rms)= 0.08 inch, (Figure 5-11) and 50% Kalker creep.

(2) The best agreement of the PSD for the rear truck, x_{TFT}, at 35 mph was also obtained for x_A (rms)= 0.08 inches and 50% Kalker creep, but the kinematic peak was not prominent in the theoretical result. (Figure 5-13).

(3) The best agreement for both trucks at 25 mph was obtained at x_A(rms) = 0.08 inches and 75% Kalker creep (Figures 5-18 and 5-19).

For Configuration 1 we obtained good agreement of analysis and test results for the frequency of the hunting mode and shape of the PSD of x_{TFT} for the front truck and poor agreement for level of response and damping (30 mph, 50% Kalker creep, x_A (rms)= 0.08 and 0.1 in; Figure 5-20). However, the limited results we obtained for Configuration 8 did not show good agreement between analysis and test results (Figure 5-21).

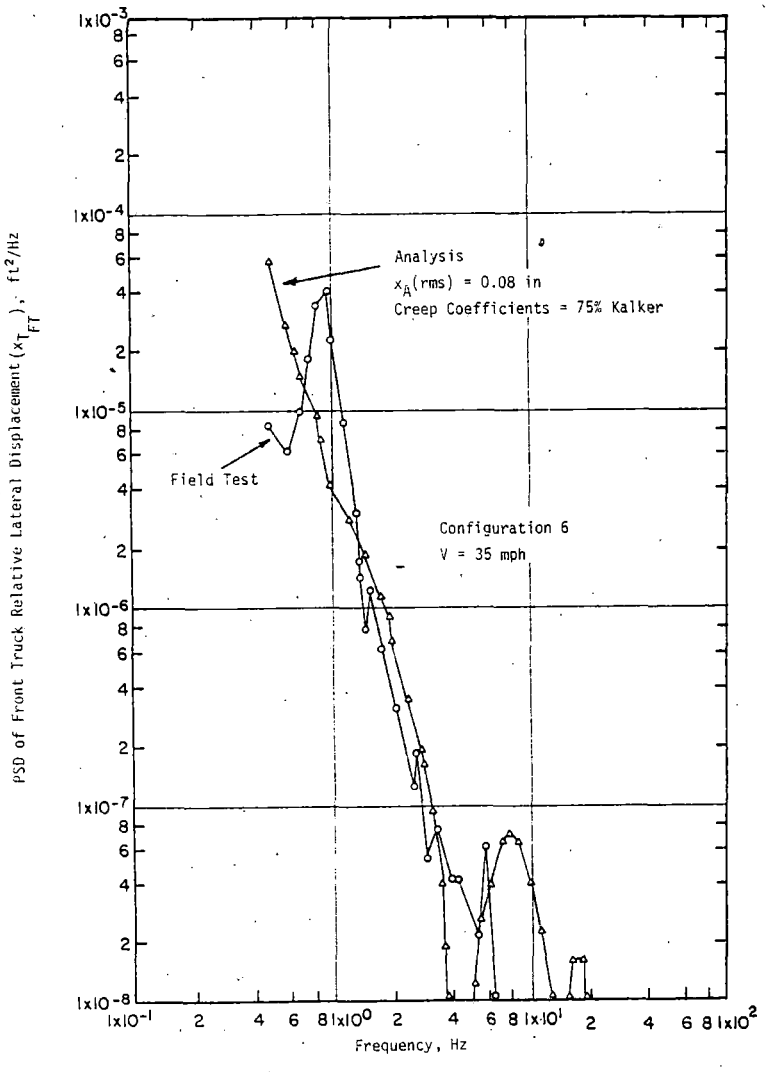

Figure 5-16. Comparison of Analysis and Test Results for Configuration 6 at 35 mph (Creep Coefficients = 75% Kalker)

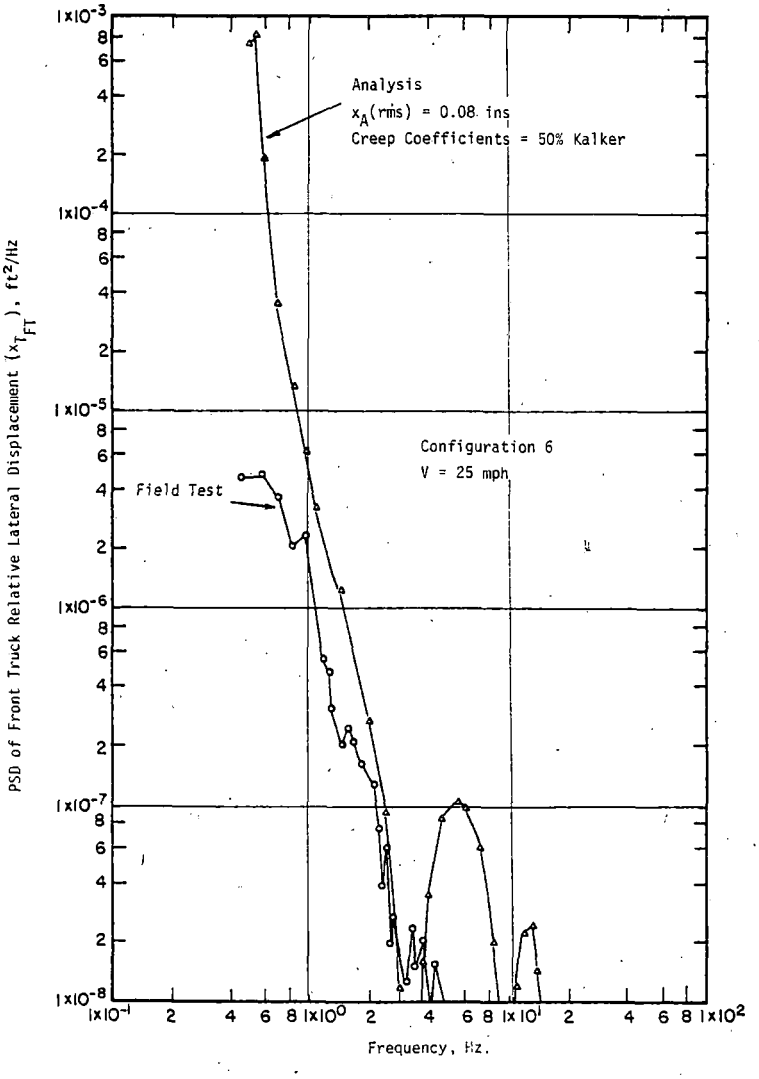

Figure 5-17. Comparison of Analysis and Test Results for Configuration 6 at 25 mph (Creep Coefficients = 50% Kalker)

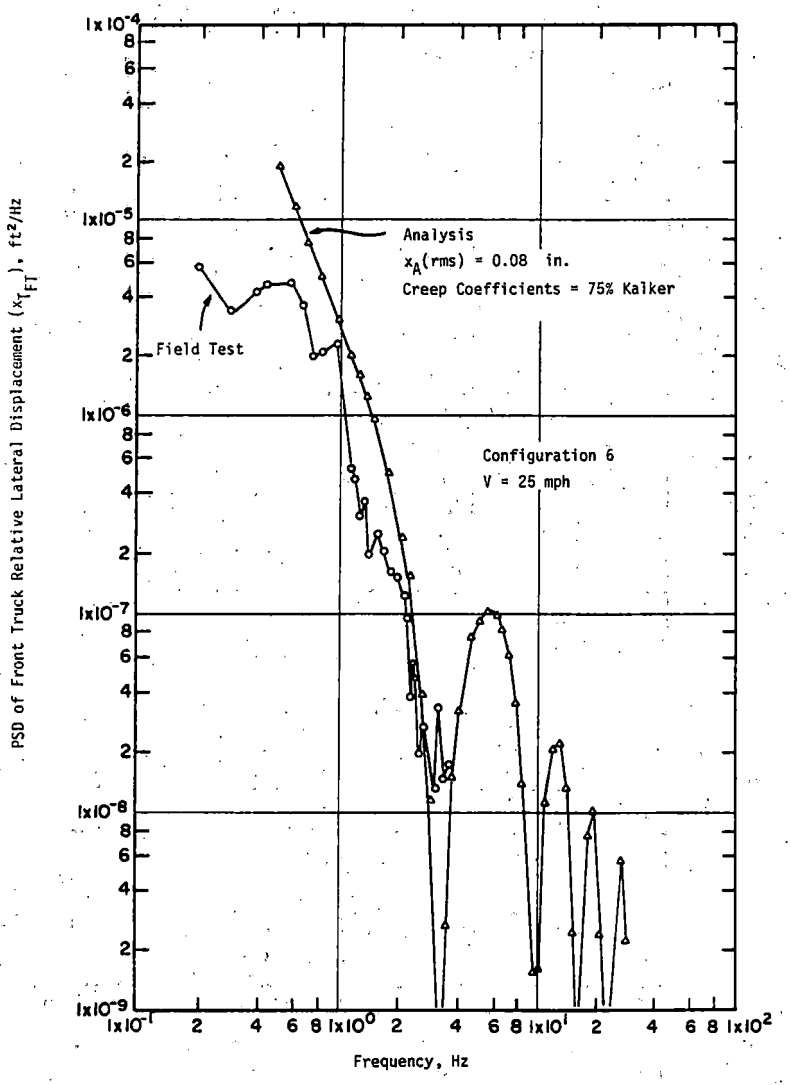

Figure 5-18. Comparison of Analysis and Test Results for Configuration 6 at 25 mph (Creep Coefficients = 75% Kalker)

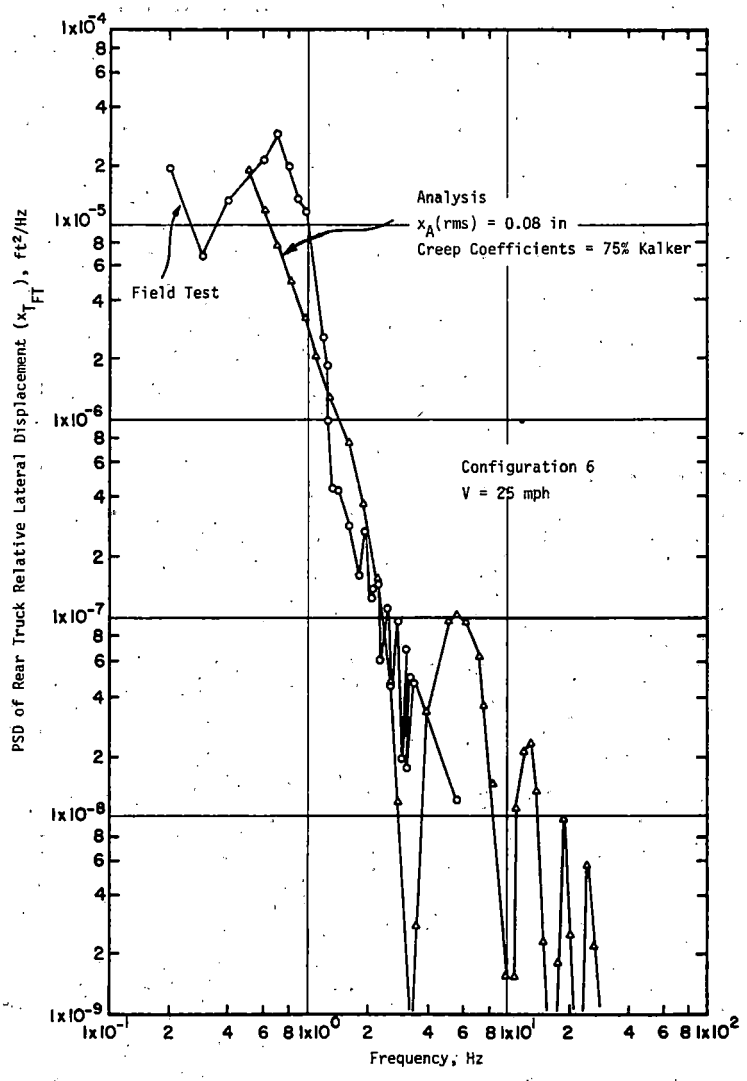

Figure 5-19. Comparison of Analysis and Test Results for Configuration 6 at 25 mph (Creep Coefficients = 75% Kalker)

A number of questions were raised in this study that could not be pursued. The results indicate that statistical linearization shows promise for predicting the response of nonlinear rail vehicles, but more work is needed to substantiate this conclusion.

HYBRID COMPUTER ANALYSIS

A simulation of a railway freight car model was conducted using the hybrid computer facility of the Clemson Engineering Computer Laboratory. This facility consists of an EAI-680 analog computer linked to a PDP-15 digital computer through an EAI-693 interface. It is described in detail in [5-6]. Although the model used was only that of a half-freight car, qualitative comparisons can be made between hybrid simulation results and those obtained during field test. This section describes the simulation, simulation results, and comparisons between simulation and test results.

Simulation Description

Due to analog equipment limitations, only a half-freight car model was simulated. This model and simulation, described completely in [5-6], consists of a two degree-of-freedom half car body mounted on a three degree-of-freedom freight car truck. The degrees of freedom are the following: truck lateral, yaw, and warp and car body lateral and roll. The actual nonlinear wheel- rail geometric constraint functions for small contact angles are used, as are simplified nonlinear approximations to the nonlinear suspension characteristics determined by tests [3-3, 3-4]. Provisions are made for excitation due to lateral track alignment irregularities. A random signal is generated and shaped by filters to give an alignment input having a PSD representative of those actually measured. This signal can be adjusted in magnitude to give the desired rms alignment.

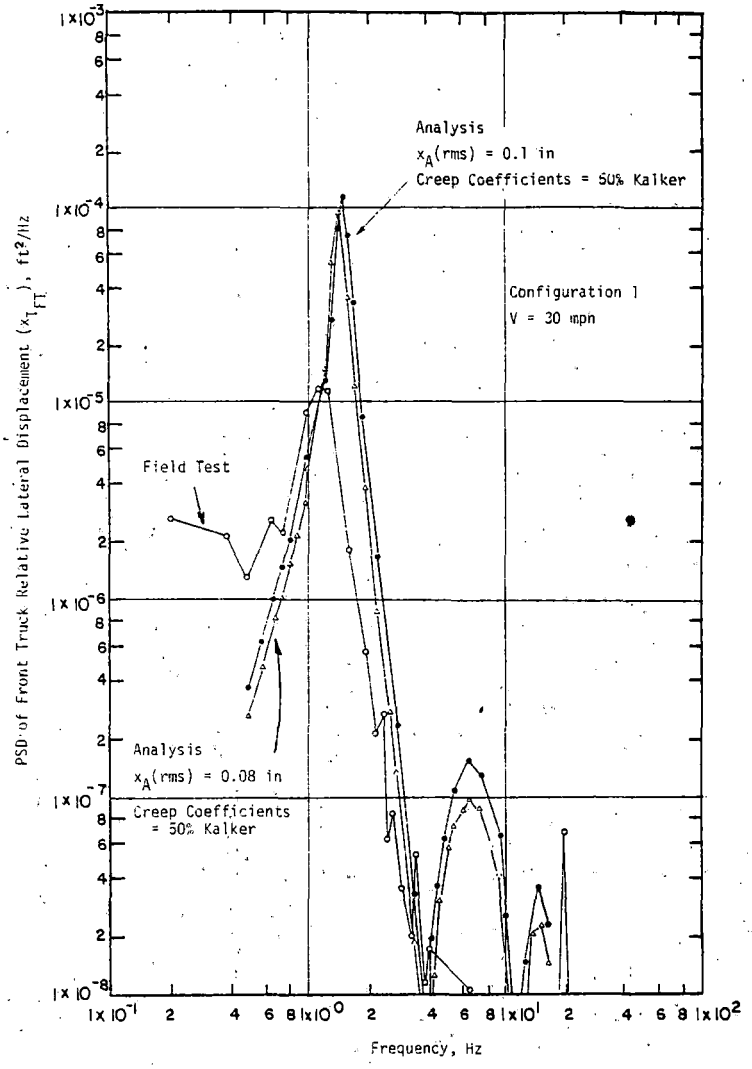

Figure 5-20. Comparison of Analysis and Test Results for Configuration 1 at 30 mph.

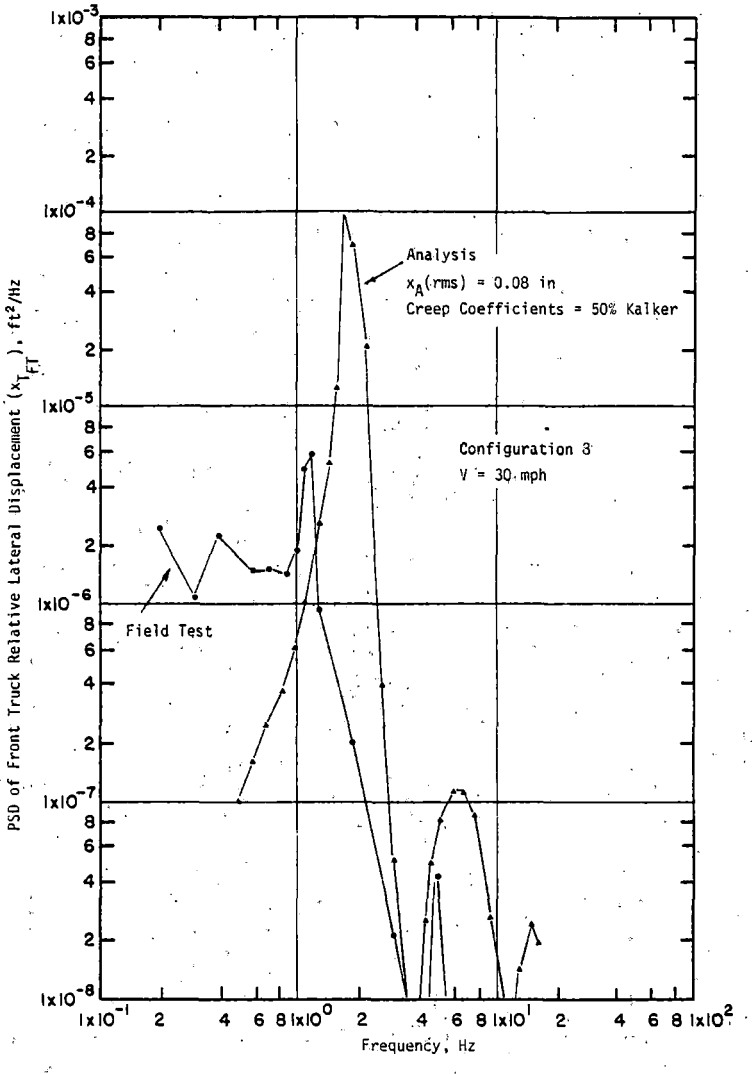

Figure 5-21. Comparison of Analysis and Test Results for Configuration 8 at 30 mph.

Only qualitative comparisons of trends can be made between the results of the hybrid simulation and field test results, because the hybrid simulation model is only a half car body with a single truck rather than a complete car with two trucks. In addition, as discussed earlier, the creep coefficient values, the rolling line offset, and the actual levels of suspension friction were not precisely known. Although the suspension friction levels were determined previously in laboratory tests, it is suspected that corrosion, contamination, and environmental effects such as humidity may influence these levels. Also, the actual inputs due to lateral alignment were never successfully determined during field tests.

Limit Cycle Studies

Figure 5-22 shows the limit cycle behavior of the hybrid simulation of Configuration 6. Dither was introduced into the friction elements of the suspension to simulate the random variation in normal force across the friction elements due to response to vertical track irregularities. The wheel-rail geometric constraint functions were smoothed to remove irregularities artificially introduced in the calculation of the functions.

The results were obtained from the response of the vehicle to initial conditions as it traversed perfectly smooth track. The dotted lines indicate unstable limit cycles while the solid line indicates the amplitude for the stable limit cycle or hunting oscillation. For example, at 50 ft/sec, an initial condition in x_T smaller than the lower dashed line would lead to a decaying oscillation. If an initial condition larger than this value occurred, the motion would grow in an oscillatory manner until the amplitude reached the value of the solid line. For values of initial conditions larger than the solid line but less than the upper dashed line, the ensuing oscillatory motion would decay in amplitude to the stable limit cycle value of the solid line. This amplitude corresponds to the flange clearance value. For initial conditions greater than the upper dashed line, the motion would grow without bound, i.e. a derailment is indicated.

Examination of this figure leads to the observation that for speeds above about 30 ft/sec, increasingly smaller values of initial

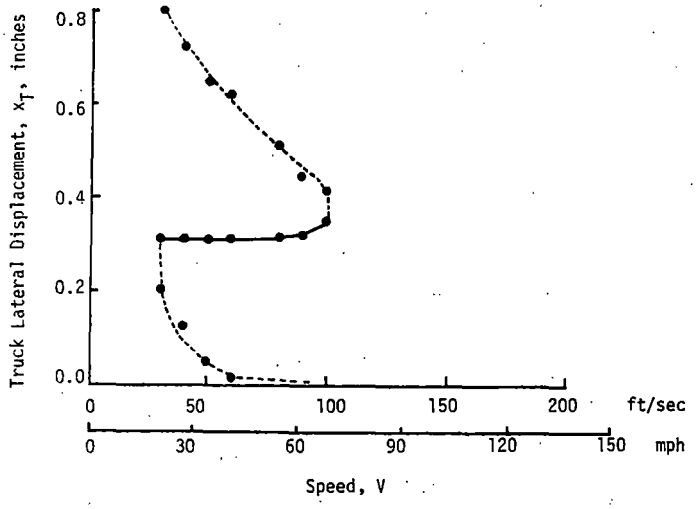

Figure 5-22. Limit Cycle Behavior of Configuration 6 With Dither and Wheel-Rail Constraint Functions Smoothed 14 Times

conditions will permit the exceedance of the lower unstable limit cycle. In practical terms, this means that for very smooth track hunting may not occur until about 100 ft/sec. At low speeds on rough track, however, track irregularities can set up motions or initial conditions that will very probably lead to hunting. As speed increases, the track must be of increasingly better quality if the truck motions are to remain small to avoid hunting. This behavior where the occurrance of hunting depends on the magnitude of initial conditions is in distinct contrast to results that would be predicted by a linear analysis (where a distinct critical speed value is predicted). This may be the reason that a range of speeds for hunting was observed during field tests (Figure 4-8).

Results for the hybrid simulation of Configuration 7* are shown in Figure 5-23. Note that the speed at which stable limit cycle is first established is between 50 and 60 ft/sec. This is higher than the corresponding value of approximately 30 ft/sec for Configuration 6. This trend is similar to that observed in field tests but, as might be expected due to the model differences, the values are not the same.

Effect of Dither

Results for Configuration 2 (the empty vehicle with CN profile A wheels) with and without the dithering effect on the normal load across the suspension friction elements are shown in Figures 5-24 and 5-25, respectively. Note that dither plays a strong role in the limit cycle behavior. With no dither, corresponding to very smooth vertical alignment characteristics,

* Recall that Configurations 6 and 7 were the empty and loaded vehicles, respectively, with 1/20 wheels.

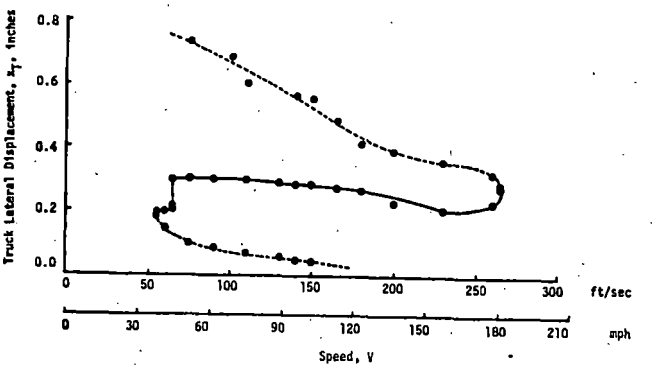

Figure 5-23. Limit Cycle Behavior of Configuration 7 with Dither and Unsmoothed Wheel-Rail Constraint Functions

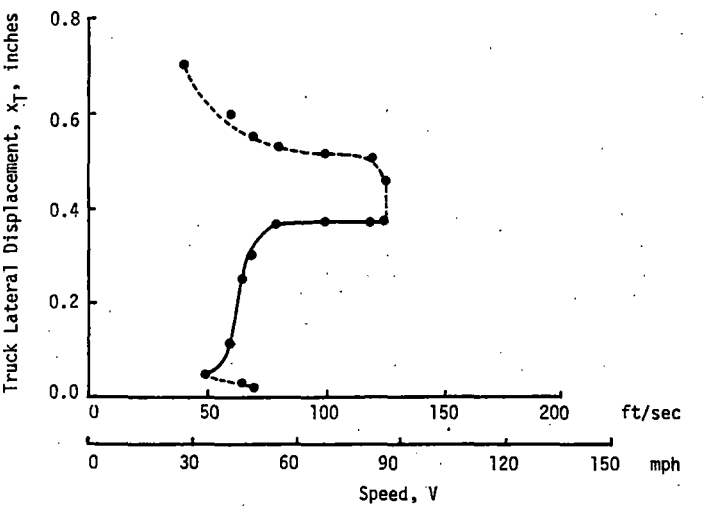

Figure 5-24. Limit Cycle Behavior of Configuration 2 With Dither and Wheel-Rail Constraint Functions Smoothed 14 Times

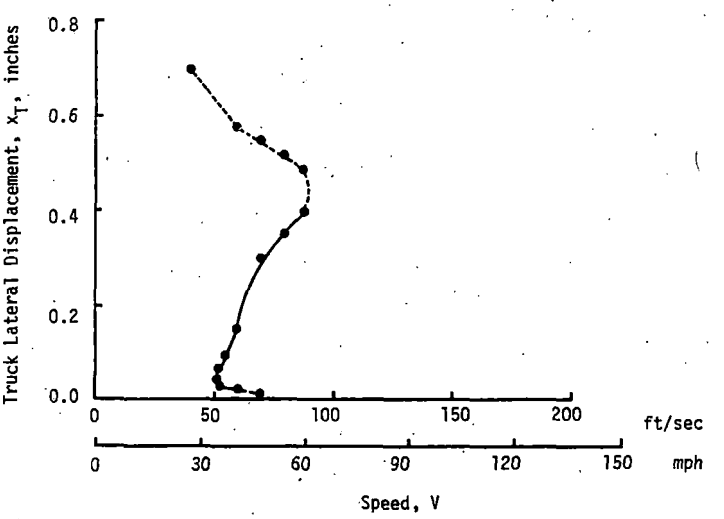

Figure 5-25. Limit Cycle Behavior of Configuration 2 Without Dither and Wheel-Rail Constraint Functions Smoothed 14 Times

there is no stable limit cycle above about 90 to 125 ft/sec. Thus dither extends the speed range for hunting oscillations and avoids the possibility of derailment suggested by Figure 5-25 for speeds over 90 ft/sec.

A second point to be emphasized is that the dither (assumed to be the result of a vertical track alignment input) affects the lateral dynamic response of the vehicle. It should be expected that this coupling between vertical and lateral motions would be exhibited for the actual vehicle and that changing the vertical inputs would change the limit cycle behavior.

Stability of Loaded vs. Empty Car

Results shown for Configurations 6 and 7 in Figures 5-22 and 5-23 indicate that when the vehicle with 1/20 wheels was loaded, hunting limit cycles could not occur until a speed of about 50 ft/sec was obtained (as contrasted with about 30 ft/sec for the empty car). Stable limit cycles could be sustained up to about 260 ft/sec for the loaded car while this speed was about 100 ft/sec for the empty car. Consequently, the loaded car would certainly appear to be more stable. This trend was seen during field tests (see Figure 4-8) where for truck A the hunting limit cycle was initiated at about 46 mph (67.5 ft/sec) for the empty vehicle as compared with about 75 mph (111.5 ft/sec) for the loaded car.

The vehicle with CN profile A wheels (see Figure 3-12) exhibited somewhat similar behavior. The results for the limit cycle study for the empty and loaded cars with CN-A profiles (Configurations 2 and 8, respectively) are shown in Figures 5-24 and 5-26. Note that although the lowest speed for a hunting limit cycle is only slightly higher for Configuration 8 (about 55 ft/sec as compared with 50 ft/sec for Configuration 2), the amplitude of the stable limit cycle is only about 0.1 inch for the loaded car as compared with a very rapid build-up to almost 0.4 inches (or flange clearance) for the empty car. This would lead an observer to consider Configuration 8 to be more stable than 2. During field tests, Configuration 8 was observed to hunt at about 50 mph (73.4 ft/sec) as compared to between 30 and 45 mph (44 and 66 ft/sec) for Configuration 2. It is possible that low amplitude hunting was obscured by the response to rough track for Configuration 8 during field tests. While the hybrid results indicate probable derailment for speeds above about 175 ft/sec for Configuration 8, it should be recalled that the actual wheel-rail contact angles will not be small as assumed, and the wheelset will not derail so easily. In fact, field test results indicate a hunting limit cycle without derailment (Figure 4-8).

Response to On-Board Forcers

The case of the on-board forcers described in Chapter 3 and 4 was also simulated on the hybrid computer. In studying the test data obtained with these forcers, we were concerned about the contamination of the transient signal by the response to the track irregularities. Consequently, we simulated the action of the forcers both on perfectly smooth track and on

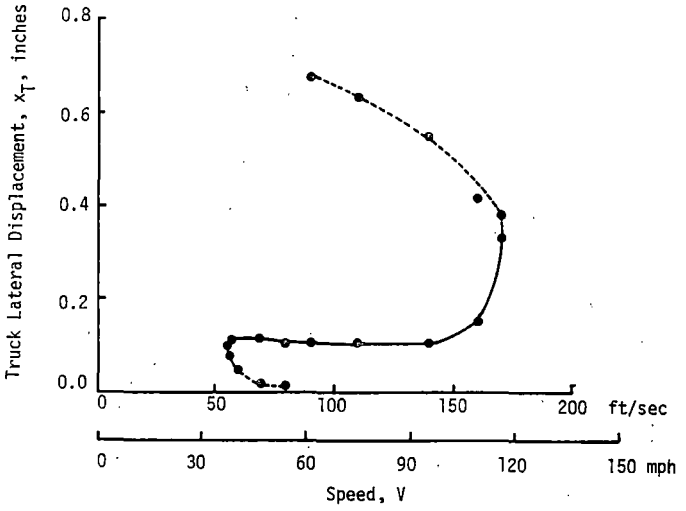

Figure 5-26. Limit Cycle Behavior of Configuration 8 With Dither and Wheel-Rail Constraint Functions Smoothed 14 Times

track with random lateral irregularities of the centerline (0.04 inches RMS). We were then able to evaluate the system damping characteristics using a simple log-decrement analysis [5-7] of the transient decay.

All time histories and estimates of damping ratio described from here on for Configuration 6 used a model for which the wheel-rail geometric constraint functions were not smoothed (in contrast to the limit cycle results shown in Figure 5-22). The results of the limit cycle study for Configuration 6 with dither but no smoothing are shown in Figure 5-27. This version of Configuration 6 exhibited a slightly higher value of speed for the onset of hunting limit cycles (about 55 ft/sec as compared with about 30 ft/sec for the smoothed wheel-rail functions).

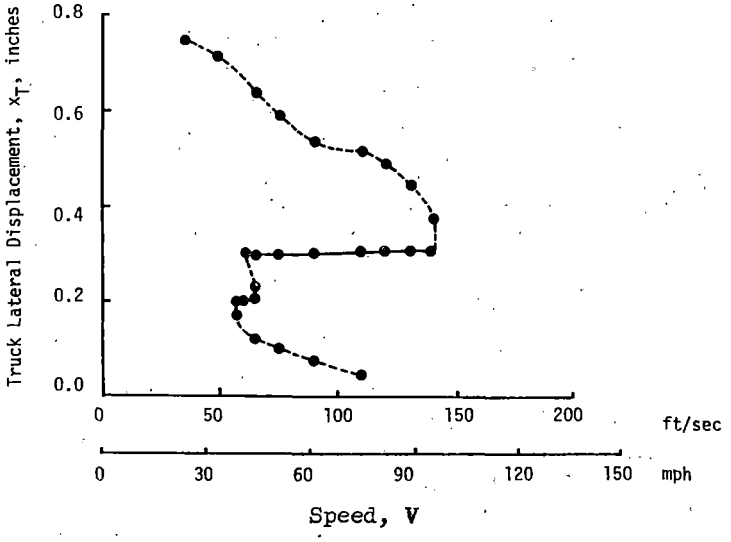

Figure 5-27. Limit Cycle Behavior of Configuration 6 with Dither and Unsmoothed Wheel-Rail Constraint Functions

Simulated time histories for the response of Configuration 6 to truck forcers on smooth track at 20.44 mph are shown in Figure 5-28. The forcers command a yaw moment or torque to the truck bolster. As the forcers are applied, the wheelsets are displaced laterally (x_1 and x_2 for front and rear wheelsets, respectively) to supply a reacting torque due to longitudinal creep forces. The other variables shown in Figure 5-28 are car body lateral (x_c), truck warp (θ_w), truck yaw (θ_T), and truck lateral (x_T). Upon release of the forcers, a well-defined transient decay occurs. Results of using log-decrement analysis at several values of speed for Configuration 6 on smooth track are shown in Figure 5-29. The damping ratio ζ, is calculated from the relationship:

$$\zeta \simeq (1/2\pi)\ln(a_1/a_2)$$

where a_1 and a_2 are the amplitudes of successive peaks of the transient decay signal. This equation is valid for values of ζ small enough that $\sqrt{1-\zeta^2} \simeq 1$. A band is shown centered about each value of ζ. This band has a width of 2σ where σ is the standard deviation of about 20 to 25 estimates of ζ. These sets of estimates were made by taking the ratios of a number pairs of peaks from a single transient signal as well as analyzing several distinct transient signals resulting from separate forcer applications. As may be seen, the width of the band is rather large and indicates the difficulty in accurately calculating ζ by this method for low values of ζ.

The response to the forcers while the vehicle traversed track with random lateral alignment irregularities was also simulated. The probability and power spectral density functions calculated for the lateral track alignment are shown in Figure 5-30 for a speed of 40 ft/sec (27.27 mph). The PSD is approximately constant out to a break frequency corresponding to 0.01 cyc/ft after which it falls off with the square of the frequency. The rms value of lateral alignment irregularities used in the simulation was 0.04 inches.

A typical response of Configuration 6 to the truck forcers as the vehicle traversed irregular track is shown in Figure 5-31. In addition to the response variables shown previously in Figure 5-28, the variable x_{TFT} and the centerline alignment input signal x_A are shown. As previously discussed, x_{TFT} is the lateral position of the wheelset relative to the track centerline, the signal called "truck lateral" in the field test data. The response of the truck to the combined forcer initial condition and x_A signal may be seen in the various response variables. The contaminating effect of x_A may be seen by comparing the x_T signals for operation on smooth and on rough track (Figures 5-28 and 5-31). Not only is the vehicle responding to both x_A and the forcers, but x_{TFT} includes the alignment signal x_A, as well. Due to the presence of x_A in the x_{TFT} signal, the peaks of the transient after forcer release are not well defined, making it difficult to apply the log- decrement procedure.

Results of applying the log-decrement procedure to the forcer response data on rough track are shown in Figure 5-32. These results

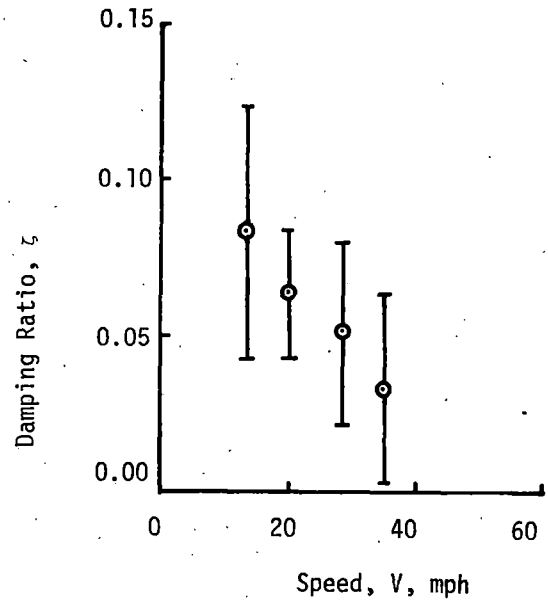

Figure 5-29. Damping Ratio versus Speed for Configuration 6 Using Log-Decrement Analysis (Hybrid Simulation).

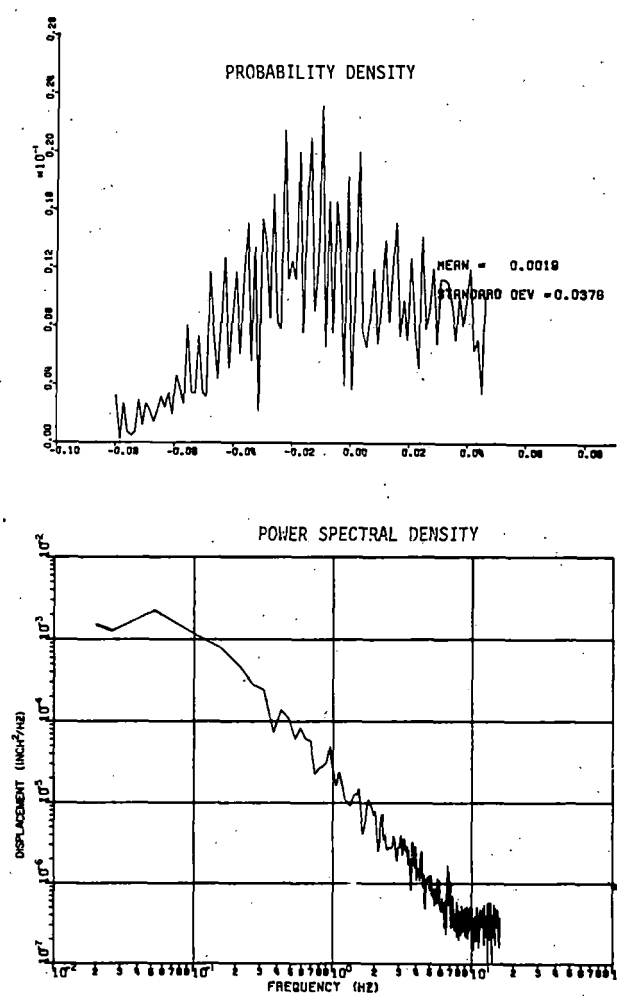

Figure 5-30. Probability Density and PSD Functions of Simulated Track Alignment Irregularities with 0.04 inches RMS Roughness for Hybrid Simulation at 27.27 mph

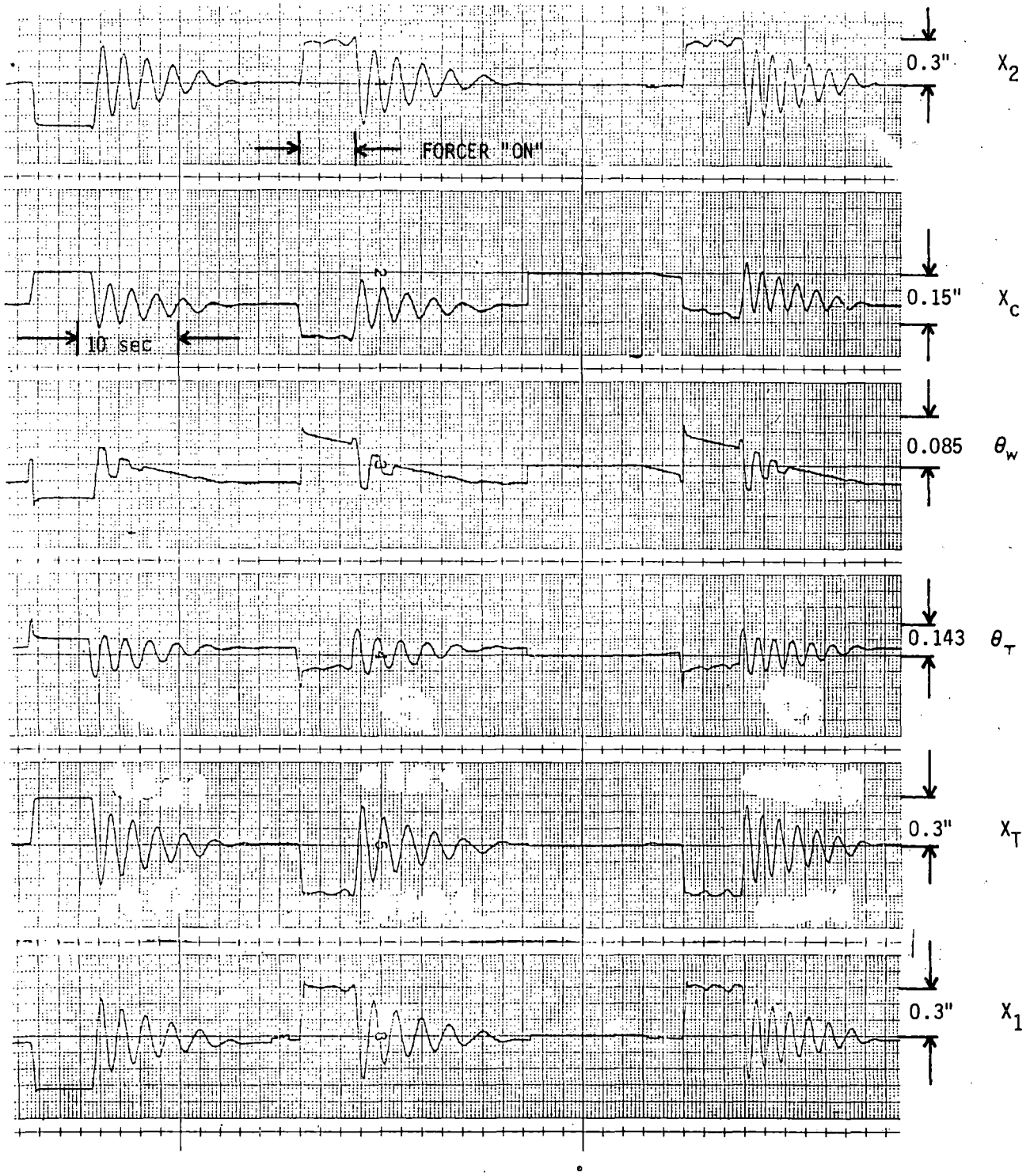

Figure 5-28. Response of Configuration 6 to Truck Forcers on a Smooth Track at 20.44 mph (Hybrid Simulation)

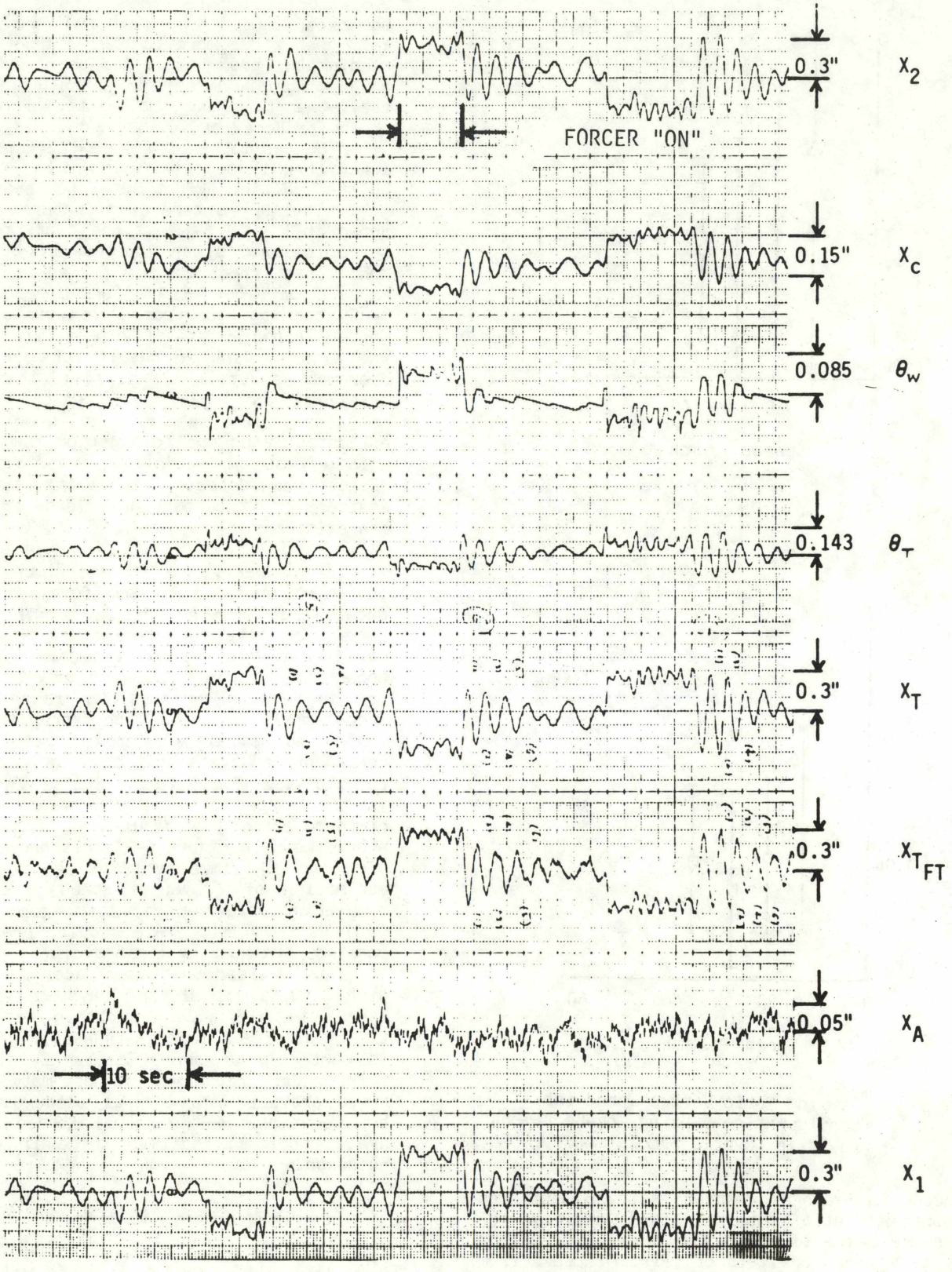

Figure 5-31. Response of Configuration 6 to Truck Forcers at 20.44 mph and Track Roughness of 0.04 inches RMS (Hybrid Simulation)

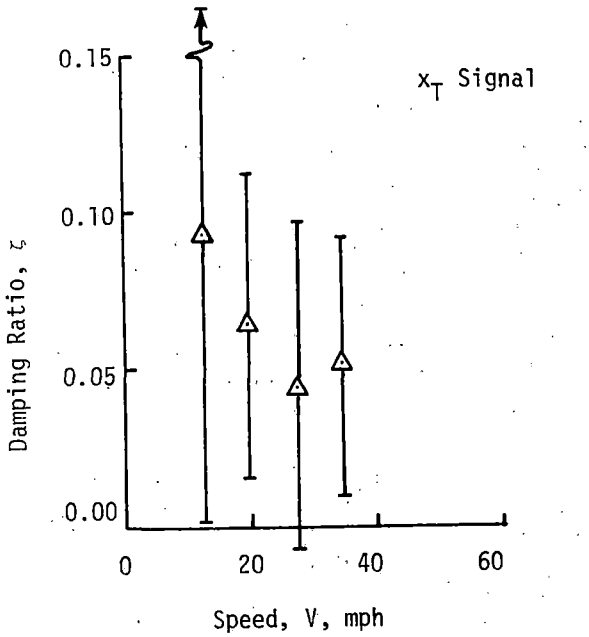

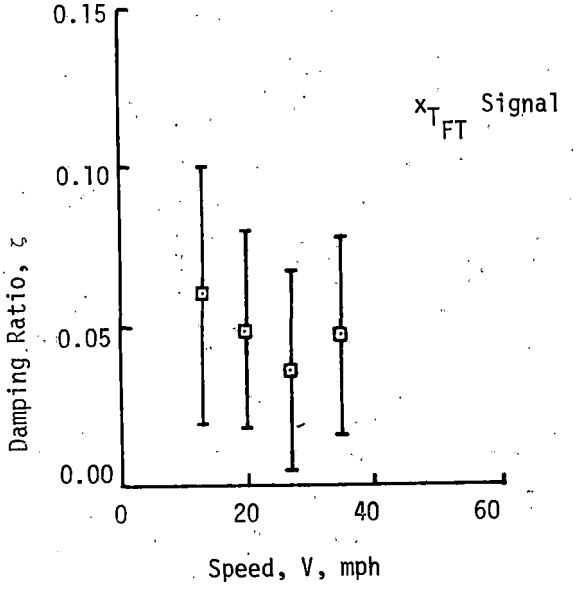

Figure 5-32. Damping Ratio Versus Speed for Configuration 6 Using Log-Decrement Analysis (Hybrid Simulation)

represent an average of about 13 to 16 estimates of damping ratio obtained from analysis of successive pairs of peaks for a given transient decay as well as analysis of pairs of peaks from distinct decay signals. As done previously in Figure 5-29, 2σ bands centered about the mean estimate for each value of ζ are also shown. Note that there is considerable uncertainty (as measured by the width of the 2σ bands) in estimating ζ via the log-decrement approach from these signals. However, the level of uncertainty for these estimates obtained from operation on rough track seems to be of the same order as that associated with the estimates obtained from operation on smooth track (Figure 5-29). Thus, the uncertainty associated with the ζ estimates is probably due more to the accuracy of actually reading the peak values (or to other causes such as the nonlinear effect of suspension friction etc.) than to either the effects of random input, or the presence of x_A in the x_{TFT} signal.

The estimates of ζ from the x_{TFT} signal are lower than those obtained from x_T. This is due to the additive effect of x_A to the response x_T. A particularly interesting feature of the plots shown in Figure 5-32 is the decrease in ζ with speed followed by an increase of ζ at about 36 mph. This effect was not present in the ζ estimates from smooth track forcer response (Figure 5-29) but was observed in analysis of field test forcer response data (Figure 4-15). This effect was also evident in results obtained by random decrement analysis of the field test data (Figures 4-12 and 4-13). The reasons for this are not clear. The rather large uncertainty in the estimates leads one to question the existence of this effect although the fact that the same effect was detected in using two different analyses of field test data lends credibility to its existence.

In summary, the investigation of the log-decrement analysis of the forcer response data showed that even on ideally smooth track, there is a high level of uncertainty associated with estimating the system damping. The level of uncertainty for response on smooth track is of the same order as that for rough track (0.04 inches rms). Straight line extrapolations of the mean damping ratio estimates obtained by log-decrement analysis of the various simulation results would indicate a value of $\zeta = 0$ somewhere in the range of 45 to 55 mph. This may be compared with the results of the limit cycle study shown in Figure 5-27 that predict the onset of a hunting limit cycle at about 40 mph. The estimation of ζ versus speed from the hybrid simulation does not yield the same speed (when $\zeta=0$) as the limit cycle studies predict for the onset of the hunting limit cycle.

It is clear that even under perfect simulation conditions, plots of system damping versus speed are difficult to obtain accurately from time histories. This is true even when the track is perfectly smooth. Similar levels of uncertainty and inaccuracy in estimating ζ versus speed prevail when lateral track irregularities both contaminate the actual forced response and are present as additive noise in the measured response.

Spectral Analysis of Simulation Data

Spectral analysis was conducted of the simulated time response for various configurations of the 5 degree-of-freedom nonlinear model. This analysis was done using the same software package that was used for the field test data. The results of these analyses can be compared qualitatively with those obtained during field tests bearing in mind that the inputs to the vehicle that occurred during field tests were never adequately determined.

The simulated time histories for Configuration 6 (with dither and unsmoothed wheel-rail geometry functions) at 34.3 mph are shown in Figure 5-33. The units for the angular response variables are degrees. Recall that the speed at which hunting limit cycles first occur for this configuration is about 39 mph. Note the response of the wheelset lateral displacements (x_1 and x_2) is typical of a narrow band random process. This also may be seen in the other response variables. The action of friction in the truck suspension may be seen clearly in the truck warp (θ_w) where the motion is "sticky" and "jerky". The presence of x_A in the x_{TFT} signal gives high frequency components that make it look "rougher" and broader band than the x_T signal (note also that the polarities are reversed for these two signals). At 46 mph, the response (as shown in Figure 5-34) clearly shows the sustained hunting limit cycle where, during much of the time, x_1 and x_2 reach amplitude values equal to the flange clearance of 0.3 inches. On smooth track, however, flange contact occurs on every cycle of the oscillation at 46 mph. The variable ϕ_c is the car body roll.

It is interesting to compare the power spectral density calculated for the absolute truck lateral displacement (x_T) with that obtained for the relative displacement (x_{TFT}). Of course, the x_T signal was not available during field tests and only x_{TFT} could be measured. The PSDs for the X_T and X_{TFT} signals obtained from the hybrid simulation are shown in Figures 5-35 and 5-36, respectively, for speeds of 24.9, 34.3, 46.0, and 53.8 mph. At these latter two speeds the vehicle is hunting as the limit cycle study (Figure 5-27) indicates the onset of a hunting limit cycle at about 39 mph.

Below the critical speed and for frequencies below that of the hunting mode, analysis of a single wheelset [1-15] indicates that the wheelset follows the track irregularities, i.e. the wheelset lateral displacement should be approximately the same magnitude and in phase with x_A while the relative displacement should be very small. As frequency increases beyond the hunting mode, the wheelset response to the irregularities decreases. As a result, the relative displacement is approximately the same magnitude and out of phase with the irregularities. As described in the statistical linearization section, these trends are similar for complete vehicles.

Note that below the critical speed (i.e., at 24.9 and 34.3 mph), the low frequency value of the PSD for x_{TFT} is smaller than that for x_T while above the hunting frequency the contribution of x_A to X_{TFT} is evident. The hunting frequency is easily found at all speeds shown as the frequency of the prominent peak response. At the two speeds above the critical speed, 46.0 and 53.8 mph, the PSDs for x_T and x_{TFT} look very similar with the exception of a somewhat more "jagged" appearance of the PSD for x_{TFT} above the hunting frequency.

The probability density functions for x_{TFT}, computed from the simulation time histories are shown in Figure 5-37 for Configuration 6. At 24.9 and 34.3 mph, the density functions for x_{TFT} appear quite similar and look like very spread out Gaussian density functions. At 53.8 mph the x_{TFT} density function shows the two-peak shape typical of a signal comprised of a sine wave plus random noise. The inference to be drawn is that the hunting limit cycle is contributing strongly to the signal. At 46 mph, the density function for x_{TFT} appears to be flat and in a transition between the spread-out (approximately) Gaussian form of 34.3 mph and the two-peak shape of 53.8 mph. The two-peak shape means that the signal is spending much of its time at the extreme values of the motion.

The PSDs calculated for Configuration 6 from the hybrid simulation (Figure 5-36) may be compared with those obtained during field tests (Figure B-6, truck lateral displacements for 24.9, 34.3, 46, and 53.8 mph). Although the peaks for the hunting mode seem to be sharper for the hybrid results (due to the lower critical speed for the hybrid simulation, about 39 mph as compared to the field test values of 46 to 53 mph for truck A, 80 mph for truck B), the frequency of the hunting mode and the general shapes of the PSDs compare well. Similarly, the general shapes of the probability density functions obtained from the hybrid simulation (Figure 5-37) compare well with those obtained from field tests (Figure 4-21) for speeds above and below the initial speed for onset of the hunting limit cycle.

As was done with the data from the field tests, system damping ratios were estimated from the PSDs calculated from the hybrid simulation data. This was done using the PSDs of both the x_T and x_{TFT} signals. The results are shown in Figure 5-38. As was the case with the results of the log- decrement analysis of the forcer response data, smaller values of damping ratio were calculated for x_{TFT} response as compared with the x_T. Again, this is due to the contaminating effect of x_A and the consequent narrowing or sharpening of the peak in the PSDs for the x_{TFT} signal. This may be seen in comparing the PSDs in Figures 5-35 and 5-36 at 24.9 and 34.3 mph. All the values of ζ calculated from the log-decrement procedure for both x_T and x_{TFT} were considerably lower than those calculated using the PSDs. This is the same type of behavior that was observed in analysis of field test data (Figures 4-13 and 4-15). Although this behavior may be due to contamination of the forcer response data by the response to x_A, even the damping values obtained from simulated forcer response data on smooth track (Figure 5-29) were considerably lower than those calculated from the PSDs of the simulated x_T and x_{TFT} response (Figure 5-38).

The simulation results obtained for response to initial conditions of different amplitudes offer some insight into the differences in damping results. Configuration 6 (without smoothing of wheel-rail functions) was run on smooth track at 44.3 mph, 5.5 mph above the approximate speed for first occurance of a stable limit cycle (Figure 5-27). For initial conditions of x_T ranging from 0.05 to 0.09 inches (below the unstable limit cycle), damping ratios from about 0.04 to 0.02, respectively, were obtained for the ensuing decay to equilibrium. Thus, as might be expected for this nonlinear system, damping at a given speed depends on the initial conditions. We would expect that this may also be true at sub-critical speeds.

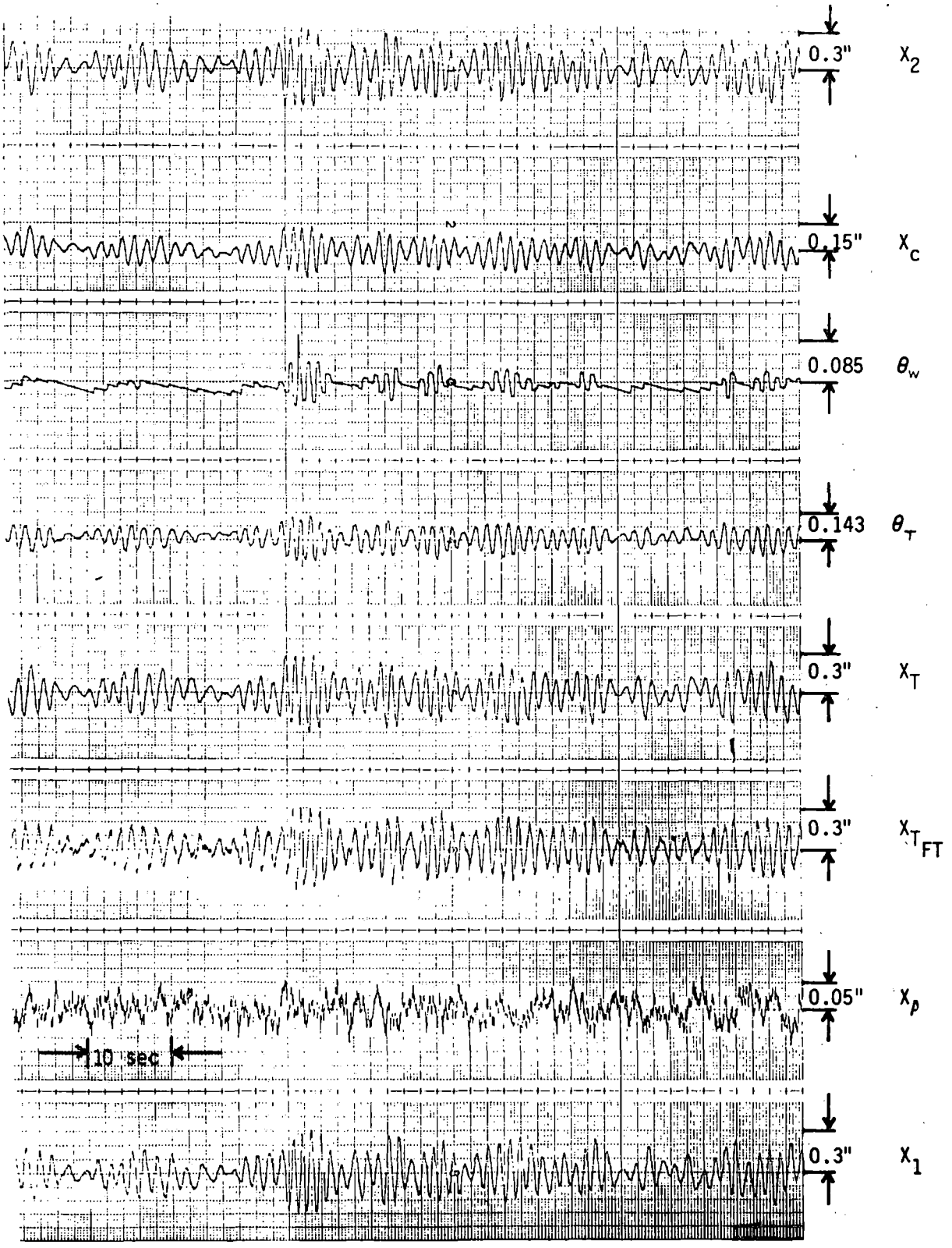

Figure 5-33. Response of Configuration 6 to Random Irregularities in Centerline Alignment at 34.3 mph (Hybrid Simulation; 0.04 inches RMS Track Centerline Alignment).

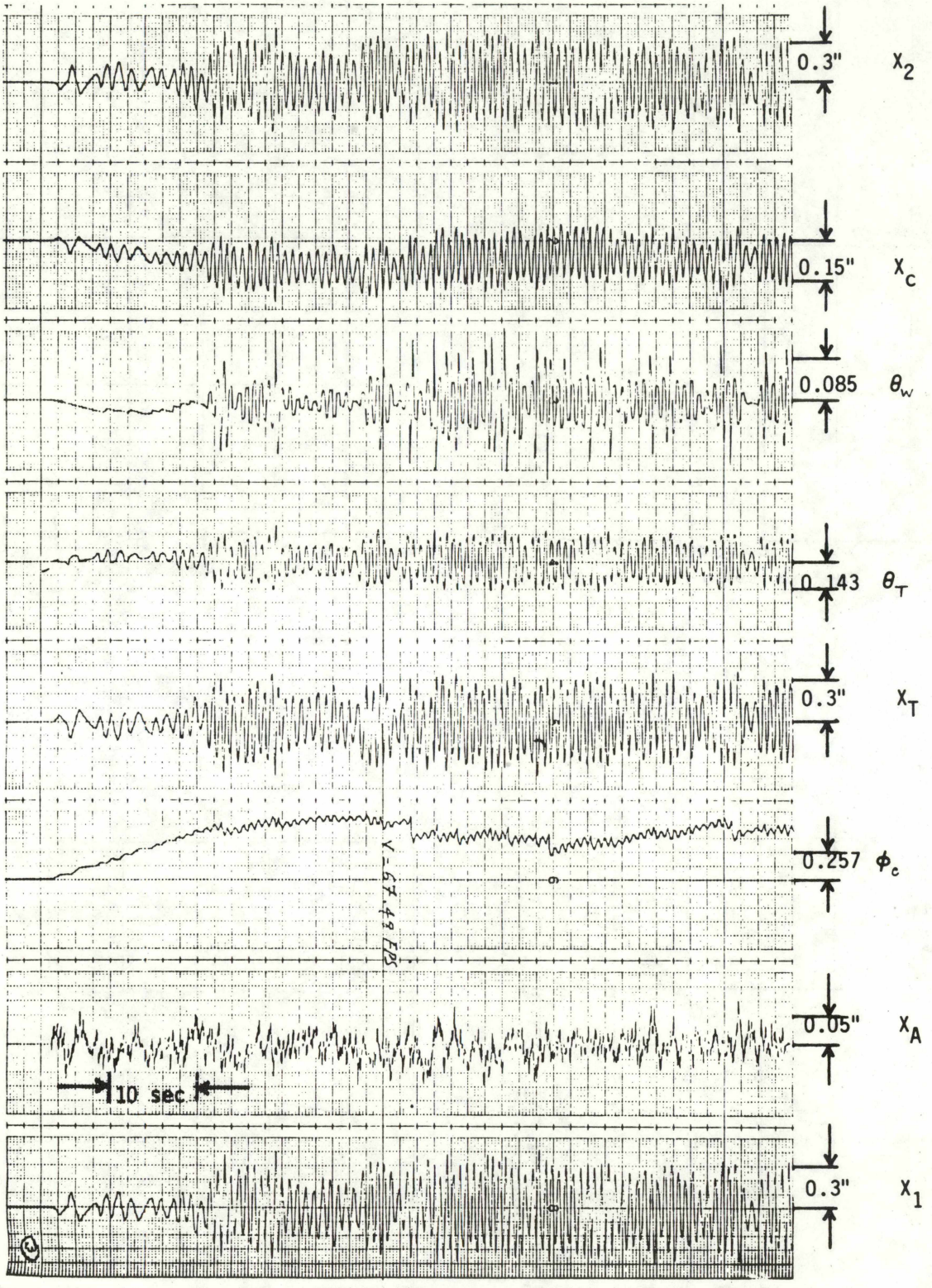

Figure 5-34. Response of Configuration 6 to Random Irregularities in Centerline Alignment at 46.0 mph (Hybrid Simulation; 0.04 inches RMS Track Centerline Alignment).

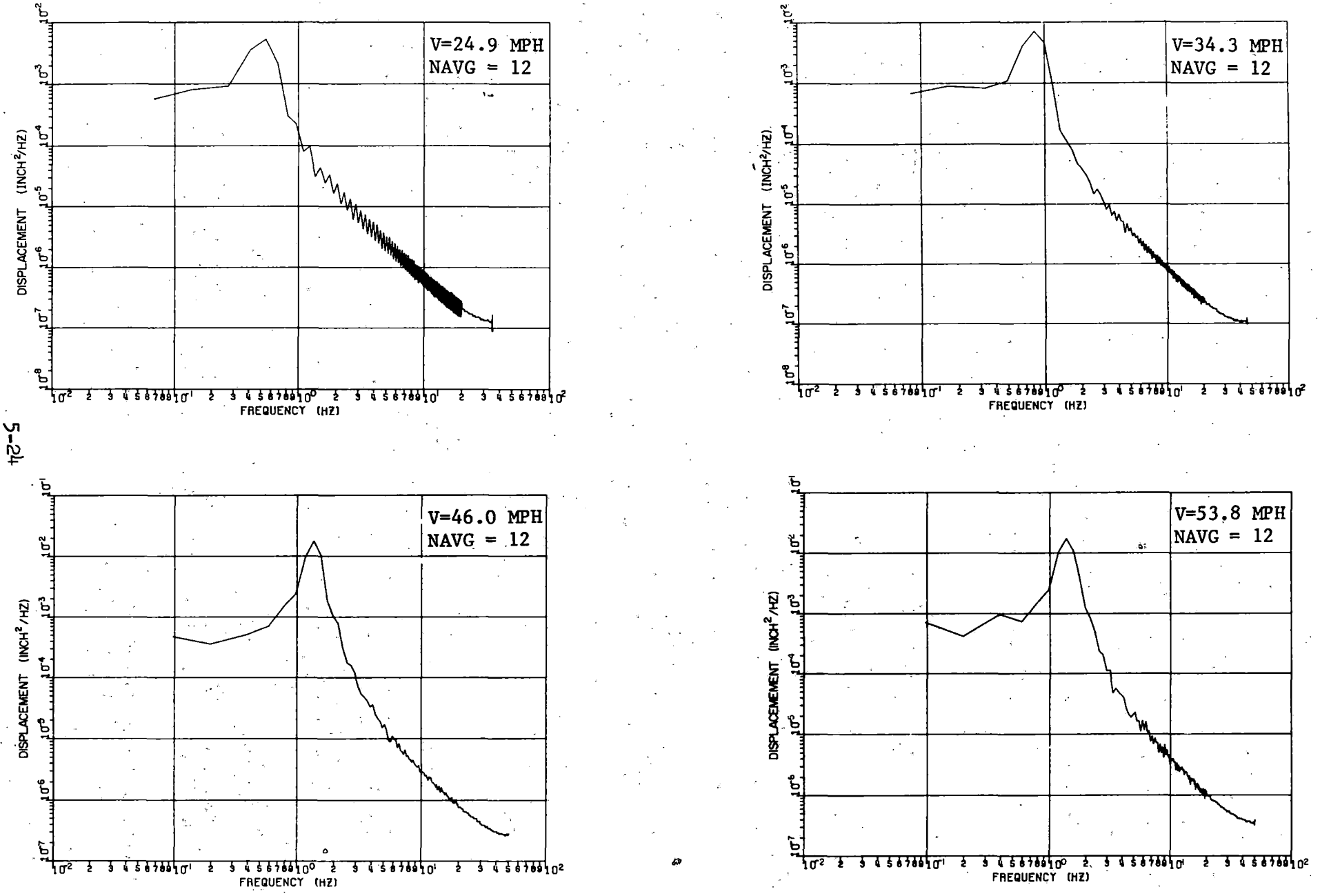

Figure 5-35. PSDs for Truck Lateral Displacement, x_T, of Configuration 6 (Hybrid Simulation; 0.04 inches RMS Track Centerline Alignment).

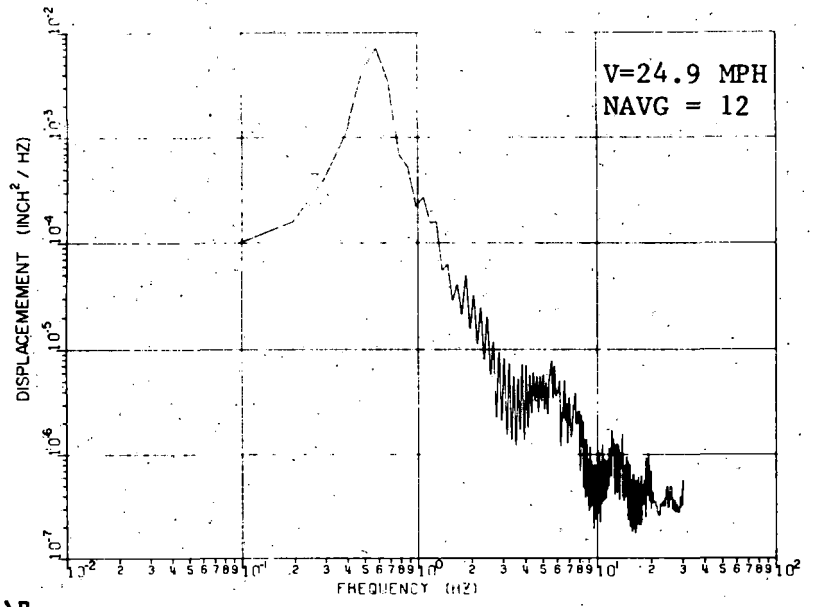

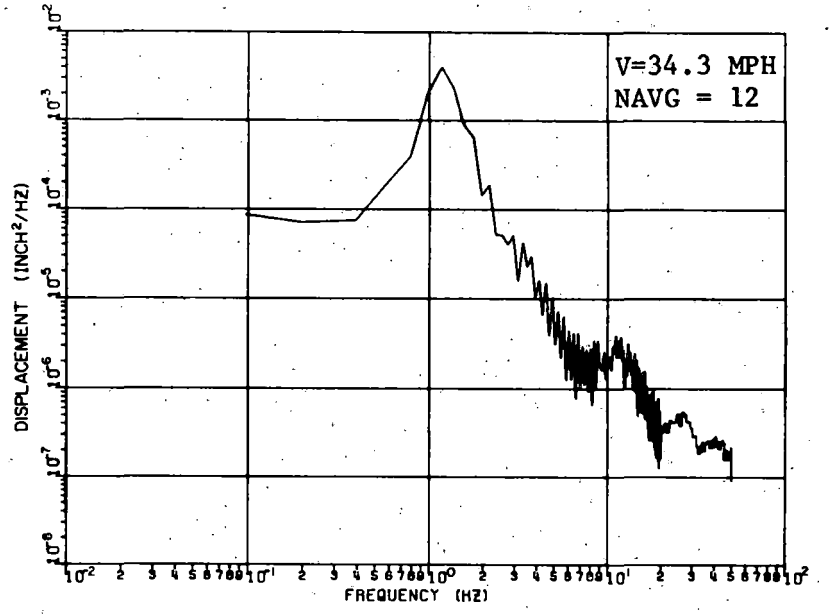

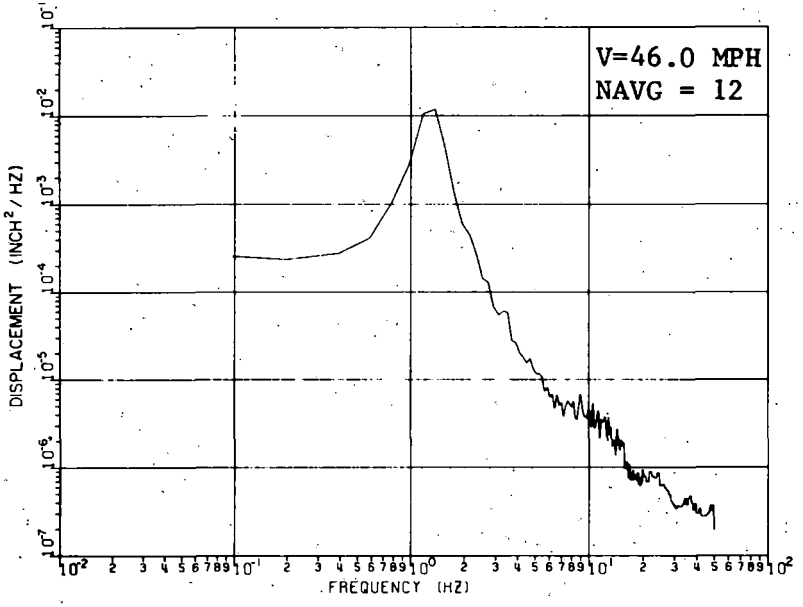

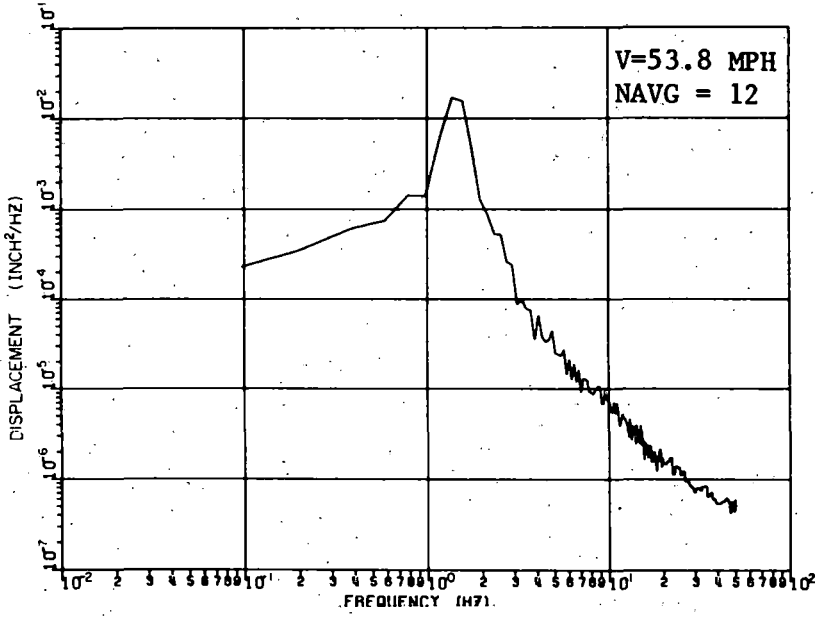

Figure 5-36. PSDs for Truck Relative Lateral Displacement, x_{TFT}, of Configuration 6 (Hybrid Simulation; 0.04 inches RMS Track Centerline Alignment).

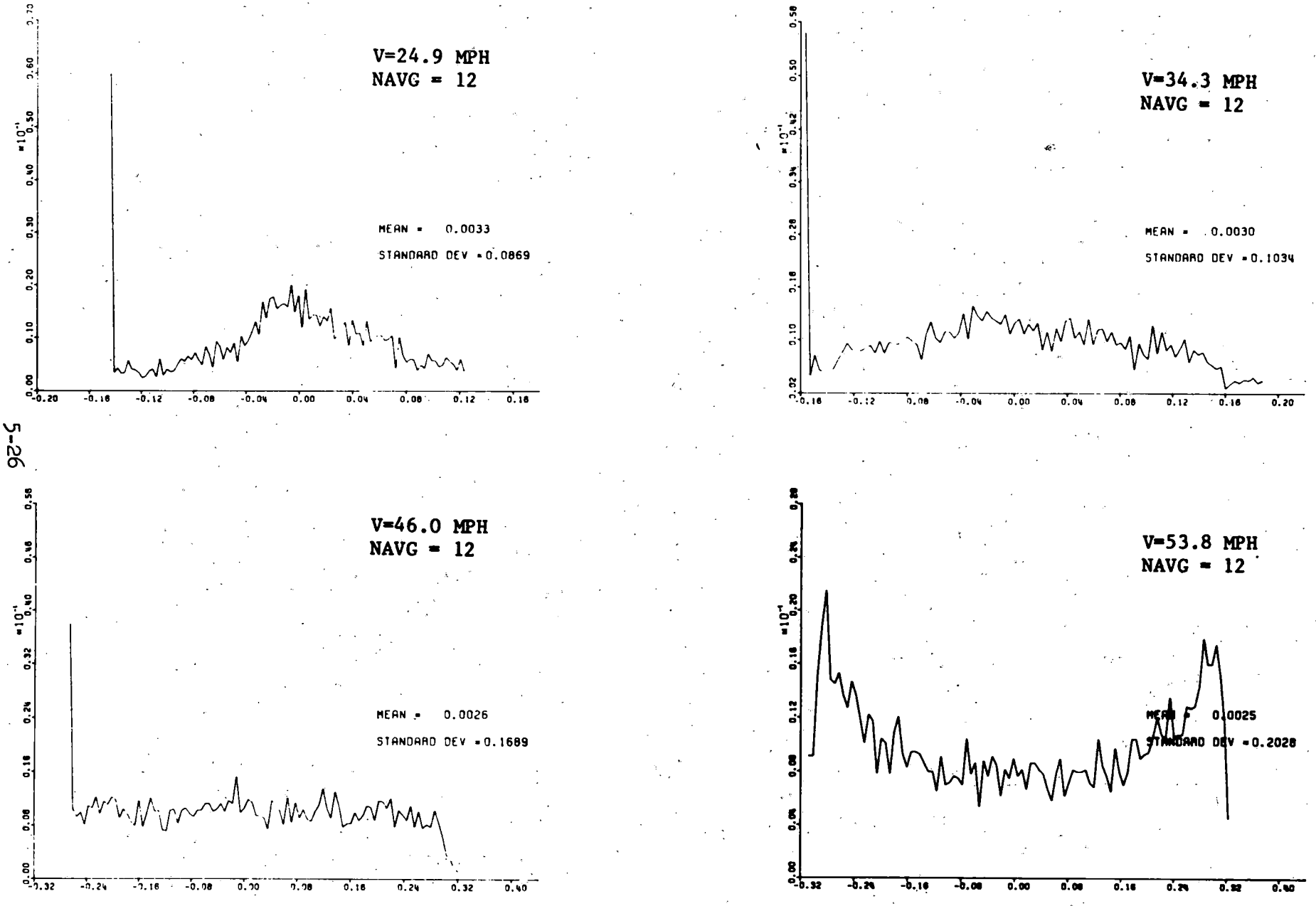

Figure 5-37. Probability Density Functions for Truck Relative Lateral Displacement, $x_{T_{FT}}$, of Configuration 6 (Hybrid Simulation; 0.04 inches RMS Track Centerline Alignment).

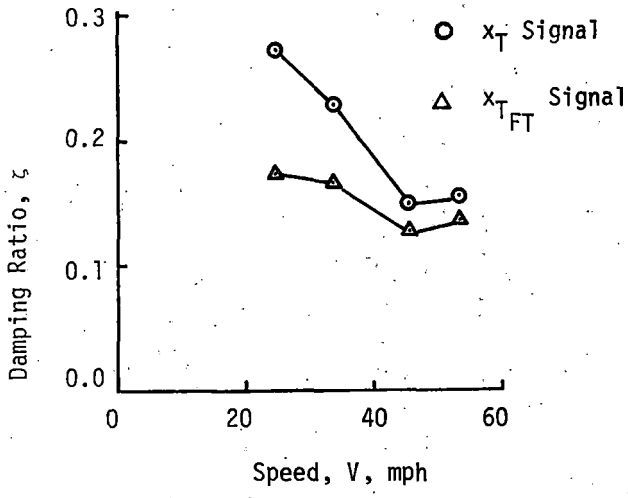

Figure 5-38. Damping Ratio versus Speed for Configuration 6 Using PSDs (Hybrid Simulation)

This dependency of damping on amplitude is not accounted for in the method used to calculate damping ratio from the peak of the PSD. In fact this method assumes that the system response in the half-power bandwidth about the peak is well approximated by the response of a linear, second-order system. In some sense, the damping ratio calculated from the peak of the PSD (at sub-critical speeds) may be an "average" with respect to amplitude and thus be different than the value that would be calculated from the responses to forcer inputs of the same amplitude. More investigation is required to resolve this question.

As can be seen in Figure 5-38, curves of ζ versus speed calculated from the PSDs also show the upswing in ζ (after a certain speed) that was obtained from the forcer response data.

It is interesting to note that although estimates of ζ differ depending on whether the x_T or x_{TFT} signal is used, the differences decrease as speed increases. This would imply that if the uncertainties surrounding the use of ζ as an indicator of hunting can be removed, ζ may be estimated using the measurable x_{TFT} signal. However, one of the purposes of constructing a plot of ζ versus speed is to estimate the stability margin at sub critical speeds. Such a plot constructed from analysis of the x_{TFT} signal may be too conservative because of the underestimation of the ζ values at the lower speeds.

Random Decrement Analysis of Simulation Data

To complete the investigation into the methods used to analyze the response data, we used the random decrement technique to estimate the system damping of the simulated response. As before, Configuration 6 with dither but no smoothing of the wheel-rail functions was used. Damping and frequency of the least damped mode were calculated using the same software package that was used for the field test data. Results of random decrement analysis of the x_T signal are shown in Figure 5-39 together with the corresponding results of the log decrement and PSD analyses. As may be seen, there is considerable disparity in the estimates of damping. However, the random decrement results are closer to those of the log-decrement analysis. This is in distinct contrast to the results of the field tests where the random decrement and PSD analyses gave very similar estimates of damping, both of which were generally higher than the damping predicted by log decrement.

As discussed in Chapter 3, a trigger level must be selected for the random decrement analysis. Except at the lowest speed, 24.9 mph, we found that the damping ratio estimates were fairly insensitive to trigger level.

The unexplained increase in damping with speed above a certain value of speed is also apparent in the random decrement analysis of the simulation data. Another interesting (and unexplained) result is the decrease of ζ with speed at low speed. This was also noted for Configuration 1 and for Configuration 2, truck B, in the field tests (Figure 4-11).

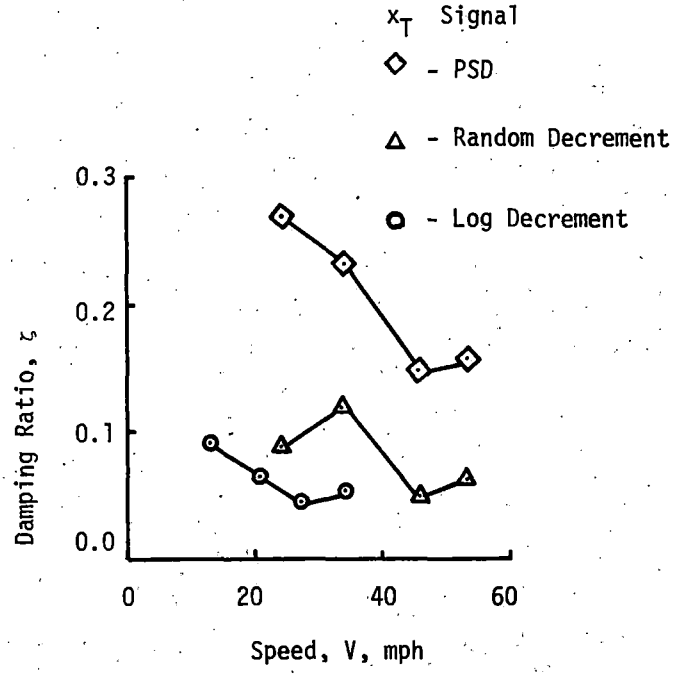

Figure 5-39. Comparison of Damping Ratio Versus Speed Characteristics of Configuration 6 as Determined by PSD, Random Decrement and Log-Decrement Analyses (Hybrid Simulation Results)

SUMMARY

Favorable qualitative comparisons were obtained for results of the hybrid simulation and field tests. These perhaps are best seen in comparing the shapes and characteristics for the PSDs obtained in each case (Figures 5-35, 5-36 and B-6).

The utility of the damping ratio, ζ, as an indicator of (a) stability margin, and (b) the possibility of a hunting limit cycle is open to question. Three different analysis techniques (log decrement, random decrement, and PSD) were used to analyze simulated response data. All three gave different answers for ζ. Furthermore, extending any ζ versus speed curve (by "eyeball") to the point where $\zeta = 0$ gives a speed value for the first occurance of the hunting limit cycle that only approximately compares with that obtained from limit cycle studies.

The concept of damping ratio is used for linear systems. Of course, in the sense of "fitting" a linear response curve to an actual nonlinear response, the idea of "damping ratio" may be used for these nonlinear systems. However, in the light of the results reported above, it does not appear to be very useful as an indicator for the purposes noted. Perhaps a better indicator of stability margin and the onset of hunting limit cycles could be derived (probably empirically) from the probability density functions for the response at various speeds or, as noted in Chpater 4, the rate of change of the RMS truck lateral displacement with speed. In the latter case a speed margin rather than a stability margin could be defined. This possibility was not examined to any significant extent during the hybrid studies and is a topic for future research.

CONCLUSION

As many questions were raised as answered in the course of this study, and unfortunately we were not given sufficient resources to find answers for most of the new questions. Nonetheless, the study shed considerable light on the nature of the freight car dynamic behavior and the adequacy of theoretical models to predict this behavior.

The comparisons of experimental test results with results of linear, quasi-linear and nonlinear theoretical results uncovered the following trends in each area:

1. Linear Modeling and Analysis

   It was seen that the linear model does not adequately represent the behavior of rail vehicles with 3 piece freight trucks. Coulomb friction in the suspension dominates the vehicle behavior and can not be adequately represented in a linear manner. Although describing functions may be used to obtain equivalent linear values, one has very little basis for choosing a priori the nonlinearity input signal needed in the describing function.

2. Statistical Linearization of the Nonlinear Model

   This technique provided encouraging results when PSDs from theory were compared with those obtained experimentally. Both the general shape and frequencies of dominant responses were in reasonable agreement. However, this approach does not provide a direct assessment of hunting stability or stability margin. However, the agreement found gives us some confidence in the model, and suggests that stability can be assessed using a sinusoidal input describing function analysis.

3. Hybrid Simulation with Nonlinear Model

   Qualitative agreement of hybrid computer results for existence of limit cycles with experimental evidence of hunting was obtained. Because the hybrid simulation was limited to a 1/2 car model, quantitative agreement was not expected. Favorable qualitative agreement for the PSDs was also obtained.

   However, this work also indicated that the damping ratio is of questionable utility as an indicator of stability for nonlinear systems such as this freight car.

Overall, the study established that the nonlinear, 9 DOF model for the freight car is capable of producing reasonable agreement of theory and experiment. A linear analysis is inadequate for this type of vehicle, except to provide guidance in a design effort. Because the statistical linearization results look reasonable, we expect that a stability analysis employing sinusoidal input describing functions will also provide reasonably accurate results.

Too many parameters were unknown and too few of the vehicle configurations tested were studied to have great confidence in the results given here. In particular, the roadbed geometry, the railhead geometry and the creep force laws that actually existed at the time of the tests were not measured or identified. These parameters and inputs, which have a very strong influence on the vehicle behavior, had to be estimated or inferred in the work done here.

We did not have resources to pursue fully either the many questions that arose with the limited number of configurations and speeds that were investigated, or investigate the other configurations, speeds, and response variables for which test data were available. As a result, we consider that the efforts described represent only a first step in the difficult process of validating the models used.

Chapter 6

CONCLUSIONS

SUMMARY

This field test and model validation research has provided a significant advancement in our understanding of rail freight car dynamics, and increased considerably our confidence in the present theory for the dynamics of such rail vehicles. As such, the many man-years of effort that went into test planning, test conduct, data analysis, theoretical developments and the comparison of theory and experiment were quite worthwhile. Nonetheless, conclusive validation of the existing theory for rail car lateral dynamics was not obtained in this project. This should not suggest that the existing theory is inadequate, but rather that the comparison process is exceedingly difficult. Uncertainties in vehicle and roadbed parameters, experimental uncertainty in the data, the strongly nonlinear behavior of the test car, as well as uncertain and variable quantities in the wheel-rail force laws prevented definitive conclusions concerning the validity of the theory. Equally important is the fact that insufficient resources were available to pursue answers for most of the questions that arose in the comparison stages of the project. Consequently, the efforts reported here must be regarded as one step in a long process toward full understanding rail vehicle dynamics.

The conclusions reached concerning each step, field testing methods, test car behavior, and model validity, are discussed below. Recommendations for future work in this area are outlined at the close of the chapter.

FIELD TESTING METHODS

Railcar field testing requires careful characterization of the vehicle and roadbed as well as careful measurement of vehicle dynamics and analysis of test data. Although a thorough effort to characterize the test vehicle was made in this project, only one truck was characterized, and that done only once. We suspect that there may be a wide variation from truck to truck in important vehicle characteristics such as suspension friction levels, and that these parameters may vary with environmental conditions. Consequently, in future tests, it would be highly desirable to completely identify the dominant vehicle characteristics several times during the test program.

One of the shortcomings of these tests was the lack of adequate roadbed geometry characterization. As explained earlier, alignment, profile and gauge data were measured only one year before and one year after the tests.

Consequently, the actual roadbed condition during the tests was not known, nor were we able to synchronize the vehicle test data with roadbed measurements. This proved to be particularly unfortunate, because nonlinear friction in the vehicle suspension causes the dynamic behavior to depend strongly on the roadbed disturbances. Thus, the roadbed geometry must be known to completely understand the rail freight car dynamic behavior.

The vehicle instrumentation and data recording system used in these tests were well thought out, and they performed well during the tests. The wheel/rail displacement probes, in particular, provided reliable and useful data. The greatest shortcoming of the tests, however, was the failure to obtain initial conditions for these devices. A simple procedure to zero these probes should have been developed.

We would have preferred, given the limitations of testing resources (and the benefit of hindsight), to have more test data for fewer vehicle configurations. Longer runs at the same speed, and runs at more speeds would have given enough data to analyze the anomalous behavior that often occurred. Holding speed more nearly constant during the test runs also would have made the data more useful.

TEST VEHICLE BEHAVIOR

Considerable insight into the nature of the test car dynamic behavior was extracted from the field test results. It was clearly seen that no unique threshold speed for the onset of hunting exists for this vehicle. Instead, a hunting speed range exists in which intermittent hunting occurs in the lower part of the range, and sustained hunting always occurs at higher speeds. The intermittent hunting confirms the nonlinear nature of the rail freight car by illustrating the dependence of vehicle dynamic behavior on the amplitudes of vehicle motions.

The kinematic mode of the test vehicle dominated the vehicle response. As expected, the frequency of this kinematic motion was very nearly directly proportional to speed. The PSD analysis showed that the majority of the energy in vehicle motion was associated with this kinematic mode.

The variations in test vehicle configuration confirmed previous experience concerning the effect of design changes on vehicle stability. Stability was increased by increasing the truck shear stiffness through the addition of truck stiffners. The stability of the vehicle was also increased by adding rotational friction between truck and car body. This was seen by noting that both the dry centerplate configuration and the constant contact sidebearing devices increased the hunting speed range. It is important to recognize that the increased friction levels mean that the friction surfaces may remain locked together under higher force or torque levels, and that one result of increasing rotational friction is to increase the effective rotational stiffness between truck and car. We suspect that the increased stability is primarily due to the increased stiffness rather than the friction itself.

One of the more surprising results found in these tests was the wide variations that may occur in parameters that we had expected to remain constant. The presence of rough as-manufactured tread surfaces on the wheels on one truck for the Configuration 6 and 7 tests (AAR 1/20 taper wheel profiles) apparently caused significantly different behavior to exist between the two trucks, the other of which had smooth treads. This difference can be attributed to a difference in creep coefficients between the two trucks.

The magnitude of the variation in wheel-rail geometric parameters (conicity and gravitional stiffness) along the track was also surprising. Theoretically, this variation should be negligible for constant taper wheels such as the AAR 1/20 profile. Although errors introduced during the wheel and rail profile digitization process caused the 1/20 taper results to be unreliable, large variations were also seen with the CN-A profile. The ratio of standard deviation to mean value of conicity for this profile ranged from 15 to 30% at different track sections. Consequently, a range of effective conicity should be anticipated for vehicles with such profiles.

MODEL VALIDITY

Comparison of the experimental results with those from the theory clearly demonstrated that a linear theory cannot adequately predict the stability or forced response of the rail freight car with three-piece trucks. The high Coulomb friction levels at the centerplate, bolster-sideframe interface, and the bearing adapter have a dominant effect of the vehicle dynamic behavior. Although the friction effects may be treated by an equivalent damping factor in a linear analysis, estimation of these equivalent factors requires knowledge of the amplitudes of vehicle motions. We found that we were not able, apriori, to accurately estimate these amplitudes.

One should keep in mind that there is still a place for linear analysis. Due to the simplicity of linear analysis, it should remain the starting point for evaluating the effects of design changes or environmental factors on vehicle dynamics, although the results can only be interpreted qualitatively. In addition, any design changes that reduce the dominance of the Coulomb friction will also increase the validity of linear models and analysis methods.

Limited comparison of quasi-linear forced random response results with test data indicated that the quasi-linear analysis adequately represents the freight car behavior. This forced response analysis employed random input describing functions. This success suggests that a quasi-linear stability analysis, using sinusoidal input describing functions may provide reasonably accurate stability information.

The nonlinear analysis carried out with a one-half car model on the hybrid computer confirmed that the nonlinear model qualitatively represents the behavior seen in the test car. Intermittent hunting and PSDs with the same shape as the experimental ones were obtained on the hybrid computer. This level of agreement suggests that the nonlinear model for the rail freight car is substantially correct.

The hybrid computer results were also used to evaluate various methods for computing the vehicle stability margin. This work revealed that the random decrement, PSD estimation and hydraulic forcer methods for obtaining a damping ratio v.s. speed curve were unreliable for the nonlinear vehicle. Although some of this unreliability is due to the random nature of the process, it appears that the damping ratio is not a good measure of stability margin for this nonlinear system. In view of the strongly nonlinear character of the vehicle, this result is not surprising. A measure of stability margin for nonlinear systems comparable to the damping ratio for linear systems has not yet been found.

FUTURE WORK

It would be highly desirable to complete the comparison process begun in this project. Due to insufficient funding, we were able only to compare theoretical results with experiment for two or three vehicle configurations. It would be quite useful to complete this work by comparisons with the other five or six configurations. In addition, the results found here suggest that a quasi-linear stability analysis would provide reasonable estimates of vehicle stability. Confirmation of this hypothesis would also be worthwhile.

The nonlinear nature of the freight car with three-piece trucks made it impossible to separate the uncertainties associated with the nonlinear behavior from those of the wheel-rail interaction. Because our first objective is to obtain an understanding of the fundamental wheel-rail interaction, future tests with a more nearly linear vehicle are needed.

The test results obtained in this program had several shortcomings. Perhaps most critical was the lack of an absolute reference for the wheel-rail measurements. This prevented our using the test data to estimate creep force laws to evaluate curving performance. Because the creep coefficient may have a dominant influence on stability, development of a means for estimating creep coefficients would be very useful.

In any dynamic test program the system parameters must be known in order to interpret the test results. We see a great need for simple parameter identification tests and analysis methods that could be used for acceptance testing and proof of concept tests as well as more research oriented testing. Such tests would replace the expensive laboratory tests used in this project to obtain the vehicle characteristics.

REFERENCES

1-1. Law, E. H., Hadden, J. A. and N. K. Cooperrider, "General Models for Lateral Stability Analyses of Railway Freight Vehicles," FRA/ORD-77/36 (PB 272371), June 1977.

1-2. Cooperrider, N.K., Law, E. H., Hull, R., Kadala, P. and J. M. Tuten, "Analytical and Experimental Determination of Nonlinear Wheel/Rail Geometric Constraints," Federal Railroad Administration Report No. FRA-OR&D-76-244 (PB 252290), December 1975.

1-3. Heller, R. and N. K. Cooperrider, "Users' Manual for Asymmetric Wheel/Rail Contact Characterization Program," Federal Railroad Administration Report No. FRA/ORD-78/05, (PB279707), December 1977.

1-4. Goree, J. G. and E. H. Law, "Users' Manual for Kalkers' Simplified Nonlinear Creep Theory," Federal Railroad Administration Report No. FRA/ORD-78/06, December 1977.

1-5. Goree, J. G., "Users' Manual for Kalker's "Exact" Nonlinear Creep Theory," Federal Railroad Administration Report No. FRA/ORD-78/50, August, 1978.

1-6. Haque, I., Law, E. H. and N. K. Cooperrider, "Users' Manual for Program for Calculation of Kalker's Linear Creep Coefficients," Federal Railroad Administration Report No. FRA/ORD-78/71, May 1979.

1-7. Haque, I., Law, E. H. and N. K. Cooperrider, "Users' Manual for Lateral Stability Computer Programs for Railway Freight Car Models," Federal Railroad Administration Report No. FRA/ORD-80/30, (PB 80-176266), April 1980.

1-8. Cooperrider, N. K. and E. H. Law, "Users' Manual for Linear Freight Car Forced Lateral Response Computer Program," Federal Railroad Administration Report No. FRA/ORD-80/85, December, 1980.

1-9. Cooperrider, N. K. and E. H. Law, "A Survey of Rail Vehicle Testing for Validation of Theoretical Analyses," ASME J. Dyn. Sys. Measurements and Control, Vol. 100, No. 4, December 1978.

1-10. Anon., "A Comparison of Theoretical and Experimental Vehicle Behavior Using a 2 Axled Special Vehicle," Report No. 2, Question C116, Interaction between Vehicle and Track, Utrecht, October 1972.

1-11. Fallon, W. J., Cooperrider, N. K., and Law, E. H., "An Investigation of Techniques for Validation of Railcar Dynamic Analyses" Federal Railroad Administration Report, FRA-OR&D-78/19 (PB 279996/AS), March 1978.

1-12. Healy, M. J., "A Computer Method for Calculating Dynamic Responses of Nonlinear Flexible Rail Vehicles, "Wyle Laboratories Report, 1976.

1-13. Platin, B. E., Beaman, J. J., Hedrick, J. K. and Wormley, D. N., "Freight Car Operation, Computational Methods and Engineering Data for Response to Track Cross-level Variation," MIT, Dept. of Mech. Engr., May, 1976.

1-14. Wickens, A. H., "The Dynamics of Railway Vehicles on Straight Track: Fundamental Considerations of Lateral Stability," Proc. Inst. Mech. Engr., Vol. 180, Part 3F, 1966, pp. 29-44.

1-15. Illingworth, R., "The Mechanism of Railway Vehicle Excitation by Track Irregularity," Ph.D. thesis, Keble College, Oxford, 1973.

2-1. Law, E. H., and Cooperrider, N. K., "Freight Car Dynamics: Final Report" Federal Railroad Administration, May, 1981.

2-2. Law, E. H., Hadden, J. A. and N. K. Cooperrider, "General Models for Lateral Stability Analyses of Railway Freight Vehicles," FRA-OR&D-77/36 (PB 272371), June 1977.

2-3. Tuten, J. M., Law, E. H., Cooperrider, N. K., "Lateral Stability of Freight Cars with Axles Having Different Wheel Profiles and Asymmetric Loading," Trans. ASME, J. Eng. for Industry, February 1979, pp 1-16.

2-4. Hedrick, J. K., Cooperrider, N. K. and E. H. Law, "The Application of Quasi-Linearization Techniques to Rail Vehicle Dynamic Analysis," Federal Railroad Administration Report No. FRA/ORD-78/56, November 1978.

2-5. Heller, R., Malstrom, C. W. and E. H. Law, "Hybrid Simulation of Rail Vehicle Lateral Dynamics," Simulation, 1977.

2-6. Cooperrider, N. K. and E. H. Law, "Users Manual for Linear Freight Car Forced Lateral Response Computer Program," Federal Railroad Administration Report No. FRA/ORD-80/85, December 1980.

2-7. Cole, H. A. Jr., "On-Line Failure Measurement and Detection of Aerospace Structures by Random Decrement Signatures," NASA-TND-4503, 1968.

2-8. Matsudaira, T., Matsui, N., Arai, S. and Yokose, K., "Problems of Hunting of a Railway Vehicle on a Test Stand," ASME J. Engr. for Industry, Vol. 91, Series B, No. 3, August 1969, pp. 879-890.

2-9. Healy, M. J. "A Computer Method for Calculating Dynamic Responses of Nonlinear Flexible Rail Vehicles," Wyle Laboratories Report, 1976.

3-1. Private Communication from I. Gitlin, AAR Research Center.

3-2. Orr, D. G., ed., "70 Ton Truck Components Data, Physical Restraints, Mechanical Properties, Damping Characteristics," Track-Train Dynamics Harmonic Roll Series, Vol. 2, 1974.

3-3. McKeown, F. S., "Torsional Resistance at a Truck Bolster/Car Body Centerplate Interface," Test Report - Part IV, ASF Participation in AAR/RPI/FRA Track-Train Dynamics Program," American Steel Foundries, Test Engineering Department, Feb. 22, 1974.

3-4. Abbott, P., "Comparison of the Nonlinear Dynamic Characteristics of the Barber S-2 and ASF Ride Control Freight Trucks," Martin Denver Division Technical Report MCR-76-475, Contract NAS 8-29882, Sept. 1976.

3-5. Anon, "Truck Hunting Model Validation Lab Test To Find Friction Coefficient at Air Bag Side Bearing/Body Bolster Wear Plate," Association of American Railroads Research Center, Informal Report, Fall 1977.

3-6. Helms, H. and Strothmann, W., "Lateral Rail Irregularities - Measurement and Application," The Dynamics of Vehicles on Roads and on Tracks, ed. Slibar and Springer, publ. by Swets and Zeitlinger B. V. - Amsterdam, Proceedings of 5th Vehicle Systems Dynamics - 2nd IUTAM Symposium, Vienna, Austria, September 1977.

3-7. Gilchrist, A. O., "Variation Along the Track of Conicity and Rolling Line Offset", British Rail Research Dept. Technical Note DYN. 62, July 1967.

3-8. Kenworthy, M. A., and Adair, J. W., "Test Results Report-Track Geometry Measurements in Support of Freight Car Lateral Dynamics Program," Department of Transportation Report DOT-FR-78-22, March 23, 1978.

3-9. Darien, N. J., "Track Train Dynamics - Phase II, Truck Hunting Model Validation Field Test, Comprehensive Document of Field Test Program," Draft of American Association of Railroads Report.

5-1. Law, E. H., Hadden, J.A. and Cooperrider, N. K., "General Models for Lateral Stability Analyses of Railway Freight Vehicles, "FRAOR&D-77-36 (PB 272371), June, 1977.

5-2. Haque, I., Law, E. H. and N. K. Cooperrider, "User's Manual for Lateral Stability Computer Programs for Railway Freight Car Model," Federal Railroad Admin. Rept. No. FRA-OR&D-80/30 (PB80176266) April 1980.

5-3. Kalker, J. J. "On the Rolling Contact of Two Elastic Bodies in the Presence of Dry Friction," Doctoral Dissertation, Technische Hogeschool, Delft, The Netherlands, 1967.

5-4. Hedrick, J. K., Cooperrider, N. K., and E. H. Law, "The Application of Quasi-Linearization Techniques to Rail Vehicle Dynamic Analyses", U. S. DOT/FRA Report FRA-OR & D-77-36, June 1977, (PB 272371)

5-5. Cooperrider, N. K., et al, "Analytical and Experimental Determination of Nonlinear Wheel/Rail Geometric Constraints", U. S. DOT/FRA Report FRA-OR&D-76-244, December 1975 (PB 252290).

5-6. Malstrom, C. W., Heller, R., Khan, M. S., "Hybrid Computation - An Advanced Computation Tool for Simulating the Nonlinear Dynamic Response of Railroad Vehicles", Proceedings on Advanced Techniques in Track/Train Dynamics and Design, Association of American Railroads, Chicago, Illinois, March 1978.

5-7. Thomson, Theory of Vibration With Applications, 2nd ed., Prentice-Hall, 1981.

APPENDIX A
WHEEL-RAIL GEOMETRY DATA ANALYSIS

The details of the wheel-rail geometry data analysis process and summary tables of the data treated by this process are given in this Appendix.

PROCESSING OF RAIL AND WHEEL PROFILES

After recording the rail profiles with the DB profilometer, the individual profile tracings were photographed and enlarged to minimize errors during the subsequent digitization process. Coordinate systems were then scribed on the photographs by extending the original vertical and horizontal reference lines until they intersected. This intersection was later defined as the origin of the coordinate system during the digitization process. A reference point 4 inches to the right of the vertical reference line was marked for each profile so that a scale factor could be found. This scale factor was then used in the subsequent conversion to actual scale of the data for the digitized enlarged profile.*

After "conditioning" the profiles in this manner, the enlargements of the rail profiles were sent to the DOT Transportation Test Center at Pueblo for digitization. The digitized profile data were recorded on magnetic tape at Pueblo and returned. This tape was then decoded onto DEC tape at the Clemson Engineering Computer Laboratory and was then further decoded from DEC tape to IBM compatible magnetic tape.

Data cards were then punched from this tape. These contained the titles, reference points and coordinate points for all the profiles taken. There were approximately 18 standard boxes of cards.

The 18 boxes of cards were separated by profile and each profile was stored on an IBM magnetic tape. At this stage the profiles were edited to eliminate spurious and unwanted points. This was done through the use of an editing program that plotted the points recorded for each profile on a video screen. At the conclusion of this step, the edited profiles were again stored on IBM magnetic tape.

At this point the profiles were ready to be used as input to the wheel-rail geometry program described in [1-3]. There were several modifications made to the wheel-rail geometry program so that the coordinate system used with the measured profiles could be used directly in the program.

ANALYSIS OF WHEEL-RAIL GEOMETRY

Using the modified wheel-rail geometry program and the digitized wheel and rail profile data as input, the wheel-rail geometry program was run for both the AAR 1/20 and the CNA wheels at each rail station recorded. Punched card output and plotter output from these runs were recorded on magnetic tape so that selected cases could be chosen for actual plotting and further analysis.

A data analysis computer program was developed and used to analyze the results of the wheel-rail geometry program. The purpose of this program was to calculate the linearized wheel-rail geometry characteristics at each rail station for the two wheel profiles used. In addition, at each station, the rail gauge and the offsets for all the wheel-rail geometric constraint functions were calculated.

The first step in the data analysis was to define the points of flange contact. For the AAR 1/20 wheel, these points were defined as the points at which an average contact angle (over three consecutive lateral increments of wheelset lateral displacement) of 0.15 rad or 8.6 deg. was exceeded. Correspondingly, for the CNA, the value for the average contact angle was taken to be 0.75 rad or 43 deg. Flange contact was then said to occur at the innermost of the three points. Straight lines were then fitted in a least square sense to the curves of $(r_L-r_R)/2a$, $(\delta_L-\delta_R)/2$, and ϕ_w in the regions within flange contact. A straight line was also fitted to the (approximately) even function, $(\delta_L+\delta_R)/2$.

The zero crossing of the straight line fit to the $(r_L-r_R)/2a$ curve was taken as an estimate of the rolling line offset and the slope of the straight line was taken as a linear estimate of the effective conicity, λ. Similarly, the offsets and slopes of the straight lines fitted to the functions $(\delta_L-\delta_R)/2$ and ϕ_w were calculated. For $(\delta_L+\delta_R)/2$, the value of the straight line fit at $x_w = 0$ was calculated.

For wheel profiles such as the AAR 1/20 that should have essentially linear wheel-rail geometry characteristics within the flange contact points, the above procedure is reasonable. However, for wheels such as the CN profile A, these characteristics can be rather nonlinear, even within the tread contact region. Thus, using the predicted rolling line offset position, we chose lateral amplitudes of $\pm$ 0.05 in. and fitted a straight line to the 0.1 in. segment. Slopes and offsets were then calculated for the constraint functions in this segment. The lateral amplitude was then incremented to $\pm$ 0.10 in. and the process repeated. A number of segments were treated in this way until the length of the segment corresponded to the distance between the flange contact points.

Summary tables for the offsets and slopes of the constraint functions for the various track sections are given in Table A-1. Sections 0 and A, given in parts (a) and (b) of the table, are tangent track sections of the UP main line. Section B (part (c)) is taken in the mainline 6 deg. curve described previously and Sections C and D (parts (d) and (e), respectively) are from the mainline 1 deg. curve and entry and exit spirals. Section E (part (f)) is a section of

* For the wheel profiles, two reference points were marked, one to the right and one to the left of the origin. These two points were 6 inches apart. This known distance allowed us to scale the photographically enlarged profiles.

tangent "passing track" adjacent to the mainline near MP 204 east of Barstow, CA.

Because dynamic response data from runs on the curve sections and passing track was not used for reasons previously stated, the table sections (c) through (f) are not discussed. However, because of the uniqueness of these data they are included here for possible use and reference by other researchers.

In the space where the standard deviation is listed for each parameter, two numbers separated by a colon are enclosed in parentheses. The first of these lists the number of the points that are within ± 3 standard deviations of the mean value; the second number denotes the total number of data points. For each entry in parts (a) and (b) of the tables, the limits of the 90% confidence interval for the true mean value are listed. These were calculated using the Student's "t" distribution.

The equations defining the parameters listed in these tables are given below:

$$(r_L - r_R)/2 = \lambda\,(x_w - x_{R_o}) - \lambda x_A \qquad \text{(A-1)}$$

$$(\delta_L - \delta_R)/2 = \Delta\,(x_w - x_{\delta_o})/a - \Delta x_A/a \qquad \text{(A-2)}$$

$$\phi_w = \Gamma\,(x_w - x_{\phi_o})/a - \Gamma x_A/a \qquad \text{(A-3)}$$

$$(\delta_L + \delta_R)/2 = \delta_o \qquad \text{(A-4)}$$

For the AAR 1/20 wheels, the values given are for straight lines fitted over the entire region of tread contact whereas for the CN wheels, values are given corresponding to segments of wheelset lateral displacement of width ± 0.15 in and ± 0.25 in centered at the rolling line offset position. For the AAR 1/20 wheels, in a large number of cases the effective conicity was so small that the rolling line offset position calculated was outside the tread contact region.

Table A-1. LINEAR ESTIMATES OF WHEEL-RAIL GEOMETRIC CONSTRAINT FUNCTIONS

(a) SECTION 0: Tangent Track; MP 208.5 West for 320 ft.		WHEEL PROFILE		
		AAR 1/20	CNA (±0.15 in)	CNA (±0.25 in)
GAUGE	MEAN (IN)	56.464	56.462	56.462
	STD. DEV. (IN)	0.050 (64:64)	0.052 (64:64)	0.052 (64:64)
	90% CONF. LIM.	(56.453, 56.474)	(56.451, 56.473)	(56.451, 56.473)
EFFECTIVE CONICITY, λ	MEAN	0.0291	0.3463	0.4154
	STD. DEV.	0.0314 (61:64)	0.1006 (64:64)	0.0586 (64:64)
	90% CONF. LIM.	(0.0224, 0.0358)	(0.3253, 0.3673)	(0.4032, 0.4276)
ROLLING LINE OFFSET, x_{R_o}	MEAN (IN)	-0.2723	-0.0376	-0.0348
	STD. DEV. (IN)	1.4630 (60:64)	0.0281 (63:64)	0.0215 (64:64)
	90% CONF. LIM.	(-0.5877, 0.0431)	(-0.0435, -0.0317)	(-0.0393, -0.0303)
CONTACT ANGLE DIFFERENCE, Δ	MEAN	-0.8811	9.3899	13.5453
	STD. DEV.	3.3621	4.1979 (64:64)	2.7055 (64:64)
	90% CONF. LIM.	(-1.5829, -0.1793)	(8.5136, 10.2662)	(12.9805, 14.1101)
CONTACT ANGLE OFFSET, x_{δ_o}	MEAN (IN)	-0.0071	-0.0060	-0.0196
	STD. DEV. (IN)	0.2688 (60:64)	0.0327 (63:64)	0.0189 (64:64)
	90% CONF. LIM.	(-0.0651, +0.0509)	(-0.0129, 0.0009)	(-0.0235, -0.0157)
ROLL ANGLE, Γ	MEAN	0.0623	0.1552	0.1619
	STD. DEV.	0.0119 (64:64)	0.0104 (63:64)	0.0123 (63:64)
	90% CONF. LIM.	(0.0598, 0.0648)	(0.1530, 0.1574)	(0.1593, 0.1645)
ROLL ANGLE OFFSET, x_{ϕ_o}	MEAN	-0.0848	-0.0644	-0.0535
	STD. DEV. (IN)	0.0666 (64:64)	0.0390 (64:64)	0.0339 (64:64)
	90% CONF. LIM	(-0.0987, -0.0709)	(-0.0725, -0.0563)	(-0.0606, -0.0464)
AVERAGE CONTACT ANGLE, δ_o	MEAN (RAD)	0.0647	0.1371	0.1519
	STD. DEV. (RAD)	0.0101 (64:64)	0.0125 (64:64)	0.0132 (64:64)
	90% CONF. LIM.	(0.0626, 0.0668)	(0.1345, 0.1397)	(0.1491, 0.1547)

TABLE A-1. LINEAR ESTIMATES OF WHEEL-RAIL GEOMETRIC CONSTRAINT FUNCTIONS (cont.)

(b) SECTION A: Tangent Track; MP 206.5 East for 320 ft.		WHEEL PROFILE		
		AAR 1/20	CNA (±0.15 in)	CNA (±0.25 in)
GAUGE	MEAN (IN)	56.676	56.676	56.676
	STD. DEV. (IN)	0.053 (24:24)	0.053 (24:24)	0.053 (24:24)
	90% CONF. LIM.	(56.657, 56.694)	(56.657, 56.694)	(56.657, 56.694)
EFFECTIVE CONICITY λ	MEAN	0.0624	0.3116	0.3012
	STD. DEV.	0.0297 (24:24)	0.0959 (24:24)	0.0403 (24:24)
	90% CONF. LIM.	(0.0520, 0.0728)	(0.2781, 0.3451)	(0.2871, 0.3153)
ROLLING LINE OFFSET, x_{R_o}	MEAN (IN)	-0.1321	-0.0679	-0.0515
	STD. DEV. (IN)	0.1654 (22:24)	0.0368 (24:24)	0.0228 (24:24)
	90% CONF. LIM.	(-0.1928, -0.0714)	(-0.0807, -0.0551)	(-0.0595, -0.0435)
CONTACT ANGLE DIFFERENCE, Δ	MEAN	-0.1789	8.5824	8.8519
	STD. DEV.	1.9758 (24:24)	3.7403 (24:24)	1.4704 (24:24)
	90% CONF. LIM.	(-0.8686, 0.5108)	(7.2768, 9.8880)	(8.3386, 9.3651)
CONTACT ANGLE OFFSET, x_{δ_o}	MEAN (IN)	0.2400	-0.0505	-0.0270
	STD. DEV. (IN)	1.4432 (22:24)	0.0464 (23:24)	0.0264 (24:24)
	90% CONF. LIM.	(-0.2892, 0.7692)	(-0.0670, -0.0340)	(-0.0362, -0.0178)
ROLL ANGLE, Γ	MEAN	0.0656	0.1379	0.1314
	STD. DEV.	0.0080 (24:24)	0.0137 (24:24)	0.0108 (24:24)
	90% CONF. LIM.	(0.0628, 0.0684)	(0.1331, 0.1427)	(0.1276, 0.1352)
ROLL ANGLE OFFSET, x_{ϕ_o}	MEAN (IN)	0.0309	-0.0690	-0.0645
	STD. DEV. (IN)	0.0488 (24:24)	0.0314 (24:24)	0.0300 (24:24)
	90% CONF. LIM.	(0.0139, 0.0479)	(-0.0800, -0.0580)	(-0.0750, -0.0540)
AVERAGE CONTACT ANGLE, δ_o	MEAN (RAD)	0.0662	0.1173	0.1168
	STD. DEV. (RAD)	0.0053 (24:24)	0.0106 (24:24)	0.0078 (24:24)
	90% CONF. LIM.	(0.0644, 0.0681)	(0.1136, 0.1210)	(0.1141, 0.1195)

Table A-1. LINEAR ESTIMATES OF WHEEL-RAIL GEOMETRIC CONSTRAINT FUNCTIONS (cont.)

(c) SECTION B: 6 Deg Curve; 840 ft through curve		WHEEL PROFILE					
		AAR 1/20		CNA (± 0.15 in)		CNA (± 0.25 in)	
GAUGE	MEAN (IN)	56.859		56.859		56.859	
	STD. DEV. (IN)	0.130	(23:23)	0.130	(23:23)	0.130	(23:23)
EFFECTIVE CONICITY, λ	MEAN	0.0694		0.2237		0.2238	
	STD. DEV.	0.0157	(22:23)	0.1201	(23:23)	0.0570	(23:23)
ROLLING LINE OFFSET, x_{R_o}	MEAN (IN)	0.1462		0.0154		0.0230	
	STD. DEV. (IN)	0.0890	(23:23)	0.0422	(23:23)	0.0361	(23:23)
CONTACT ANGLE DIFFERENCE, Δ	MEAN	0.9613		6.6493		6.3038	
	STD. DEV.	0.7205	(23:23)	3.7758	(23:23)	1.5904	(23:23)
CONTACT ANGLE OFFSET, x_{δ_o}	MEAN (IN)	0.0952		0.0213		0.0272	
	STD. DEV. (IN)	0.1586	(21:23)	0.0418	(22:23)	0.0481	(23:23)
ROLL ANGLE, Γ	MEAN	0.0569		0.0749		0.0806	
	STD. DEV.	0.0066	(23:23)	0.0216	(23:23)	0.0177	(23:23)
ROLL ANGLE OFFSET, x_{ϕ_o}	MEAN (IN)	0.1395		0.0252		0.0235	
	STD. DEV. (IN)	0.0677	(23:23)	0.0534	(23:23)	0.0524	(23:23)
AVERAGE CONTACT ANGLE, δ_o	MEAN (RAD)	0.0551		0.0690		0.0784	
	STD. DEV. (RAD	0.0042	(23:23)	0.0175	(23:23)	0.0142	(23:23)

(d) SECTION C: 1 Deg. Curve; 400 ft West through curve and spiral		WHEEL PROFILE					
		AAR 1/20		CNA (± 0.15 in)		CNA (± 0.25 in)	
GAUGE	MEAN (IN)	56.564		56.564		56.564	
	STD. DEV. (IN)	0.078	(11:11)	0.078	(11:11)	0.078	(11:11)
EFFECTIVE CONICITY, λ	MEAN	0.0742		0.3585		0.3685	
	STD. DEV.	0.0278	(11:11)	0.0743	(11:11)	0.0379	(11:11)
ROLLING LINE OFFSET, x_{R_o}	MEAN (IN)	- 0.0153		0.0243		0.0234	
	STD. DEV. (IN)	0.1439	(11:11)	0.0303	(11:11)	0.0281	(11:11)
CONTACT ANGLE DIFFERENCE, Δ	MEAN	- 1.0940		9.8686		11.5357	
	STD. DEV.	3.1917	(11:11)	2.9857	(11:11)	1.2148	(11:11)
CONTACT ANGLE OFFSET, x_{δ_o}	MEAN (IN)	0.0814		0.0371		0.0364	
	STD. DEV. (IN)	0.1377	(10:11)	0.0383	(11:11)	0.0247	(11:11)
ROLL ANGLE, Γ	MEAN	0.0625		0.1396		0.1342	
	STD. DEV.	0.0101	(11:11)	0.0132	(11:11)	0.0109	(11:11)
ROLL ANGLE OFFSET, x_{ϕ_o}	MEAN (IN)	0.1627		0.0388		0.0417	
	STD. DEV. (IN)	0.0621	(11:11)	0.0338	(11:11)	0.0332	(11:11)
AVERAGE CONTACT ANGLE, δ_o	MEAN (RAD)	0.0592		0.1217		0.1257	
	STD. DEV. (RAD)	0.0093	(11:11)	0.0150	(11:11)	0.0120	(11:11)

Table A-1. LINEAR ESTIMATES OF WHEEL-RAIL GEOMETRIC CONSTRAINT FUNCTIONS (cont.)

(e) SECTION D: 1 Deg Curve; 160 ft East through curve and spiral		WHEEL PROFILE		
		AAR 1/20	CNA (± 0.15 in)	CNA (± 0.25 in)
GAUGE	MEAN (IN)	56.606	56.606	56.606
	STD. DEV. (IN)	0.031 (4:4)	0.031 (4:4)	0.031 (4:4)
EFFECTIVE CONICITY, λ	MEAN	0.0599	0.2965	0.3287
	STD. DEV.	0.0318 (4:4)	0.0365 (4:4)	0.0273 (4:4)
ROLLING LINE OFFSET, x_{R_o}	MEAN (IN)	- 0.0951	- 0.0026	0.0144
	STD. DEV. (IN)	0.0652 (4:4)	0.0305 (4:4)	0.0130 (4:4)
CONTACT ANGLE DIFFERENCE, Δ	MEAN	- 0.0368	7.8591	10.0908
	STD. DEV.	0.6273 (4:4)	1.9427 (4:4)	1.2471 (4:4)
CONTACT ANGLE OFFSET, x_{δ_o}	MEAN (IN)	- 1.0673	0.0166	0.0278
	STD. DEV. (IN)	2.7486 (4:4)	0.0216 (4:4)	0.0087 (4:4)
ROLL ANGLE, Γ	MEAN	0.0630	0.1401	0.1351
	STD. DEV.	0.0061 (4:4)	0.0086 (4:4)	0.0054 (4:4)
ROLL ANGLE OFFSET, x_{ϕ_o}	MEAN (IN)	0.1597	0.0223	0.0285
	STD. DEV. (IN)	0.0168 (4:4)	0.0116 (4:4)	0.0098 (4:4)
AVERAGE CONTACT ANGLE, δ_o	MEAN (RAD)	0.0632	0.1345	0.1298
	STD. DEV. (RAD)	0.0048 (4:4)	0.0063 (4:4)	0.0055 (4:4)

(f) SECTION E: Tangent passing track MP 204 East for 480 ft		WHEEL PROFILE		
		AAR 1/20	CNA (± 0.15 in)	CNA (± 0.25 in)
GAUGE	MEAN (IN)	56.330	56.247	56.324
	STD. DEV. (IN)	0.1072 (19:19)	0.132 (30:30)	0.109 (18:18)
EFFECTIVE CONICITY, λ	MEAN	0.0443	0.5612	0.5954
	STD. DEV.	0.0449 (17:19)	0.1736 (30:30)	0.1280 (18:18)
ROLLING LINE OFFSET, x_{R_o}	MEAN	- 0.2908	- 0.0143	- 0.0123
	STD. DEV. (IN)	0.4420 (18:19)	0.0285 (30:30)	0.0202 (18:18)
CONTACT ANGLE DIFFERENCE, Δ	MEAN	- 2.7506	20.7927	21.9099
	STD. DEV.	1.9279 (17:19)	8.3788 (30:30)	5.7542 (18:18)
CONTACT ANGLE OFFSET, x_{δ_o}	MEAN (IN)	0.1534	0.0020	- 0.0028
	STD. DEV. (IN)	0.2342 (18:19)	0.0330 (30:30)	0.0201 (18:18)
ROLL ANGLE, Γ	MEAN	0.0611	0.1939	0.2129
	STD. DEV.	0.0172 (19:19)	0.0334 (29:30)	0.0465 (18:18)
ROLL ANGLE OFFSET, 0	MEAN (IN)	0.0421	- 0.0226	- 0.0184
	STD. DEV. (IN)	0.0912 (19:19)	0.0393 (30:30)	0.0319 (18:18)
AVERAGE CONTACT ANGLE, δ_o	MEAN (RAD)	0.0636	0.1885	0.2005
	STD DEV. (RAD)	0.0155 (19:19)	0.0343 (30:30)	0.0356 (18:18)

APPENDIX B

POWER SPECTRAL DENSITIES

OF SELECTED VARIABLES FROM

FIELD TEST RESULTS

This appendix contains PSDs of the truck A and B lateral displacement variables for all configurations tested. In addition, it contains PSDs of all computed model variables for Configuration 6. The method of combining field test signals to obtain model variables is given in Appendix C.

The PSDs shown here are actually one side of a two-sided spectrum. As a result, the amplitudes are lower by a factor of two than would normally be seen on a single-sided PSD. The PSDs were computed by Fast Fourier Transformation of 1024-point data records. Each plot shows the number of data records that were ensamble averaged to obtain the PSD. All data was prewhitened and windowed using an approximate Hanning method before analysis.

The times shown on the plots correspond to real time during the tests, referred to zero at the beginning of each data tape file.

Each plot shows train speed and direction. Speeds given to the nearest tenth mile per hour are computed averages, and speeds shown to the nearest mile per hour are nominal speeds. The latter speeds are shown for test runs on which the speed channel was inoperative.

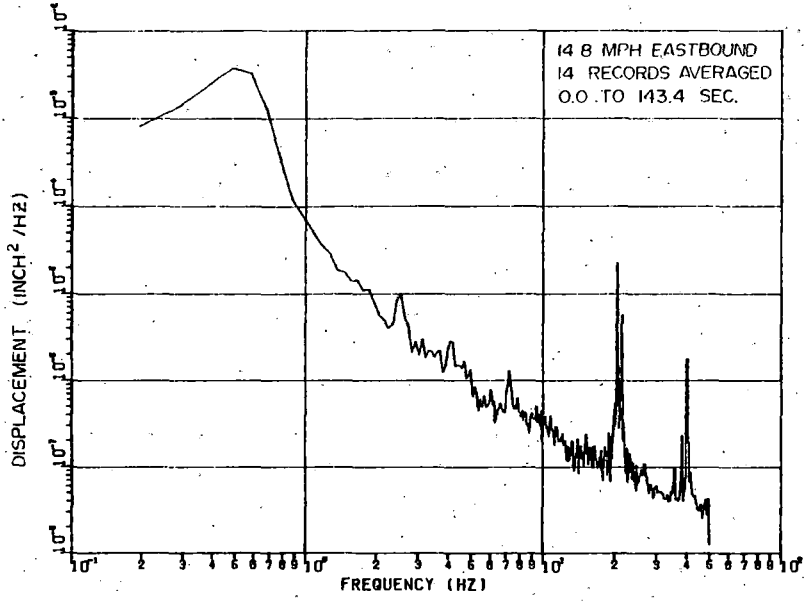

a. TRUCK-A LATERAL DISPLACEMENT

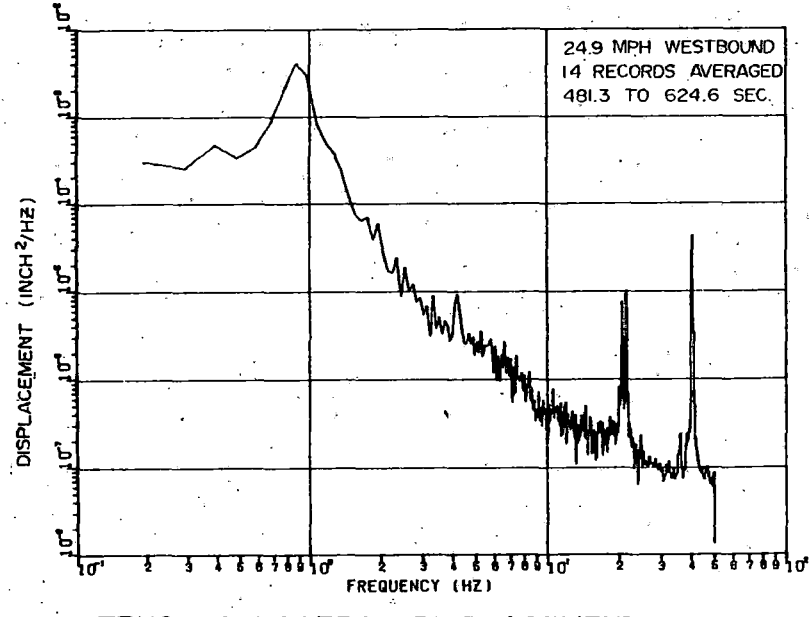

c. TRUCK-A LATERAL DISPLACEMENT

FIGURE B-1. CONFIGURATION I

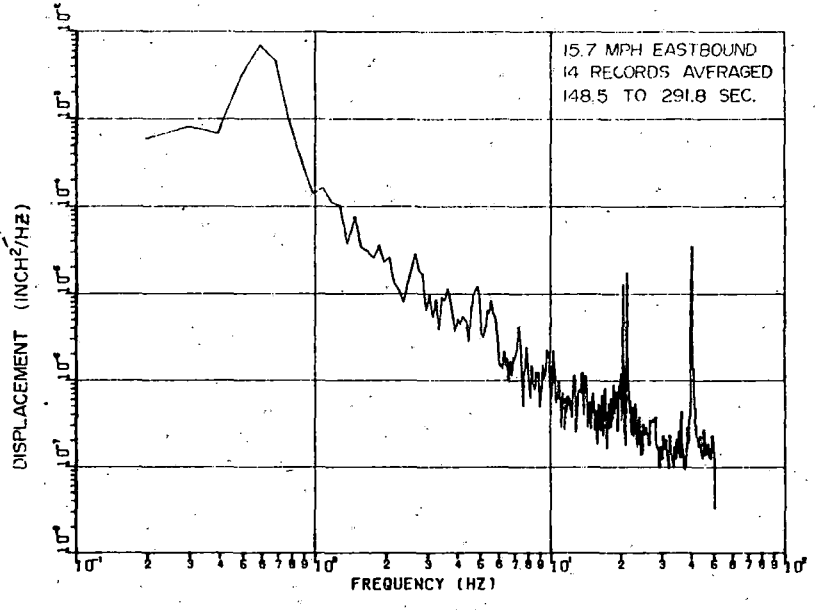

b. TRUCK-A LATERAL DISPLACEMENT

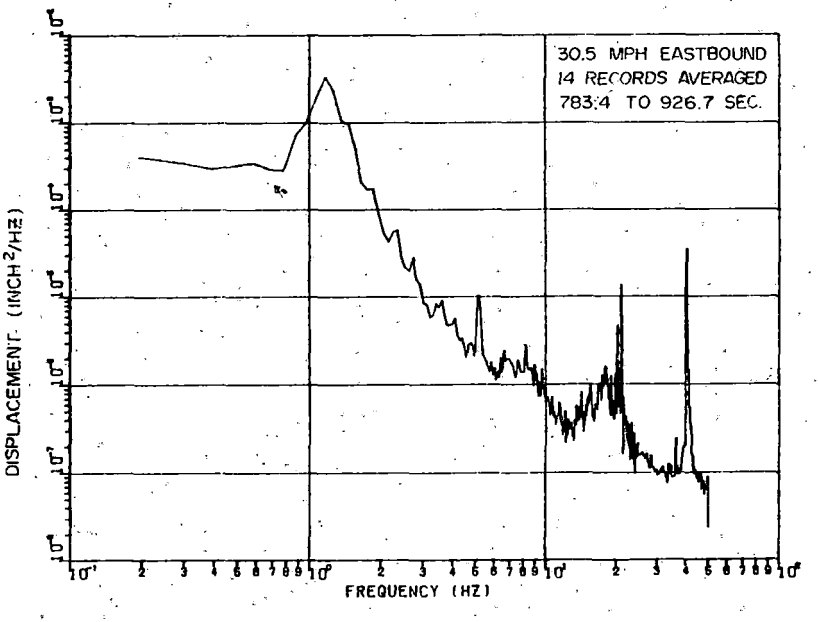

d. TRUCK-A LATERAL DISPLACEMENT

POWER SPECTRAL DENSITIES

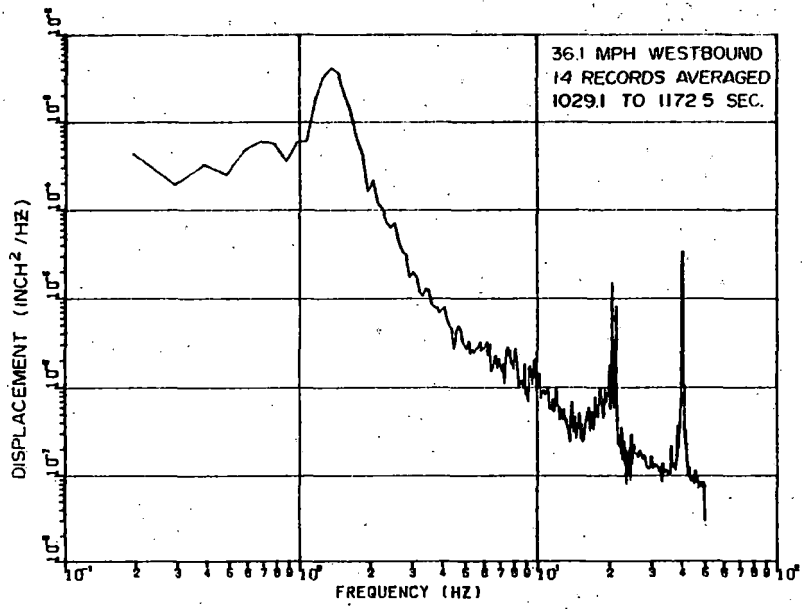

e. TRUCK-A LATERAL DISPLACEMENT

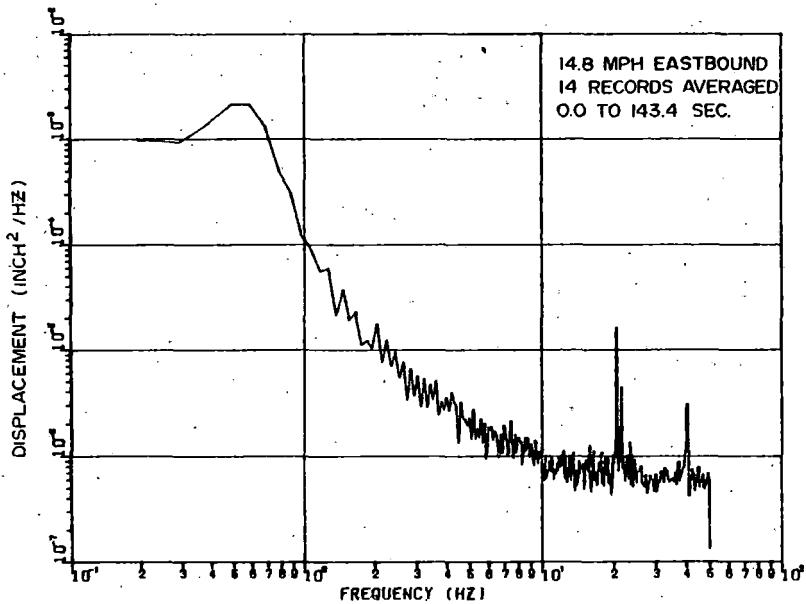

g. TRUCK-B LATERAL DISPLACEMENT

FIGURE B-1. CONFIGURATION I

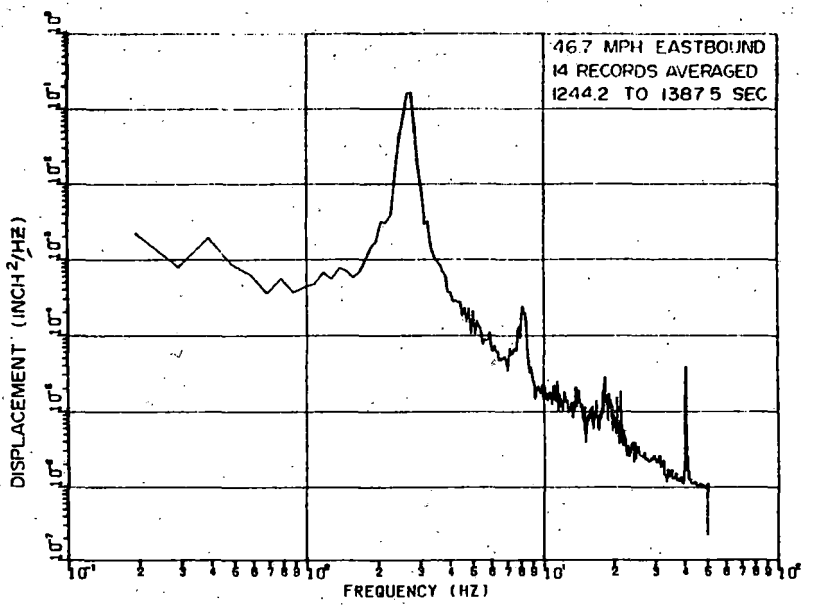

f. TRUCK-A LATERAL DISPLACEMENT

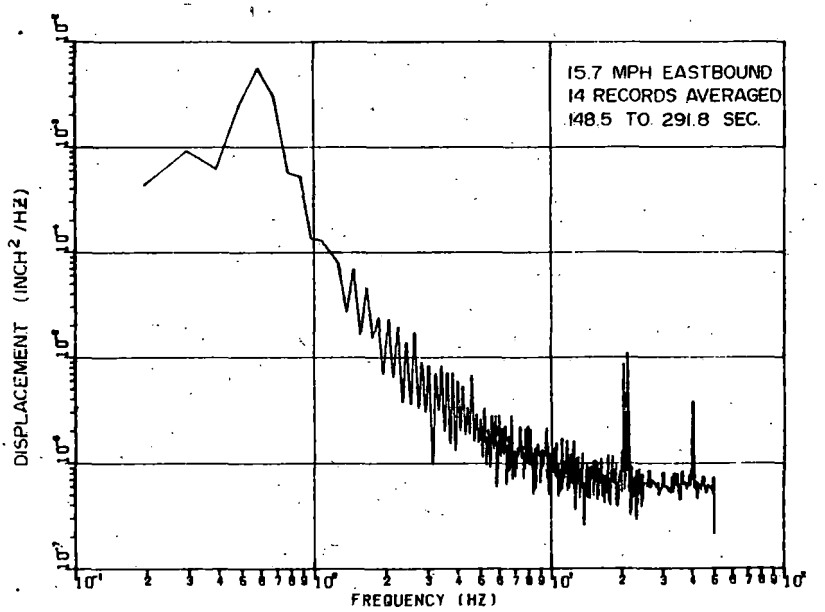

h. TRUCK-B LATERAL DISPLACEMENT

POWER SPECTRAL DENSITIES

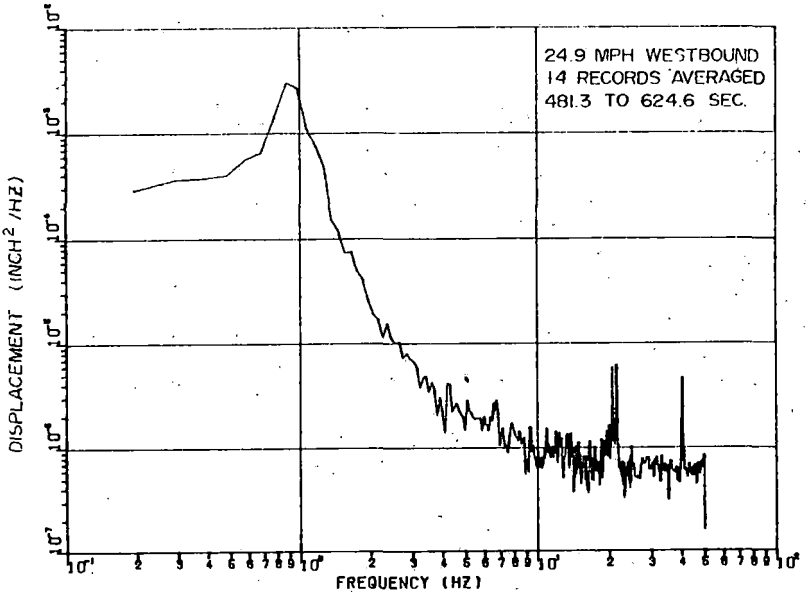

i. TRUCK-B LATERAL DISPLACEMENT

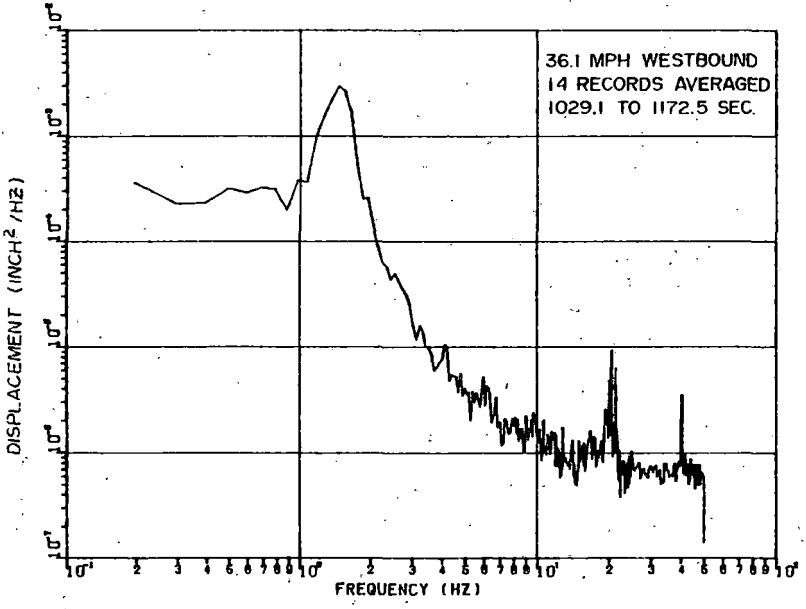

k. TRUCK-B LATERAL DISPLACEMENT

FIGURE B-1. CONFIGURATION I

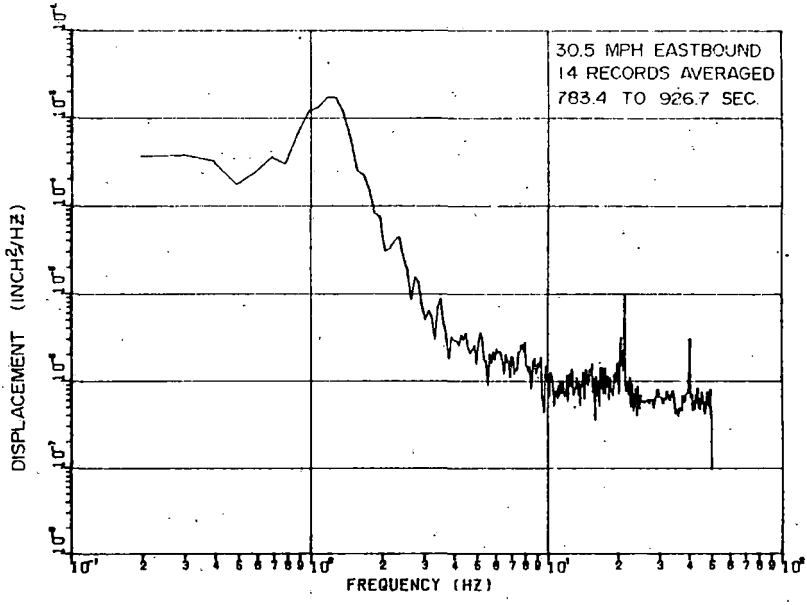

j. TRUCK-B LATERAL DISPLACEMENT

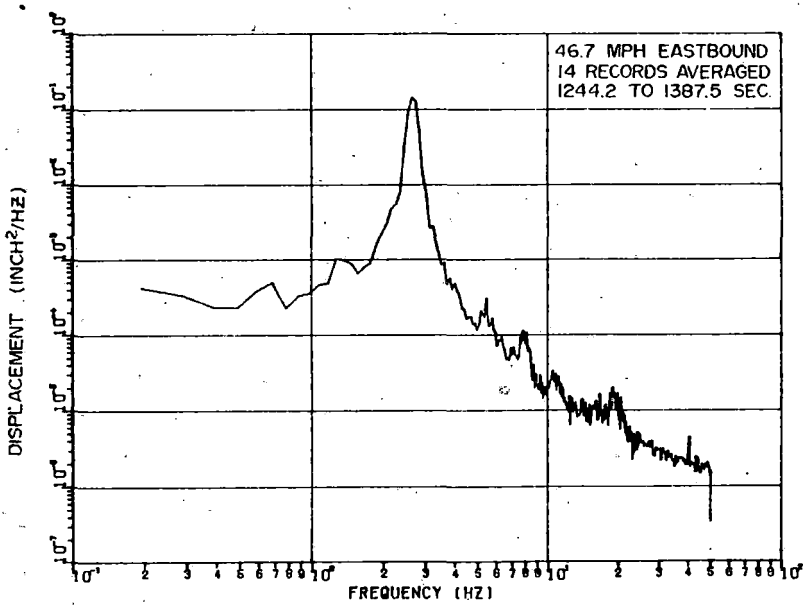

l. TRUCK-B LATERAL DISPLACEMENT

POWER SPECTRAL DENSITIES

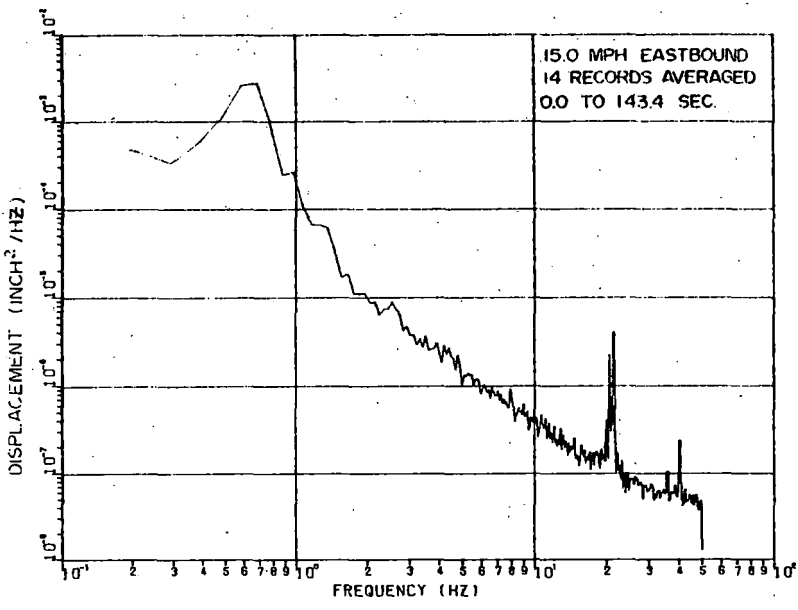

a. TRUCK-A LATERAL DISPLACEMENT

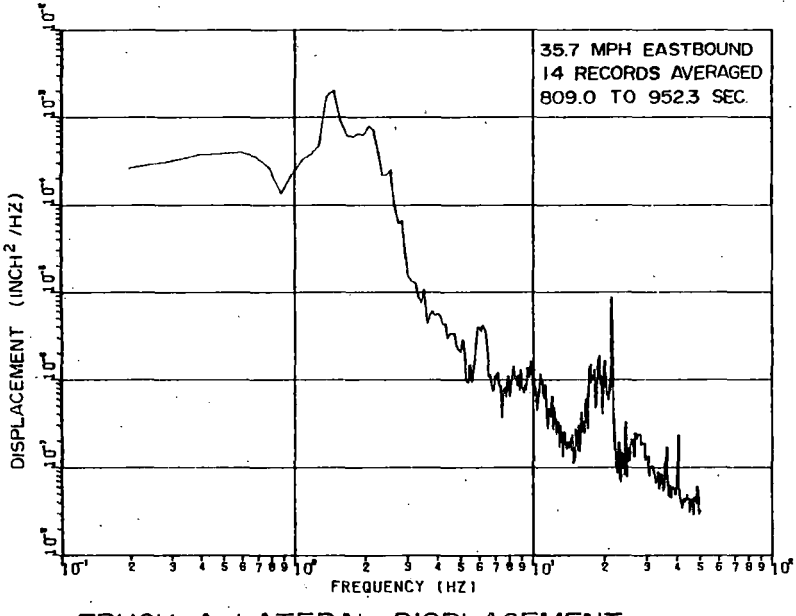

c. TRUCK-A LATERAL DISPLACEMENT

FIGURE B-2. CONFIGURATION 2

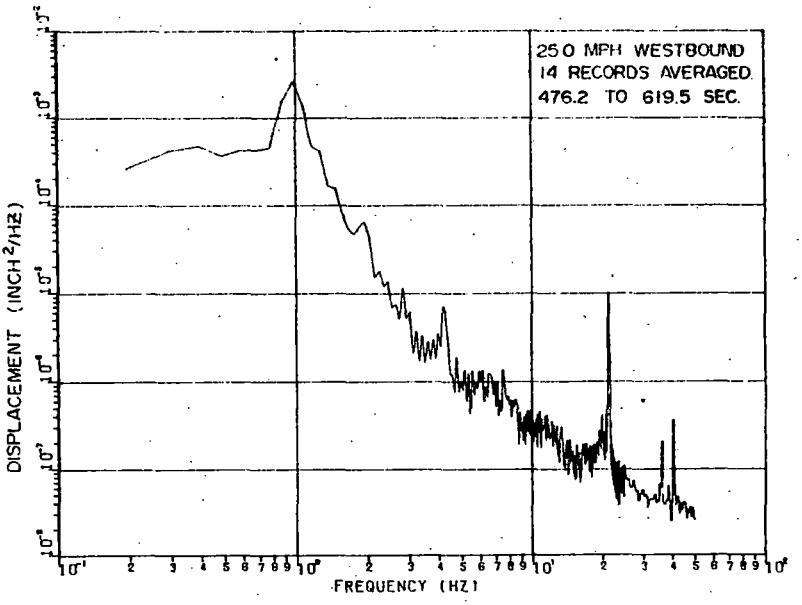

b. TRUCK-A LATERAL DISPLACEMENT

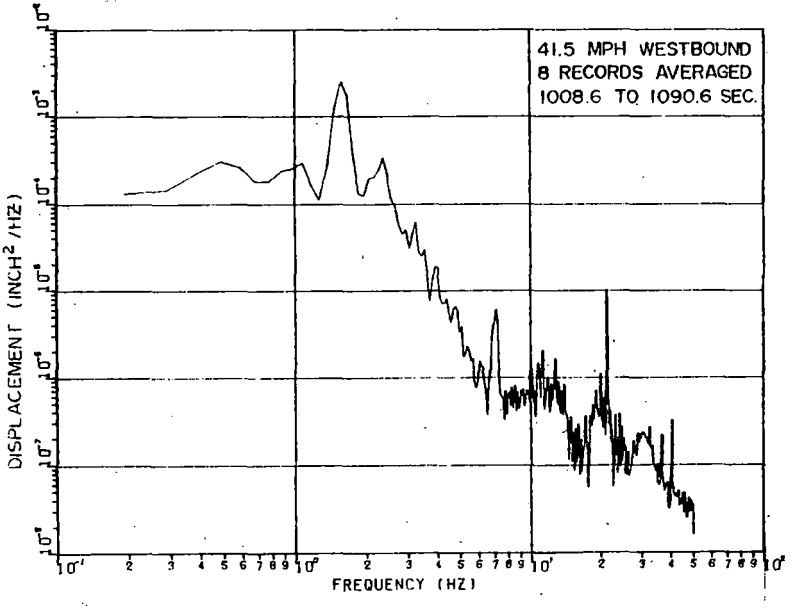

d. TRUCK-A LATERAL DISPLACEMENT

POWER SPECTRAL DENSITIES

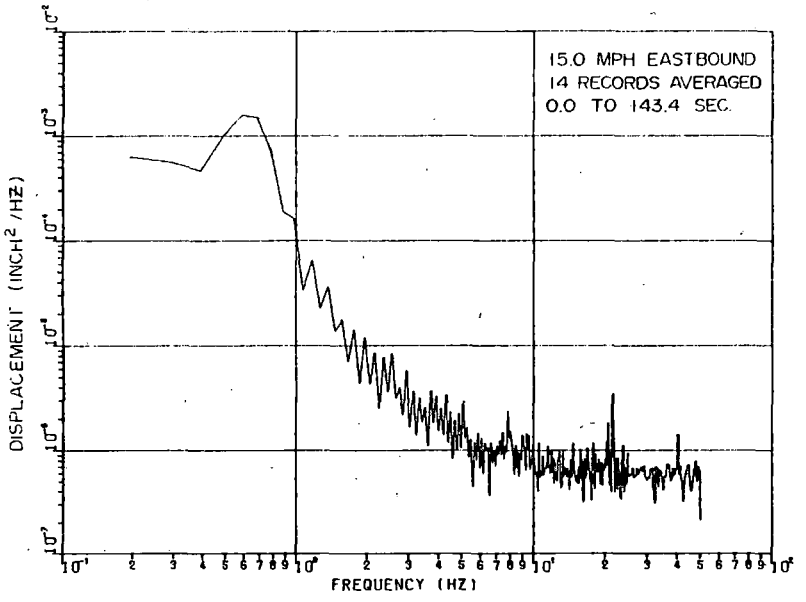

e. TRUCK-B LATERAL DISPLACEMENT

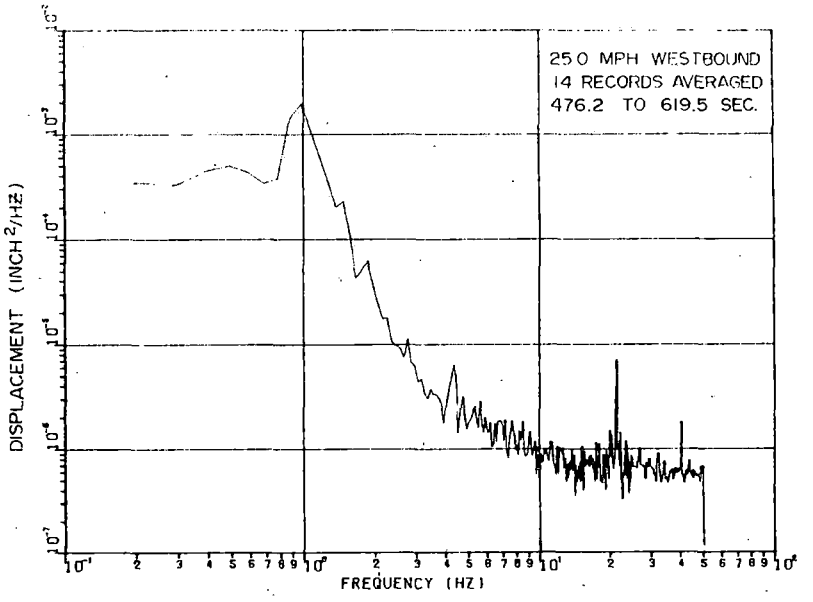

f. TRUCK-B LATERAL DISPLACEMENT

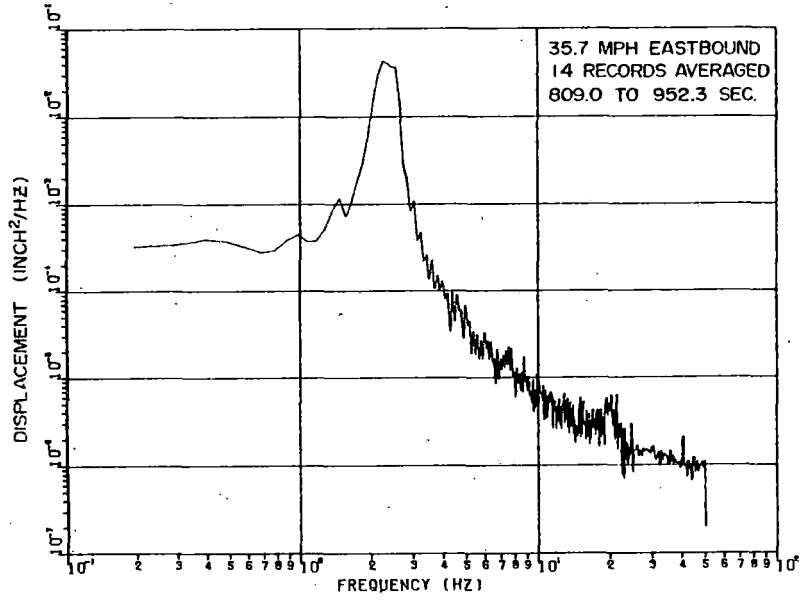

g. TRUCK-B LATERAL DISPLACEMENT

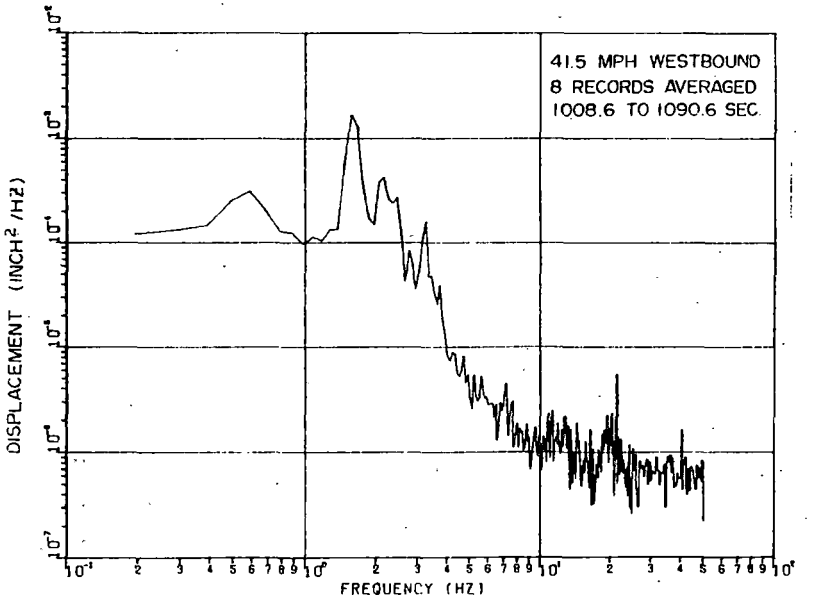

h. TRUCK-B LATERAL DISPLACEMENT

FIGURE B-2. CONFIGURATION 2 POWER SPECTRAL DENSITIES

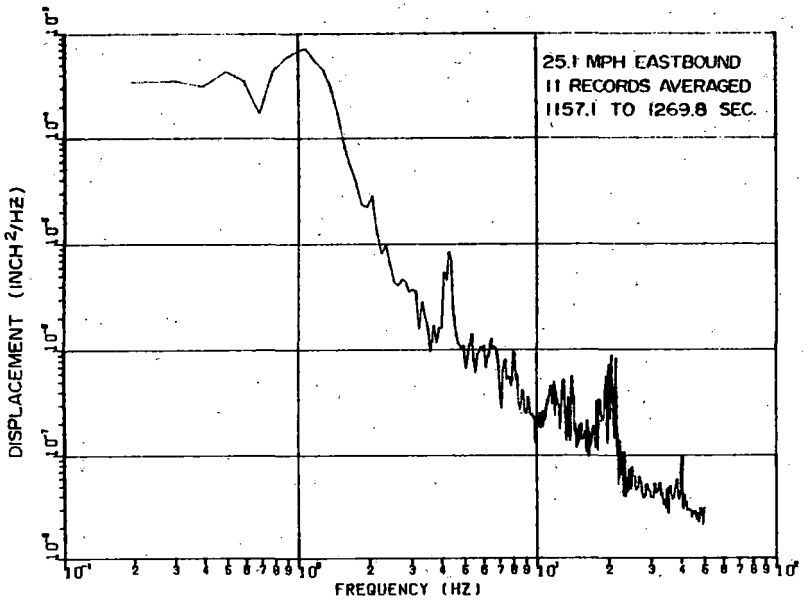

a. TRUCK-A LATERAL DISPLACEMENT

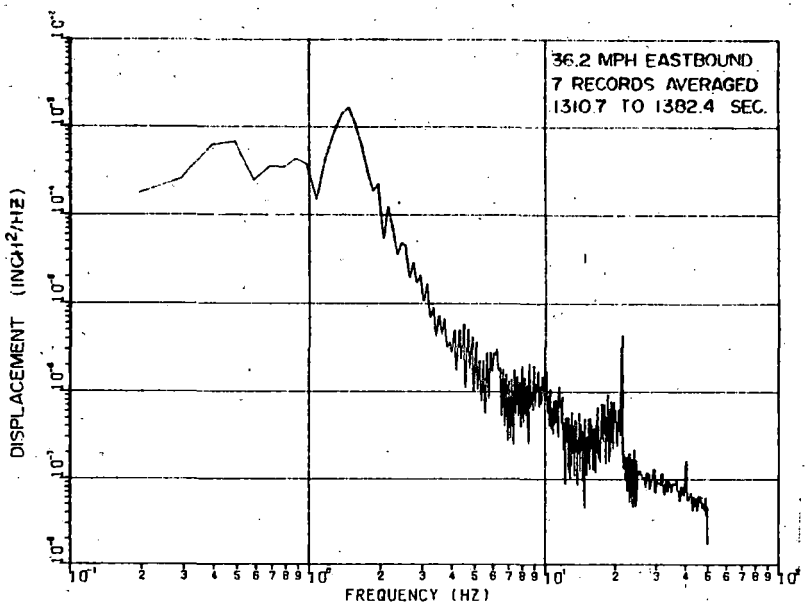

b. TRUCK-A LATERAL DISPLACEMENT

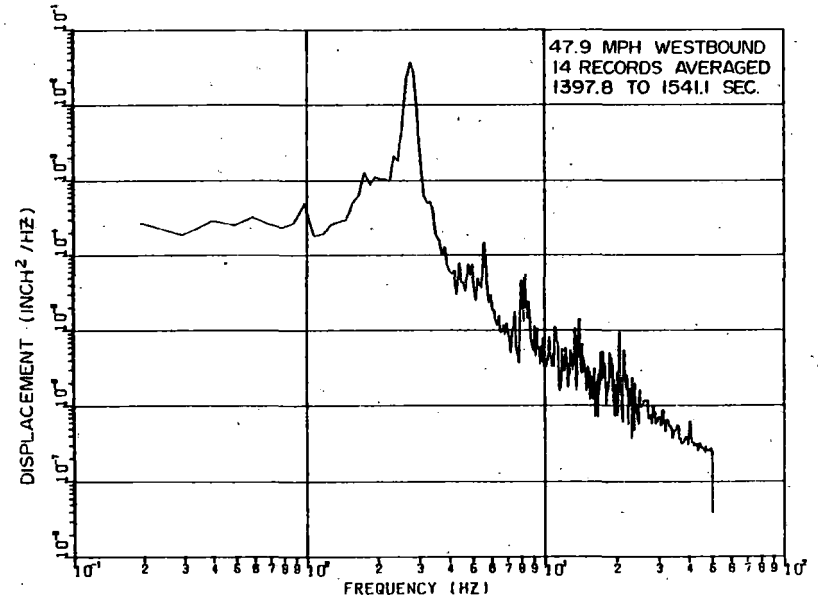

c. TRUCK-A LATERAL DISPLACEMENT

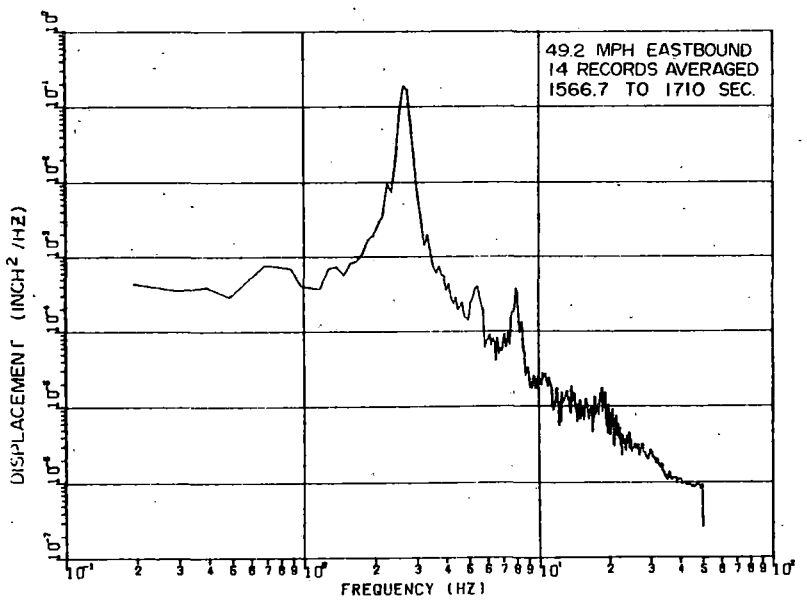

d. TRUCK-A LATERAL DISPLACEMENT

FIGURE B-3. CONFIGURATION 3 POWER SPECTRAL DENSITIES

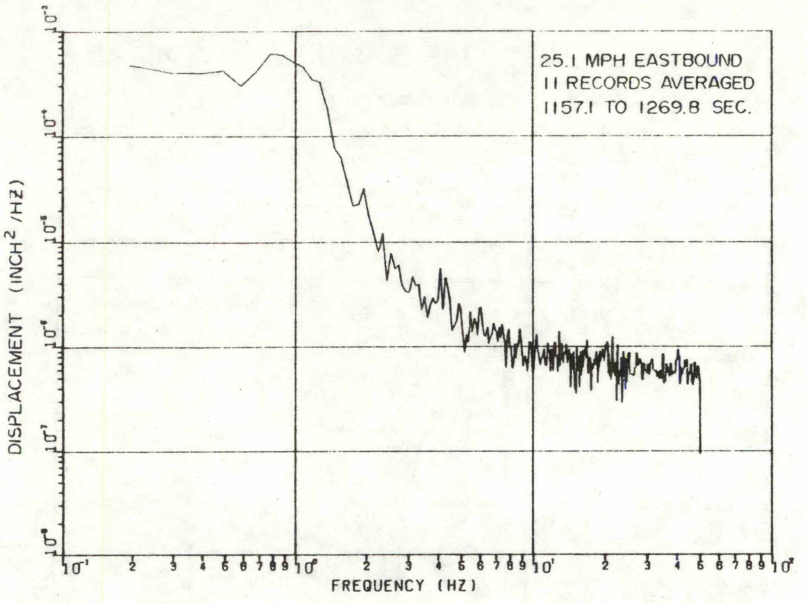

e. TRUCK-B LATERAL DISPLACEMENT

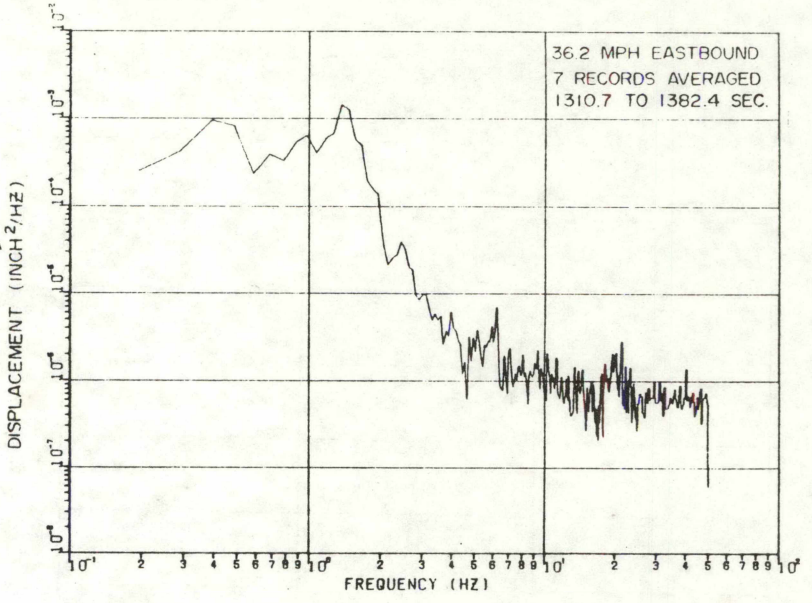

f. TRUCK-B LATERAL DISPLACEMENT

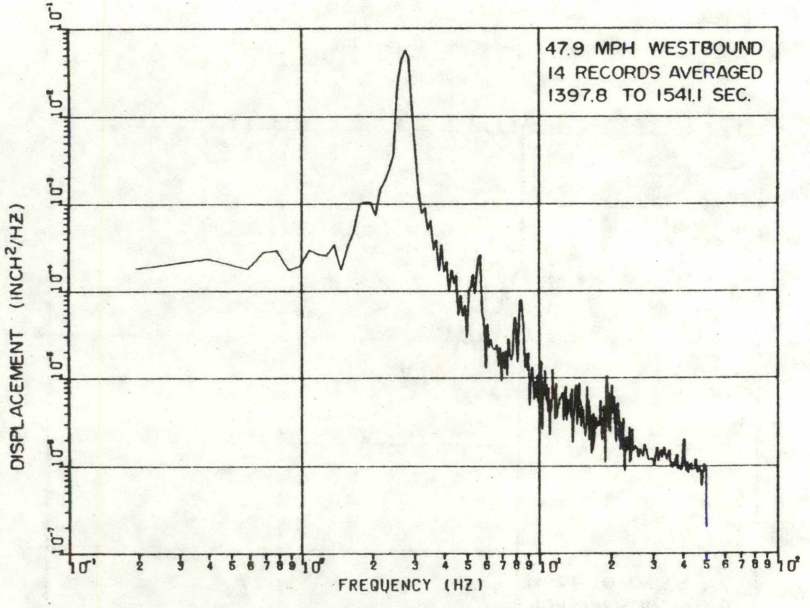

g. TRUCK-B LATERAL DISPLACEMENT

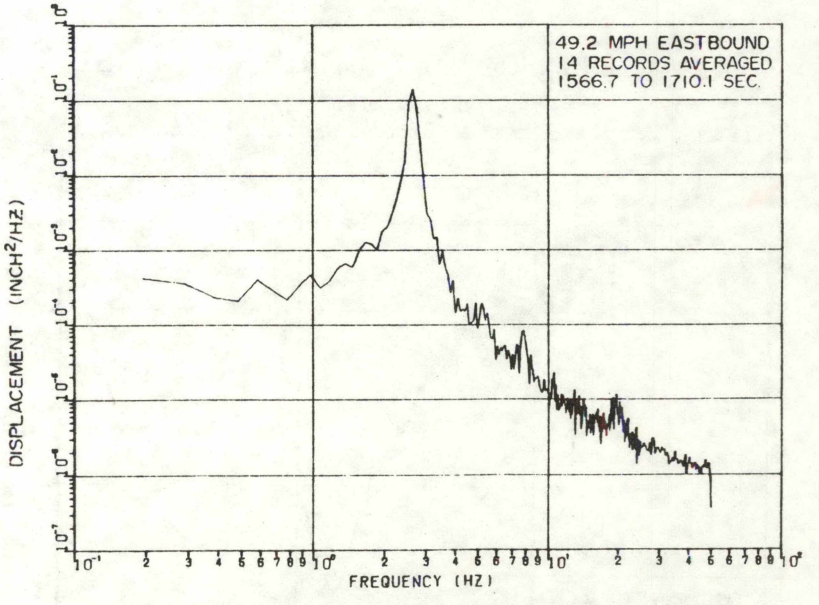

h. TRUCK-B LATERAL DISPLACEMENT

FIGURE B-3. CONFIGURATION 3 POWER SPECTRAL DENSITIES

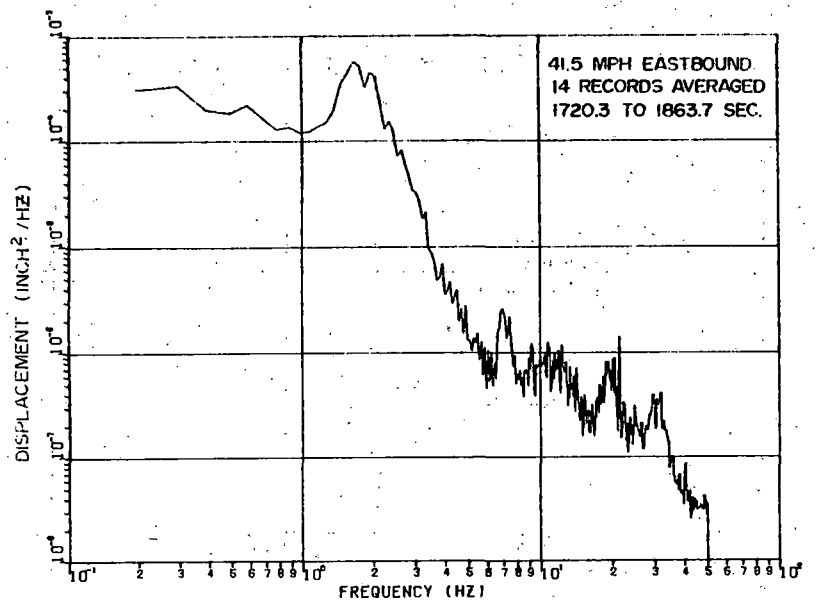

a. TRUCK-A LATERAL DISPLACEMENT

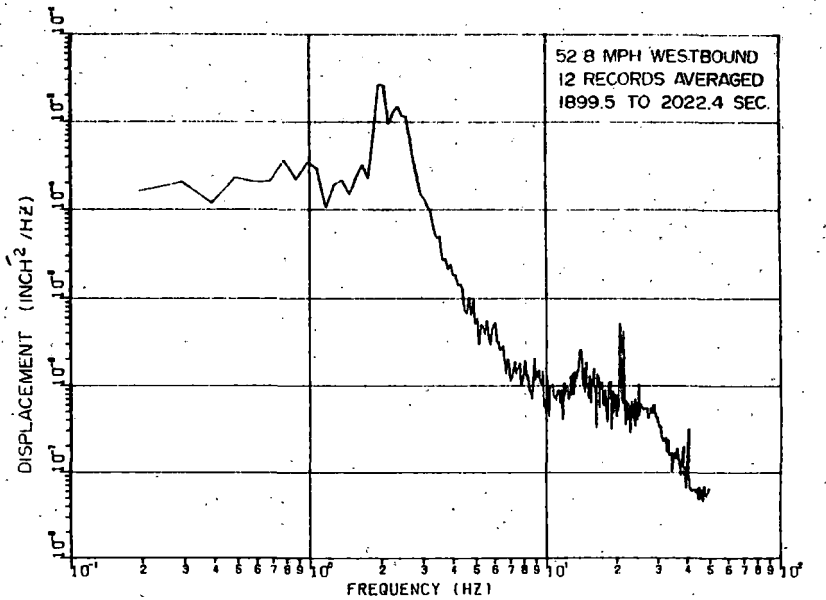

b. TRUCK-A LATERAL DISPLACEMENT

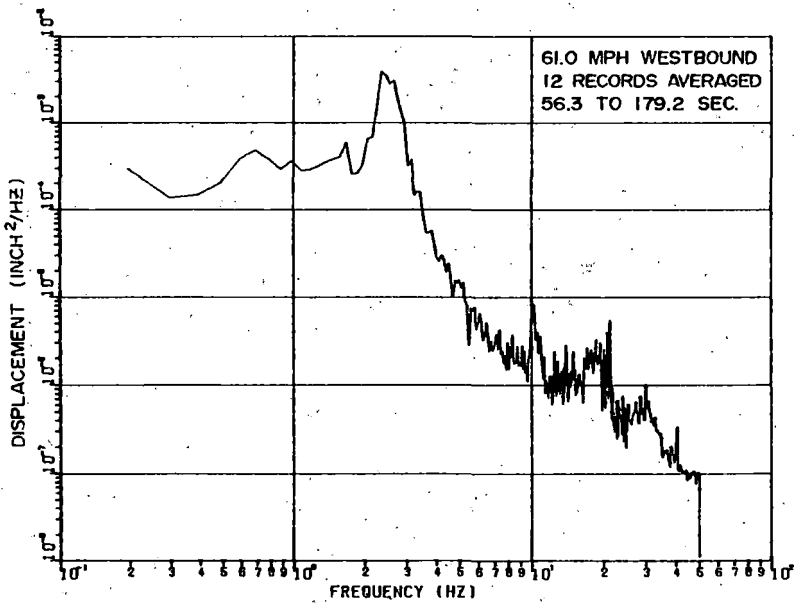

c. TRUCK-A LATERAL DISPLACEMENT

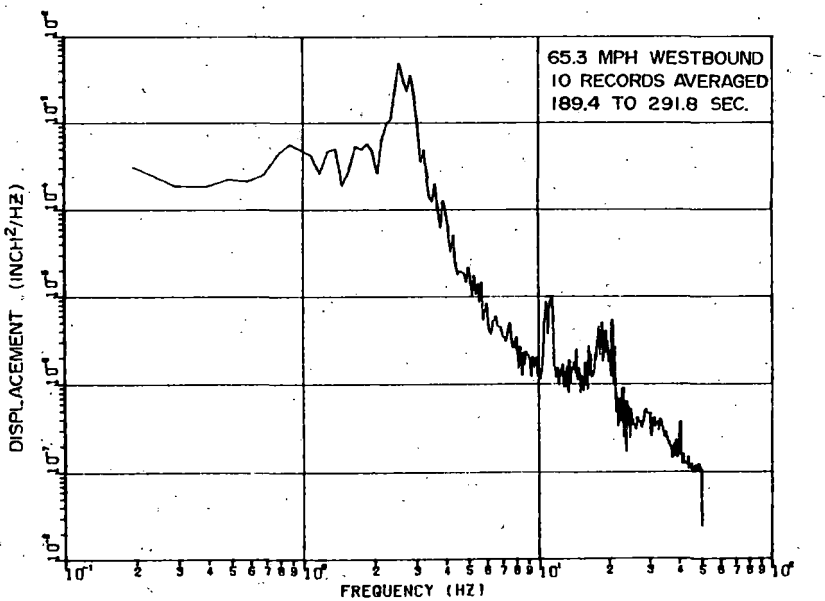

d. TRUCK-A LATERAL DISPLACEMENT

FIGURE B-4. CONFIGURATION 4 POWER SPECTRAL DENSITIES

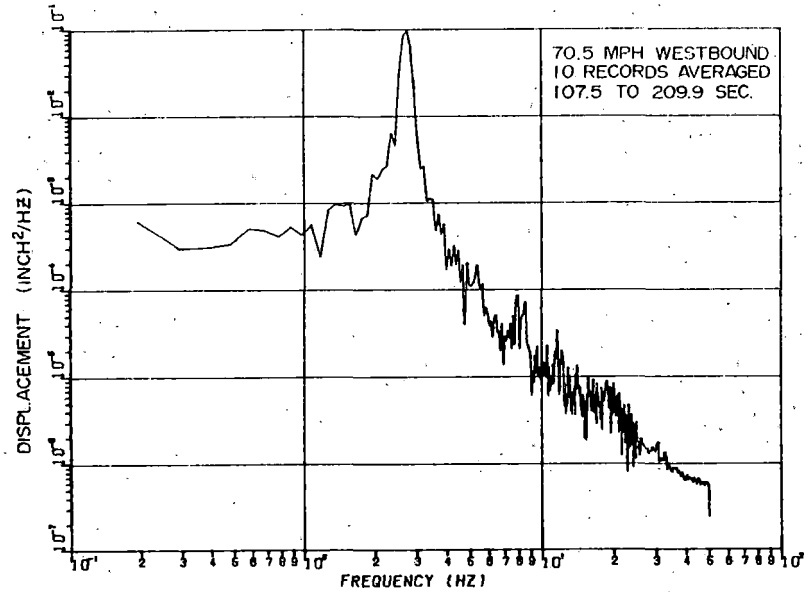

e. TRUCK-A LATERAL DISPLACEMENT

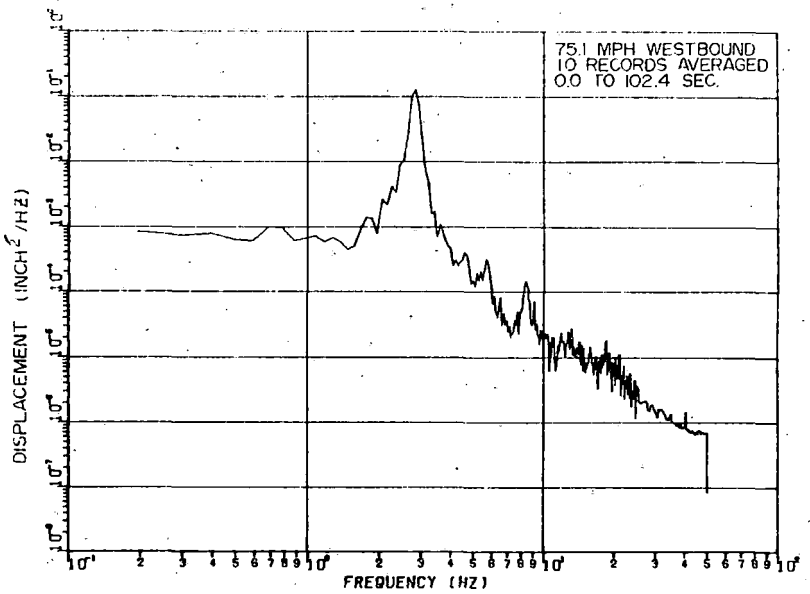

f. TRUCK-A LATERAL DISPLACEMENT

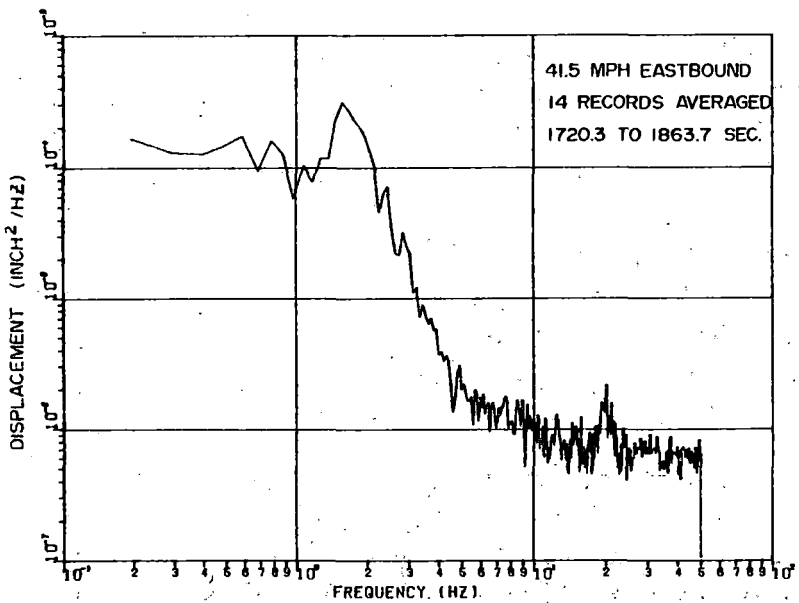

g. TRUCK-B LATERAL DISPLACEMENT

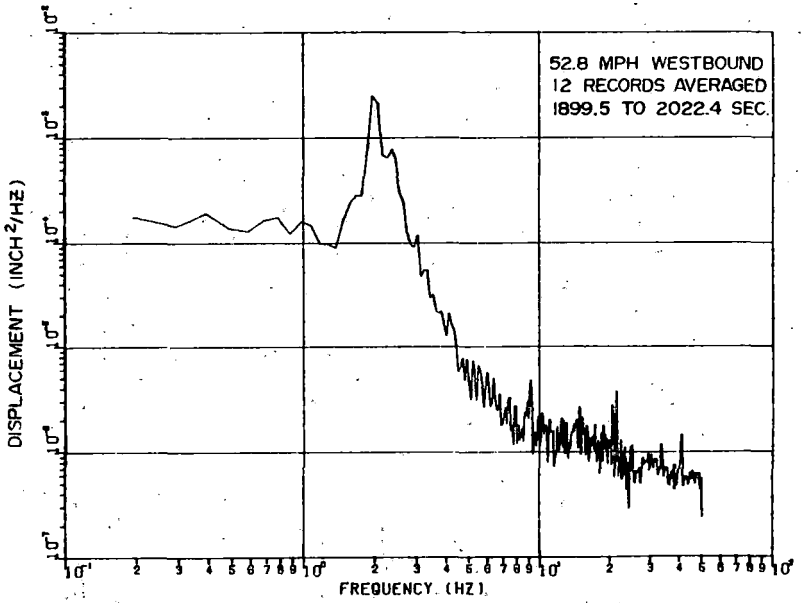

h. TRUCK-B LATERAL DISPLACEMENT

FIGURE B-4 CONFIGURATION 4 POWER SPECTRAL DENSITIES

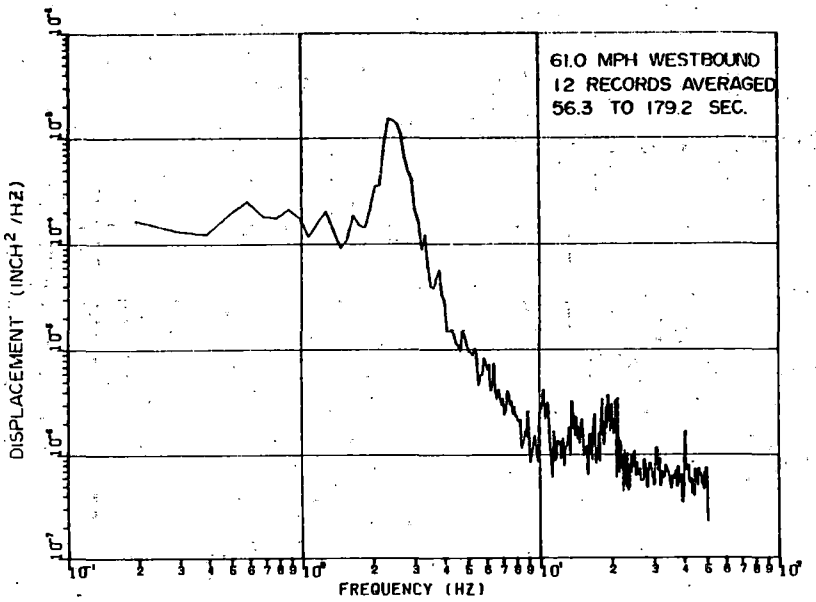

i. TRUCK-B LATERAL DISPLACEMENT

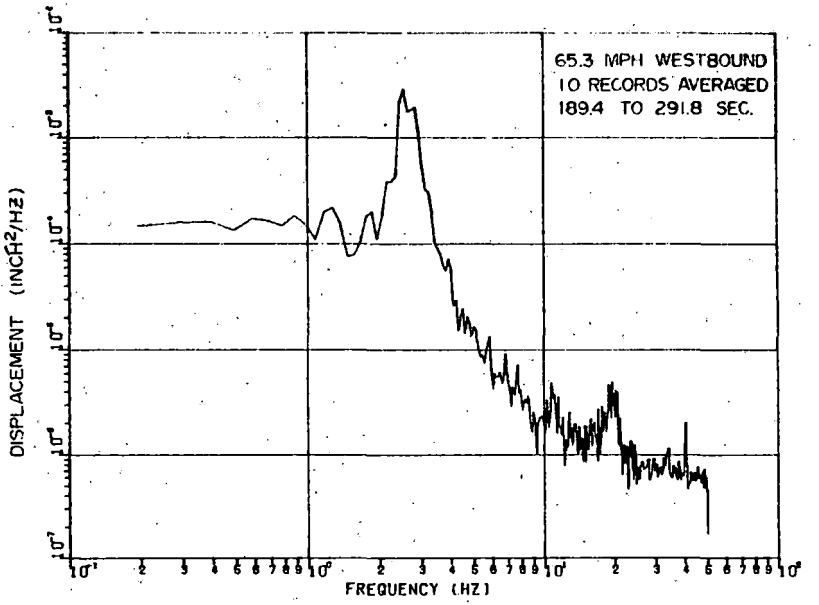

j. TRUCK-B LATERAL DISPLACEMENT

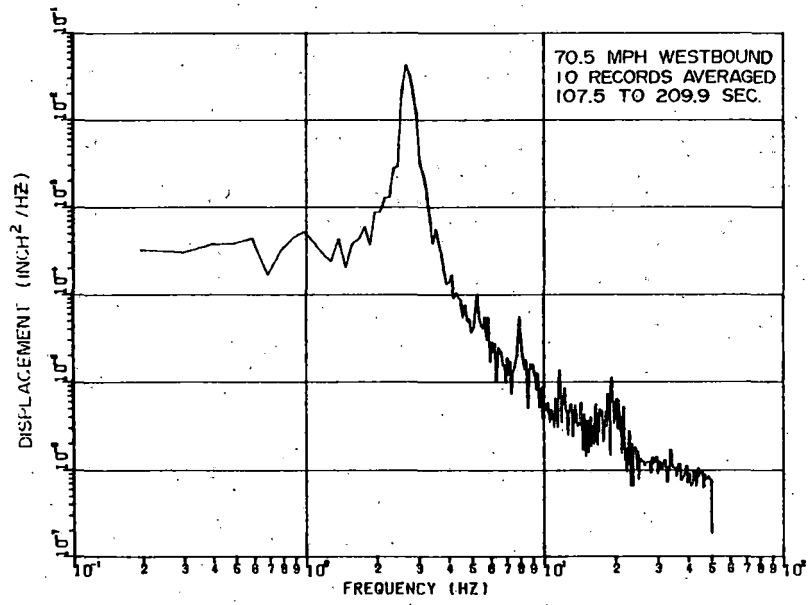

k. TRUCK-B LATERAL DISPLACEMENT

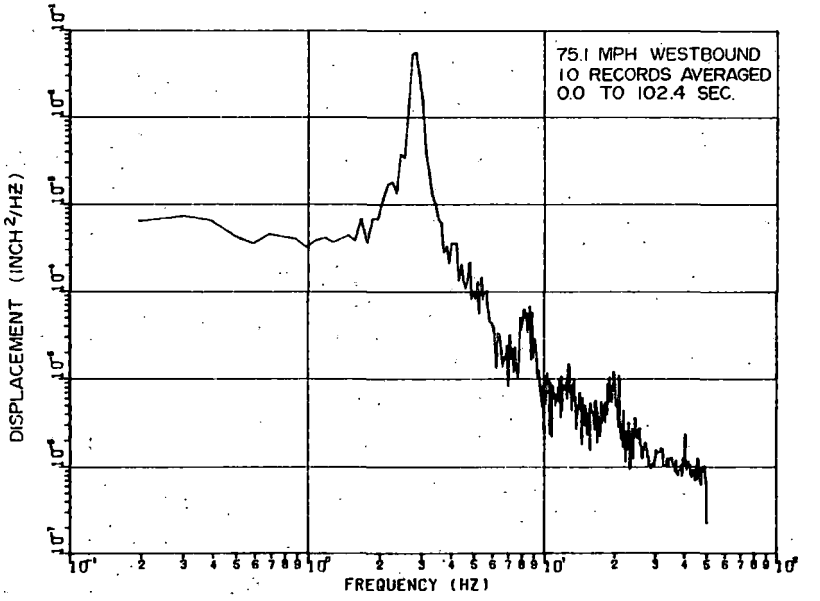

l. TRUCK-B LATERAL DISPLACEMENT

FIGURE B-4. CONFIGURATION 4 POWER SPECTRAL DENSITIES

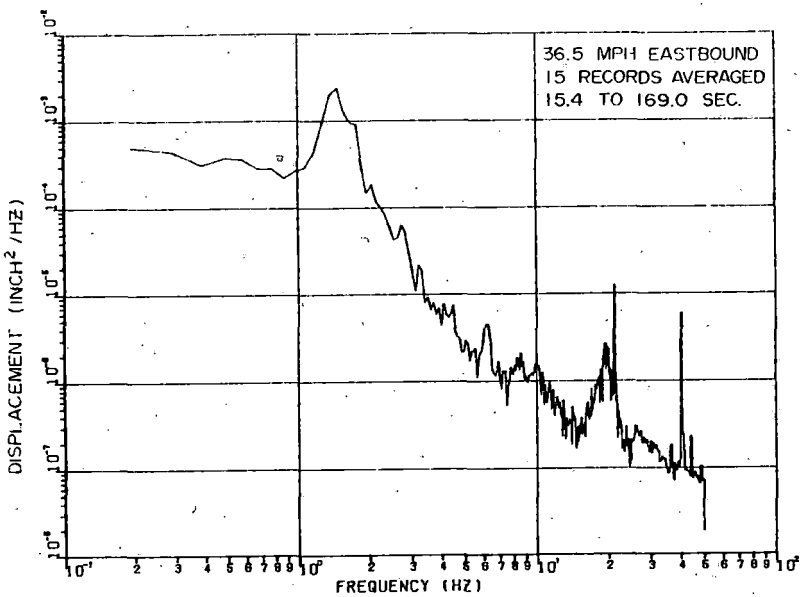

a. TRUCK-A LATERAL DISPLACEMENT

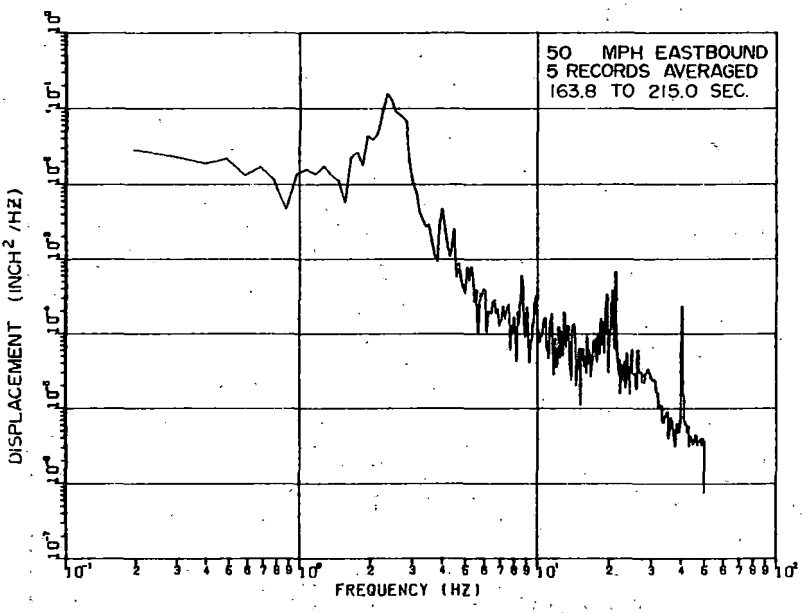

c. TRUCK-A LATERAL DISPLACEMENT

FIGURE B-5. CONFIGURATION 5

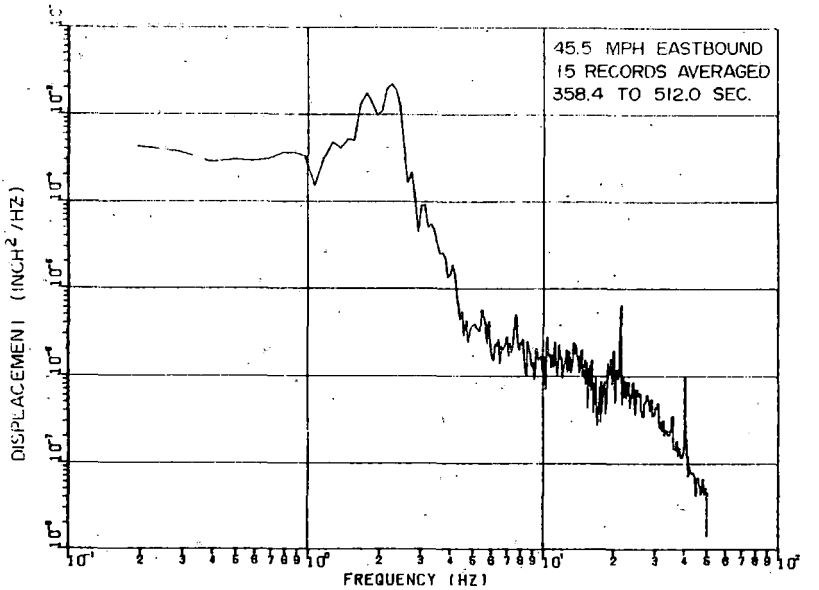

b. TRUCK-A LATERAL DISPLACEMENT

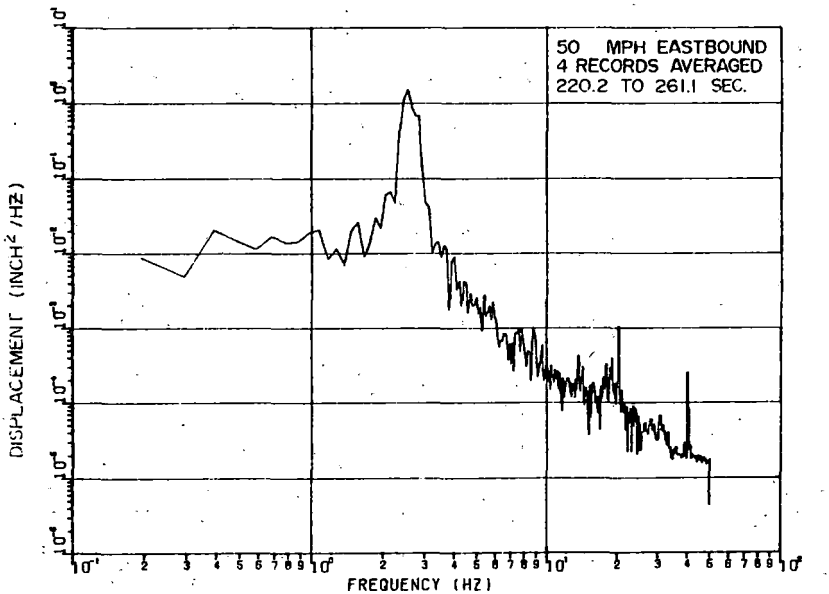

d. TRUCK-A LATERAL DISPLACEMENT

POWER SPECTRAL DENSITIES

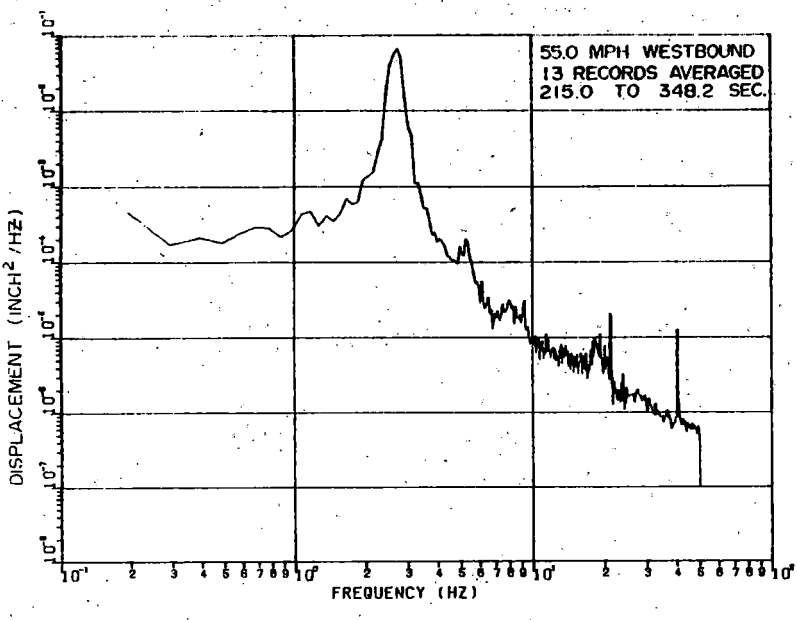

e. TRUCK-A LATERAL DISPLACEMENT

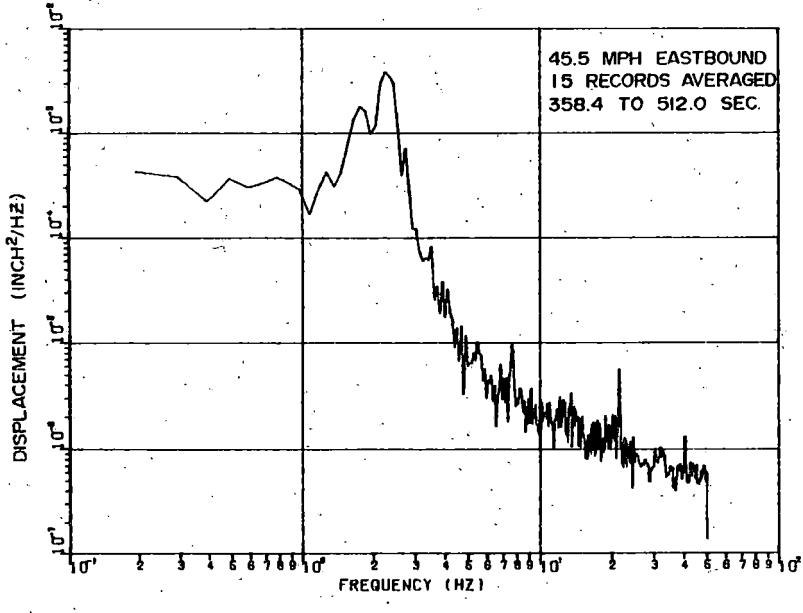

g. TRUCK-B LATERAL DISPLACEMENT

FIGURE B-5. CONFIGURATION 5

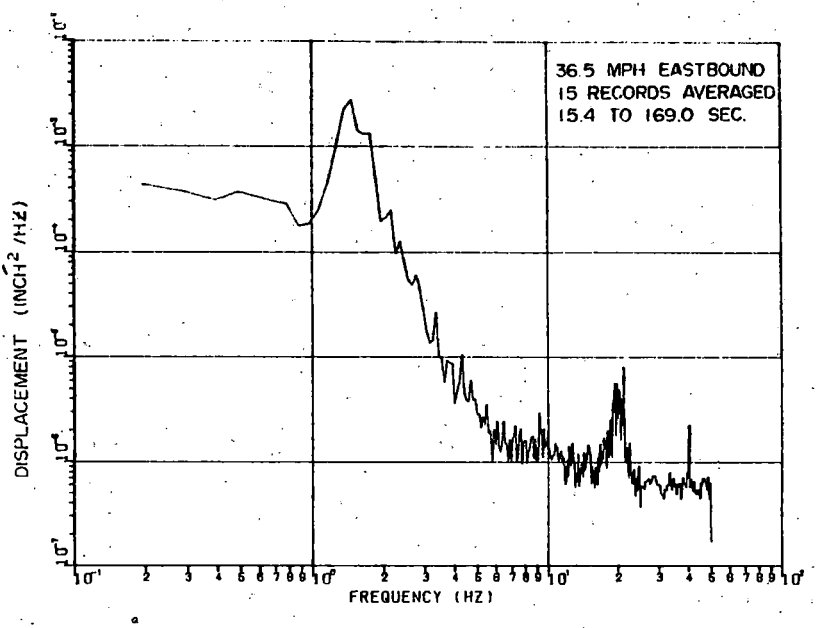

f. TRUCK-B LATERAL DISPLACEMENT

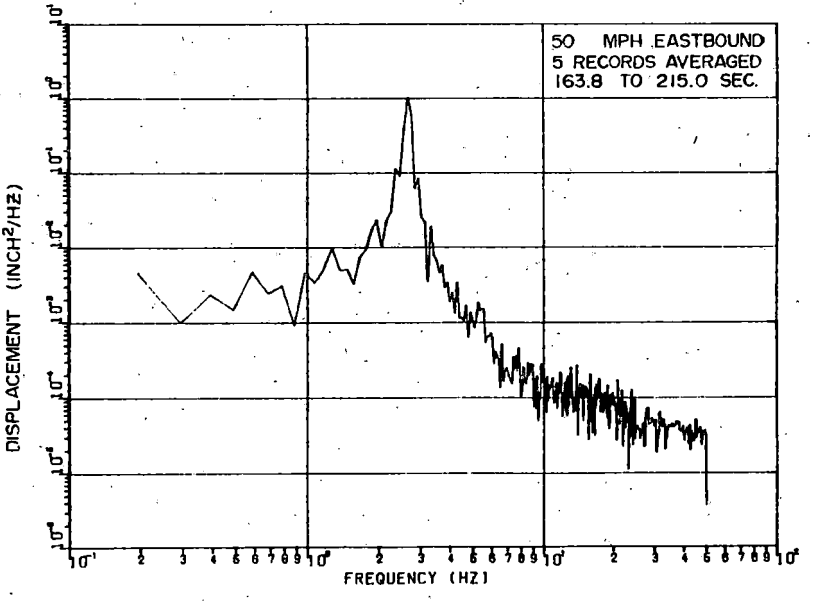

h. TRUCK-B LATERAL DISPLACEMENT

POWER SPECTRAL DENSITIES

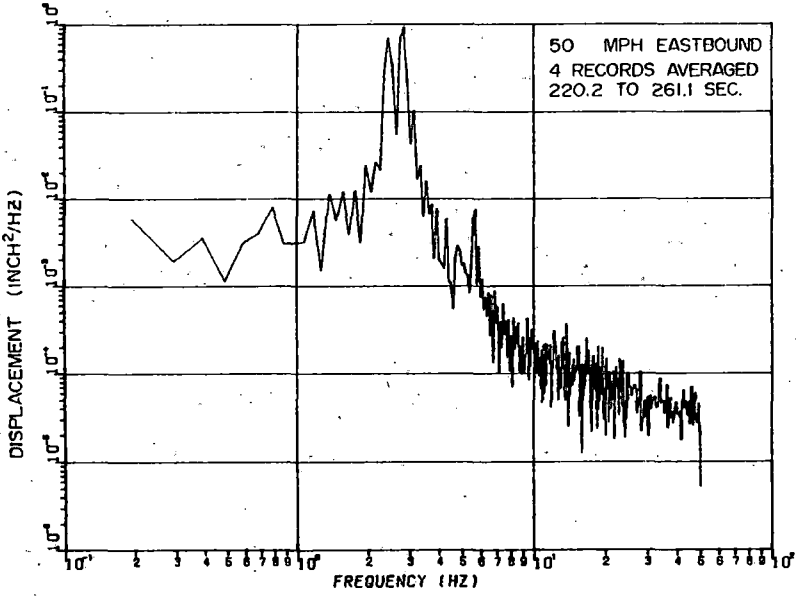

i. TRUCK-B LATERAL DISPLACEMENT

FIGURE B-5. CONFIGURATION 5.

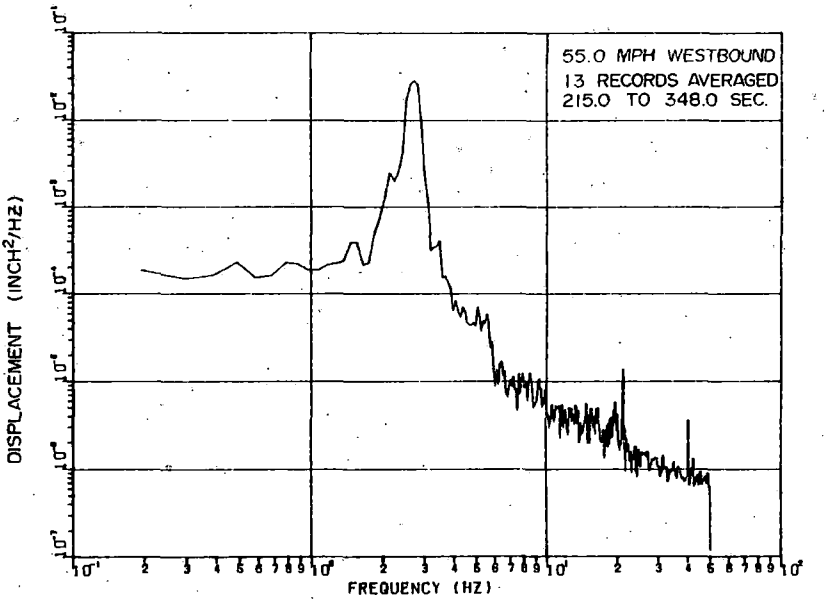

j. TRUCK-B LATERAL DISPLACEMENT

POWER SPECTRAL DENSITIES

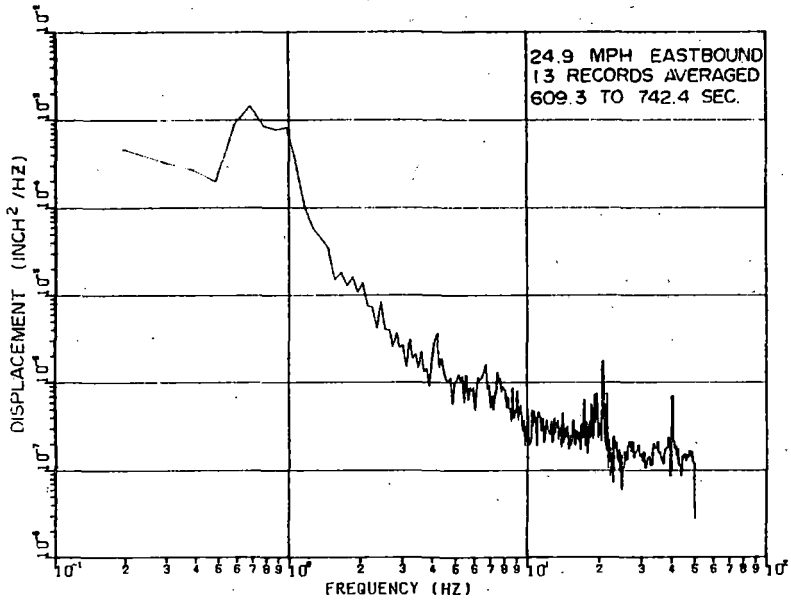

1 a. CARBODY LATERAL DISPLACEMENT

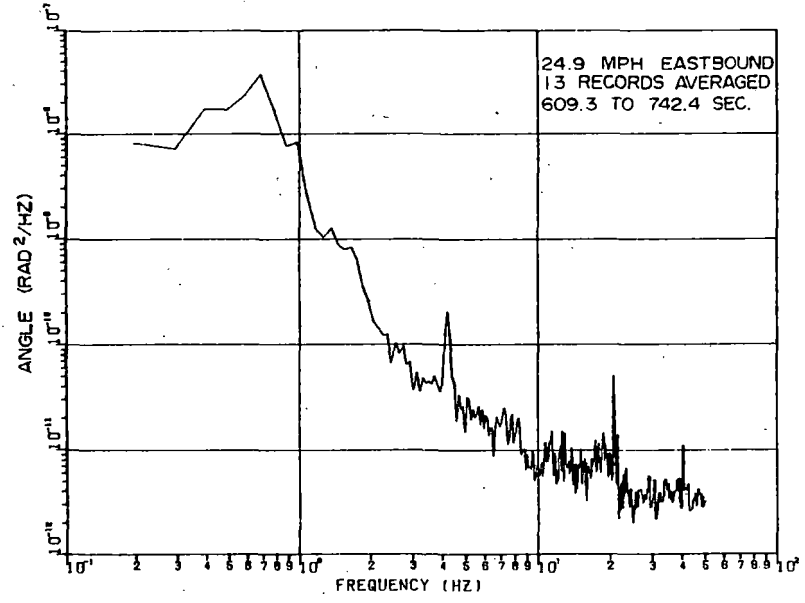

1c. CARBODY YAW ANGLE

FIGURE B-6. CONFIGURATION 6

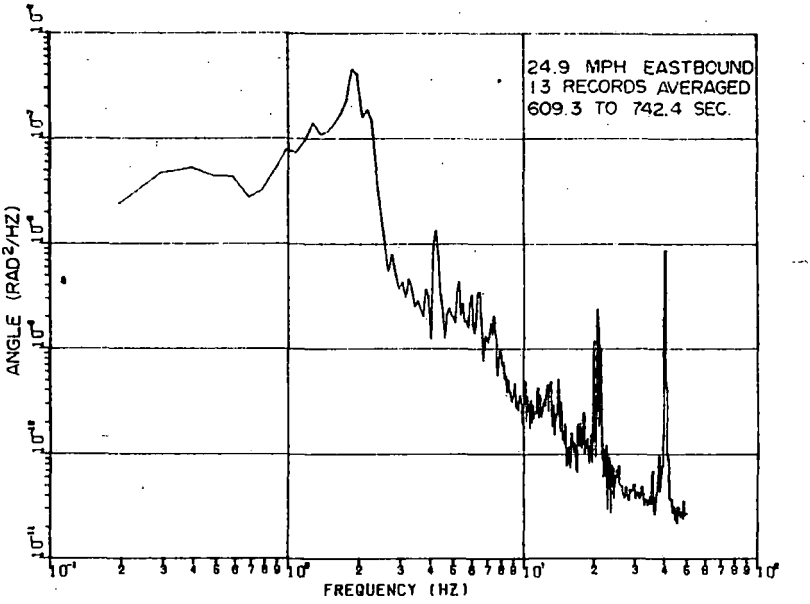

1b. CARBODY ROLL ANGLE

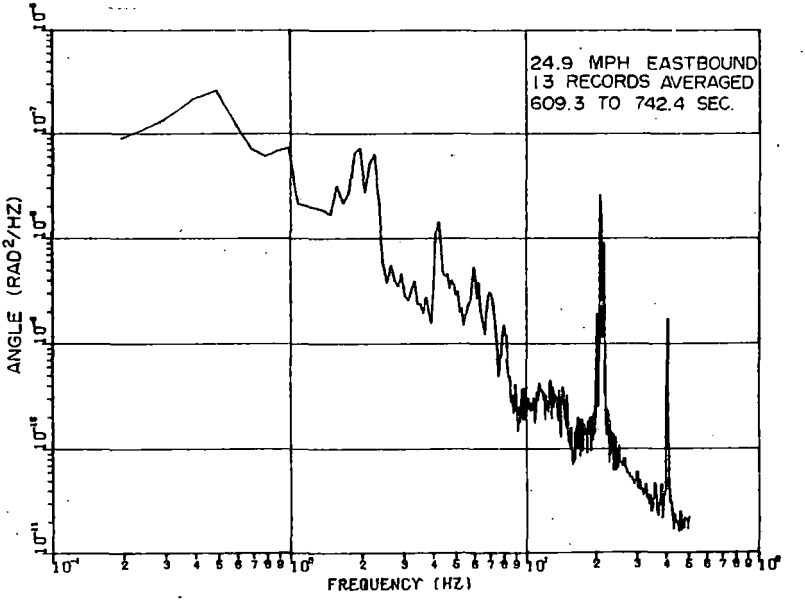

1d. CARBODY LONGITUDINAL TORSION

POWER SPECTRAL DENSITIES

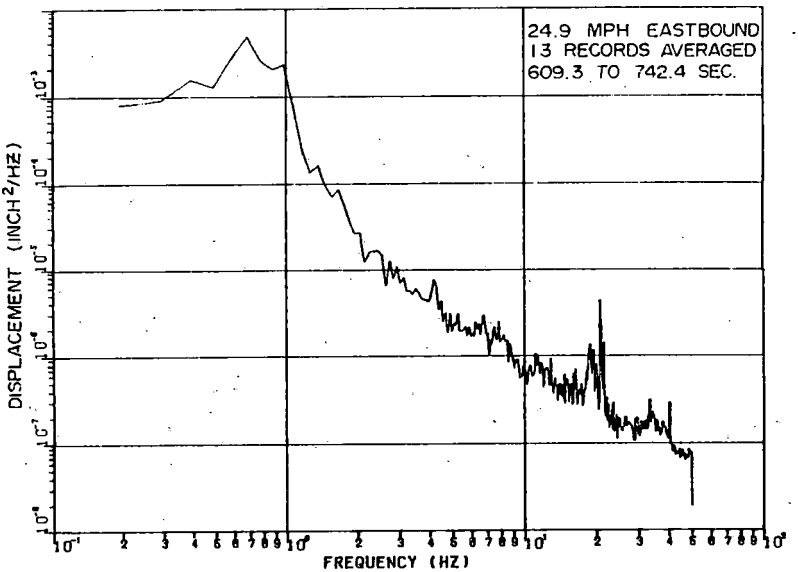

1 e. TRUCK-A LATERAL DISPLACEMENT

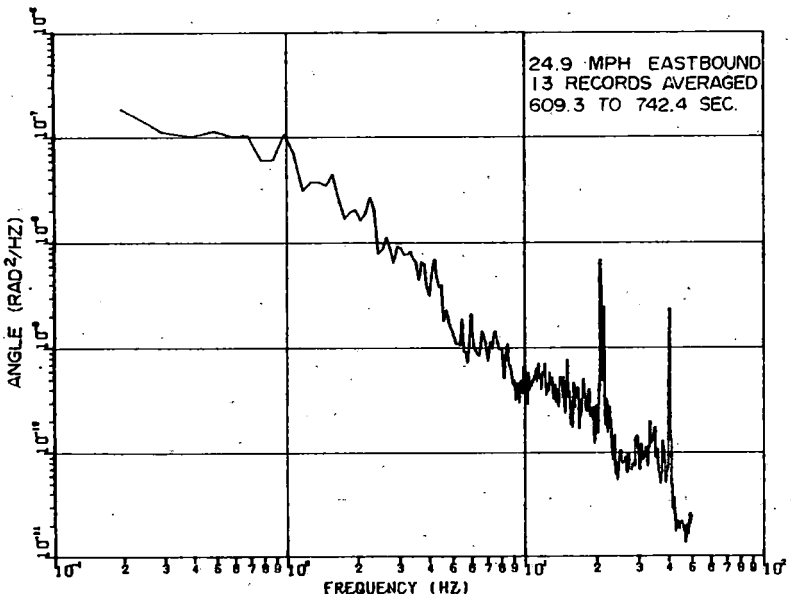

1 g. TRUCK-A WARP ANGLE

FIGURE B-6. CONFIGURATION 6

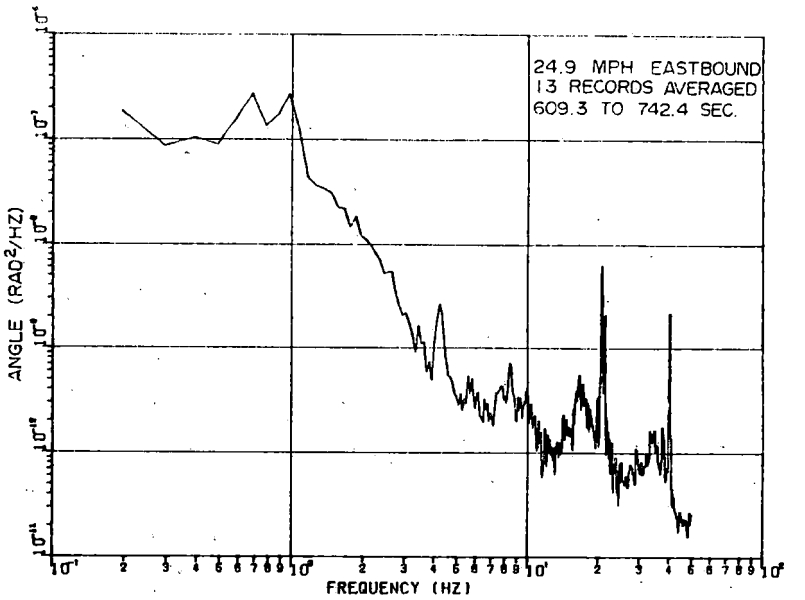

1 f. TRUCK-A YAW ANGLE

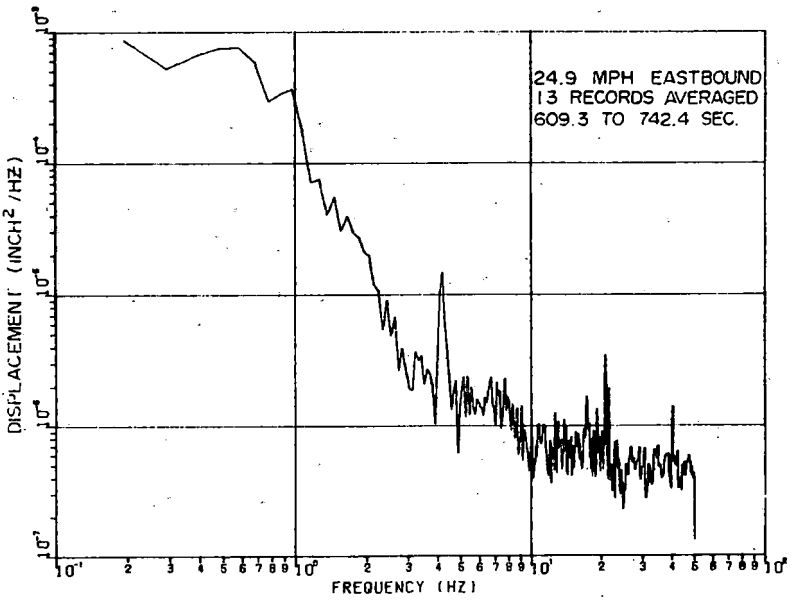

1 h. TRUCK-F LATERAL DISPLACEMENT

POWER SPECTRAL DENSITIES

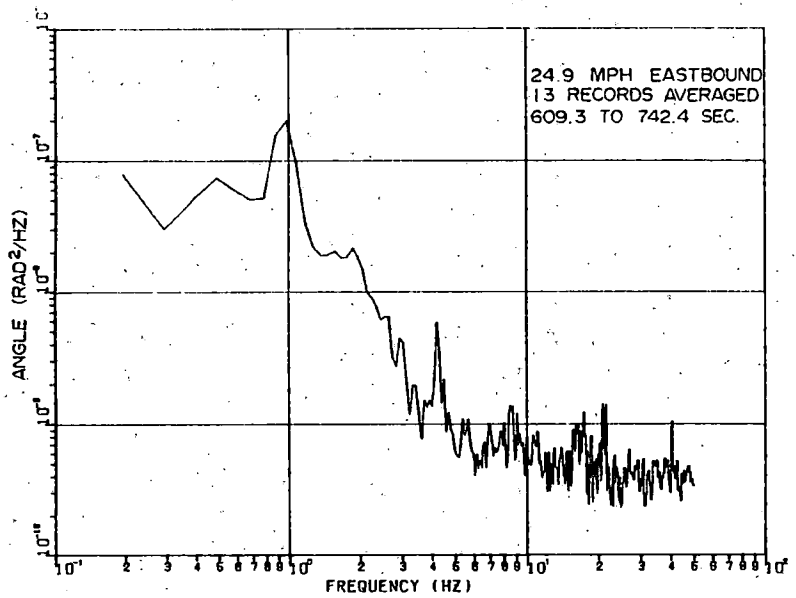

1 i. TRUCK-B YAW ANGLE

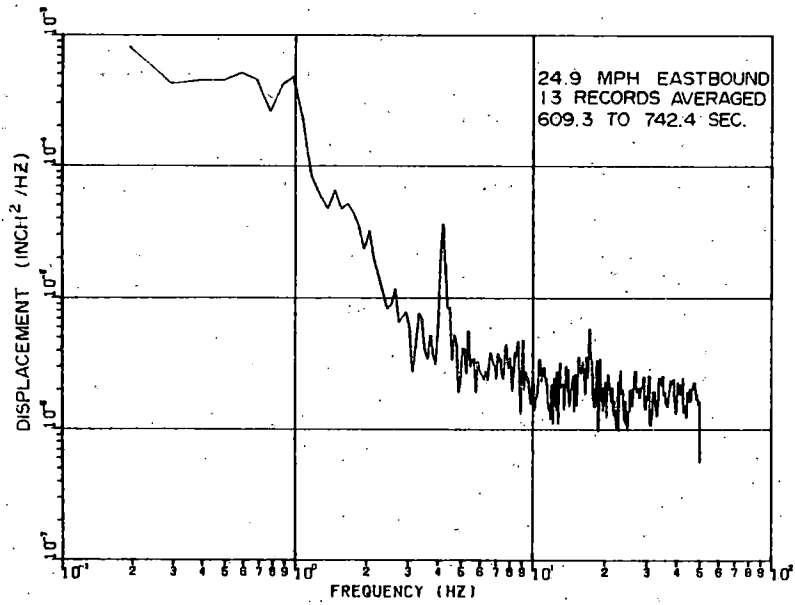

1 k. WHEELSET-1 LATERAL DISPLACEMENT

FIGURE B-6. CONFIGURATION 6

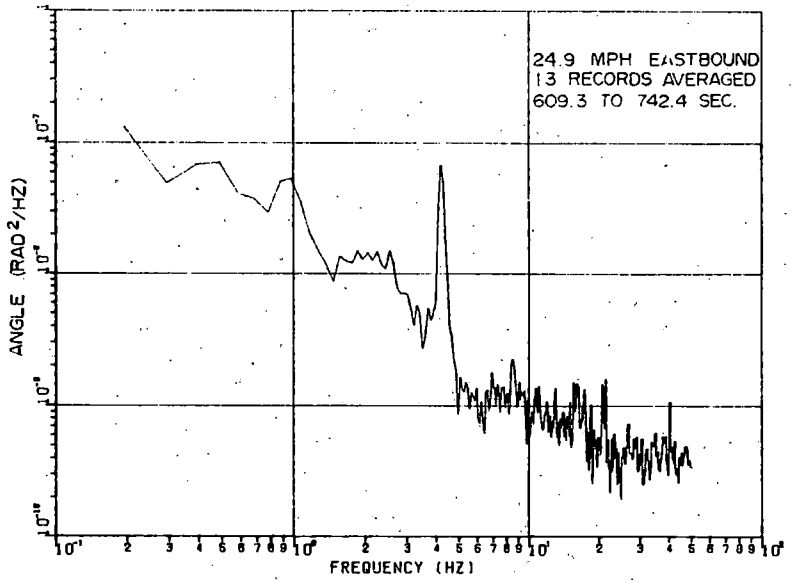

1 j. TRUCK-B WARP ANGLE

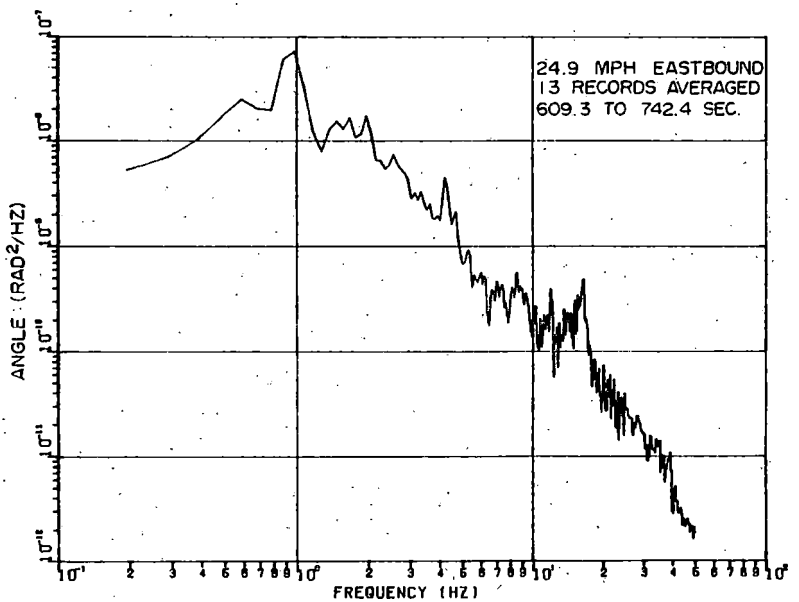

1 l. WHEELSET-1 YAW ANGLE

POWER SPECTRAL DENSITIES

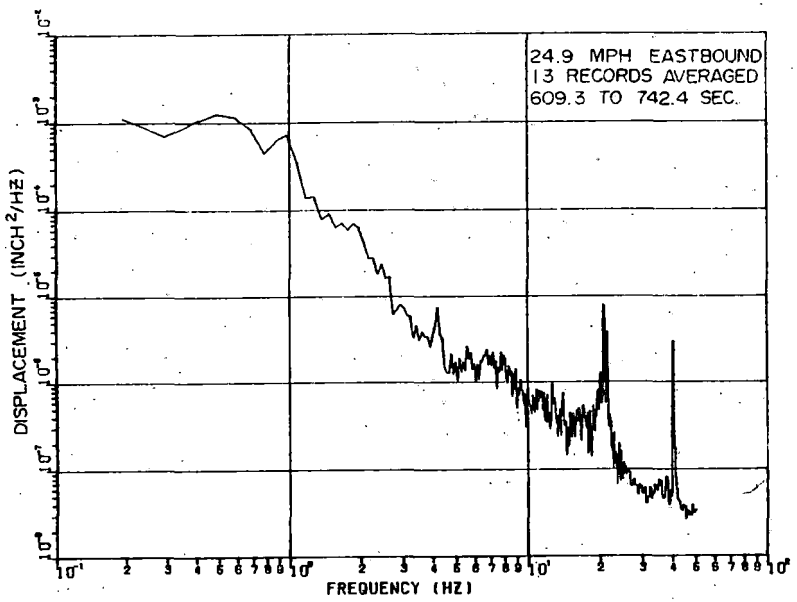

1m. WHEELSET-2 LATERAL DISPLACEMENT

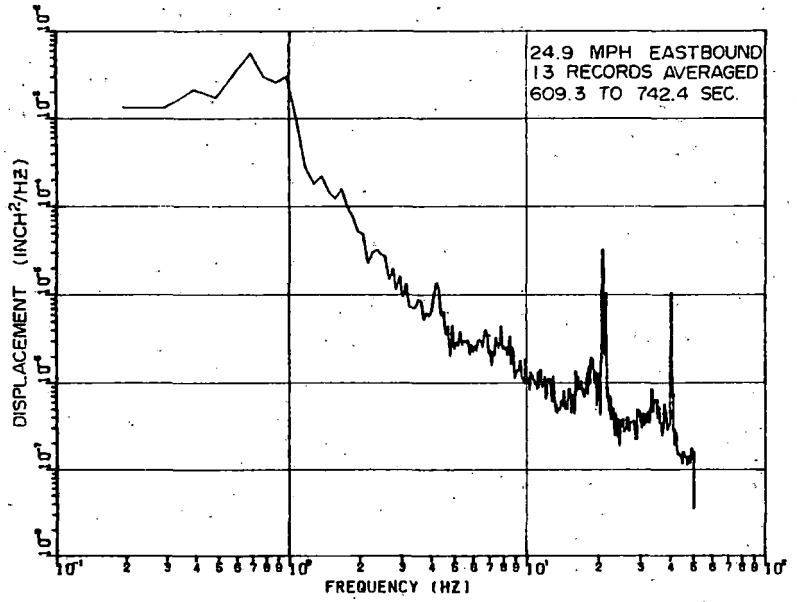

1o. WHEELSET-3 LATERAL DISPLACEMENT

FIGURE B-6. CONFIGURATION 6

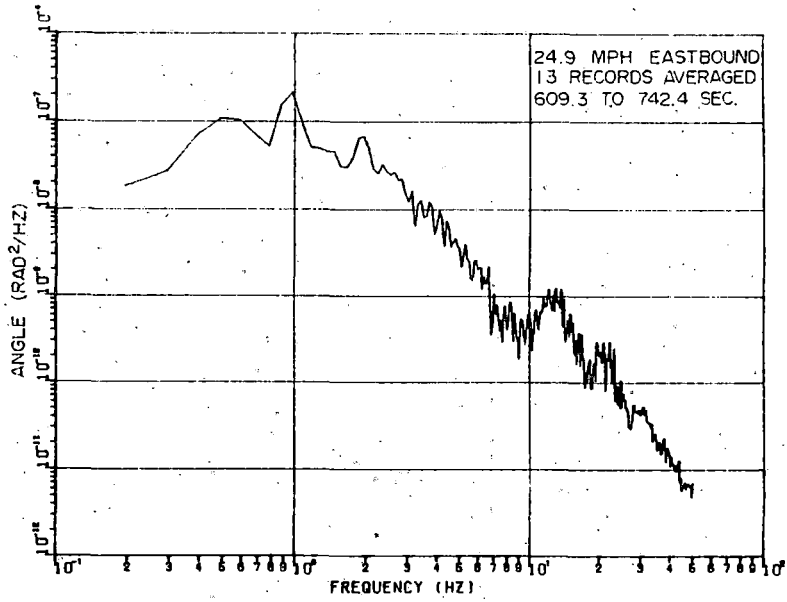

1n. WHEELSET-2 YAW ANGLE

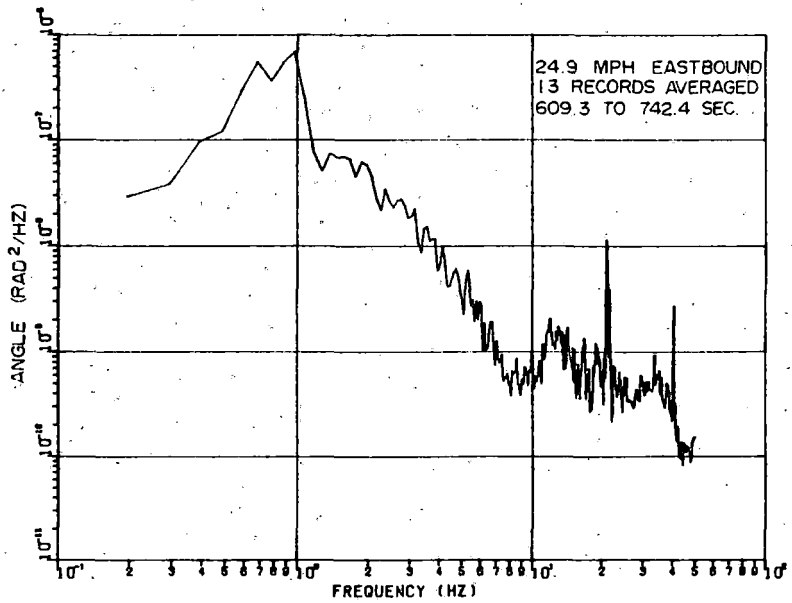

1p. WHEELSET-3 YAW ANGLE

POWER SPECTRAL DENSITIES

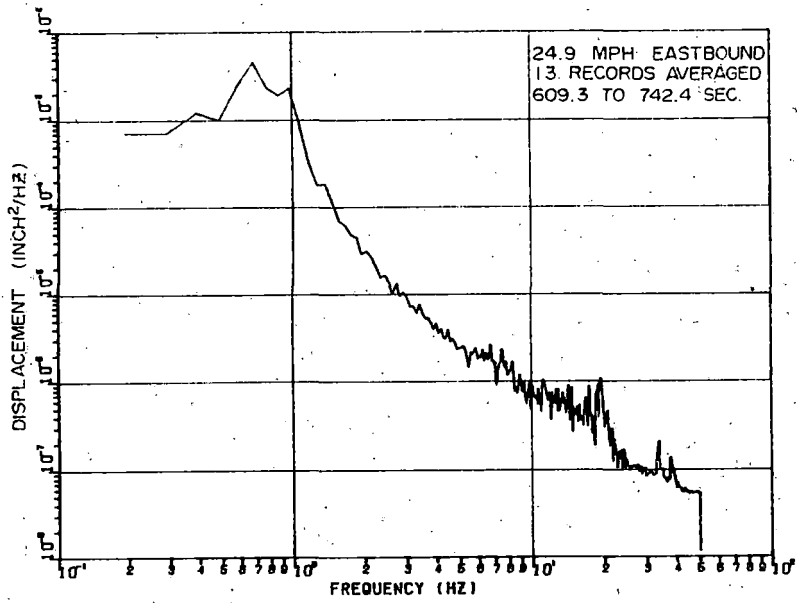

1 q. WHEELSET-4 LATERAL DISPLACEMENT

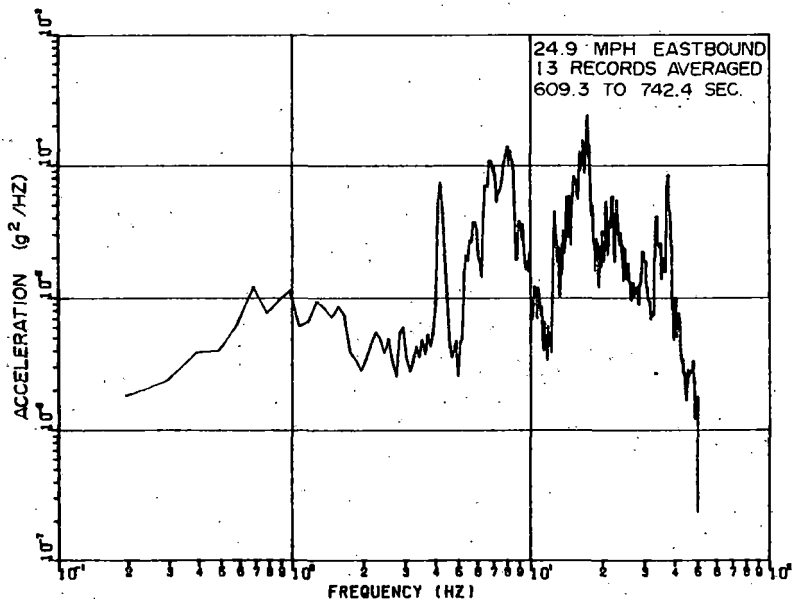

1 s. SIDEFRAME LATERAL ACCELERATION
AXLE-4 RIGHT SIDE

FIGURE B-6. CONFIGURATION 6

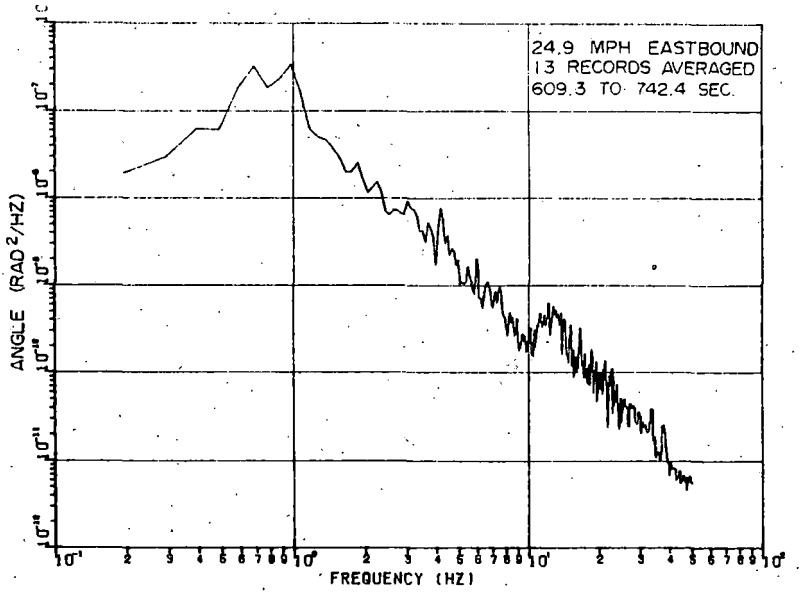

1r. WHEELSET-4 YAW ANGLE

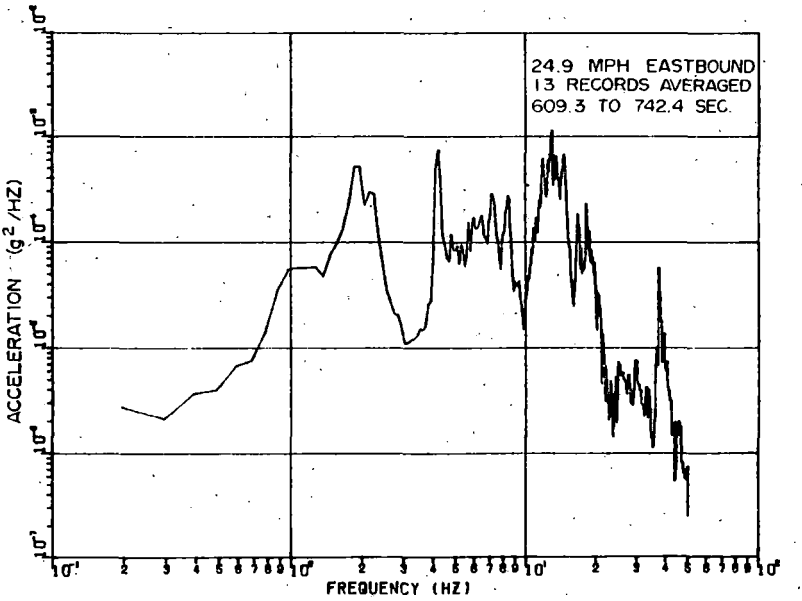

1t. CARBODY VERTICAL ACCELERATION
B-END RIGHT SIDE

POWER SPECTRAL DENSITIES

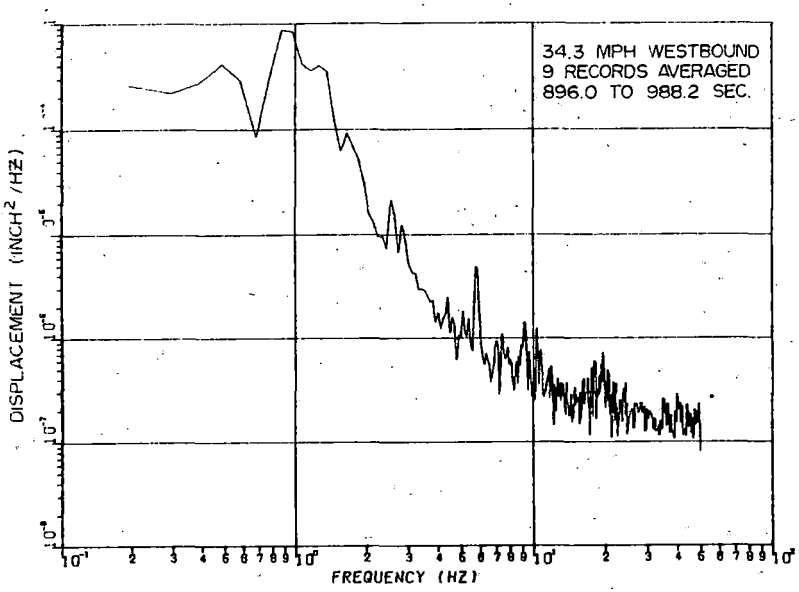

2 a. CARBODY LATERAL DISPLACEMENT

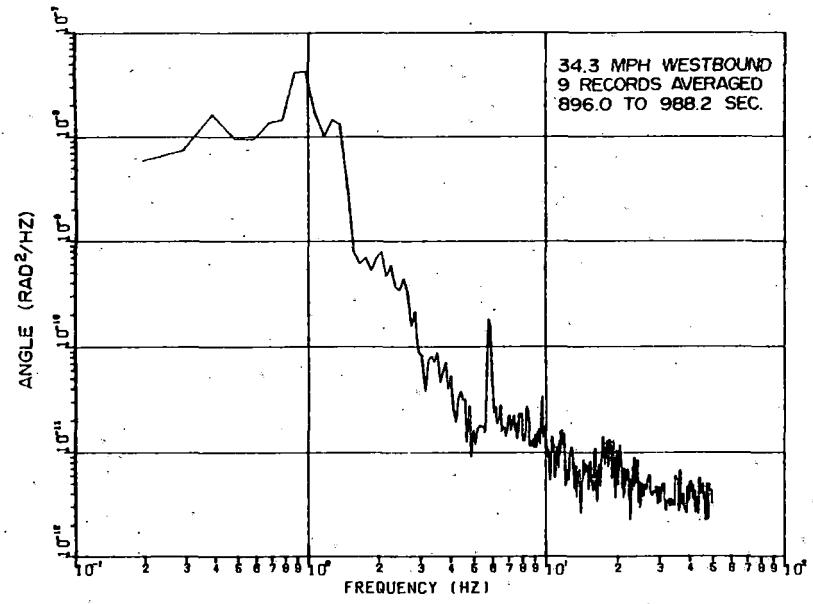

2 c. CARBODY YAW ANGLE

FIGURE B-6. CONFIGURATION 6

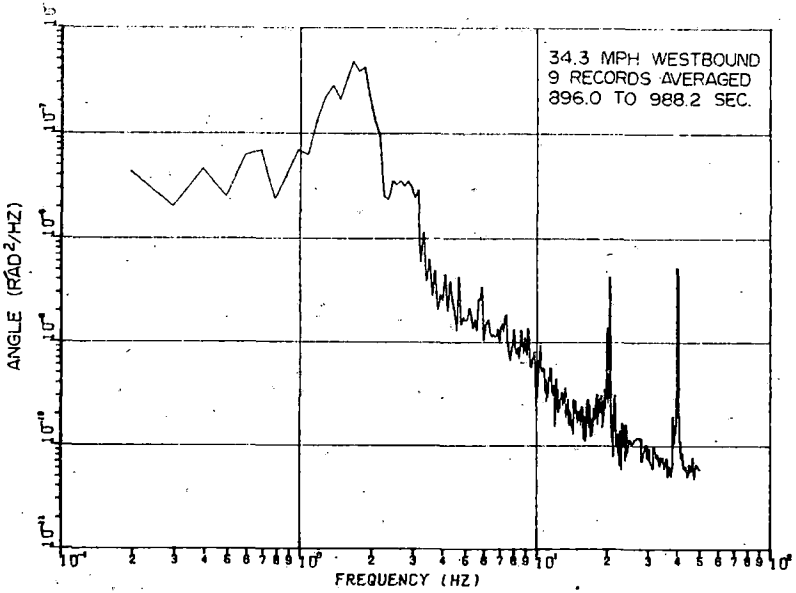

2 b. CARBODY ROLL ANGLE

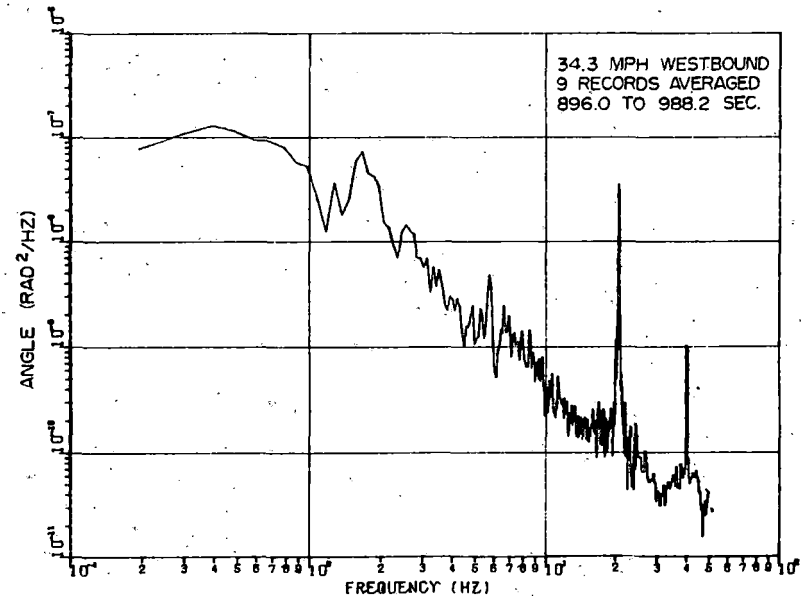

2 d. CARBODY LONGITUDINAL TORSION

POWER SPECTRAL DENSITIES

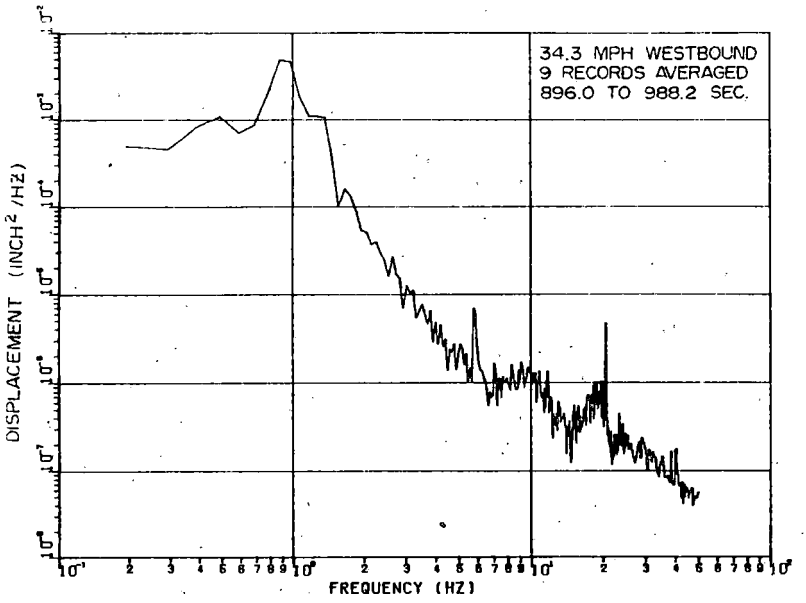

2 e. TRUCK-A LATERAL DISPLACEMENT

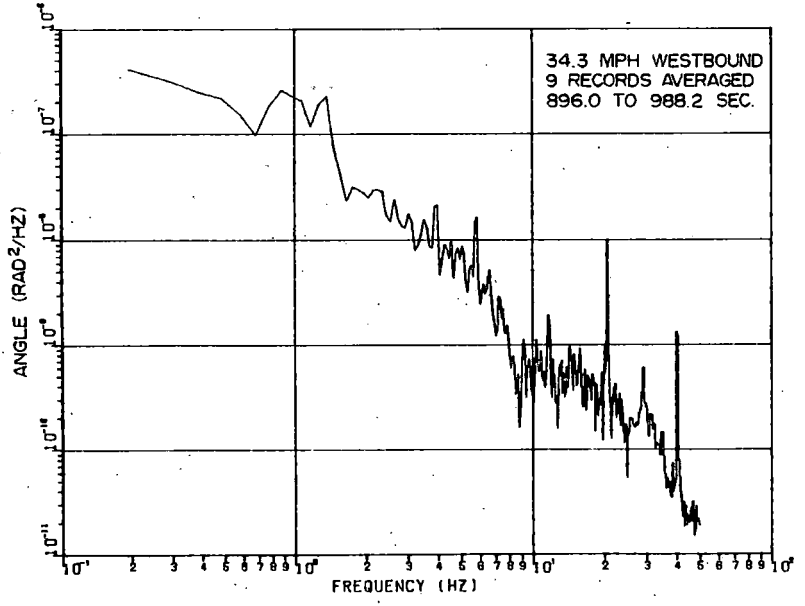

2 g. TRUCK-A WARP ANGLE

FIGURE B-6. CONFIGURATION 6

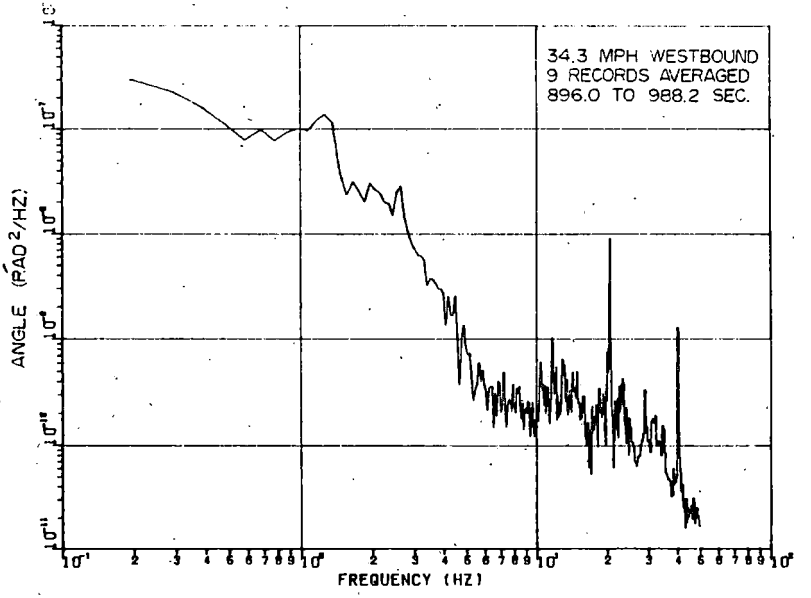

2 f. TRUCK-A YAW ANGLE

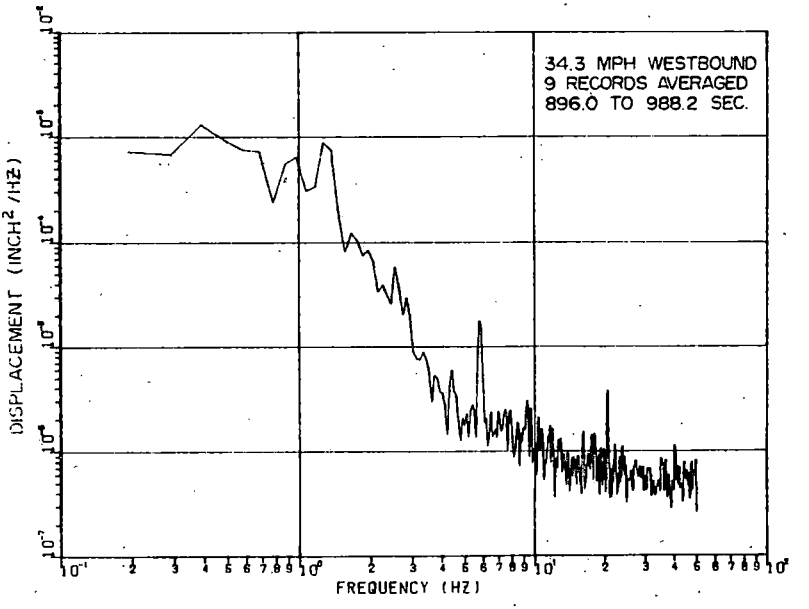

2 h. TRUCK-B LATERAL DISPLACEMENT

POWER SPECTRAL DENSITIES

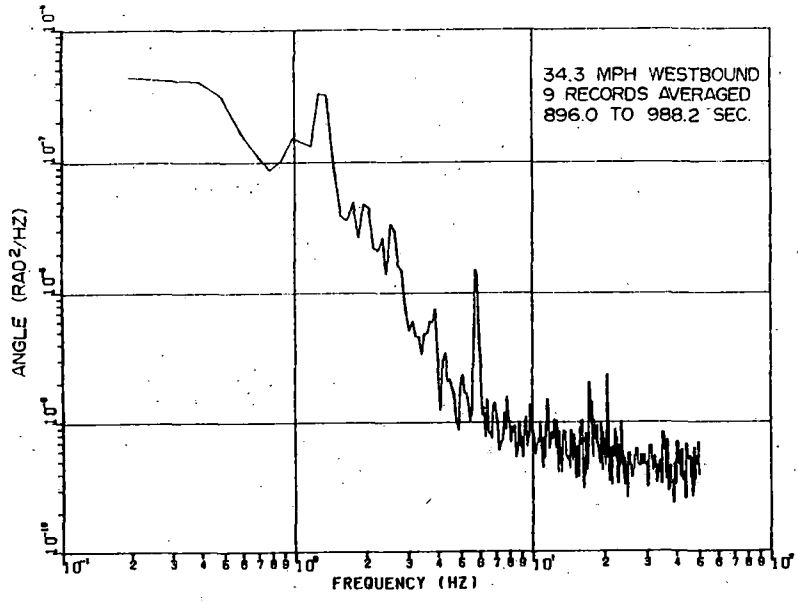

2 i. TRUCK-B YAW ANGLE

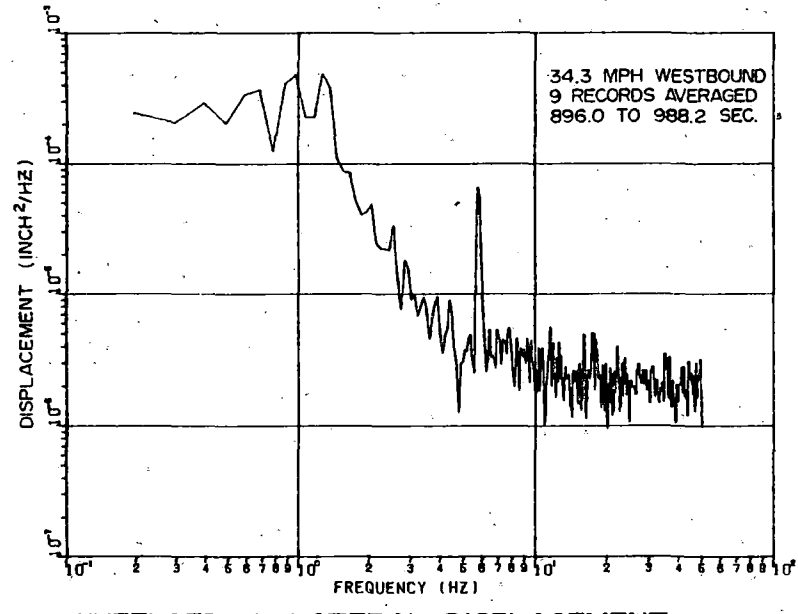

2.k. WHEELSET-1 LATERAL DISPLACEMENT

FIGURE B-6. CONFIGURATION 6

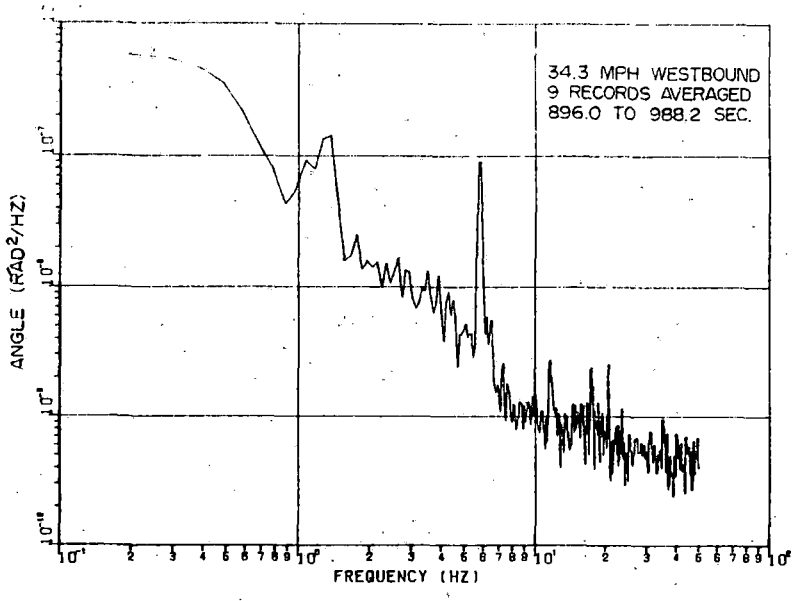

2 j. TRUCK-B WARP ANGLE

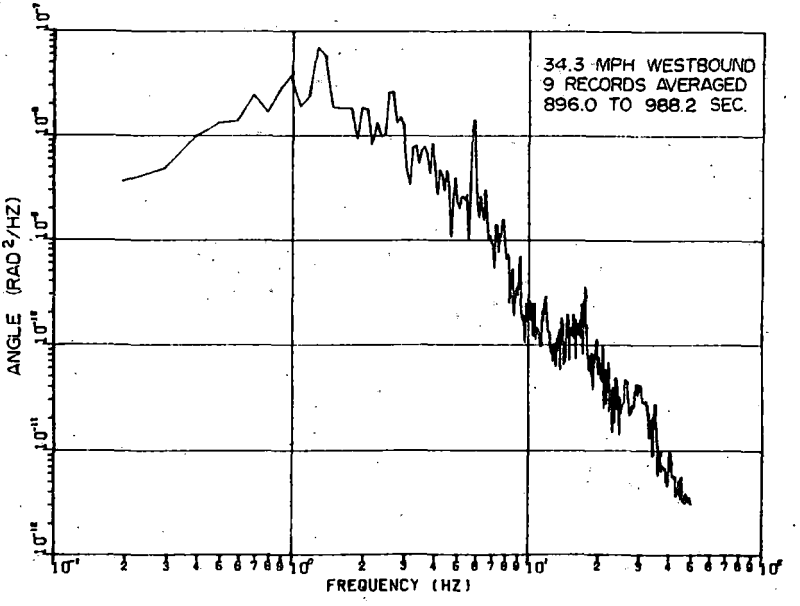

2 l. WHEELSET-1 YAW ANGLE

POWER SPECTRAL DENSITIES

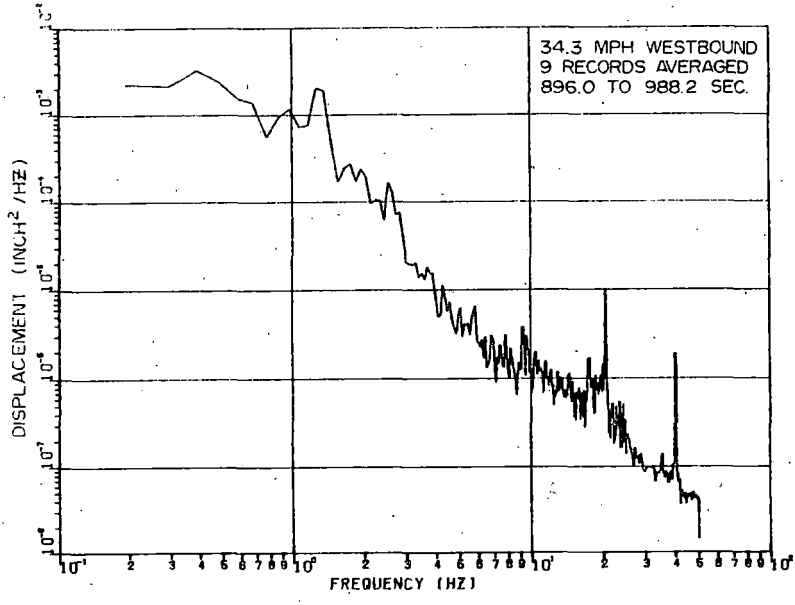

2m. WHEELSET-2 LATERAL DISPLACEMENT

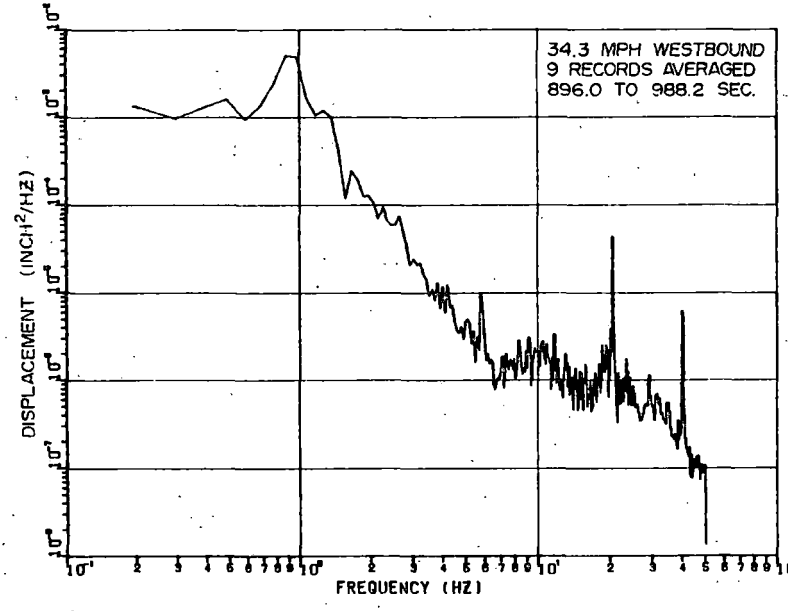

2o. WHEELSET-3 LATERAL DISPLACEMENT

FIGURE B-6. CONFIGURATION 6

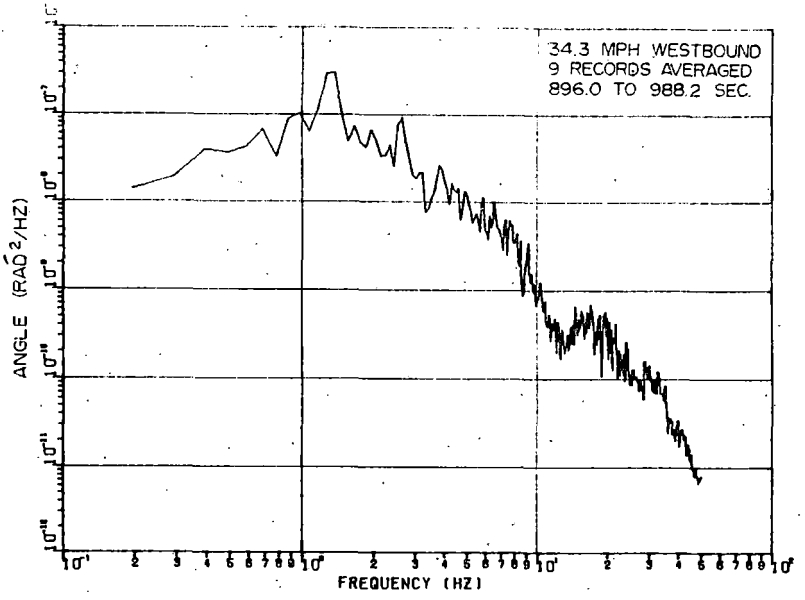

2 n. WHEELSET- 2 YAW ANGLE

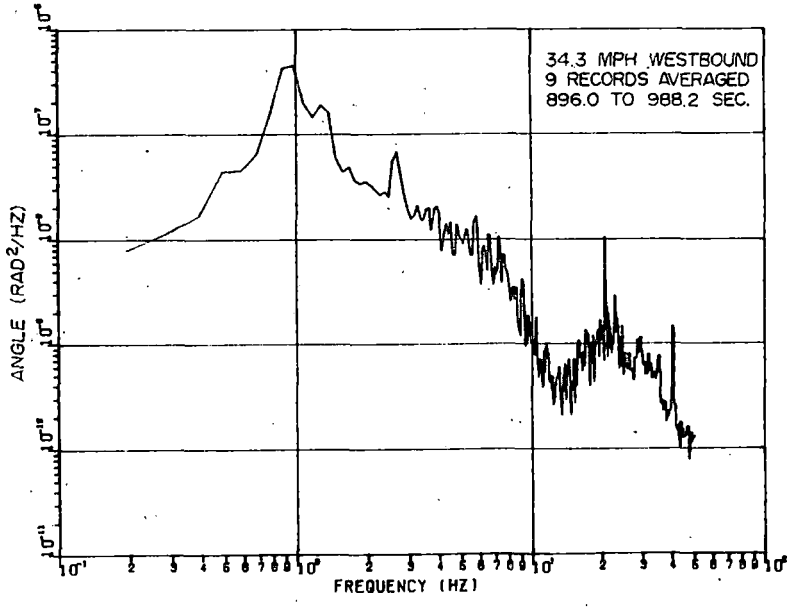

2 p. WHEELSET- 3 YAW ANGLE

POWER SPECTRAL DENSITIES

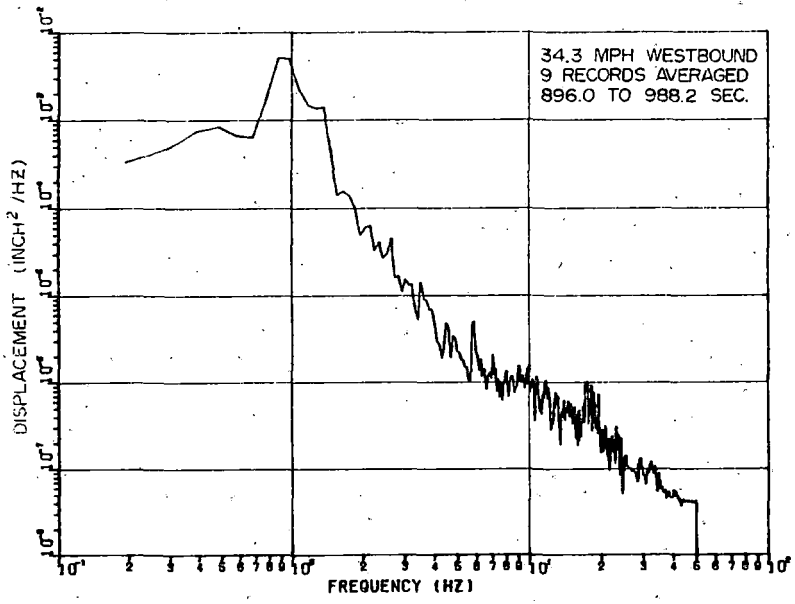

2q. WHEELSET-4 LATERAL DISPLACEMENT

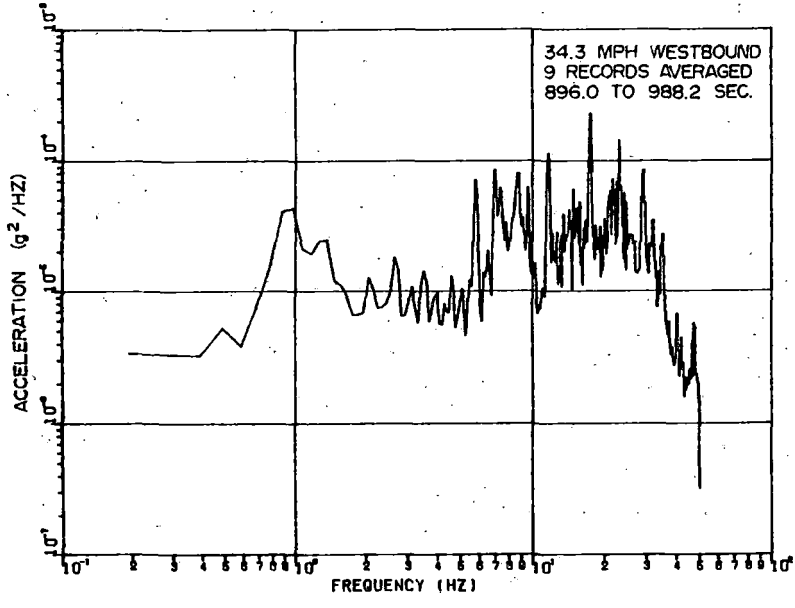

2s. SIDEFRAME LATERAL ACCELERATION
AXLE-4 RIGHT SIDE

FIGURE B-6. CONFIGURATION 6

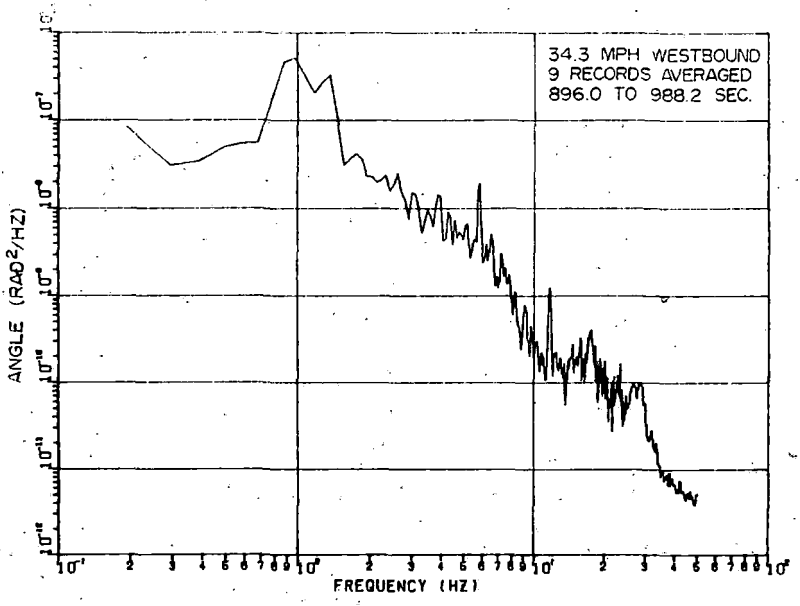

2r. WHEELSET-4 YAW ANGLE

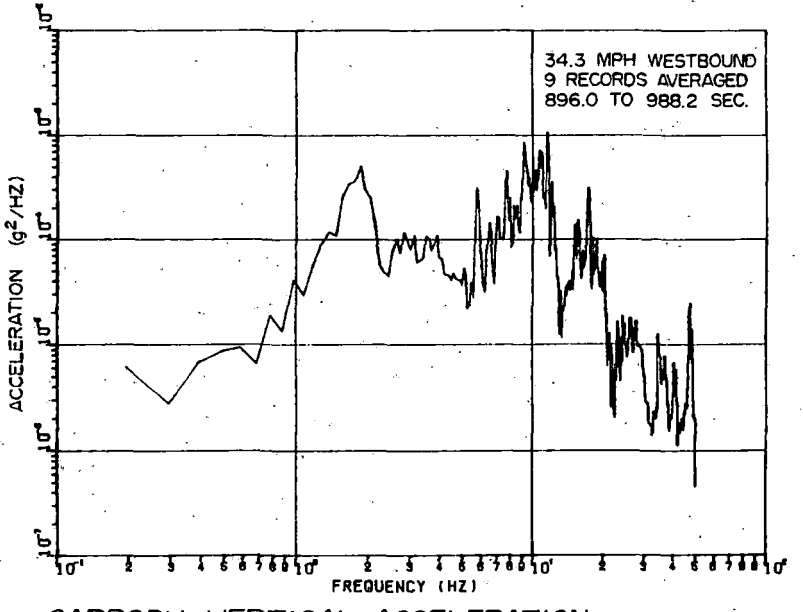

2t. CARBODY VERTICAL ACCELERATION
B-END RIGHT SIDE

POWER SPECTRAL DENSITIES

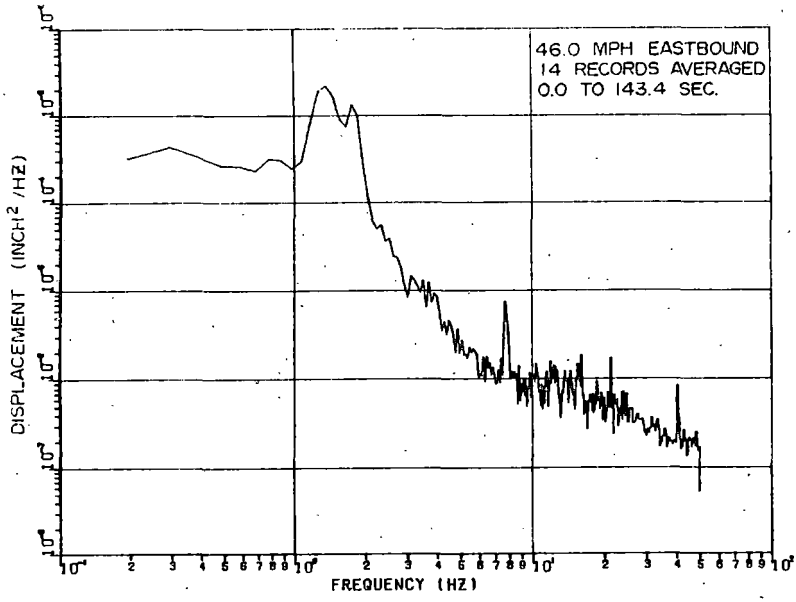

3 a. CARBODY LATERAL DISPLACEMENT

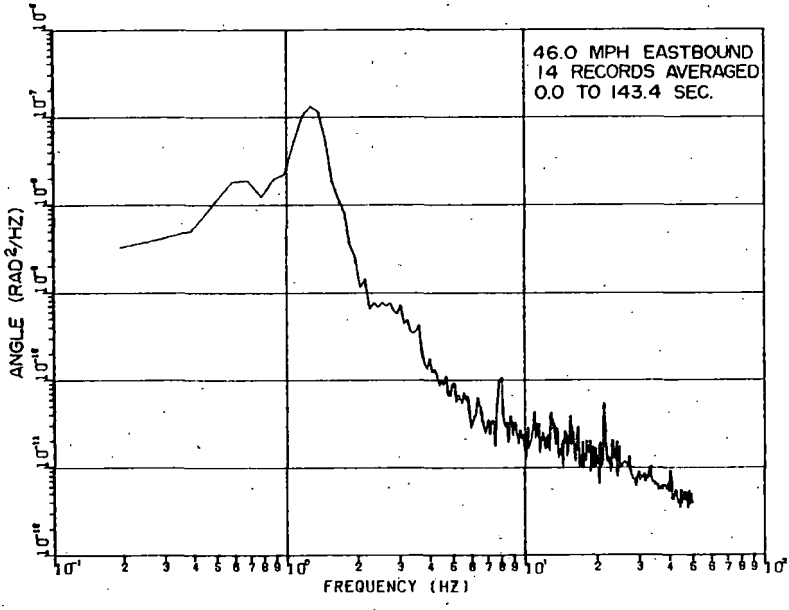

3 c. CARBODY YAW ANGLE

FIGURE B-6. CONFIGURATION 6

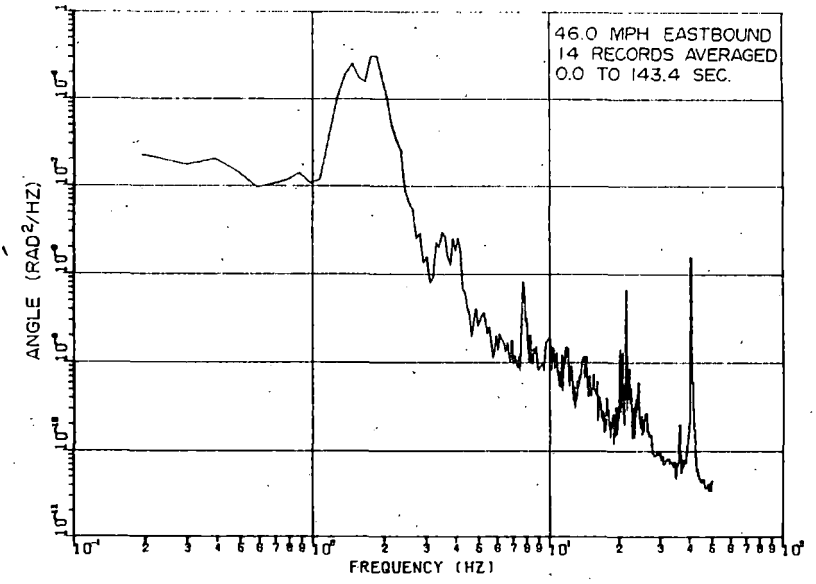

3 b. CARBODY ROLL ANGLE

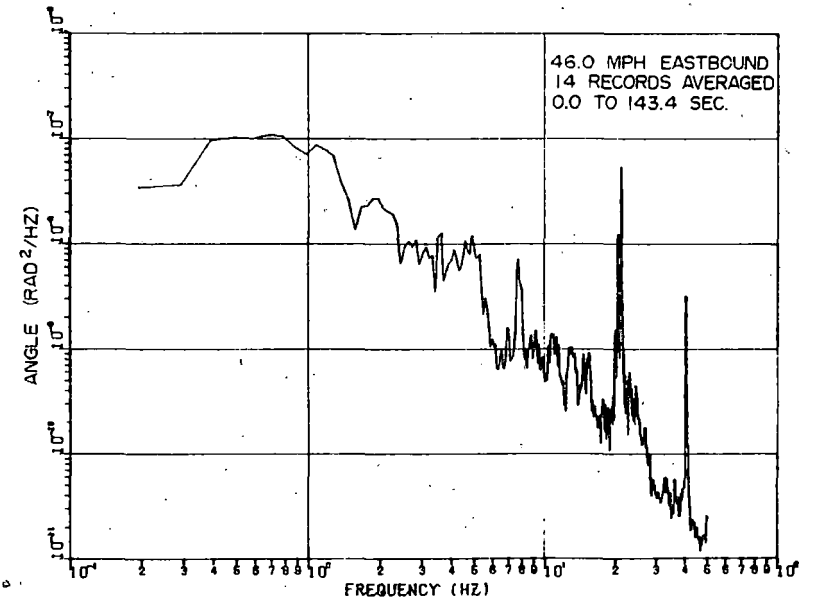

3 d. CARBODY LONGITUDINAL TORSION

POWER SPECTRAL DENSITIES

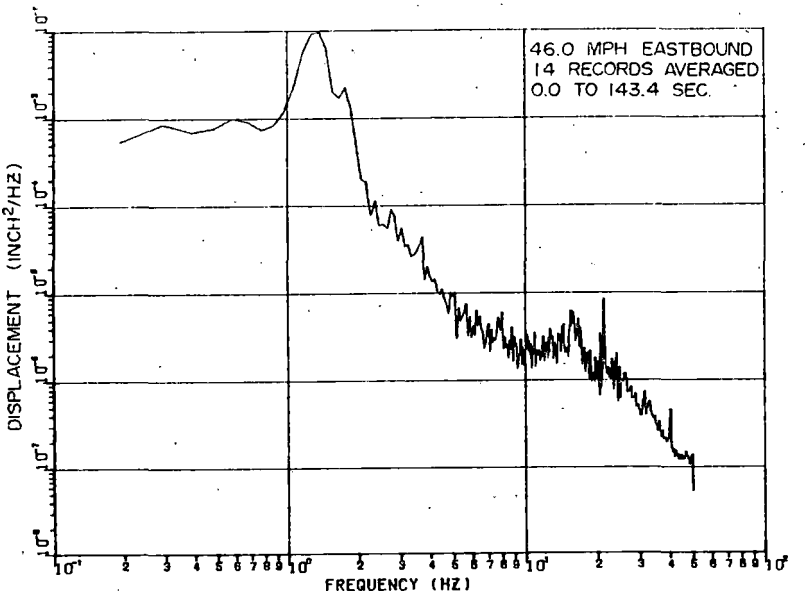

3e. TRUCK-A LATERAL DISPLACEMENT

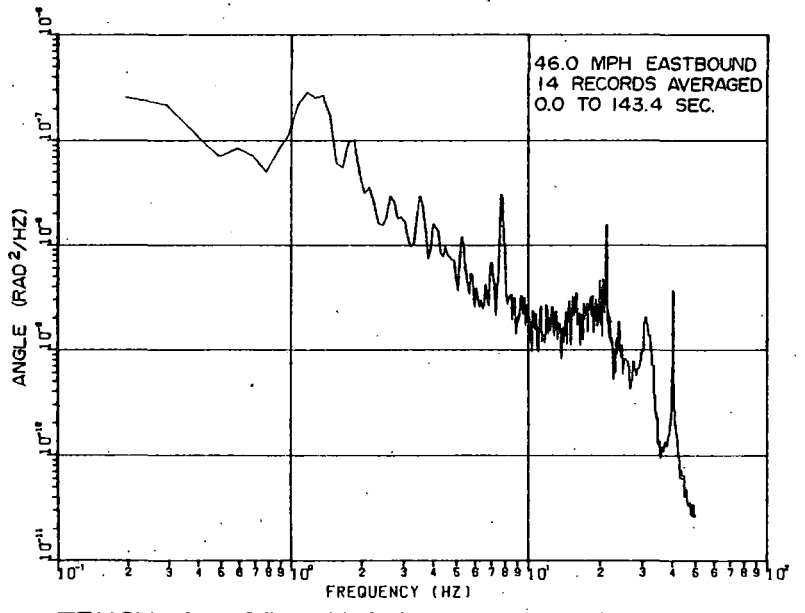

3g. TRUCK-A WARP ANGLE

FIGURE B-6. CONFIGURATION 6

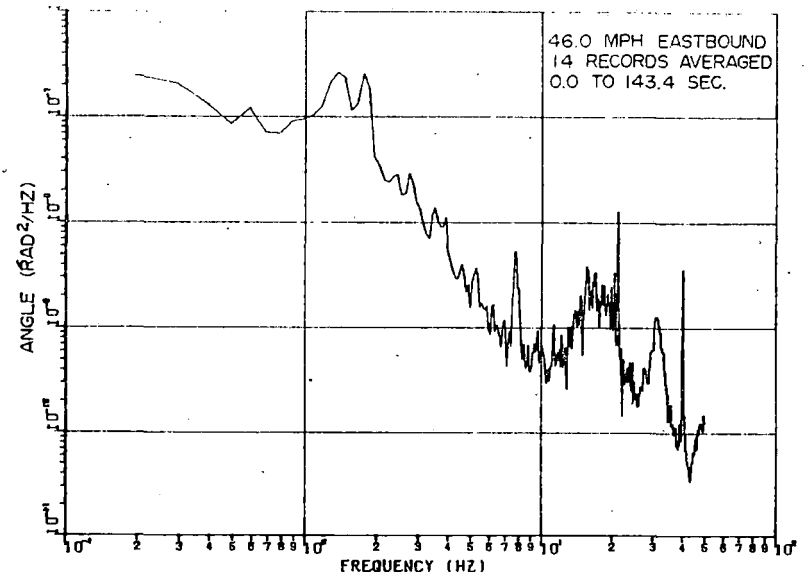

3 f. TRUCK-A YAW ANGLE

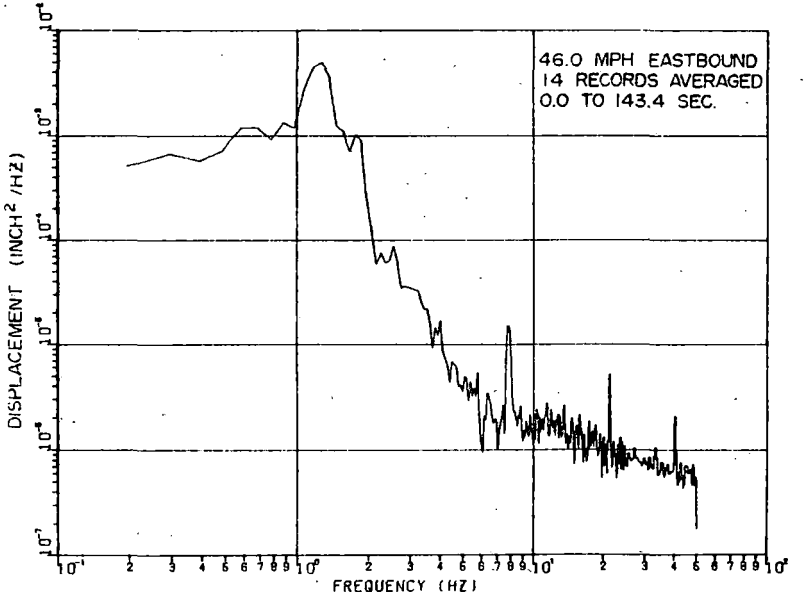

3 h. TRUCK-B LATERAL DISPLACEMENT

POWER SPECTRAL DENSITIES

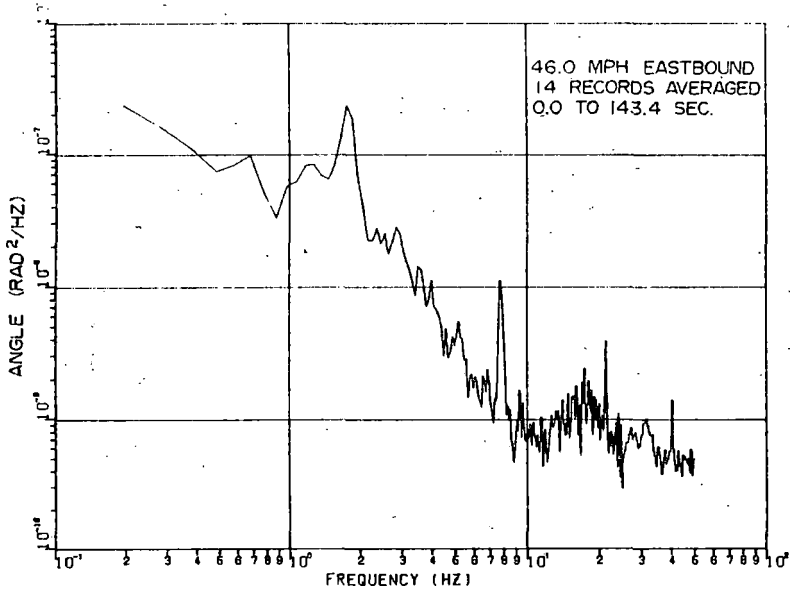

3i. TRUCK-B YAW ANGLE

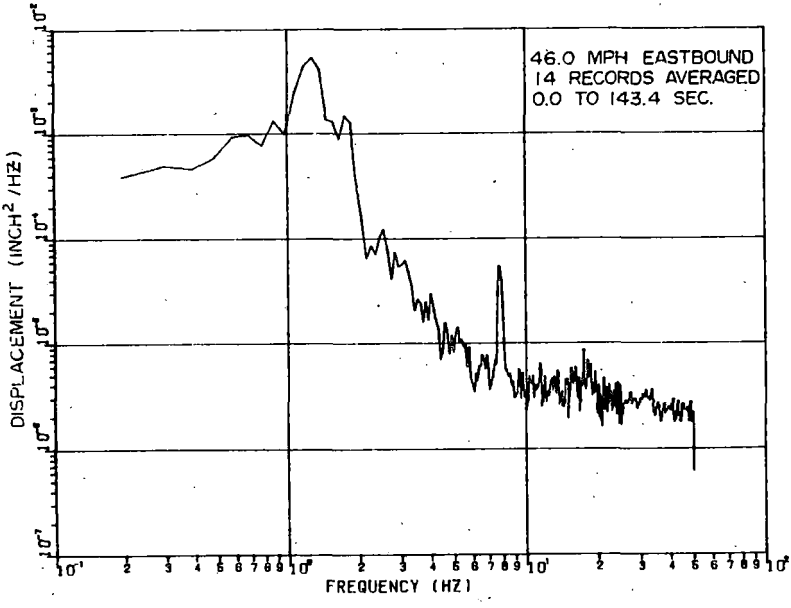

3k. WHEELSET-1 LATERAL DISPLACEMENT

FIGURE B-6. CONFIGURATION 6

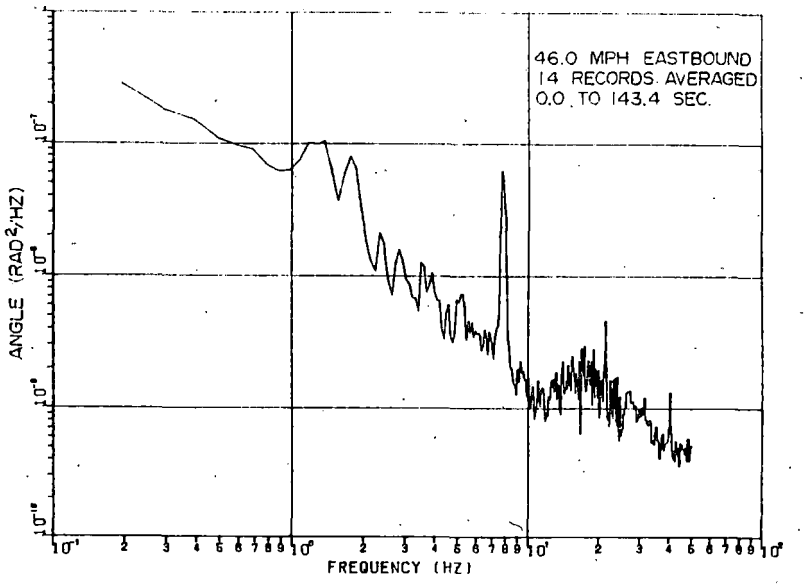

3 j. TRUCK-B WARP ANGLE

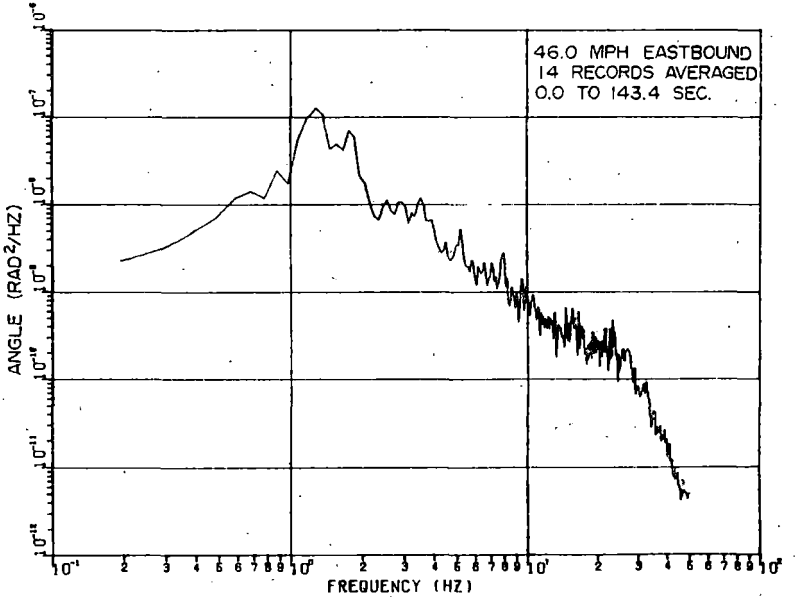

3 l. WHEELSET-1 YAW ANGLE

POWER SPECTRAL DENSITIES

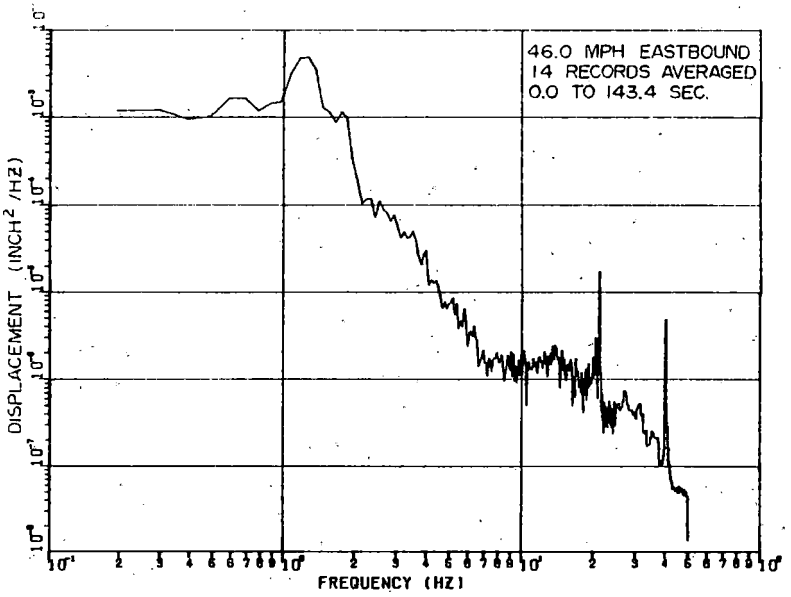

3m. WHEELSET-2 LATERAL DISPLACEMENT

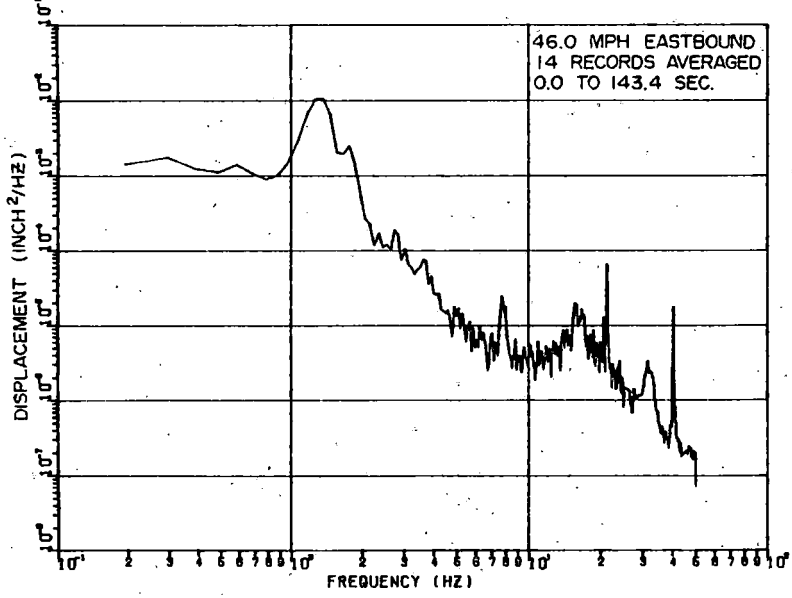

3o. WHEELSET-3 LATERAL DISPLACEMENT

FIGURE B-6. CONFIGURATION 6

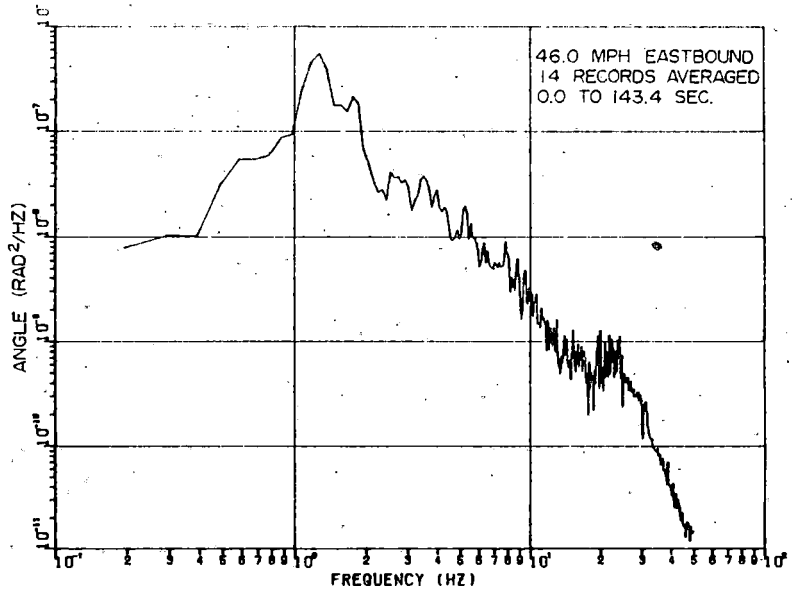

3n. WHEELSET-2 YAW ANGLE

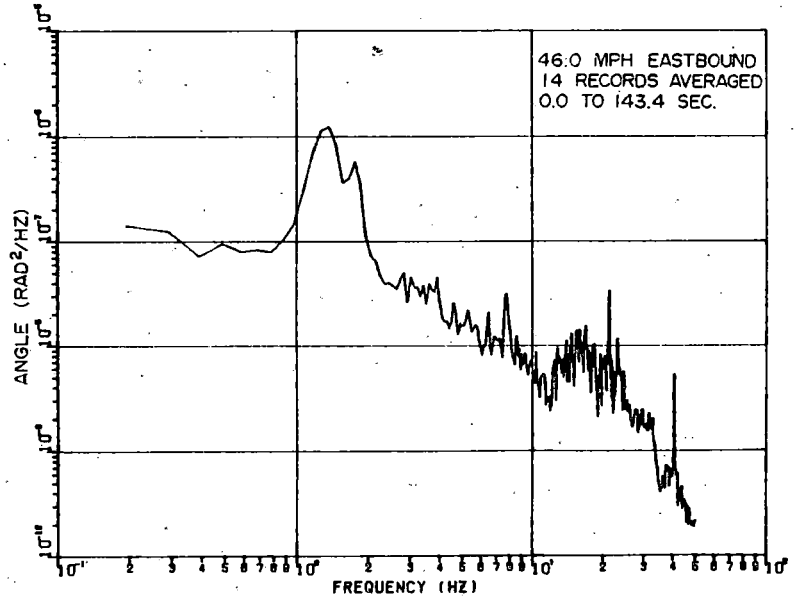

3p. WHEELSET-3 YAW ANGLE

POWER SPECTRAL DENSITIES

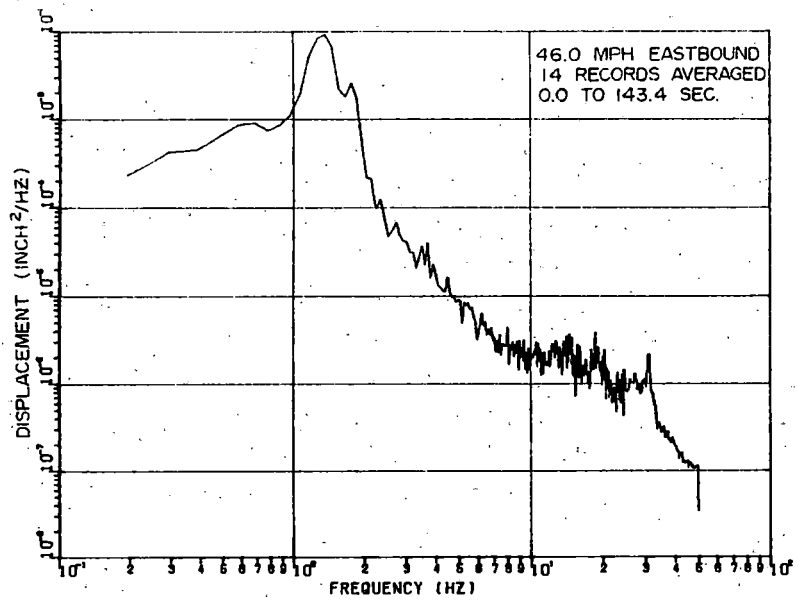

3q. WHEELSET-4 LATERAL DISPLACEMENT

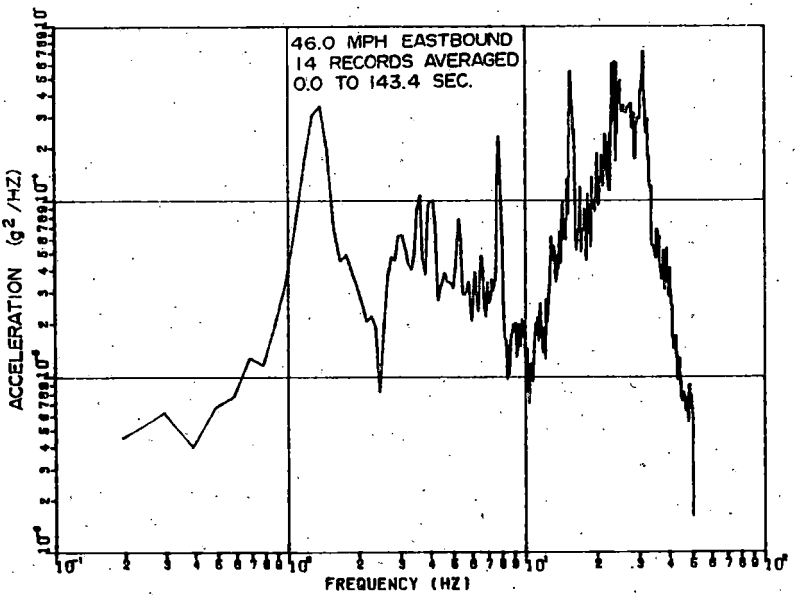

3s. SIDEFRAME LATERAL ACCELERATION
AXLE-4 RIGHT SIDE

FIGURE B-6. CONFIGURATION 6

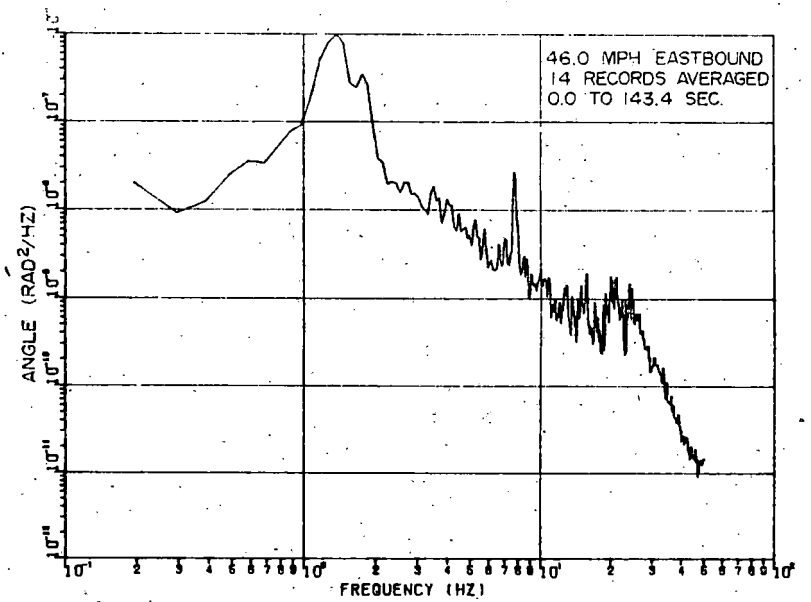

3f. WHEELSET-4 YAW ANGLE

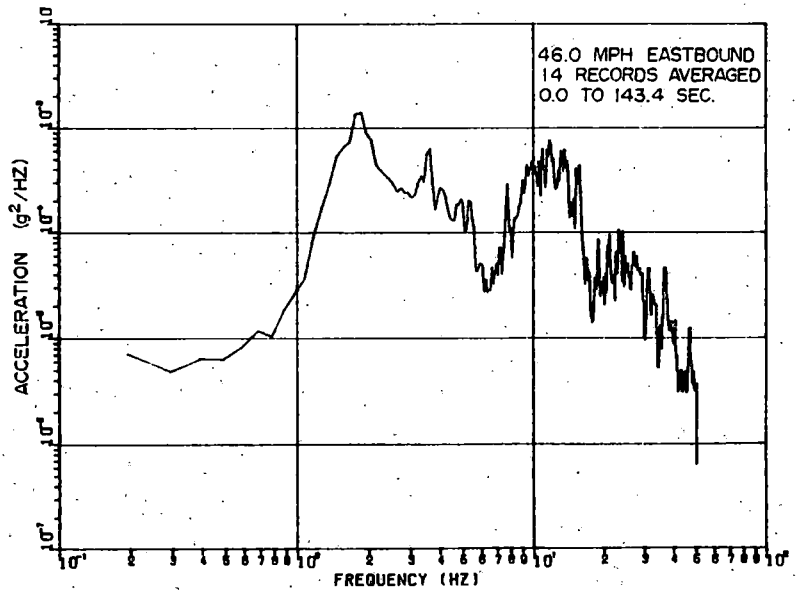

3t. CARBODY VERTICAL ACCELERATION
B-END RIGHT SIDE

POWER SPECTRAL DENSITIES

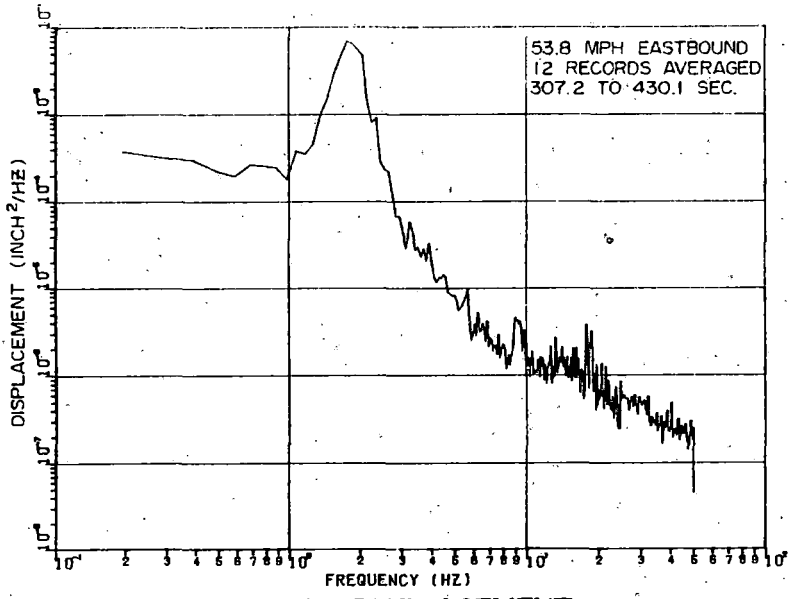

4 a. CARBODY LATERAL DISPLACEMENT

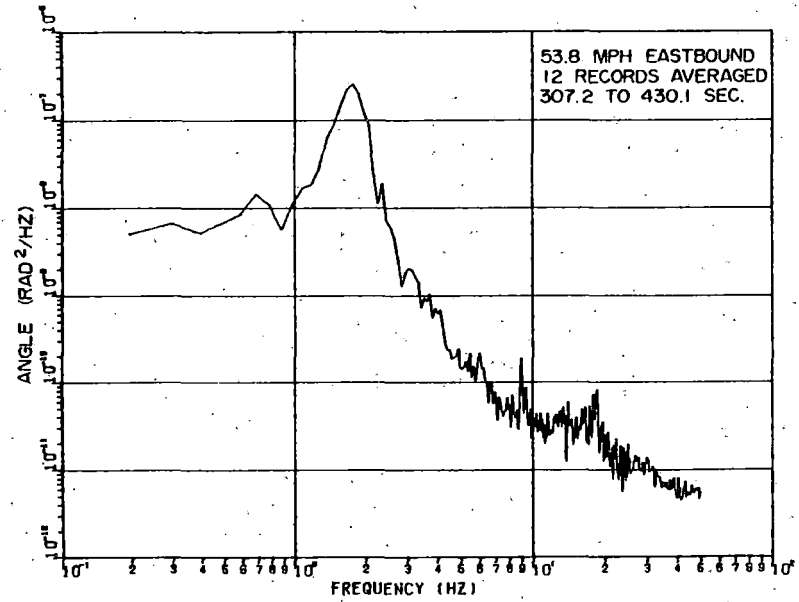

4 c. CARBODY YAW ANGLE

FIGURE B-6. CONFIGURATION 6

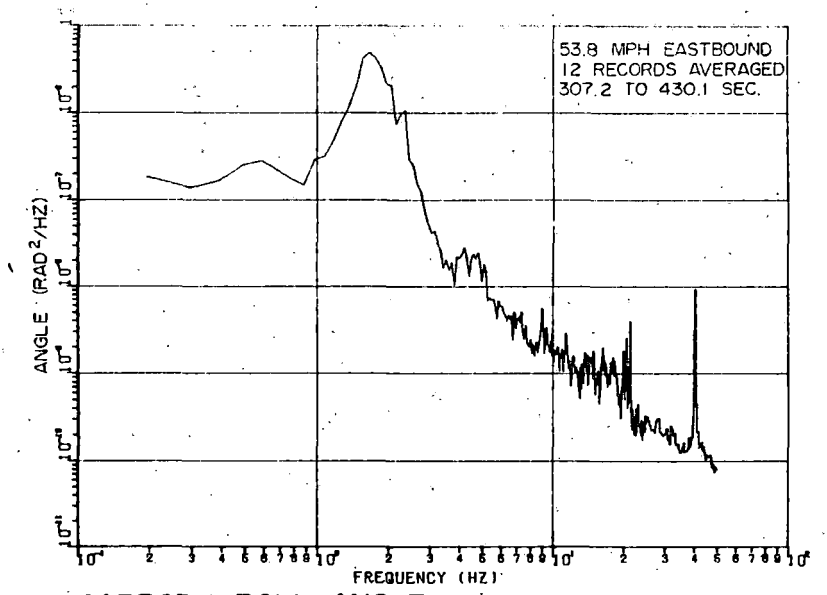

4 b. CARBODY ROLL ANGLE

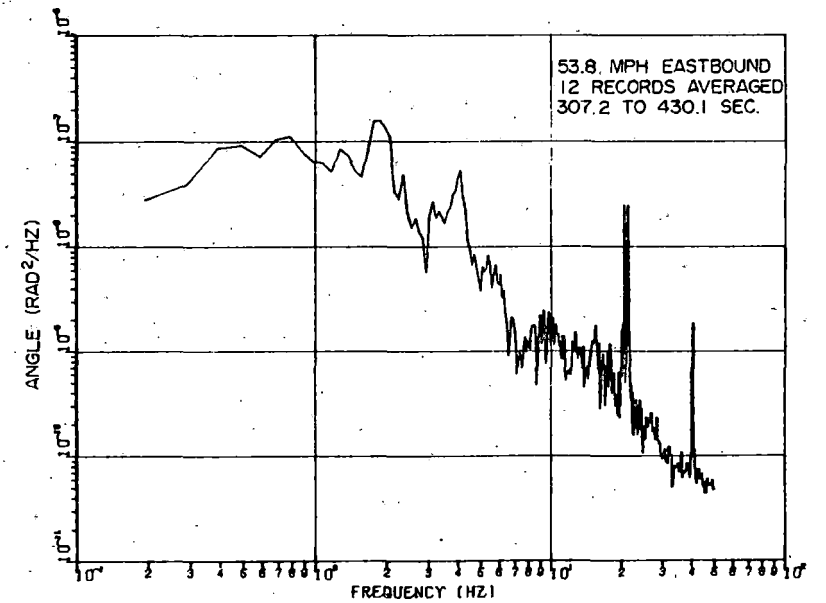

4 d. CARBODY LONGITUDINAL TORSION

POWER SPECTRAL DENSITIES

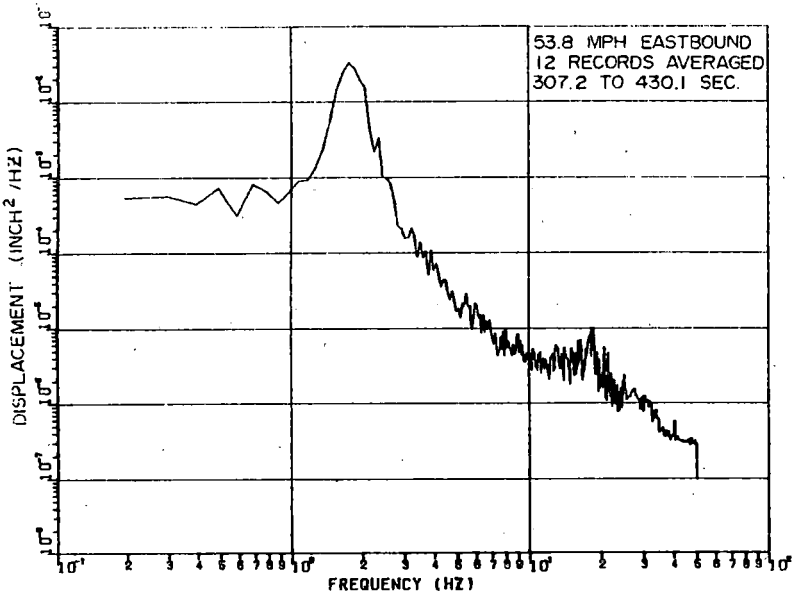

4 e. TRUCK-A LATERAL DISPLACEMENT

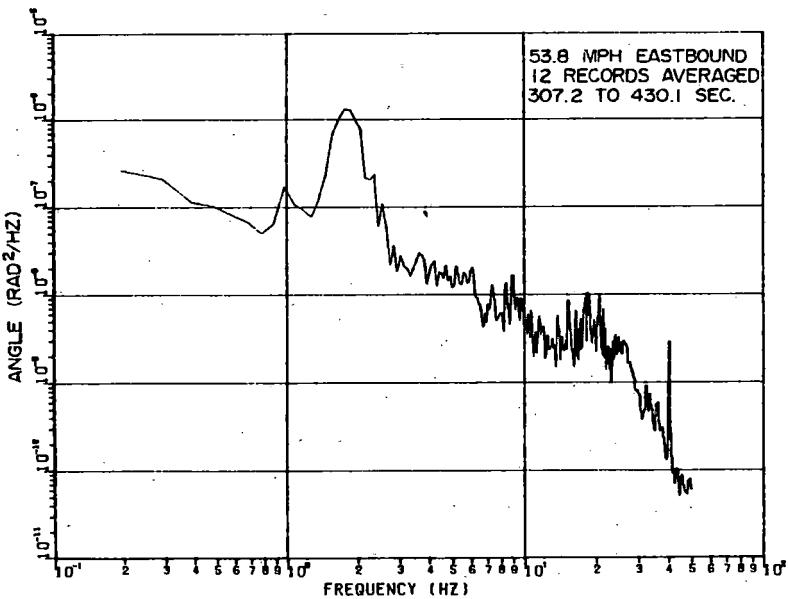

4 g. TRUCK-A WARP ANGLE

FIGURE B-6. CONFIGURATION 6

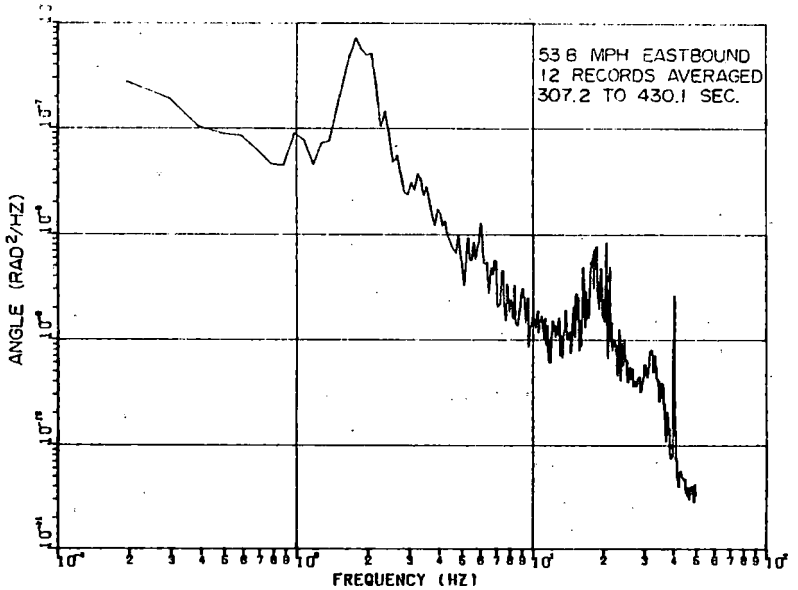

4 f. TRUCK-A YAW ANGLE

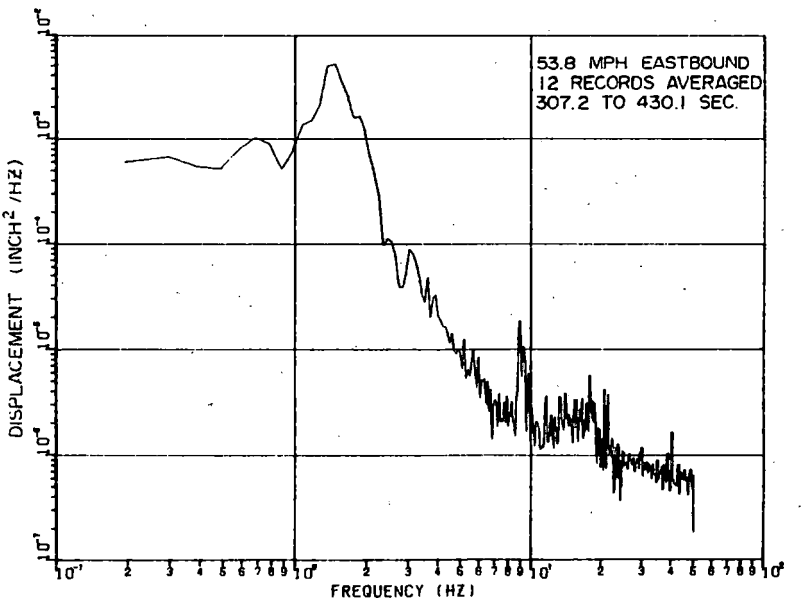

4 h. TRUCK-B LATERAL DISPLACEMENT

POWER SPECTRAL DENSITIES

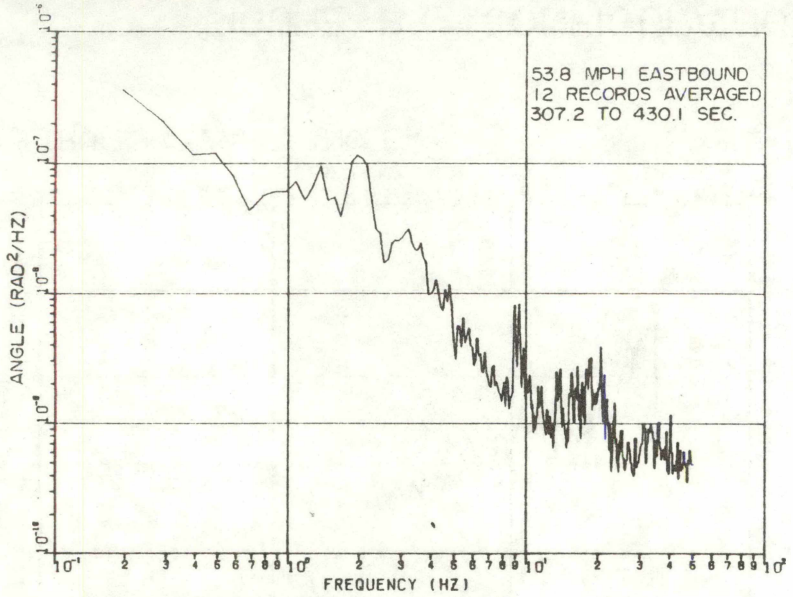

4 i. TRUCK-B YAW ANGLE

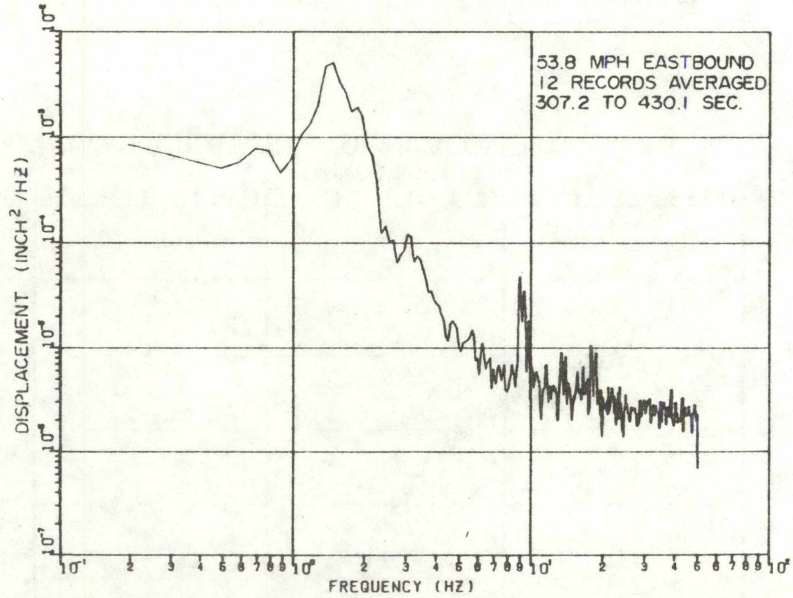

4 k. WHEELSET-1 LATERAL DISPLACEMENT

FIGURE B-6. CONFIGURATION 6

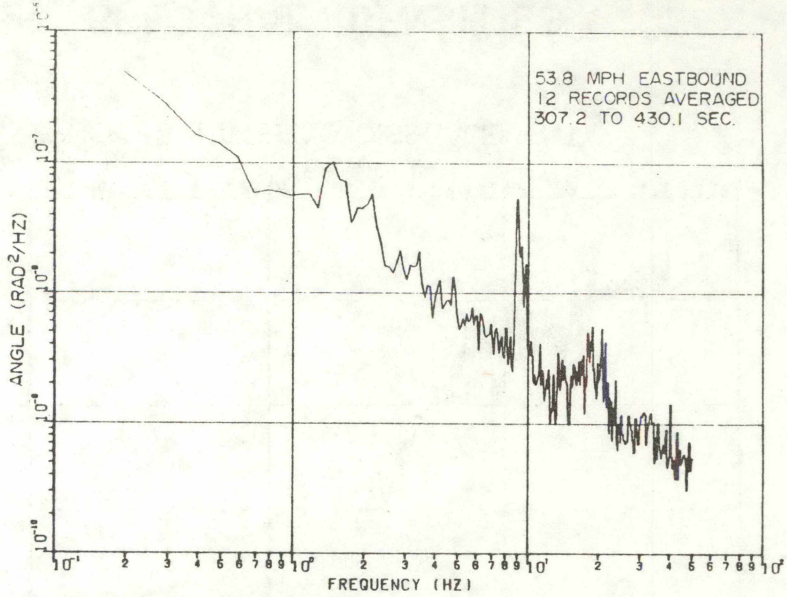

4 j. TRUCK-B WARP ANGLE

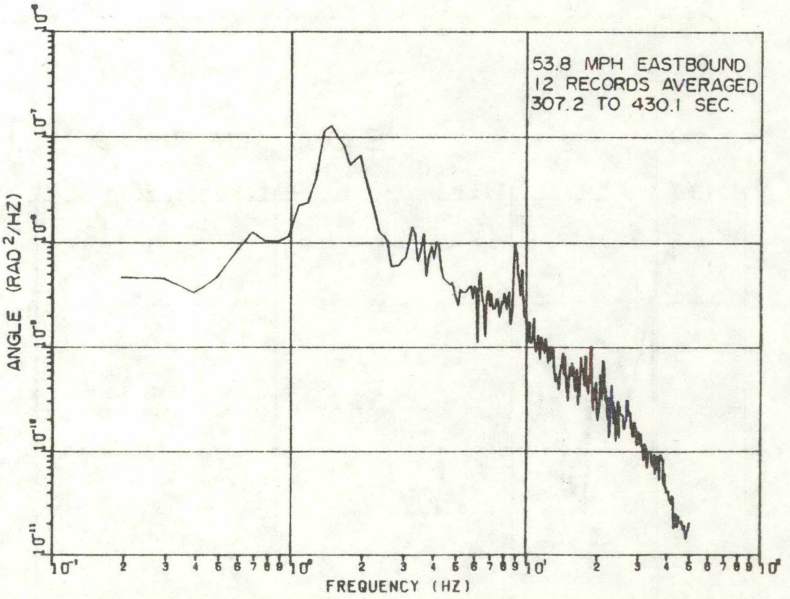

4 l. WHEELSET-1 YAW ANGLE

POWER SPECTRAL DENSITIES

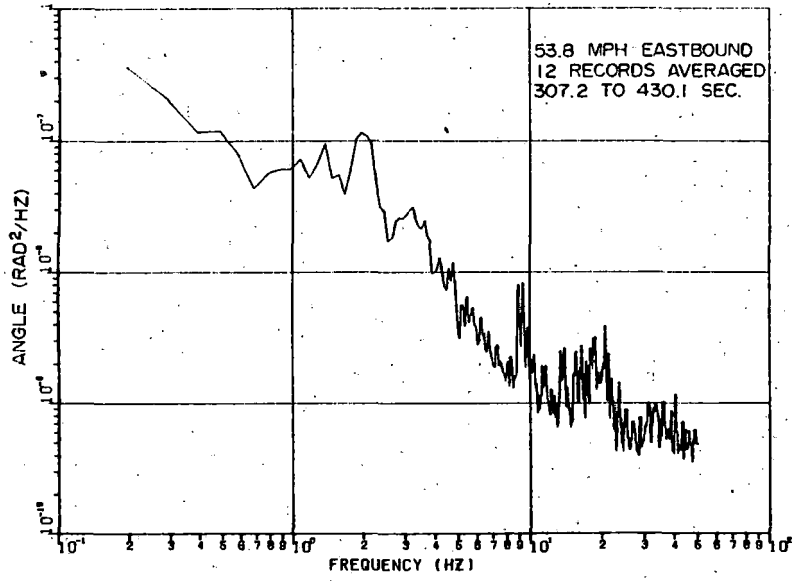

4 i. TRUCK-B YAW ANGLE

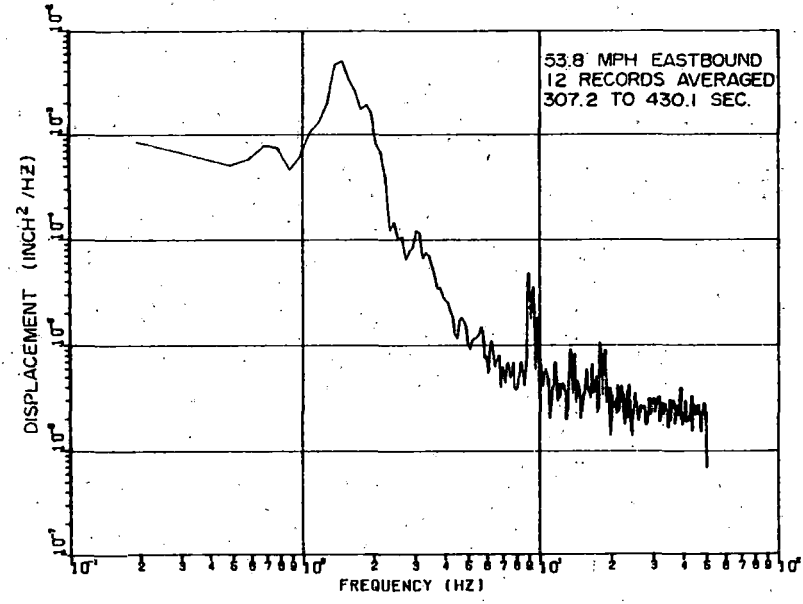

4 k. WHEELSET-1 LATERAL DISPLACEMENT

FIGURE B-6. CONFIGURATION 6

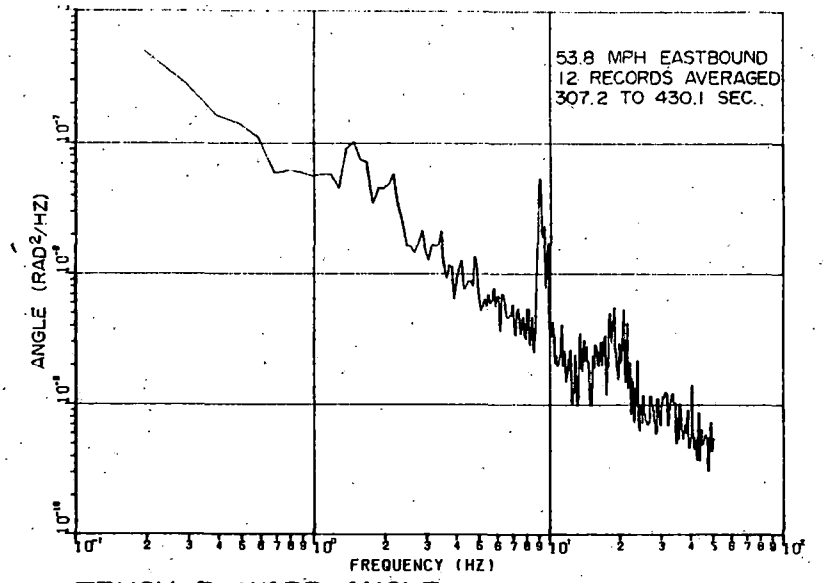

4 j. TRUCK-B WARP ANGLE

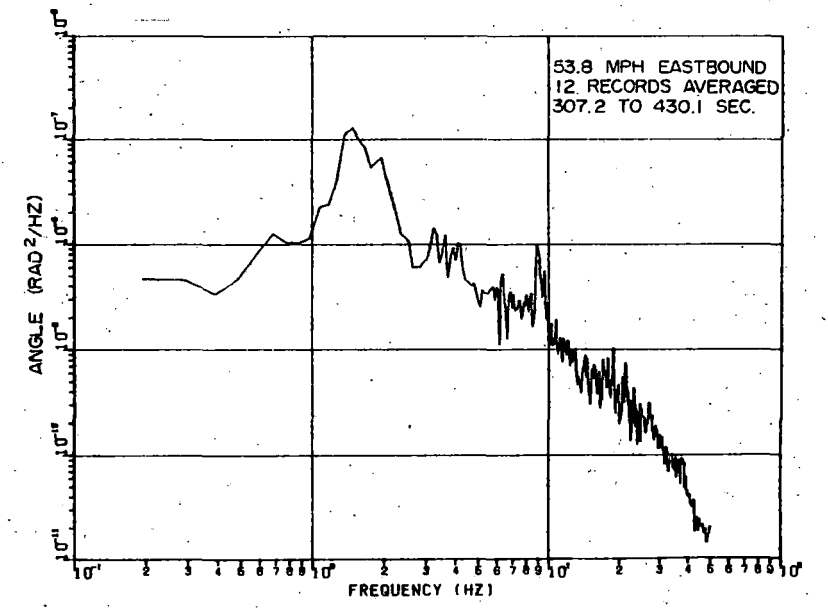

4 l. WHEELSET-1 YAW ANGLE

POWER SPECTRAL DENSITIES

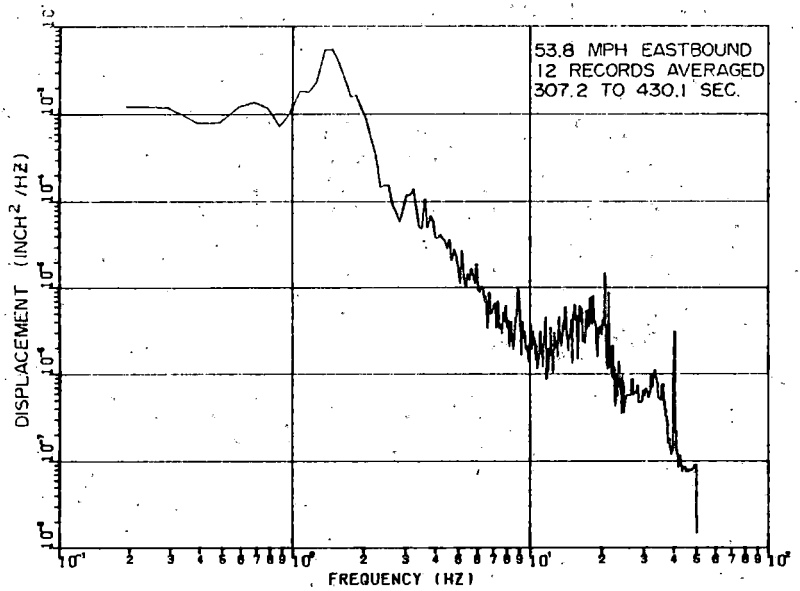

4m. WHEELSET-2 LATERAL DISPLACEMENT

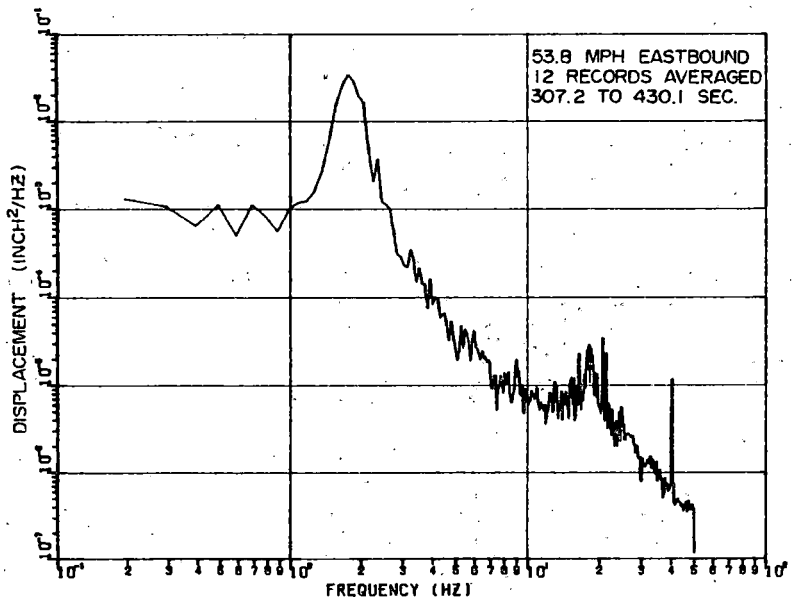

4o. WHEELSET-3 LATERAL DISPLACEMENT

FIGURE B-6. CONFIGURATION 6

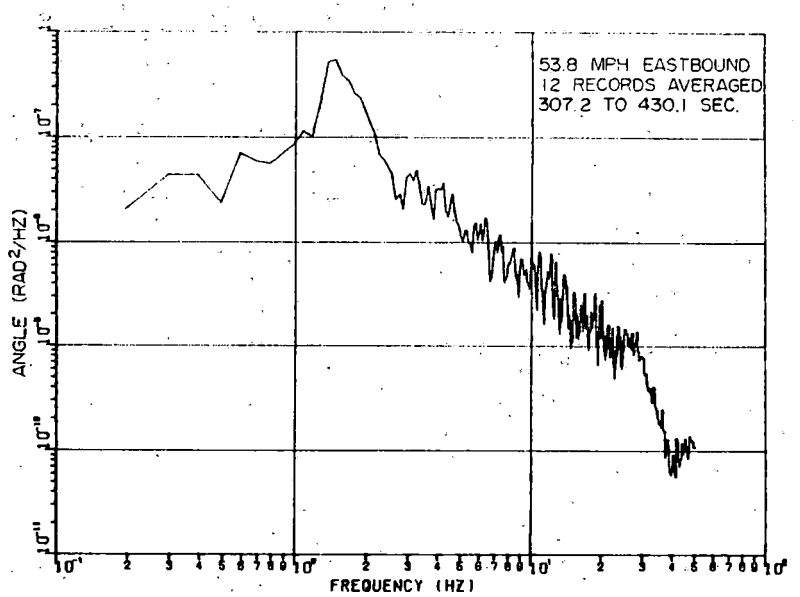

4n. WHEELSET-2 YAW ANGLE

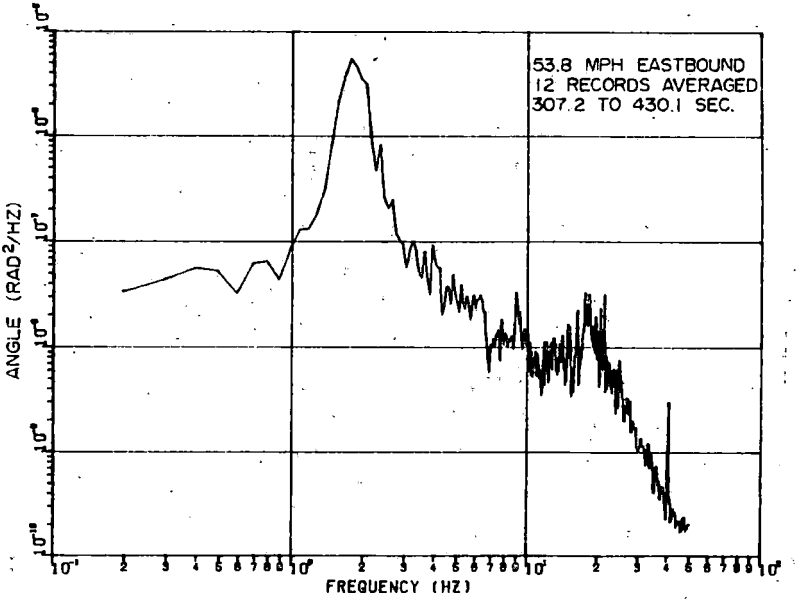

4p. WHEELSET-3 YAW ANGLE

POWER SPECTRAL DENSITIES

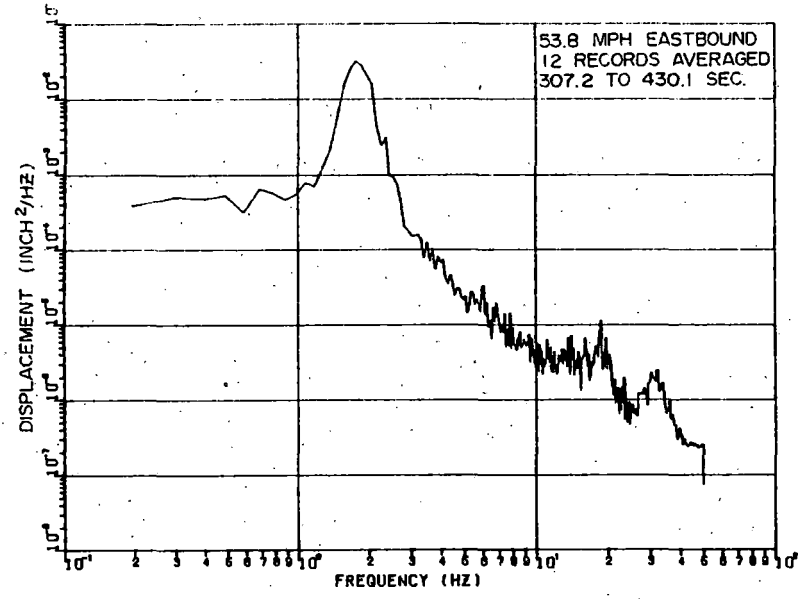

4 q. WHEELSET-4 LATERAL DISPLACEMENT

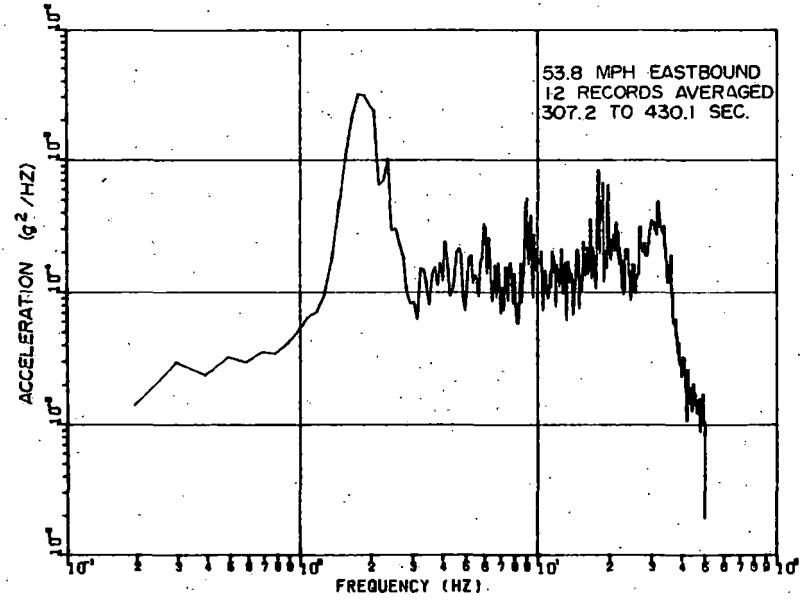

4 s. SIDEFRAME LATERAL ACCELERATION
AXLE-4 RIGHT SIDE

FIGURE B-6. CONFIGURATION 6

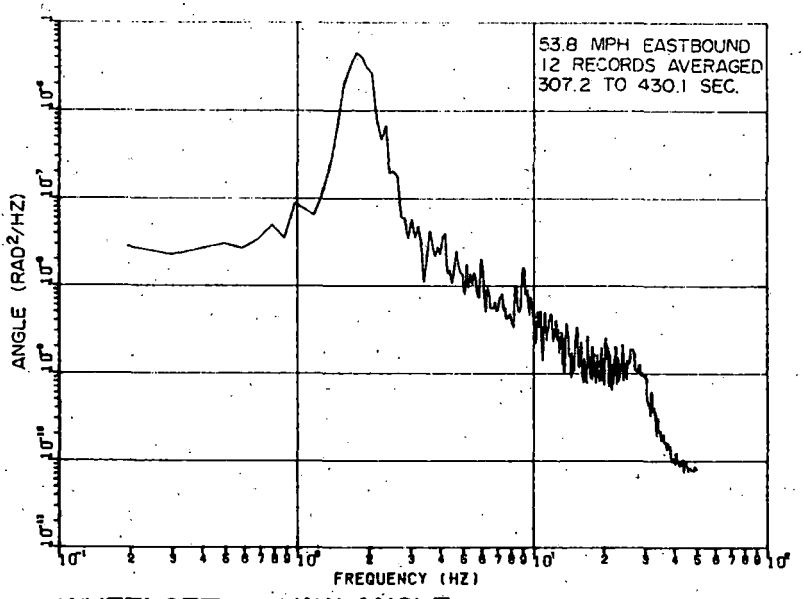

4r. WHEELSET-4 YAW ANGLE

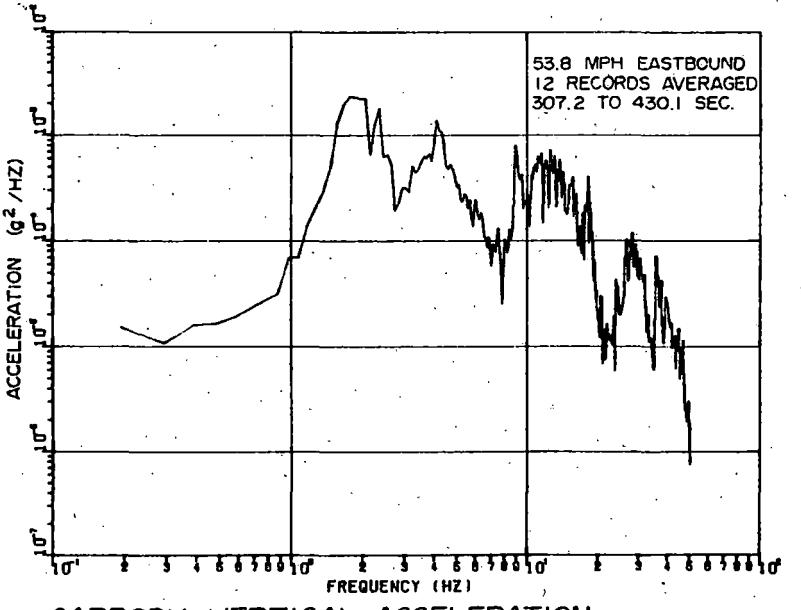

4t. CARBODY VERTICAL ACCELERATION
B-END RIGHT SIDE

POWER SPECTRAL DENSITIES

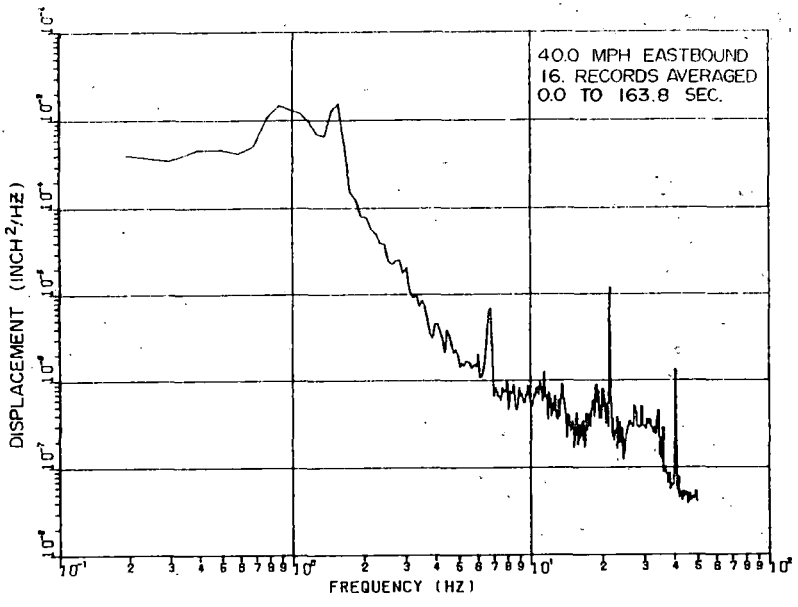

a. TRUCK-A LATERAL DISPLACEMENT

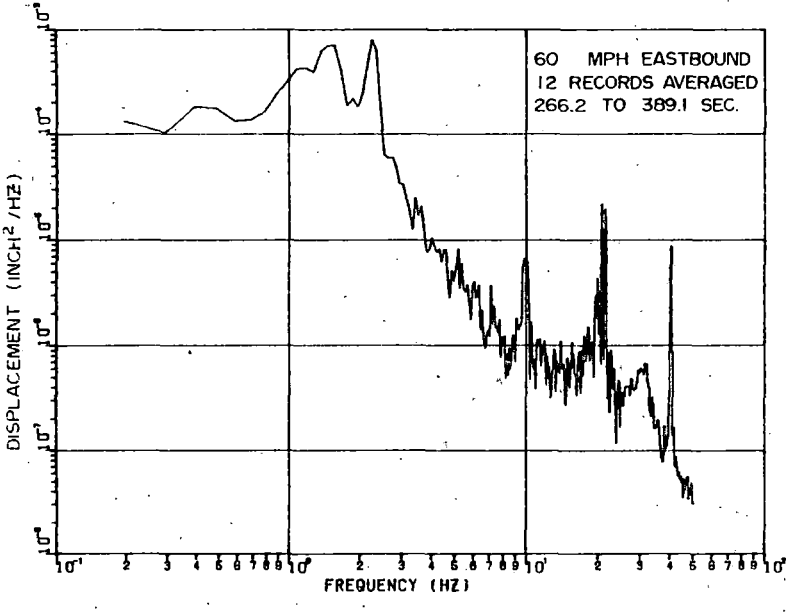

c. TRUCK-A. LATERAL DISPLACEMENT

FIGURE B-7. CONFIGURATION

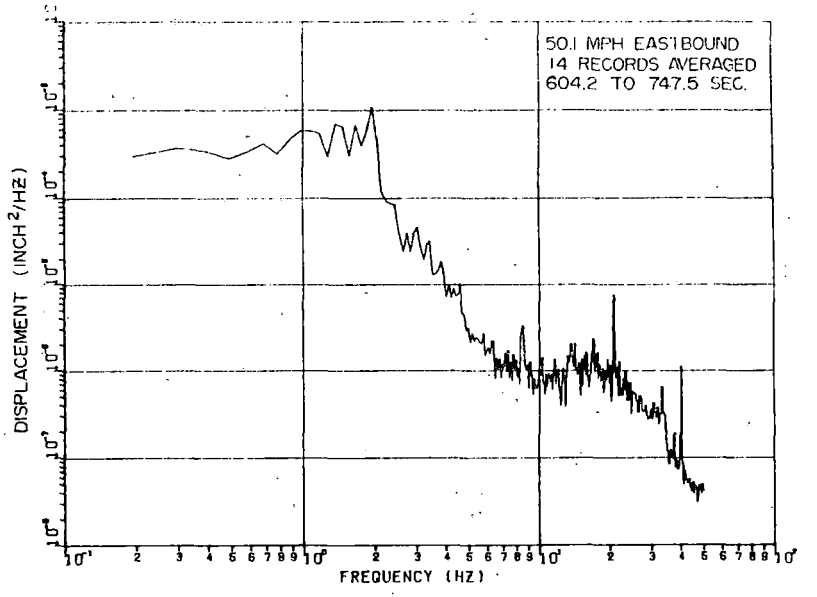

b. TRUCK-A LATERAL DISPLACEMENT

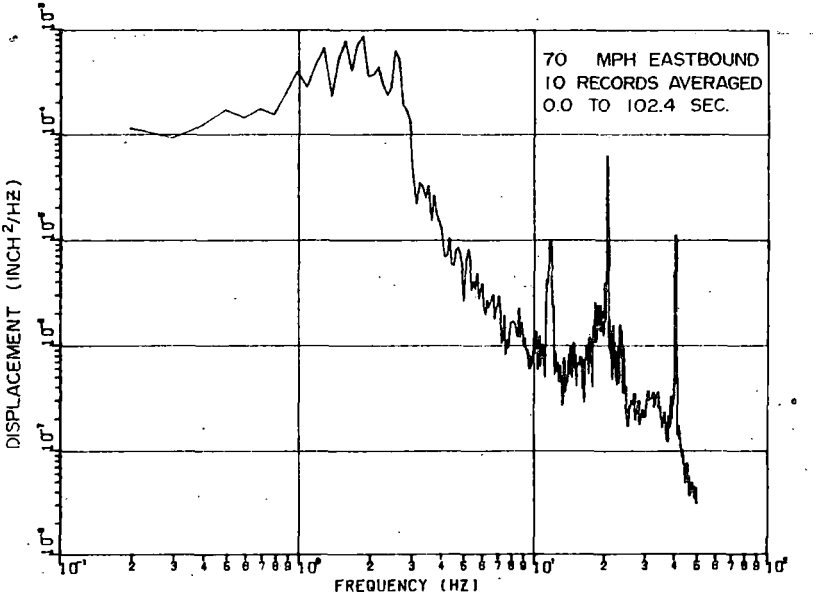

d. TRUCK-A LATERAL DISPLACEMENT

7 POWER SPECTRAL DENSITIES

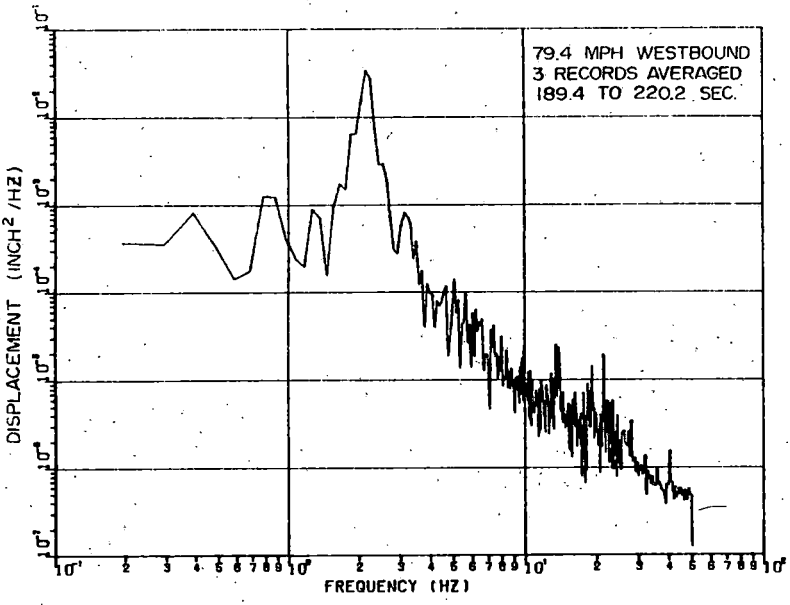

e. TRUCK-A LATERAL DISPLACEMENT

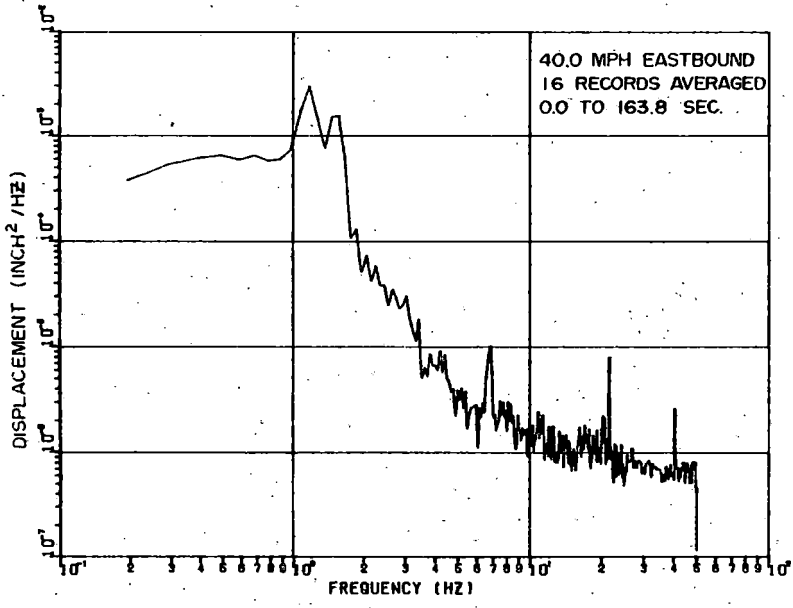

g. TRUCK-B LATERAL DISPLACEMENT

FIGURE B-7. CONFIGURATION 7

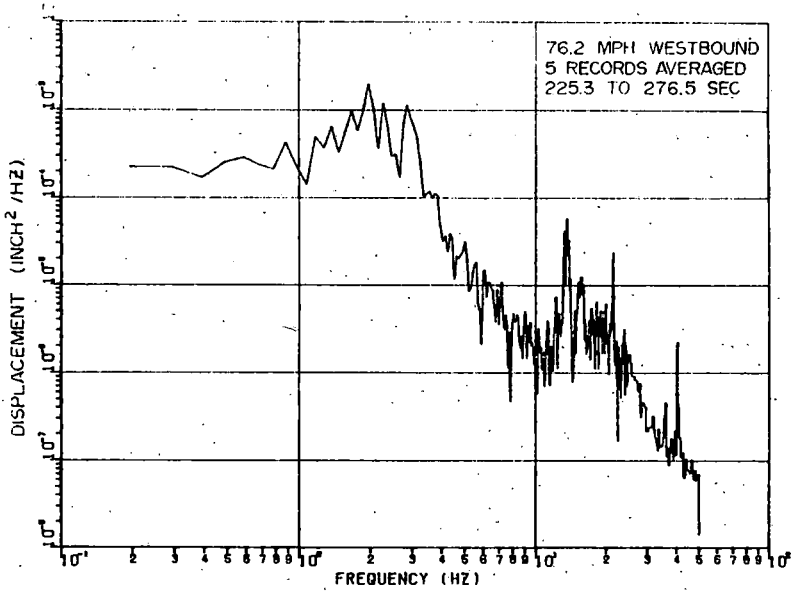

f. TRUCK-A LATERAL DISPLACEMENT

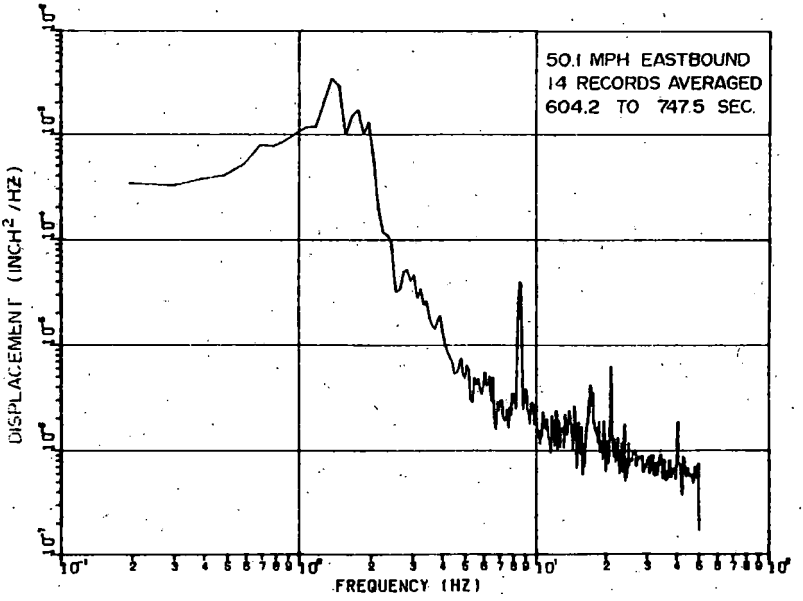

h. TRUCK-B LATERAL DISPLACEMENT

POWER SPECTRAL DENSITIES

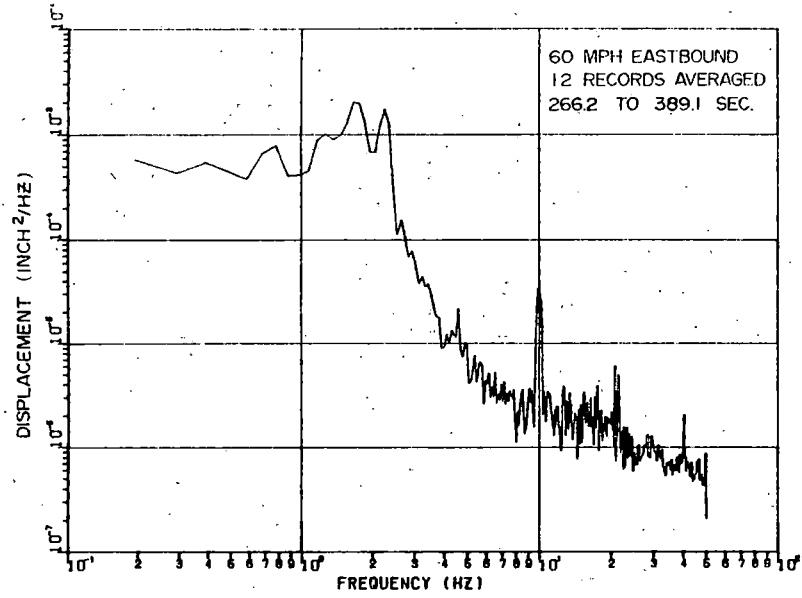

i. TRUCK-B LATERAL DISPLACEMENT

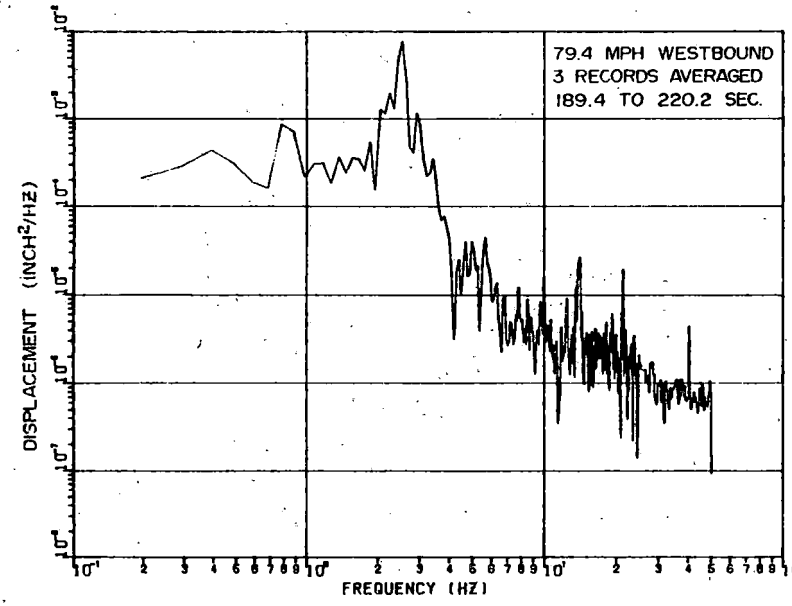

k. TRUCK-B LATERAL DISPLACEMENT

FIGURE B-7. CONFIGURATION 7

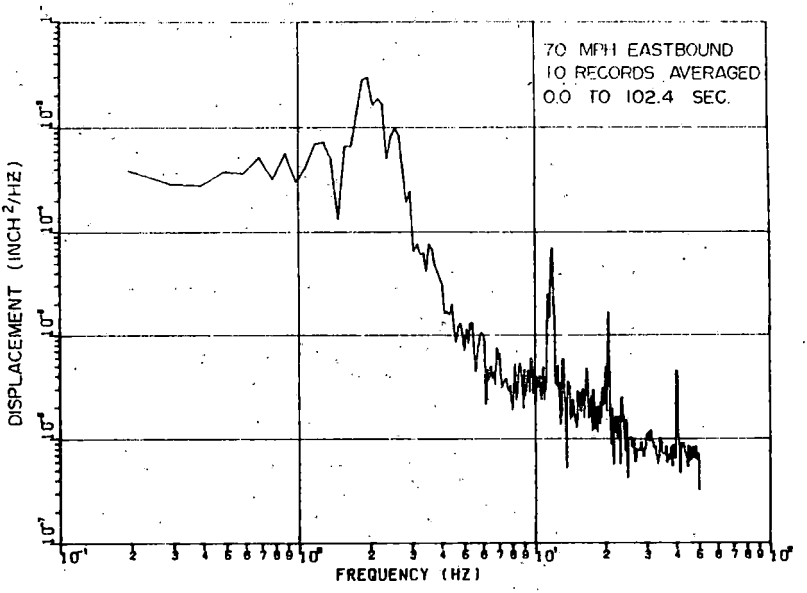

1. TRUCK-B LATERAL DISPLACEMENT

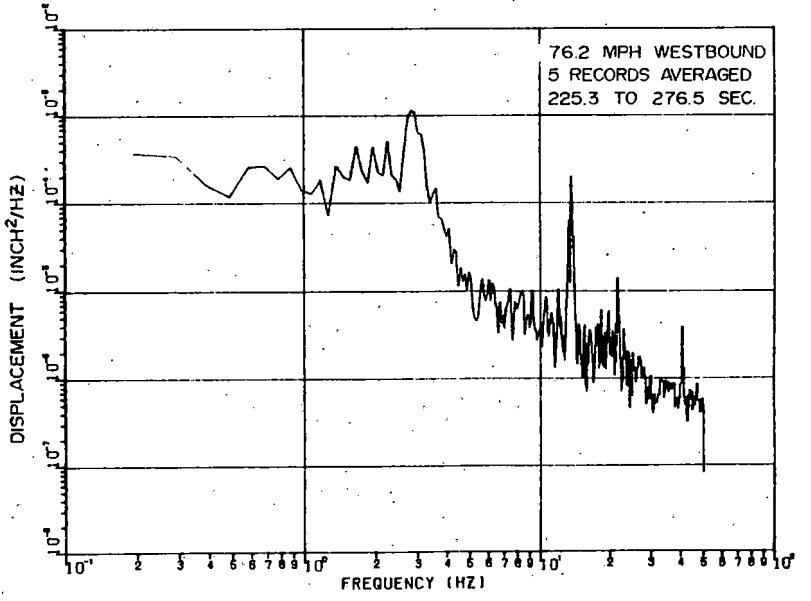

1. TRUCK-B LATERAL DISPLACEMENT

POWER SPECTRAL DENSITIES

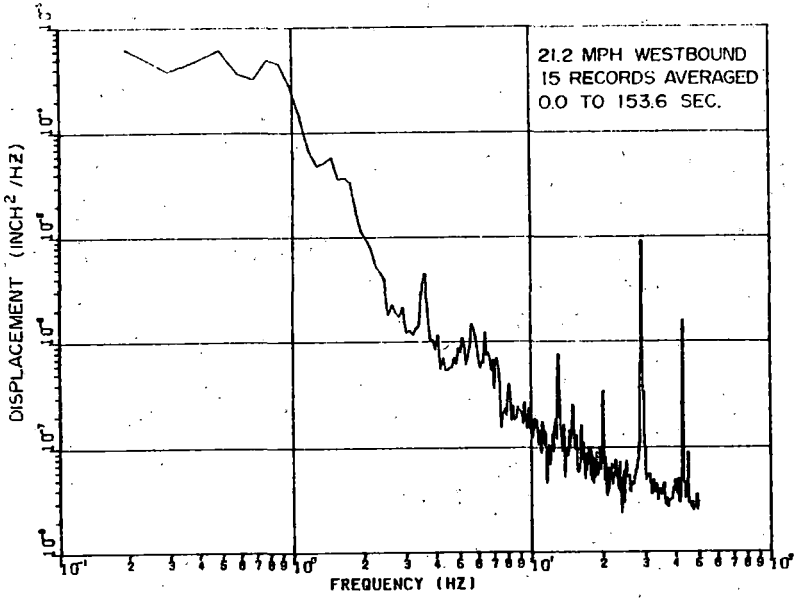

a. TRUCK-A LATERAL DISPLACEMENT

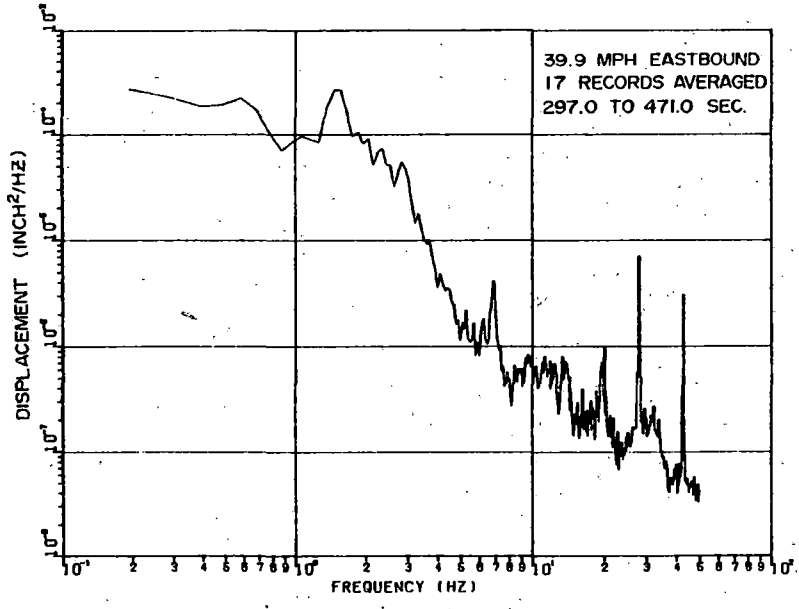

c. TRUCK-A LATERAL DISPLACEMENT

FIGURE B-8. CONFIGURATION 8

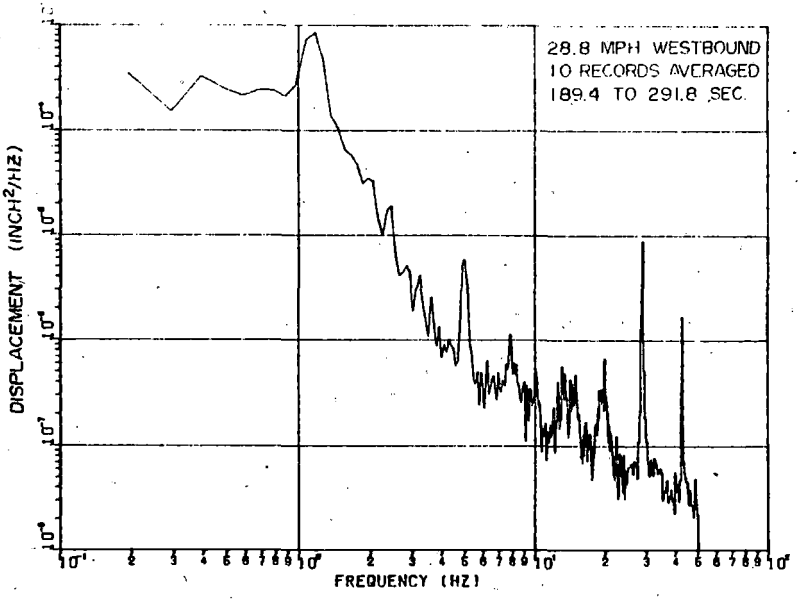

b. TRUCK-A LATERAL DISPLACEMENT

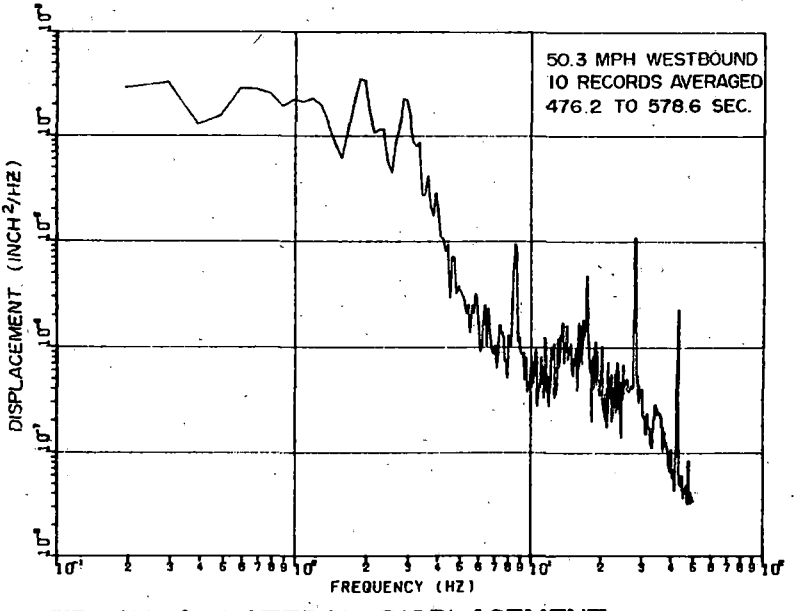

d. TRUCK-A LATERAL DISPLACEMENT

POWER SPECTRAL DENSITIES

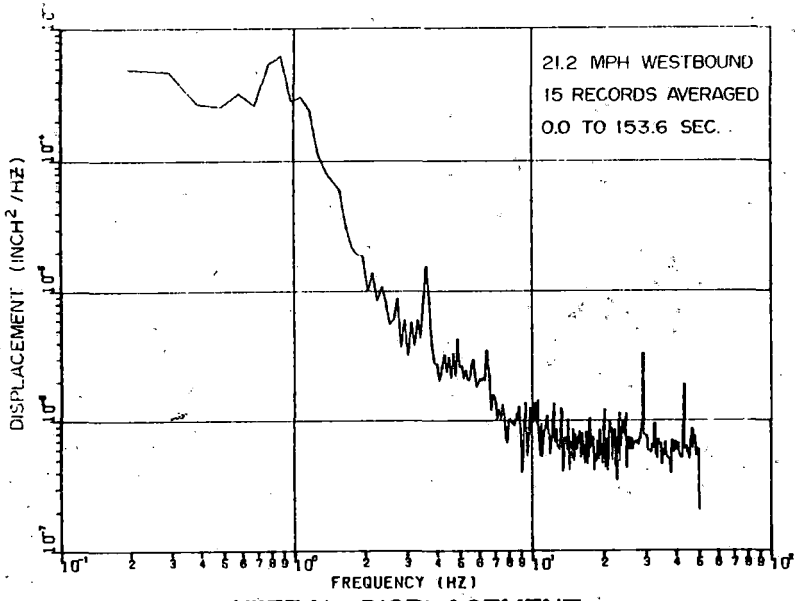

e. TRUCK-B LATERAL DISPLACEMENT

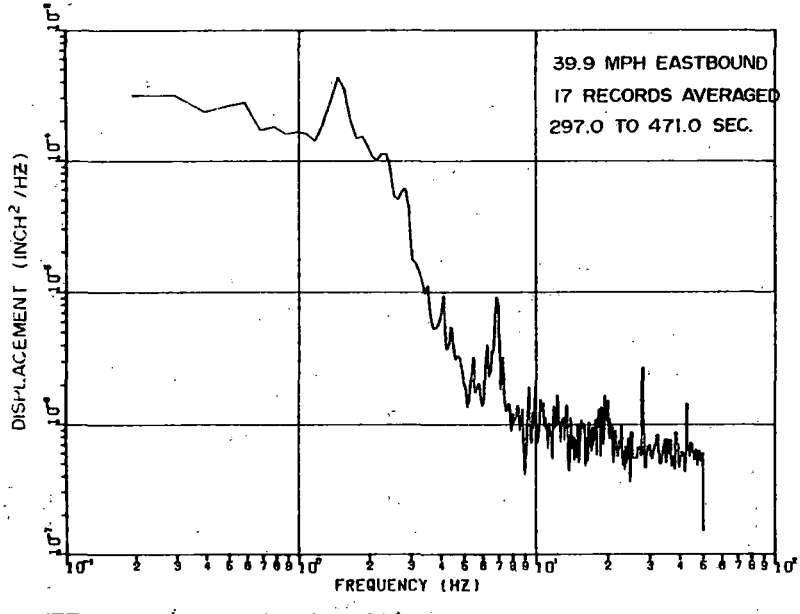

g. TRUCK-B LATERAL DISPLACEMENT

FIGURE B-8. CONFIGURATION 8

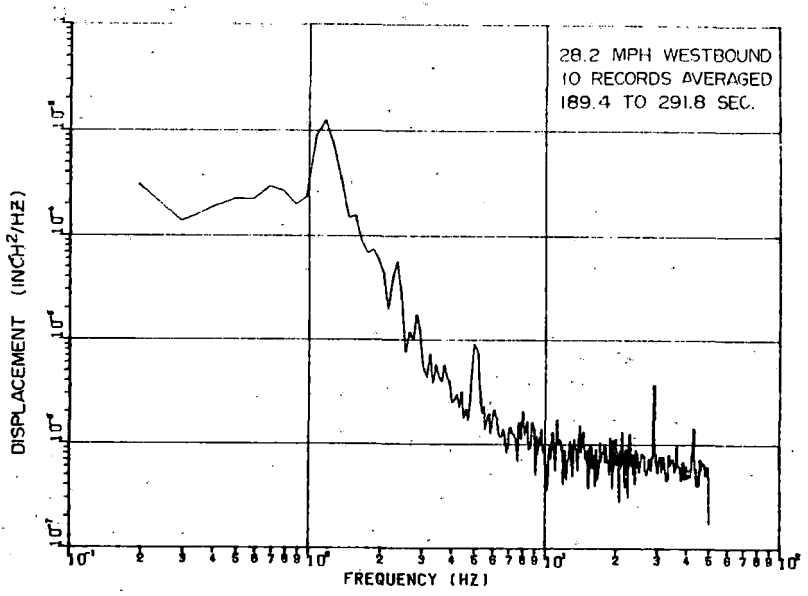

f. TRUCK-B LATERAL DISPLACEMENT

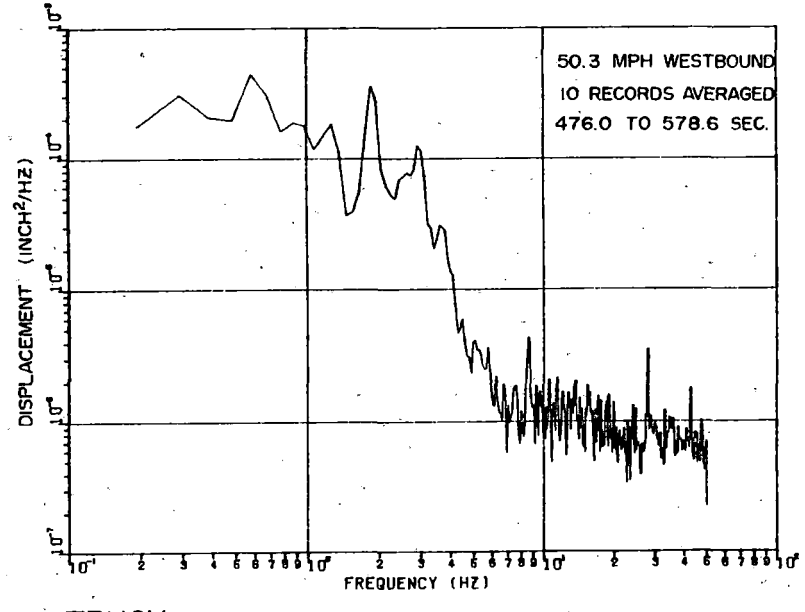

h. TRUCK-B LATERAL DISPLACEMENT

POWER SPECTRAL DENSITIES

APPENDIX C

DEFINITION OF MODEL VARIABLES AND JOINT DISPLACEMENT VARIABLES

Data from the various transducers comprising the instrumentation compliment were combined to form variables of a 19-DOF freight car model. We have referred to these computed variables as model variables.

Beginning with the individual channels shown in Table 3-10, a set of intermediate variables was first computed. Table C1 shows the definitions of these intermediate variables.

The 19-DOF model variables were then computed using the intermediate variables and the individual channels. Table C2 shows the definitions of the model variables.

The joint displacements discussed in Chpater 4 and shown in Table 4-4 were computed from the model variables as shown in Table C3.

Table C3. Joint Displacement Variables

$$\text{CPROT-A} = \theta_C - \theta_{TA} - \theta_{WA}$$

$$\text{CPROT-B} = \theta_C - \theta_{TB} - \theta_{WB}$$

$$\text{BOSF-A} = X_C + \theta_C/203 - X_{TA}$$

$$\text{BOSF-B} = X_C - \theta_C/203 - X_{TA}$$

$$\text{SFVERT} = \phi_C/39$$

Table C1. Intermediate Combined Variables.

101. WRLD-BR1 = (WRLD-BR1a + WRLD-BR1b)/2
102. WRLD-BL1 = (WRLD-BL1a + WRLD-BL1b)/2
103. WRLD-BL2 = WRLD-BL2a + WRLD-BL2b)/2
104. WRLD-AR3 = (WRLD-AR3a + WRLD-AR3b)/2
105. WRLD-AL3 = (WRLD-AL3a + WRLD-AL3b)/2
106. WRLD-AR4 = (WRLD-AR4a + WRLD-AR4b)/2
107. WRLD-AL4 = (WRLD-AL4a + WRLD-AL4b)/2
108. AXAT-BR1 = (WRLD-BR1a - WRLD-BR1b)/D
109. AXAT-BL1 = (WRLD-BL1b - WRLD-BL1a)/D
110. AXAT-BL2 = (WRLD-BL2b - WRLD-BL2a)/D
111. AXAT-B1 = (AXAT-BR1 + AXAT-BL1)/2
112. AXAT-AR3 = (WRLD-AR3a - WRLD_AR3b)/D
113. AXAT-AL3 = (WRLD-AL3b - WRLD-AL3a)/D
114. AXAT-AR4 = (WRLD-AR4a - WRLD-AR4b)/D
115. AXAT-AL4 = (WRLD-AL4b - WRLD-AL4a)/D
116. AXAT-A3 = (AXAT-AR3 + AXAT-AL3)/D
117. AXAT-A4 = (AXAT-AR4 + AXAT-AL4)/2
118. AXDPS-A = (AXDSP-AR3 - AXDSP-AL3)/W1
119. AXDSP-B = (AXDSP-BR2 - AXDSP-BL2)/W1
120. BOROL-A = (SPTR-AL - SPTR-AR)/W2
121. BOROL-B = (SPTR-BL - SPTR-BR)W2
122. BOSF-A = (BOSF-AL - BOSF-AR)/2
123. BOSF-B = (BOSF-BL - BOSF-BR)/2
124. CONGA-A = (WRLD-AR4 = WRLD-AL4)/2
125. CONGA-B = (WRLD-BRL + WRLD-BL1)/2
126. CVRT-A = (CVRT-AR + CVRT-AL)/2
127. CVRT-B = (CVRT-BR + CVRT-BL)/2
128. CROL-A = (CVRT-AL - CVRT-AR)/W3
129. CROL-B = (CVRT-BL - CVRT-BR)/W3
130. SFLAT-AR = (SFLAT-AR3 + SFLAT-AR4)/2
131. SFLAT-AL = (SFLAT-AL3 + SFLAT-AL4)/2
132. SFALT-BR = (SFLAT-BR1 + SFLAT-BR2)/2
133. SFLAT-BL = (SFLAT - BL1 + SFLAT-BL2)/2
134. SFLAT-A = (SFLAT-AR - SFLAT-AL)/2
135. SFLAT-B = (SFLAT-BR - SFLAT-BL)/2
136. SFYAW-AR = (SFLAT-AR4 - SFLAT-AR3)/L
137. SFYAW-AL = (SFLAT-AL3 - SFLAT-AL4)/L
138. SFYAW-BR = (SFLAT-BR2 - SFLAT - BR1)/L
139. SFYAW-BL = (SFLAT-BL1 - SFLAT-BL2)/L
140. SFYAW-A = (SFYAW-AR + SFYAW-AL)/2
141. SFYAW-B = (SFYAW-BR + SFYAW-BL)/2
142. SFWRP-A = (SFLNG-AR - SFLNG-AL)/W4
143. SFWRP-B = (SFLNG-BR - SFLNG-BL)/W4
144. ASLAT-AR3 = (ASLAT-AR3u + ASLAT-AR3d)/2
145. ASLAT-AL3 = (ASLAT-AL3u + ASLAT-AL3d)/2
146. ASLAT-AR4 = (ASLAT-AR4u + ASLAT-AR4d)/2
147. ASLAT-AL4 = (ASLAT-AL4u + ASLAT-AL4d)/2
148. ASLAT-AR = (ASLAT-AR3 + ASLAT-AR4)/2
149. ASLAT-AL = (ASLAT-AL3 + ASLAT-AL4)/2
150. SFROL-AR = [+(ASLAT-AR3u + ASLAT-AR4u) + (ASLAT-AR3d + ASLAT-AR4d)]/F
151. SFROL-AL = ([ASLAT-AL3u + ASLAT-AL4u) - (ASLAT-AL3d + ASLAT-AL4d)]/F
152. ASYAW-AR = (ASLAT-AR4 - ASLAT-AR3)/L
153. ASYAW-AL = (ASLAT-AL3 - ASLAT-AL4)/L

Note: See Table C2 for distance definitions.

Table C2. 19-DOF Model Variables

D.O.F.	SYMBOL	DESCRIPTION	DISPLACEMENT	ACCELERATION
1	X_c	Carbody Lat. Disp.	$(X_{TA}+X_{TB}$ + BOSF-A + BOSF-B)/2	(BOLAT-A + BOLAT-B)/2
2	ϕ_c	Carbody Roll Angle	(BOROL-A + BOROL-B)/2 - (CRBOV-A + CRBOV-B)/2G	(CROL-A + CROL-B)/2
3	θ_c	Carbody Yaw Angle	$-(X_{TB}$ + BOSF-B - X_{TA} - BOSF-A)/M	(BOLAT-A - BOLAT-B)/M
4	γ_c	Carbody Longitudinal Torsion	(BOROL-A - BOROL-B) - (CRBOV-A - CRBOV-B)/G	(CROL-A - CROL-B)/2
5	η_c	Carbody Lateral Bending	Not Measured (NM)	NM
6	X_{TA}	Truck A Lat. Disp.	$(X_{TW3}+X_{TW4}$+ASLAT-AL + ASLAT-AR)/2	SFLAT-A
7	θ_{TA}	Truck A Yaw Angle	$-(X_{TW3} - X_{TW4})/L$ + (ASYAW-AR + ASYAW-AL)/2	SFYAW-A
8	θ_{WA}	Truck A Warp Angle	θ_{TW4}+(SFAX-AR4 - SFAX-AL4)/W + $(X_{TW3} - X_{TW4})/L$	SFWRP-A - SFYAW-A
9	X_{TB}	Truck B Lat. Disp.	$(X_{TW1} + Y_{TW2})/2$	SLAT-B
10	θ_{TB}	Truck B Yaw Angle	$-(X_{TW1} - X_{TW2})/L$	SFYAW-B
11	θ_{WB}	Truck B Warp Angle	θTW_1 + (SFAX-BR1 - SFAX-BL1)/W + $(X_{TW1} - X_{TW2})/L$	SFWRP-B - SFYAW-B
12	X_{TW1}	Wheelset 1 Lat. Disp.	(WRLD-BR1 - WRLD-BL1)/2	NM
13	θ_{TW1}	Wheelset 1 Yaw Angle	AXAT-B1	NM
14	X_{TW2}	Wheelset 2 Lat. Disp.	- WRLD-BL2	NM
15	θ_{TW2}	Wheelset 2 Yaw Angle	AXAT-BL2	NM
16	X_{TW3}	Wheelset 3 Lat. Disp.	(WRLD-AR3 - WRLD-AL3)/2	NM
17	θ_{TW3}	Wheelset 3 Yaw Angle	AXAT-A3	NM
18	X_{TW4}	Wheelset 4 Lat. Disp.	(WRLD-AR4 - WRLD-AL4)/2	NM
19	θ_{TW4}	Wheelset 4 Yaw Angle	AXAT-A4	NM

Distances

G = centerplate to CRBOV Xducer = 18 in.
M = bolster A to bolster B = 406 in.
L = axle to axle = 68.5 in.
F = ASLAT-u to ASLAT-d = 12 in.
D = WRLD-a to WRLD-b = 50 in.
W = SFAX to SFAX = 95.5 in.
W1 = AXDSP to AXDSP = 101 in.
W2 = SPTR to SPTR = 95.5 in.
W3 = CVRT to CVRT = 123 in.
W4 = SFLONG to SFLONG = 68.5 in.

NM = Not Measured

Freight Car Dynamics: Field Test Results and Comparison with Theory (Interim Report), 1981
US DOT, FRA, NK Cooperrider, EH Law, RH Fries

PROPERTY OF FRA
RESEARCH & DEVELOPMENT
LIBRARY